Mass balance investigations at Glaciar Chico, Southern Patagonia Icefield, Chile

Andrés Rivera

A thesis submitted to the University of Bristol

in accordance with the requirements of the degree of

Doctor of Philosophy in the Faculty of Science

School of Geographical Sciences

University of Bristol

May 12, 2004

Abstract

The Southern Patagonia Icefield (SPI) is the largest temperate ice mass at mid-latitudes in the Southern Hemisphere, and an area where most glaciers have been retreating during the last 50 years. Based on field data, vertical aerial photographs and satellite images, the changes experienced by Glaciar Chico, are presented. These glacier variations are compared to climatic changes recorded in Patagonia during recent decades through modelling of the glacier mass balance, using a degree-day factor model forced with climatic and field data. The main aim of this work is to analyse the mass balance of Glaciar Chico, in order to distinguish climatically driven glacier behaviour from that which could be related to ice dynamics. Between the end of the Little Ice Age and the middle of the 20th Century the glacier retreated at relatively low rates, but in recent decades there has been an acceleration in the rate of ice thinning and area loss of up to 0.33 ± 0.22 km^2 a^{-1}. In total, the volume lost due to frontal retreat and area change between 1975 and 2001 is -1.73 ± 1.43 km^3 water equivalent (w. eq.). Although the glacier was slowly thinning before 1975, during recent decades the rate of thinning has accelerated to reach a maximum of -5.4 ± 0.55 m a^{-1} at the glacier front. From GPS data, ice thinning was also observed at the lower elevations of the accumulation area, at an average rate of -1.9 ± 0.14 m a^{-1} between 1998 and 2001. Interestingly, the thinning rate in the lower accumulation zone is three times higher than the mass balance estimated for that part of the glacier. Analysis of climatic data showed a warming trend of up to $+0.033$°C a^{-1} between 1969 and 1990, and a trend of decreasing precipitation of up to -27 mm a^{-2} between 1961 and 1990. The mass balance model was run several times in order to obtain the best-fit parameters which were calibrated with direct observations of accumulation and ablation from glaciers across Patagonia. The resulting net mass balance for Glaciar Chico obtained from the model yielded an average of -0.165 ± 0.059 km^3 a^{-1} w. eq. between 1975 and 2001, but this only accounts for three quarters of the volume lost by the glacier due to ice elevation changes (-0.226 ± 0.081 km^3 a^{-1} w. eq.). It is therefore concluded that in addition to the response of Glaciar Chico to climatic changes, a dynamic component also affects its behaviour, which could possibly be related to enhanced sliding generated by an increase in melt water, and/or a long term change in the glacier and its neighbours in the SPI.

Acknowledgments

I declare that the work in this dissertation was carried out in accordance with the Regulations of the University of Bristol. The work is original, except where indicated by special reference in the text, and no part of the dissertation has been submitted for any other academic award. Any views expressed in the dissertation are those of the author.

Andrés Rivera

May 12, 2004

TABLE OF CONTENTS

CHAPTER FIVE
REGIONAL CLIMATOLOGY

CHAPTER SEVEN
DISCUSSION AND CONCLUSIONS

REFERENCES

TABLE OF FIGURES

LIST OF TABLES

1.- INTRODUCTION

1.1 Background

One of the most important consequences of global atmospheric warming observed during recent decades is the shrinking and thinning of mountain glaciers (Meier and others, 2003). Since 1976 this is a process that appears to have been accelerating (Haeberli and others, 1999), in response to a higher global warming rate (IPCC, 2001).

One result of this global warming trend is the enhanced contribution of glaciers and ice caps to the eustatic sea-level rise, which has been estimated to be 0.2 to 0.4 mm a^{-1} averaged over the 20th Century (Church and others, 2001).

Among the regions on Earth with the highest glacial contribution to sea level rise are the Andes of southern South America (Rignot and others, 2003; Meier, 1984). This is a region that has been under-represented in global mass balance models, largely because of the lack of data, in particular the absence of a systematic, long term and validated mass balance programme (Dyurgerov and others, 1997a), as exists for Norway, Canada and the Alps (IAHS/UNESCO, 2001).

This deficiency of data from southern Patagonia can be attributed to several factors. The region from 46°S to 51°S is heavily glaciated due to its location within the Andes, along the western margin of the South American

continent. It also lies in the zone of the roaring forties, a belt of frequent cyclone tracks, characterised by high precipitation, low temperatures and semi-permanent cloud cover conditions (Streten and Troup, 1973). Together, these conditions have imposed logistical constraints to large-scale attempts to access the area and conduct scientific research.

Until the end of the 1990s very little was known about this region (Warren and Sugden, 1993), however, in recent years an increasing number of scientists have been working in Patagonia, significantly improving our knowledge of these remote glaciers (Casassa and others, 2002).

Nevertheless, because there are no systematic mass balance programmes, the existing climatological station network is very sparse, and above all, there is little information from the accumulation areas of the Patagonian glaciers our present glaciological knowledge is still insufficient to fully understand the causes of the significant changes experienced by the main ice fields.

Among the glaciers of southern Patagonia (Figure 1.1), the Northern and Southern Patagonian icefields (NPI and SPI respectively) have been the focus of an increased research effort in recent decades. These are considered to contain the largest glaciers in the Southern Hemisphere (Naruse and Aniya, 1992), and they are also representative of typical temperate mid-latitude terrestrial ice masses (Warren and Sugden, 1993). Moreover, these icefields are thought to have generated a large contribution to sea-level rise during the past 50 years, due to the retreat

and thinning of their glaciers (Aniya, 1999; Rivera and others, 2002; Rignot and others, 2003).
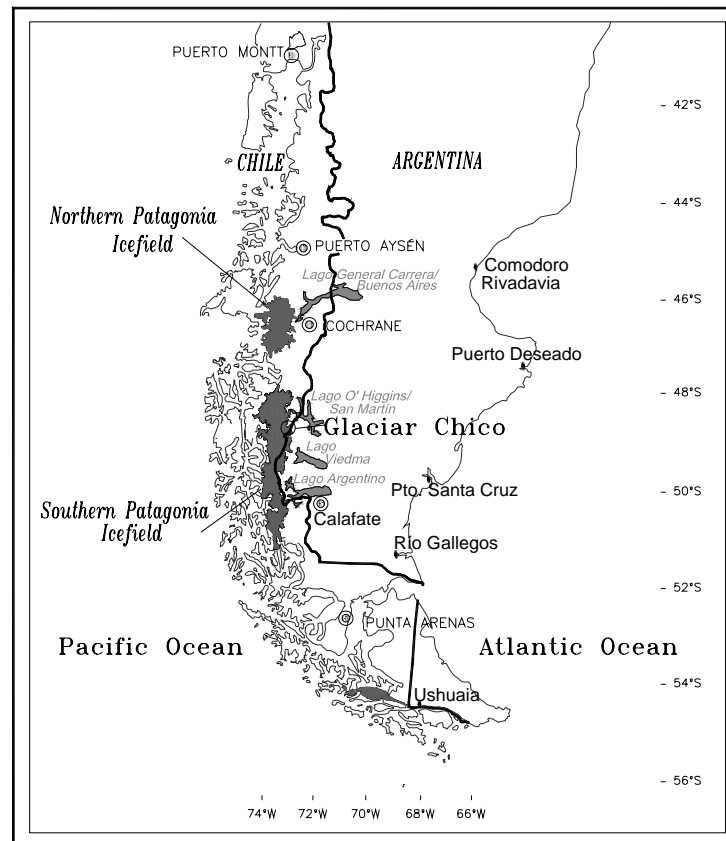
Figure 1.1 Northern and Southern Patagonia Icefields.

This process of recent glacier retreat (Aniya and others, 1997; Aniya, 2001) has been associated with atmospheric warming (Rosenblüth and others, 1997) and a reduction in precipitation (Rosenblüth and others, 1995) observed during the last Century at the majority of the climatological stations of Chilean and Argentinean Patagonia. Additionally, the dynamic components of the glaciers have been considered to be of importance in

accounting for the glacier responses (Skvarca and others, 2002; Rignot and others, 2003).

1.1.1 Glacier mass balance measurements

Glacier mass balance studies have been recognised as a key area of study in the evaluation of the contribution of glaciers and ice caps to eustatic sea-level rise, because they represent a realistic, cheap and globally applicable procedure of accounting for changes in the ice volume (UNESCO, 1998).

Among several methods used to account for the glacier mass balance, two have been widely used in the last 50 years; namely the direct and indirect (Paterson, 1994; Krimmel, 1999).

The direct method is based upon field measurements of accumulation/ablation at a stake network, as well as the use of snow pits to obtain the density and other properties of the snow. This method has been widely used since the 1940s to obtain a highly detailed mass balance record that includes both winter and summer balances of each year of measurement. However, in recent years the number of glaciers measured directly has dropped, due primarily to the logistical cost associated with field campaigns (Dyurgerov and Meier, 1997a).

The indirect method is an independent mass balance approach, where the surface elevation of a glacier is measured instantaneously with reference to the unchanging non ice-covered terrain. If the surface is measured

repeatedly the difference represents the mass balance over the measurement period. This method has been considered more reliable than direct measurements, providing the surface topography derivation for each date is accurate and related to the non-changing surfaces, "the bedrock control" (Krimmel, 1999). With this method, an inter-annual estimation of the mass balance can be obtained, covering a long time series, so long as information on the surface topography is available i.e. since the Little Ice Age (Haakensen, 1986).

For many glaciers, the indirect method has been compared with, and complemented by, direct measurements (Schöner, 1995; Reinwarth and Rentsch, 1994; Conway and others, 1999), with the purpose of extending the mass balance of each glacier to longer-term time scales (Haeberli, 1998).

These two methods and their combinations have been applied globally to more than 250 glaciers during the last 50 years, contributing valuable information about the dynamic responses of glaciers to climate change (Dyurgerov, 2002). But these programmes do exhibit some weaknesses:

- Number of glaciers

According to the last report of the World Glacier Inventory (IAHS/UNESCO, 2001), the mass balance of only 65 glaciers worldwide has actually been reported by direct measurements. Although many other glaciers have been directly measured following the first successful programme in 1946, most

were cancelled after only a few years (Cogley and Adams, 1998) due to expense and difficult logistical constraints. In recent years, an increasing number of glaciers have been studied by indirect methods, in response to the growing amount of remotely sensed data available, as well as new topographic survey techniques.

- Geographical distribution

There is poor regional representation of the present mass balance measurements. For instance, in the Southern Hemisphere large areas of South America have no mass balance studies, in spite of a total glacier area of 25,063 km^2 (USGS, 1998). Only small glaciers in the central Andes of South America have been measured, for example Glaciar Echaurren Norte in Chile since 1975 (Escobar and others, 1995), Glaciar Zongo in Bolivia since 1992 (Francou and others, 1995), and Glaciar Piloto Este in Argentina since 1979 (Leiva and Cabrera, 1996). Further south, in Patagonia, where more than 83% of the South American glacier area is located, only Glaciar de Los Tres has been measured since 1996 (Popovnin and others, 1999). By comparison, the European Alps with a total glaciated area of 2,909 km^2, contain many well studied glaciers, with 14 records of mass balance at present, some of them extending over 50 years (IAHS/UNESCO, 2001).

- Size of monitored glaciers

The vast majority of glaciers with mass balance measurements are small or medium-sized (0.1 to 20 km^2). The small glaciers (mainly cirque glaciers)

reflect annual changes in climate and mass balance almost immediately; medium-sized glaciers (mountain glaciers) react dynamically to decadal variations in climatic and mass balance changes with a lag of several years (Haeberli, 1998).

The largest valley glaciers and ice caps are the most suitable for detecting long-term changes in climate at regional scales, because they exhibit a strong and more efficiently smoothed signals of secular trends with response periods of several decades (Haeberli, 1998). However, these glaciers (large mountain glaciers, ice caps, piedmont, tidewater, freshwater, sub-polar glaciers and temperate ice fields) are poorly represented in the mass balance programmes, but they are nevertheless very important in terms of their areal ice surface and their contribution to sea-level rise (Dyurgerov, 2002).

- Type of glaciers

Nearly 70% of the glaciers monitored for mass balance purposes are located in maritime environments. This creates a bias in the distribution of the results, with a high predominance in Scandinavia, Svalbard, Canada and Iceland (Dyurgerov and Meier, 1997a and b).

To address some of these problems, a wide range of recommendations were presented by UNESCO (1998), including the urgent necessity of expanding the existing network of mass balance surveys to the Southern

Hemisphere, where large glaciers (ice caps, valley glaciers or ice fields) must be monitored.

Taking into account the above recommendations for new mass balance programmes, one of the most suitable icefields in the Southern Hemisphere, due to its size, location, availability of data and glaciological characteristics, is the SPI.

1.1.2 Mass balance of the SPI

As the SPI is composed of many different glaciers, a mass balance study for the whole area must have a wide approach with a low spatial resolution. Casassa and Rivera (1999) studied the whole area by applying a topographic mass balance model; however this was not fully validated due to the limited data for many of the glaciers. Consequently, a potentially more suitable approach is to select a glacier of the SPI which is deemed representative of the processes affecting the region.

Most of the direct measurements of mass balance data of the SPI have been obtained during field campaigns conducted in the lower ablation areas of a few glaciers, like Pío XI, Perito Moreno, Tyndall and Grey (Figure 1.2). In the accumulation areas, the available data are much more sparse, with a few exceptions for Glaciares Chico, Tyndall and Moreno (Casassa and others, 2002).

Many indirect measurements have been obtained for the whole SPI, using remotely sensed satellite data for example (Aniya and others, 1996: Aniya and others, 1997), but detailed analysis only exists for a small number of glaciers including Perito Moreno, (Stuefer, 1999) and Pío XI (Rivera and others 1997a and b).

Considering the lack of a systematic mass balance programme for the SPI glaciers and the high cost of initiating such a programme, a combination of direct and indirect mass balance methods is proposed in this thesis. These include satellite-based remote sensing techniques for the measurement of ice elevation changes, in conjunction with direct field measurements where available and a degree-day factor mass balance model.

Given the relatively large number of direct measurements, the availability of remotely sensed data, aerial photographs and surface topography for different dates, one of the main glaciers of the SPI for which the mass balance can be analysed in detail is Glaciar Chico. Direct measurements of ice elevation changes are available between 1996 and 2001, for both the accumulation and ablation areas of this glacier. During this period scientists were logistically supported by Chilean helicopters and Twin Otter aeroplanes that landed at the plateau of Paso de los Cuatro Glaciares of the SPI (Figure 1.3). In addition to these direct measurements, several photogrammetric surveys have been carried out on the glacier, allowing investigation of ice elevation changes since 1975.

Glaciar Chico is one of the largest glaciers of the SPI with an area of 193 km^2 and a total length of 25 km. The glacier basin is located on the Northeast side (continental margin) of the SPI, and has been retreating at a relatively low rate (~40 m a^{-1}) between 1945 and 1995 (Rivera and others, 2002). The lower ice front is partially calving into an arm of Lago O'Higgins, where the ice is grounded on a small island, which was first visible in the 1975 aerial photographs. This island is believed to be acting as a local pinning point, stabilising the glacier front and reducing the calving activity, which is much less than other calving glaciers of the SPI (Rivera and Casassa, 2000). The relatively low calving rates suggest that Glaciar Chico may be more sensitive to climatic forcing factors, than to local factors such as the geometry of the valleys, depth of the fjords and buoyancy at the ice front (Warren and others, 2001). Through analysis of the available field data and the surface topography from different dates, this thesis investigates the mass balance of the glacier and its relationship with ongoing climate changes affecting southern Chile.
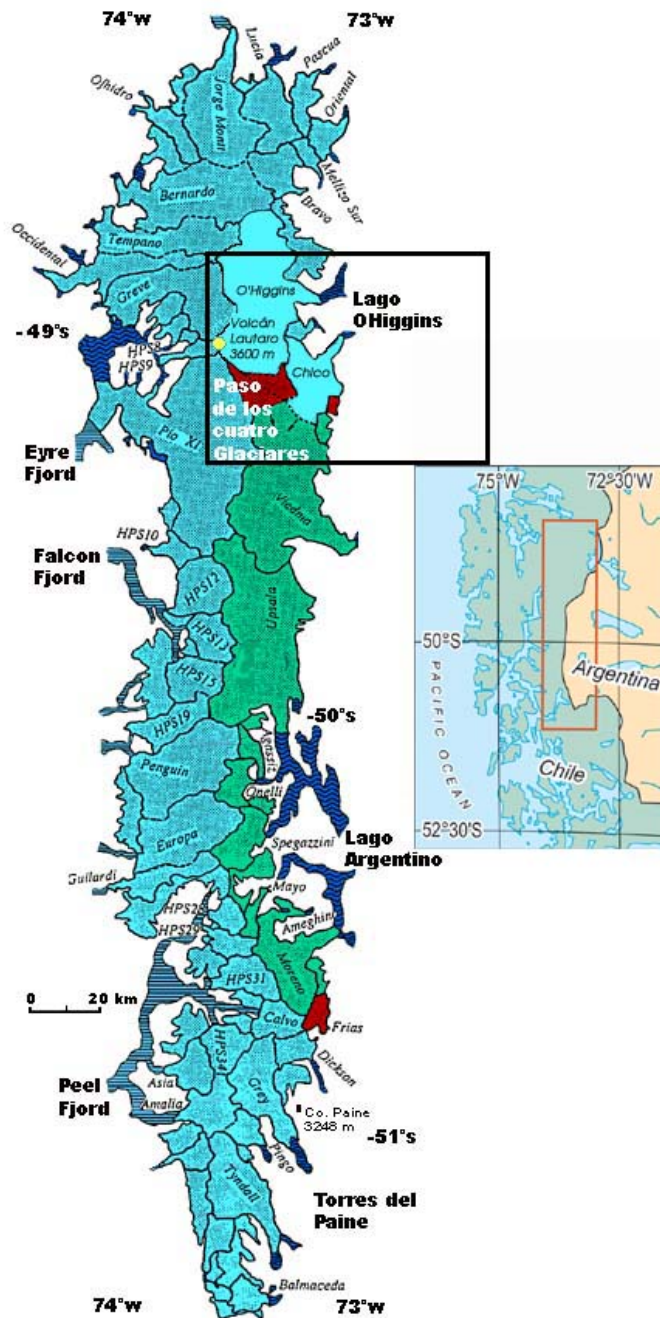
Figure 1.2 Southern Patagonia Icefield and study area. Figure adapted from Naruse and Aniya (1992) showing the main glaciers of the SPI. Glaciers contributing melt water to the Pacific Ocean are shown in blue. Glaciers contributing melt water to the Atlantic Ocean are shown in green. Areas shown in red indicate poor definition of ice divides, especially in Paso de los Cuatro Glaciares where Glaciar Chico is located. The inset shows the general location of the SPI in southern Chile and Argentina.

This kind of study is important for a country like Chile, where the lack of funds for direct measurements of glacier mass balance is endemic. Indirect measurements of glacier mass balance using remote sensing techniques could significantly increase the number of studied glaciers, extending our knowledge of glacier variations and dynamics to areas where very little is known, and where any direct approach is very expensive. A validated indirect approach will also provide data for many topics, such as calibration of models, environmental assessments and decision making, hydrological power projects, risk analysis, impacts of climate changes, new areas for colonization and water resources management.

1.2 The Southern Patagonian Icefield

1.2.1 Physical characteristics

The SPI extends north-south for 350 km between 48°20′ S and 51°30′ S, at an average longitude of 73°30′ W along the western margin of the South American continent, with a maximum elevation of 3600 m at the active Volcán Lautaro. The SPI has been divided into 48 main glacier basins (Aniya and others, 1996), mainly flowing to the east, where the glaciers generally terminate with calving fronts in freshwater lakes, and to the west with termini into Pacific Ocean fjords (Figure 1.2). In the accumulation area, most of the glaciers share relatively flat plateaus at an altitude between 1400 and 1800 m. The Equilibrium Line Altitude (ELA) of most of the glaciers is located between 900 and 1500 m, with an average

Accumulation Area Ratio (AAR) of 68% for the 48 main glaciers of the SPI (Aniya, 1999).

The SPI is located within the area affected by the southern westerlies (Lawford, 1993). Consequently, due to the effects of orography, the western margin of the SPI receives a high amount of precipitation, with an estimated annual maximum of >8 m water equivalent (w. eq.) on the icefield plateau (DGA 1987). Conversely, the eastern margin of the SPI receives little precipitation, amounting to a few hundreds of mm in the Argentine pampas (Ibarzabal y Donángelo and others, 1996).

The mean annual temperature of the marginal lower areas of the SPI is approximately 6 °C (Peña and Gutiérrez, 1992), which allows a unique ecosystem of beech forests to exist around the glacier fronts. The 0 °C isotherm is approximately located at 1100 m in winter and 1400 m in summer (Carrasco and others, 2002). Considering the regional reduction of mean temperatures with latitude (~-0.2 °C °Latitud at the eastern margin of the SPI), the likely altitudinal difference of the 0°C isotherm between the northern and southern tip of the SPI is approximately 130 m.

As the great majority of the lower tongues of the SPI calve into lakes or fjords, their frontal variations, their response time and their dynamic properties are largely controlled by local characteristics, which are often not directly related to climate change (Warren and Rivera, 1994). In this sense, it is difficult to consider just one glacier as representative of the complex processes taking place in the whole SPI, therefore, in this thesis will be

selected a glacier where the local characteristics are less important, not necessarily representing the typical calving behaviour of the Patagonian glaciers, but where the climatic changes are potentially more directly related to glacier responses.

1.2.2 Previous research

Aniya and others, (1997) determined the areal and frontal variations of the 48 major glaciers of the SPI between 1944 and 1986, based on 1:250,000 "preliminary" maps, aerial photographs and satellite imagery. These authors indicated a general trend of retreat for 42 glaciers, while 4 glaciers were in equilibrium (HPS 13, HPS 15, Calvo and Spegazzini, Figure 1.2), and 2 advanced during the same time (Pío XI and Moreno, Figure 1.2).

Other authors have extended the time series using historical data and recent aerial photographs or satellite images of individual glaciers. The glacier with the longest record of frontal variations in the SPI is Glaciar Pío XI, also called Brüggen or Ana María (Rivera, 1992). This was first described in the reports from the HMS Adventure, commanded by Lieutenant Skyring, who visited and mapped the area between January and April 1830, during the hydrographic expedition of captain P.P. King to western Patagonia (Rivera and others, 2000). Since then, the glacier advanced to an initial maximum in 1928 (Agostini, 1945), then retreated until 1945. It then began to advance at an average rate of 288 m a^{-1} to a new maximum frontal position in 1994, at which time it was destroying trees more than 350 years old (Rivera and others, 1997a). Since 1995, the

glacier has again been retreating at low rates (Rivera and others, 2000). The glacier with the largest and longest retreat rate is Glaciar O'Higgins, which, during the period 1896-1995, retreated 14.6 km (Casassa and others, 1997). Another glacier with a long series of recorded frontal variations is Glaciar Perito Moreno, first mapped in 1899. Since then, the glacier front has been oscillating in a near equilibrium position, with a net area gain of 4.1 km^2 between 1947 and 1986 (Skvarca and Naruse, 1997).

Ice elevation changes have been measured in several ablation areas of the SPI glaciers, using diverse methods including direct theodolite surveys, comparison of historical records with actual maps and evaluation of regular cartography from different dates (Casassa and others, 2002). Rignot and others (2003), analysed ice elevation changes in most of the NPI and SPI glaciers, comparing all the available regular cartography (1969, 1975 and 1995) with recently declassified Shuttle Radar Topography Mission (SRTM) data obtained in 2000, revealing a significant thinning rate for most of the ablation areas. The higher plateaus of the SPI were poorly represented in all the regular cartography, and therefore the estimation of thinning in the accumulation areas was inadequately characterised. Nevertheless, using thinning rates obtained at an altitude close to the ELA of many glaciers, it was possible to extrapolate the amount of thinning to the accumulation areas.

The longest record of ice elevation changes has been obtained for Glaciar O'Higgins, where historical records and topographic maps available from 1913 have been compared. These indicate thinning rates in the range -2.5

and -11 m a^{-1} between 1975 and 1995, which, compared with smaller rates measured during previous periods, suggest an acceleration of the thinning rates in recent years (Casassa and others, 1997).

Another glacier where ice elevation changes have been systematically measured is Glaciar Tyndall. In 1985 a mid-altitude topographic profile (at ~700 m) was surveyed with a theodolite installed at the rock margin (Naruse and others, 1987). Since then, the same profile has been re-surveyed several times with a theodolite (Nishida and others, 1995), and more recently using a Global Positioning System (GPS), allowing an estimation of ice elevation changes during recent decades. Raymond and others (In press), have compiled and reduced all available measurements to a common reference datum, homogenising the differences between methods, and determining an accelerated thinning rate of -3.6 m a^{-1} between 1993 and 2002.

Glaciar Pío XI is the exception to the high thinning rate trend observed in most of the SPI glaciers. Using Digital Elevation Models (DEMs) obtained from available regular cartography, Rivera and Casassa (1999) compared the surface topography of the ablation area of the glacier between 1975 and 1995, obtaining an average surface thickening of 2.2 m a^{-1}. This anomalous behaviour is well correlated with the unique state of advance of its southern tidewater front since 1945 (Rivera and others, 1997b) and its northern freshwater front since 1976 (Warren and others, 1997). Since 1995, Rignot and others (2003) have detected a thinning, in combination with a small retreat of the tidewater front.

1.2.3 Contribution of Patagonian glaciers to global sea level

Based upon the available glacier inventory as well as frontal and areal changes, plus some other assumptions (with respect to ice thickness, density of the ice, etc), Aniya (1999) estimated the contribution of the SPI glaciers to the eustatic sea level rise between 1944/45 to 1996 to be 505 $\pm$ 203 km^3 w eq. Dividing this value by the total ocean area of the world results in a contribution of 1.39 $\pm$ 0.54 mm in the 51 year-period from 1945 to 1996, that is 0.027 $\pm$ 0.011 mm a^{-1}. This means that the SPI contributed about 6% of the total sea level rise of small glaciers and ice caps as estimated by Meier (1984). Rignot and others (2003), analysed volumetric changes for the SPI and NPI between 1975 and 2000, and obtained a total contribution to sea level rise similar to Aniya's estimations. However, when the ice elevation changes between 1995 and 2000 were considered, the result was more than doubled compared with the previous estimation, indicating that a thinning acceleration trend is affecting the whole region.

This contribution to sea level rise from Patagonia could be considered not significant when compared with other major contributing factors such as thermal expansion of the ocean or Antarctica and Greenland, however, the Patagonian icefields have been considered one of the areas where the wasting ice is proportionally much higher and faster than Alaska for instance (Rignot and others, 2003), therefore, it is worth to examine the SPI in more detail in order to improve our understanding of a possible enhanced regional climate change.

1.3 General characteristics of Glaciar Chico

Glaciar Chico (49° 00′S, 73° 04′W) is one of the outlet glaciers of the Paso de Los Cuatro Glaciares (P4G), a 15×15 km plateau located at 49°10′S, 73°20′W (Figure 1.3). This plateau has an altitude of between 1450 and 1800 m, and is surrounded by mountain ranges (Volcán Lautaro - Cordón Mariano Moreno to the west, Cordón Pirámide to the north, and Cordón Marconi to the east). The plateau was first visited and named by Kölliker and others (1917), who estimated that it was the origin of four glaciers, namely Glaciares O'Higgins, Viedma, Pío XI and Chico. These first explorers assumed that during the expedition they reached the continental ice divide at a nunatak at the foot of Cordón Mariano Moreno (also named by them), where they left a bottle with a message, before returning to the east. In 1998 the author of this thesis found the bottle and message left by Kölliker in 1916. The site where the bottle was found was entirely within Glaciar Viedma, 12 km eastward of the present continental ice divide with Glaciar Pío XI. Actually, the P4G is only shared by two glaciers (Viedma and Chico), because the ice divide with Glaciar O'Higgins is located approximately 18 km further north. The bad weather conditions, logistic difficulties and rudimentary instruments used by Kölliker's expedition prevented a better survey of the area, which was also partially cloud covered in the west at the time of the expedition.

The frontal tongue of the glacier at Brazo Chico of Lago O'Higgins was first mapped by the Chilean-Argentinean boundary commission who visited the

area between 1894 and 1899 and produced several maps. One of these maps was reproduced by Risopatron (1905).
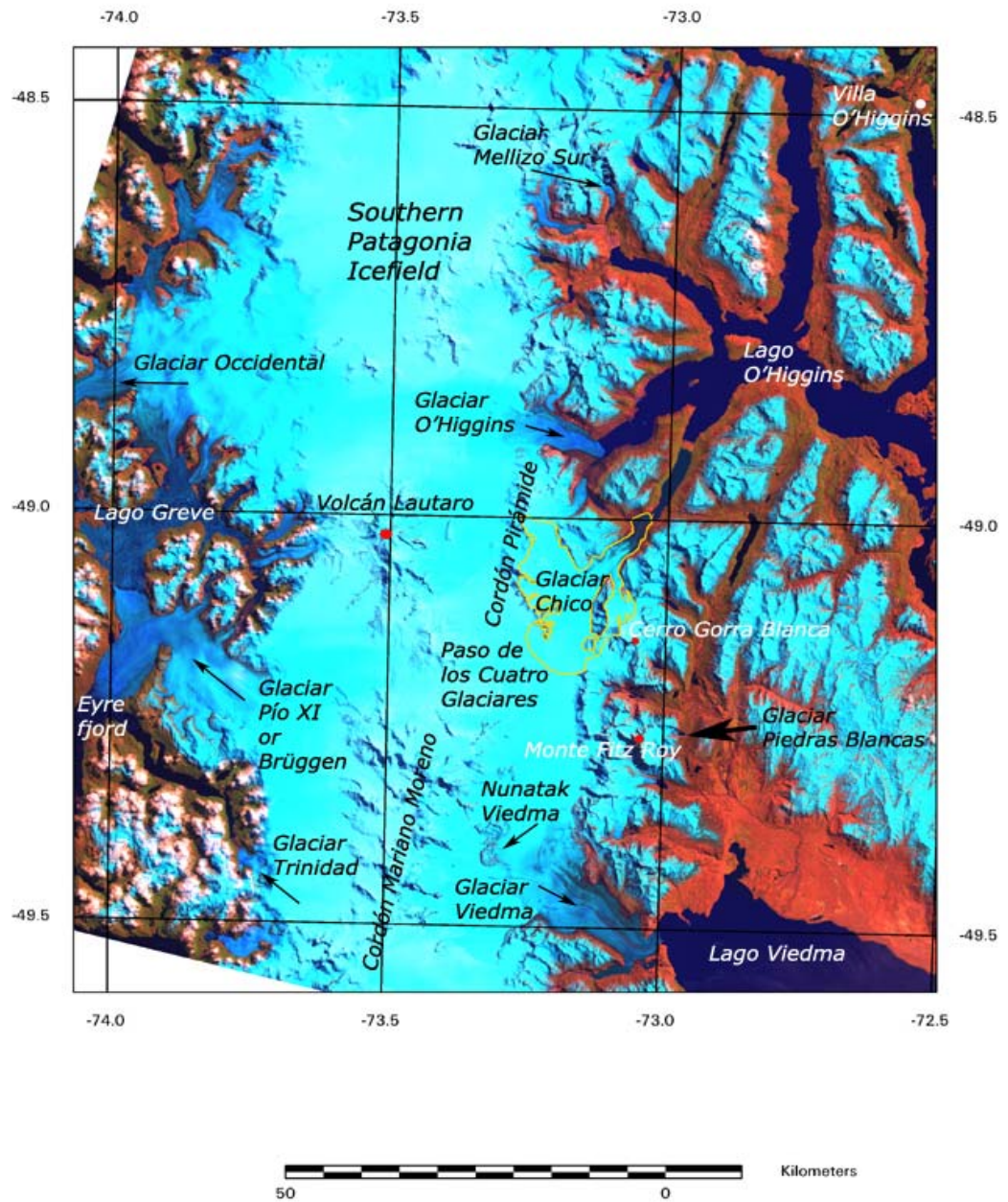
Figure 1.3 Landsat ETM+ false colour composite image (bands 1, 4 and 5) acquired on October 27, 2000. The outline of Glaciar Chico basin in 2001 is shown in yellow. Other glaciers discussed in the text are labelled.

Glaciar Chico flows from a maximum altitude of 2810 m at Cerro Gorra Blanca, to 250 m at its frontal tongue, which is partially calving into the freshwater Brazo Chico of Lago O'Higgins (one arm of O'Higgins Lake). During the last Century, the lower tongue has retreated at low rates, with a decelerating trend over recent years (Rivera and Casassa 2000).

The ice basin is well defined for most of the glacier, with the exception of three places where the boundary is ambiguous due to the uniformity of the topography: namely the ice divides between Glaciares Chico and Viedma, between Glaciares Chico and Marconi, and between Glaciares Chico and Gaea.

Three main basins comprise the accumulation area. The biggest one is located at P4G between Cordón Pirámide and Cerro Gorra Blanca. Second in size is the basin located between Cerro Pirámide and Glaciar Gaea, and finally the smallest and steepest basin is located at the northern side of Cerro Gorra Blanca.

The ablation area is lightly covered by fluvio-glacial sediments, volcanic ash and debris. These materials originate at a central moraine, which extends from one of the foothills of Cerro Pirámide.

The altitude of the plateau in the accumulation area of Glaciar Chico fluctuates between 1300 and 1500 m. The ELA of the glacier was approximately located by Rivera and Casassa (2000) at an elevation between 1300-1400 m.

Most of the present knowledge of the glacier has been obtained during the Hielo Azul annual operation carried out by the Chilean Air Force since 1996, with the main aim of training pilots on snow landing and take off of UH-1 helicopters (Figure 1.4) and Twin Otter aeroplanes equipped with skis. During these operations, scientists have had the opportunity and logistical support to study the area, including measurements of surface topography with GPS, ice thickness with Radio Echo Sounding (RES) systems, snow densities, snow accumulation/ablation, local meteorology, gravity and ice velocities. All these datasets will be used in this thesis, in combination with data obtained from remotely sensed imagery, in order to account for the mass balance of the glacier over recent decades.

Figure 1.4 Base camp at the accumulation area of Glaciar Chico (flowing to the North, left in the photograph) in September 1997, where two UH-1 helicopters were giving logistic support to the Hielo Azul operation. In the background, Cerro Gorra Blanca 2810 m asl.

1.4 Hypothesis and aims

The glaciers of southern South America have been retreating, thinning and shrinking during recent decades in response to a negative mass balance trend, which is explained by a regional increase in temperature and reduction in precipitation. However, not all the glacier variations are explained by the concept of negative mass balance. Most of the Patagonian glaciers have calving fronts, and therefore, their dynamic responses are also controlled by local factors like the geometry and bathymetry of the lakes or fjords into which they are calving.

Calving glaciers have been considered more sensitive to climate changes than non-calving glaciers, and, once pushed out of equilibrium with the climate, they can undergo large aclimatic changes, controlled mainly by their calving dynamics.

In Patagonia, it is thought that the recent variations in glacier dynamics have been triggered by climate change, but have been enhanced by calving processes, thus accounting for the high thinning and retreat rates compared with other temperate glaciated areas of the Earth.

In order to test this hypothesis, the variations experienced by a glacier with small or near absent calving activity will be analysed in detail, and compared with a degree-day factor mass balance model, forced with climatic stations and field data.

The main aim of this thesis is to analyse the mass balance of Glaciar Chico with a combined method using direct measurements from the field and ice elevation changes determined by subtracting DEMs generated from different dates. By comparing the results of this combined method with a degree-day mass balance model, it will be possible to identify and distinguish climatically driven glacier responses from those initiated by dynamics components.

1.5 Outline of thesis structure

The central background ideas contributing to this thesis have been discussed in this chapter, namely the necessity of a combined mass balance approach for glaciers in southern Chile, from where little is known in spite of recent research carried out in the region. Significant previous research related to mass balance and glacier variations has been described, emphasizing the frontal variations and ice elevation changes experienced by the glaciers of the SPI and their contribution to sea level rise. The hypothesis and aims of this thesis have also been declared.

Below is a brief description of the following chapters within the thesis.

Chapter 2: Data sets

This chapter describes the available datasets used to carry out the research, including topographic information (SRTM and previous cartography), data obtained from field campaigns (GPS data, mass balance

measurements, meteorological observations) and remotely sensed imagery, including aerial photographs and satellite images.

Chapter 3: DEM generation and errors

This chapter describes the methods employed to generate DEMs from the available datasets, their main sources of errors and the corrections applied to reduce them. These DEMs will be used in Chapter 4 to account for the ice elevation changes experienced by the glacier.

Chapter 4: Glacier characteristics and variations

This chapter includes the main results of this thesis regarding the physical characteristics, the glacial history of the region since the Little Ice Age (LIA) and the frontal, areal and ice elevation changes of Glaciar Chico. The variations of neighbouring glaciers are also included (GAEA, O'Higgins and Viedma), in order to evaluate possible relationships between their variations and those recorded for Glaciar Chico.

Chapter 5: Regional climatology

This chapter deals with the main climatological characteristics of the Patagonian region on both sides of the SPI, with emphasis on the precipitation and temperatures changes observed from instrumental data available in the region. The characteristics of the data, methods of completion of partial time-series, and methods of analysis of series are

discussed. The precipitation and temperature series of several stations, mainly on the eastern side of the SPI where Glaciar Chico is located, are analysed in detail. The results are compared with the Pacific Decadal Oscillation (PDO) index, in order to explain and contextualize the main observed changes with respect to large scale atmospheric-oceanic phenomena.

Chapter 6: Mass balance

This chapter presents a degree-day model designed for Glaciar Chico, in order to estimate the main components of the mass balance of the glacier, based upon the available direct measurements of ablation and accumulation, as well as the temperature and precipitation variations experienced by nearby stations. This model is compared with mass balance measurements obtained at the mast installed in 1996 at the base camp used during the Hielo Azul operations in the accumulation area of the glacier, as well as mass balance measurements carried out for other glaciers in Patagonia. Different future climatic scenarios are tested.

Chapter 7: Discussion, conclusions and future research

This chapter summarizes the main findings of this thesis through discussion of the key results obtained from analysis and interpretation of the glacier variations with respect to the mass balance model and the climatological data series. A proposal for future research is also presented.

2.- Data sets

2.1 Previous cartography

The southern part of South America has been cartographically mapped many times, especially the western part of the Andes, where fjords and channels were used for maritime traffic between the Americas and Europe through the Magellan Strait. Most of this historical cartography was catalogued by Martinic (1999). In some cases, this cartography can be very useful for determining the frontal position of a few glaciers (Rivera and others, 2000; Casassa and others, 1997).

In the austral summer 1944/45, the U.S.A. Air Force made the first aerial survey of the Southern Patagonia Icefield area, taking the so called TRIMETROGON flight. These photographs were used to produce the first complete "preliminary" cartography for the area at a 1:250,000 scale, including coverage of most of the SPI. Unfortunately, the topographic information is of relatively low quality, due to lack of control points on the ground.

Only a section of Glaciar Chico was covered by an initial survey by the Instituto Geográfico Militar (IGM) of Chile, based upon 1975 aerial photographs. This section is close to Lago O'Higgins, from where the IGM had logistic facilities to access the SPI and obtained a few control points on rocks in the vicinity of Glaciar Chico. Poor coverage of contour lines over the upper part of the glacier was obtained, due to a lack of stereoscopic vision

in the aerial photographs, resulting in a 1:50,000 scale cartography with contour lines every 50 m covering the lower part of the glacier and rock outcrops, but not the accumulation area of Glaciar Chico. Several spot heights are available from summits and other distinctive features in the accumulation area (Table 2.1).

With aerial photographs from 1995, the IGM made a second regular cartography at a 1:50,000 scale (Table 2.1) of almost the same area using similar photogrammetric procedures. The emphasis was on contour line coverage, in particular of those areas with poor stereoscopic vision in the 1975 aerial photographs. Most of this cartography is confidential and has not been yet published, however, the IGM allowed the author restricted access to some of the 1995 data. This cartography was controlled with GPS measurements which were added to the national geodetic network, in order to provide a high quality link between them and the contour lines generated from the aerial photographs of the SPI (IGM, personal communication).

The available regular cartography did not include all the SPI, but several glaciers were covered in both topographic charts. These common areas include both glacier accumulation and ablation zones. For Glaciar Chico, only a small area located at the frontal tongue of the glacier was covered by both surveys.

A regular cartography at 1:100,000 scale produced by IGM Argentina, based upon 1968 aerial photographs is also available. This cartography includes all the eastern portion of the SPI, including Glaciar Chico and P4G,

with 50 m contour lines. Unfortunately, the contour lines covering the western side of the SPI are very unreliable because they exhibit concentric patterns and other artefacts that are very unlikely to be real. When a DEM generated from this Argentinean cartography was compared with SRTM data, Rignot and others (2003) concluded that the error of the IGM DEM could reach 50 m. The maps are in Transverse Mercator (TM, Gauss-Krüger) projection referring to the geodetic datum of Campo Inchauspe.

Table 2.1 Regular cartography characteristics.

	1975 cartography	1995 cartography
Aerial photographs	Mc Hurd	SAF
Photograph scale	1:75,000	1:50,000
Chart scale	1:50,000	1:50,000
Datum	SAD 1969	WGS 1984
Altitude reference	Mean Sea Level	Mean Sea Level
Ground control	Many Astronomical and Doppler points measured at lower altitudes.	Many GPS points measured at lower altitudes, and a few at high altitudes across the SPI.
Contour intervals	50 m (100 m for a few areas)	50 m (25 m for a few glacier areas)
Restrictions	No	Yes

2.2 SRTM

On February 11, 2000, the U.S.A. launched the space shuttle Endeavour with the SRTM payload onboard. The mission had the aim of acquiring topographic elevation information of the Earth surface between 60 °N and

57 °S, covering approximately 80% of the Earth's land mass. These data provided the most up-to-date, complete and accurate topographic coverage of Patagonia, and covered many areas that are still unmapped by traditional photogrammetric means. SRTM data were originally acquired at a 30 m pixel size, but the declassified data in the public domain outside the U.S.A are only available at 90 m. These data cover most of the SPI, with the exception of small areas with steep slopes and southern aspects, where the interferometry procedure used in the SRTM elevation generation was unsuccessful (Figure 2.1).
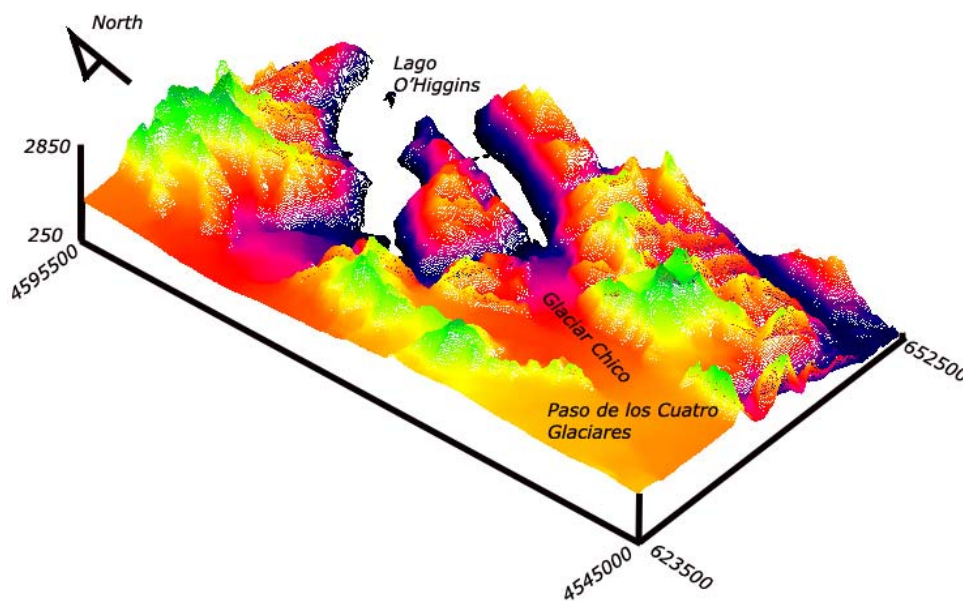
Figure 2.1 Digital Elevation Model of Glaciar Chico derived from SRTM data. UTM-18S co-ordinates and altitude in m.

2.3 Data obtained from field campaigns to Glaciar Chico

- 1996

The first campaign was carried out in the accumulation area of Glaciar Chico in January 1996, when a 13 m metal mast was buried 3 m in snow at the base camp, located at 1450 m on a flat area with a 1.4° surface slope, approximately 1 km north from the local ice divide between Glaciares Chico and Viedma. The mast was fixed with cables to wood boards buried in snow, to prevent its collapse due to strong winds. Unfortunately, only navigator quality GPS receivers were used during this campaign, therefore, the mast site was only located with a precision of 90 m. However, a basic triangulation was performed using marks placed on two rock outcrops located at the margin of the ice. From these marks the vertical and azimuth angles toward the mast were measured using a compass with inclinometer and telescope, mounted on a tripod.

A 3 m snow pit was dug at the mast location, and snow samples were collected every 20 cm vertically with a 500 cm^3 metal cylinder. Samples were weighed with a digital weight balance and analysed using a magnifying glass in order to determine ice crystal sizes. Snow temperatures were also measured every 20 cm with a digital thermometer equipped with a 5 cm probe. Snow stratigraphy was recorded for each level including the presence of ice layers, sediments, ice pipes and columns.

Discrete measurements were performed at stakes installed every 100 m along a 1 km profile located in the vicinity of the base camp. At each stake the snow height and density were measured using a stainless steel snow sampling tube Model 3600 "Federal" also called Mt. Rose, allowing estimation of densities of the snow/firn layer to a depth of 2 m.

-   1997

The second campaign was carried out in October 1997 with the base camp situated at approximately the same site as in 1996. The mast installed in 1996 was found to have been buried by a few metres and had inclined by a few degrees from the vertical.

Topographic quality Trimble Geoexplorer II GPS receivers were used to survey more than 2900 points over the glacier surface (Figure 2.2). The receivers allow single frequency data collection in coarse/acquisition (C/A) code mode with phase information, and 2 to 7 m vertical precision after applying differential correction.

One snow pit was dug to a depth of 3.8 m at the mast location. Snow densities and temperatures were measured with the same equipment and procedures used in the previous campaign. Snow stratigraphy was also observed and recorded. The snow accumulation in the 1996-1997 winter was calculated based upon the mast and snow pit measurements.

The ice thickness of Glaciar Chico was also measured along 25 profiles radiating out from the base camp in all directions of the P4G. A low frequency (2.5 MHz) RES system was used, in a profiling configuration pulled by snowmobiles and tied by mountaineering ropes. The RES measurements were collected every 2 seconds, and were geo-located using GPS receivers.

- 1998

During September and October 1998 a new Hielo Azul campaign was conducted to the same area of the P4G as in the previous two years. The base camp was again located at the site where the mast had been installed. Since the 1997 campaign, the mast had been buried a few more metres but was still visible.

The surface topography of the P4G was measured using Topcon Turbo-SII and Leica model 300 geodetic quality GPS receivers, with dual frequency and C/A code and phase information allowing 10 to 30 cm vertical precision after application of differential correction procedures.

More than 1800 points were measured over the surface of the glacier (Figure 2.2). Many of these were located along profiles similar to those measured in 1997, plus some new areas, especially at Corredor Hicken. Several 3 m long stakes made of coligües (Chilean bamboo) were installed between the base camp and the temporal snowline of Glaciar Chico (at approximately 1200 m in October). The locations of these stakes were

measured using a rapid-static procedure, allowing a minimum of 15 minutes for each measurement. The snow height variation was also recorded for each stake. Some of the stakes were re-surveyed at the end of the campaign, allowing a first estimation of ice velocities.

Several discrete snow density measurements were carried out using a Mt. Rose equipment, allowing determination of snow density in the upper 2 to 3 m snow-firn layer.

A stake network was installed at an undisturbed place close to the base camp, where snow height was measured daily. A 2 m snow pit was dug, and snow densities and temperatures were measured using the same instruments and procedures as described above.

A portable meteorological station (California Technology instruments, model TAMMS), was installed on a tripod 2 m above the snow surface. Several parameters, including air temperature, humidity and pressure, as well as wind speed and direction, were collected every 30 minutes and recorded on a battery powered data logger. The data were then transferred to a laptop computer, where they were stored and analysed.

-   2000

In October 2000, the area was visited during a new Hielo Azul operation and the base camp again installed at the site where the mast was found. Unfortunately, the weather conditions were appalling and only limited data

could be collected. The mast was measured in detail, allowing an estimation of snow height variation. A 2m snow pit was dug in the vicinity of the mast, where snow temperature, ice crystal size and snow stratigraphy were recorded.

-   2001

In October 2001 the last Hielo Azul campaign to the area was carried out. The base camp was located close to the mast, which was still visible a couple of metres above the snow surface. A snow pit was dug to a depth of 2 m at an undisturbed site in the vicinity of the base camp, where snow densities and temperatures were measured using the same 500 cm^3 cylinder described above. Geodetic quality GPS receivers (Topcon Turbo-SII and Ashtech model ZXII) were used to survey the surface topography of the area. Almost 1600 points were measured over the surface of Glaciar Chico, including several points located in similar positions to previous surveys (Figure 2.2).
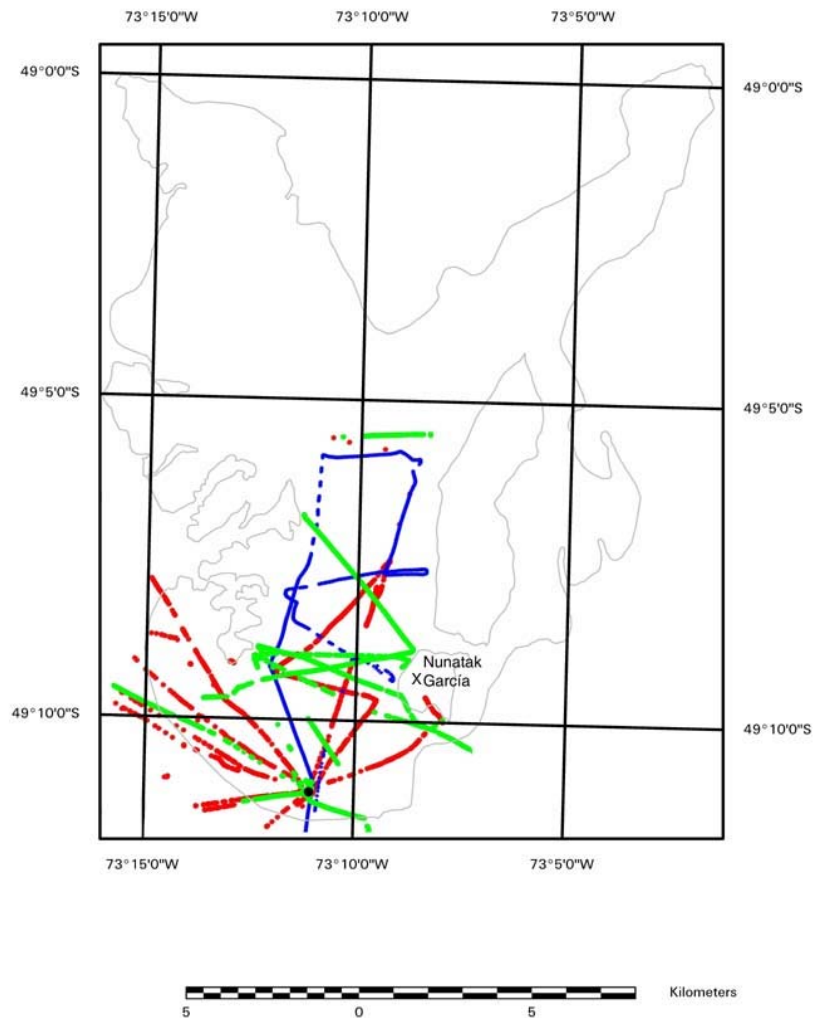
Figure 2.2   Distribution of GPS points measured in 1997 (green), 1998 (red) and 2001 (blue). The black circle illustrates the location of the base camp utilized during the campaigns. The "X" on Nunatak García shows the GCP on rock. The 2001 boundary of Glaciar Chico is in light grey.

None of the stakes installed in 1998 were found, however, 25 new stakes were installed in approximately the same positions as the 1998 stakes (Figure 2.3). The new locations were determined by navigation with topographic quality GPS receivers, and as in 1998 a rapid-static procedure was adopted allowing a minimum of 15 minutes for surveying each stake.

At each stake the snow height variation and the snow density were also measured, using a Mt. Rose equipment.

Figure 2.3 The author of this thesis measuring in September 2001 one of the stakes installed on Glaciar Chico near the ELA of the glacier, using a geodetic quality GPS receiver.

A network of stakes was installed close to the base camp, where snow height variations were measured daily. A digital thermistor, model TyniTalk, was installed 2 m above the snow surface, where it recorded air temperatures every 15 minutes over a 15 day period.

2.4 Aerial photographs

Several sets of aerial photographs from the period 1945-1997 have been used (Table 2.2). Most of the photographs were acquired in the austral summer (February-March), when the snow coverage is at its minimum extent. The date of the TRIMETROGON photographs is not available, but the one used here for Glaciar Chico, was dated by Lliboutry (1998) to be January 23 1945. TRIMETROGON has the unique ability of taking three photographs at the same time, two oblique (left and right) and one vertical.

The photographs cover most of the ablation area of Glaciar Chico, and are of sufficiently high resolution to permit a detailed analysis of the glacier features, ice fronts and surrounding rock outcrops. However, due to the image saturation generated by highly reflective snow surfaces, the accumulation areas are uniformly white and without any contrast, thus preventing stereo matching when analysed with a stereoscope.

The vertical aerial photographs of 1975, 1981 and 1997 were scanned and ortho-rectified using PCI commercial software. See Section 2.1.2 for more details. Analysis of the stereo pairs allowed interpretation of frontal and areal changes, as well as the location of the snow line at the time of image acquisition. Some of the photographs were also used for DEM generation purposes.

Table 2.2 Vertical aerial photographs.

Flight name	Nominal Scale	Date	Focal length (mm)	Type
TRIMETROGON	1:70,000	1945 January 23*	n/d	Two oblique and one vertical
Mc Hurd	1:75,000	1975 March 15	152.46	Vertical
SAF-Argentina	1:100,000	1981 January 24	87.96	Vertical
SAF-Chile	1:100,000	1995 May 26	88.09	SAF-Chile
Geotec	1:70,000	1997 March 15	153.32	Vertical

Note: * Lliboutry (1998)

2.5 Satellite images

Only a few moderate to high spatial resolution satellite images with low cloud coverage have been acquired for the SPI (Table 2.3), the majority being Landsat images covering the entirety of Glaciar Chico and most of the northern half of the SPI. However, as experienced with the aerial photographs, the main plateau of Glaciar Chico is generally saturated due to the lack of contrast across the highly reflective snow surfaces.

The oldest Landsat Multi Spectral Scanner (MSS) images from 1973 and 1976 were obtained from the Global Land Cover Facility (GLCF) of the University of Maryland. The images were provided in an ortho-rectified

format based on the satellite orbital parameters (Tucker and others, 2004).

Table 2.3 Satellite images.

Sensor	Date	Spatial resolution (m)	Azimuth angle (degrees)	Sun elevation angle (degrees)	Source
Landsat MSS	1973, September 11	57×79	61.1	44.1	GLCF
Landsat MSS	1976, February, 25	57×79	65.6	31.8	GLCF
Landsat TM	1984, December 26	28.5	68.7	47.9	USGS
Landsat TM	1986, January 14	28.5	70	44	Naruse and Aniya (1992)
Landsat ETM+	2000, October 27	28.5	50.9	44.5	USGS
Terra ASTER	2001, October 14	15	38.6	43.4	USGS
Landsat ETM+	2002, January 18	28.5	64.7	46.3	USGS

The more recent Landsat Enhanced Thematic Mapper plus (ETM+) and Thematic Mapper (TM) images were obtained from GLCF and the United States Geological Survey (USGS). These images were geo-rectified using IDRISI32 commercial software and 17 control points (CPs) obtained from

the regular cartography of the area, yielding an average horizontal error of 43 m.

The Landsat images were ortho-rectified using Erdas Imagine 8.2 commercial software. SRTM elevation data were used for this process, as well as the azimuth and sun elevation angles of each image (Table 2.3).

One Advanced Space-borne Thermal Emission and Reflection Radiometer (ASTER) satellite image (descending path, 12.5° scene orientation angle) acquired on October 14, 2001 was obtained directly from the USGS EROS Data Center. This sensor is mounted on the Terra Platform, which follows the track of the Landsat ETM+ orbit by approximately 1 hour, acquiring images in 14 spectral bands. The 0.8µm channel acquires images at both a forward and backward looking angle, which is useful for DEM generation purposes (ERSDAC, 2001).

Due to the gain values used to acquire the ASTER image (Normal), the upper accumulation area of the SPI is "saturated" (i.e. there is no variation in brightness), preventing discrimination of different snow surfaces or variations in albedo. There is, however, adequate contrast for the ablation area. The ASTER image was geo-located using 16 CPs obtained from the available regular cartography and GPS measurements, yielding a horizontal error of 15 m. PCI commercial software was used for the geo-location, ortho-rectification and DEM generation from the ASTER image (more details in Section 2.1.3).

2.6 Summary

In this chapter has been described the data sets utilised in this thesis, with emphasis in the GPS and mass balance data collected during field campaigns carried out between 1996 and 2001, as well as remotely sensed imagery, including aerial photographs acquired since 1945 and satellite images acquired since 1973.

3. DEM GENERATION AND ERRORS

3.1 DEM generation

3.1.1. DEMs from GPS data

All GPS data were collected from areas covered by snow during the field campaigns, mainly in the accumulation area of the glacier, where snowmobiles transporting the GPS receivers could move easily over snow with minimal risk of falling into crevasses (Figure 2.2). As the field campaigns were carried out between September and October (early spring), some measurements took place in the upper ablation area of the glacier, although snowmobile operation there was difficult due to the presence of wet snow and melt water.

Most of the GPS data were obtained in kinematic mode, where one receiver was installed onboard a snowmobile, collecting data every 5 seconds. A second receiver was installed simultaneously on a rock outcrop (Nunatak García, Figure 3.1) located approximately 5 km away from the base camp. The receiver was attached to a 10 cm metal pin glued into a hole drilled in the rock. This second receiver was configured as a base station, collecting data every 5 seconds. A total of 25 points were measured in 1998 and 2001, using a rapid-static procedure, where a geodetic quality GPS receiver was installed on a stake for approximately 15 minutes, collecting data every 5 seconds. All GPS data were analysed using Geogenius commercial software version 1.6, with application of a differential correction procedure.

GPS measurements were recorded in UTM 18-South co-ordinates, datum WGS-1984, EGM 1996 geoidal model. Orthometric mean sea level height was used as a reference. The majority of the GPS data points were distributed between the temporal snowline and the ice divide with Glaciar Viedma (Figure 3.1).
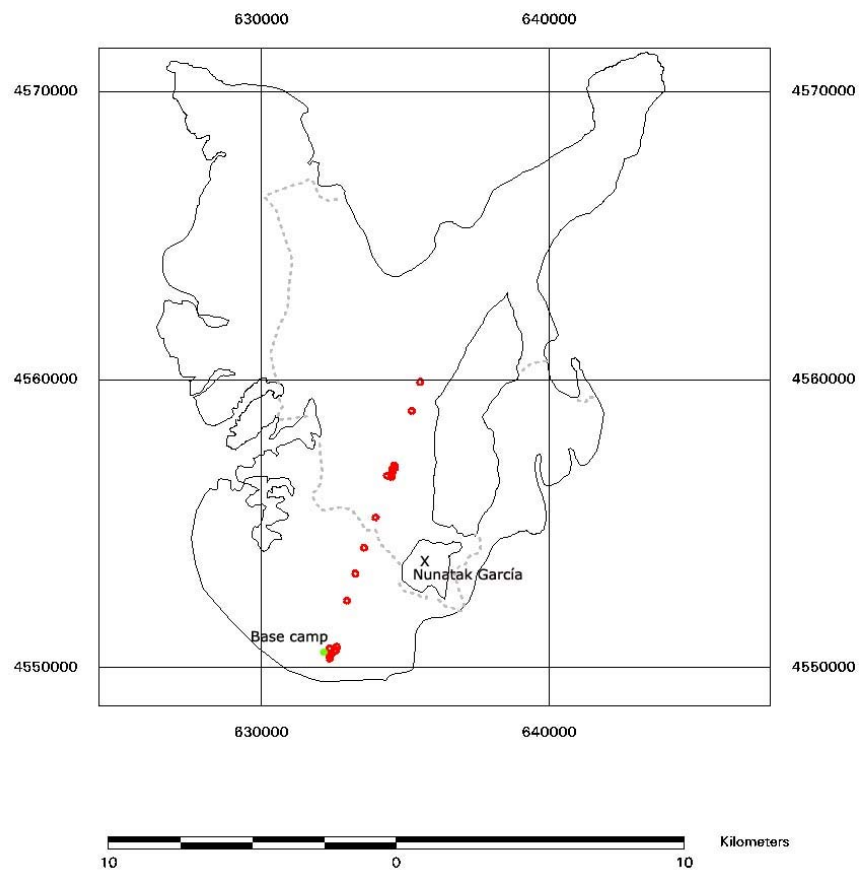
Figure 3.1 GPS measurements carried out at identical locations in 1998 and 2001 (in red). The ELA of the glacier in 2001 is shown by the grey dashed line. The "x" on Nunatak García shows the base station used in both campaigns.

3.1.2 DEMs from aerial photographs

From vertical aerial photographs (1975, 1981 and 1997), DEMs were generated using Socet Set version 4.4.0, professional digital photogrammetry software, at the University of Zurich, Switzerland. For this purpose, the photographic paper copies were scanned at 800 dpi using an EPSON expression 1640 XL scanner, resulting in a pixel resolution equivalent to 2.5 m on the ground. The calibration information of the camera (co-ordinates of the fiducial marks and the camera focal length) was used to define the internal orientation of the stereoscopic pair. Tens of tie-points were used to link together all the photographs from each date, generating a photogrammetric mosaic with relative internal orientation (known as an image block). A set of 16 ground control points (GCPs) located on rocks shown in the regular cartography, as well as from some GPS points measured in the vicinity of the glacier, were used to assign an absolute georeference to the photogrammetric pairs (known as models). These points were selected from distinguishable landmarks present in the aerial photographs, such as summits, peninsulas and geologic features.

Triangulation and bundle adjustment were calculated for each model, using GCPs and tie points, allowing;

- calculation of the position and orientation of each image at the time of photographic or image exposure
- determination of the ground coordinates of any tie points measured on the overlapping areas of multiple images

- distribution and reduction of the errors associated with the imagery, image measurements and GCPs (ERDAS, 2001).

With the bundle adjusted model it was possible to calculate the absolute orientations of the entire image block. Once the first image block was solved, the second and third blocks were adjusted to each other by using tie points obtained simultaneously from all the blocks. From the resulting oriented imagery, the photogrammetric software automatically calculated an absolute DEM for each date, at a 50 m pixel size using the WGS-1984 datum, UTM co-ordinates and mean sea level altitude reference. The 50 m pixel size was chosen to allow for possible deformations arising from the process of scanning the aerial photographs, as well as other horizontal inaccuracies introduced by the geo-location of GCPs.

The stereo-matching process was most successful for DEM creation for the ablation area of the glacier. The DEMs generated for the upper snow covered regions were incomplete, especially in the area around the mast installed in 1996 where the low contrast in the aerial photographs prevented any altitude information from being obtained (Figure 3.2).

3.1.3 DEM from ASTER image

Based upon bands 3N and 3B images from an ASTER scene acquired on October 14, 2001, a DEM was generated using PCI Geomatica commercial software at the University of Zurich, Switzerland. The same data set of GCPs used for the generation of DEMs from aerial photographs was used for

the bundle adjustment of the ASTER bands. These points were used in the absolute rectification of the model. Approximately 80 tie points were selected on the screen from all around the image, in order to ensure inter-band registration. These points were selected from rock outcrops with similar surface features, for example geologic faults, summits and vegetation, as well as ice surface characteristics like crevasses, central moraines and boulders. By using all the tie points, an epi-polar image was generated by means of rotation and resampling of the bands, from which a relative DEM was automatically extracted. This was used in combination with the GCPs in the geo-coding process to generate an absolute DEM with the WGS-1984 datum, UTM co-ordinates and mean sea level altitude reference. This resulting DEM was edited in order to eliminate areas subject to artefacts (speckle data), especially in the accumulation area of the glacier, where the lack of contrast prevented effective stereo-matching. The 50 m pixel size was chosen in order to homogenise all data for further comparisons, as well as accommodate possible horizontal displacements due to the geo-location of GCPs. The ASTER derived DEM covered most of the ablation zone of the glacier, but not the high albedo snow surface areas, where the saturation of the satellite image prevented stereo-matching. For further details on DEM generation from ASTER along-track stereo imagery see Toutin and Cheng (2001) or Hirano and others (2003).
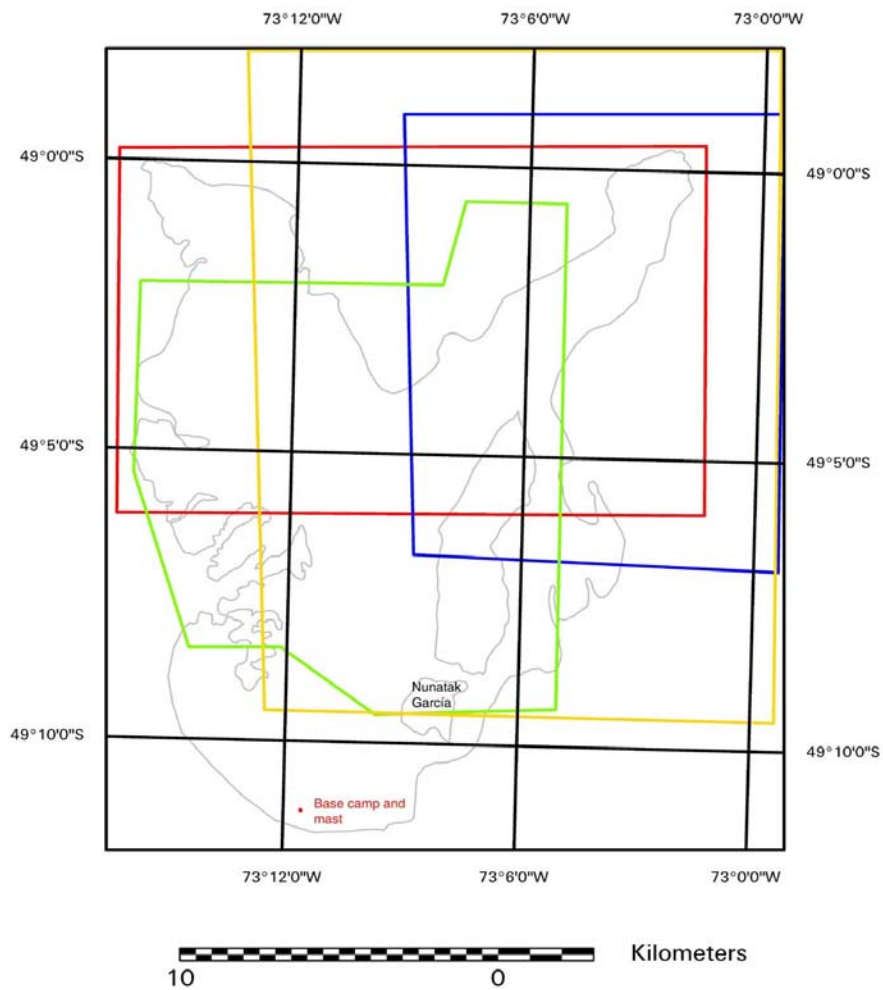
Figure 3.2 Area covered by DEM-1975 (yellow), DEM-1981 (green), DEM-1997 (blue) and ASTER-DEM (red). The boundary of Glaciar Chico in 2001 is in light grey, and the base camp used during field campaigns is shown in red.

3.1.4 DEMs from regular cartography

DEMs were generated by interpolation of contour lines digitised from the available regular cartography of 1975 and 1995 provided by the IGM Chile. Three interpolation methods were applied to a test area located at the mid-altitude region of Glaciar Chico: Inverse Distance Weighing (IDW), Triangulated Irregular Network (TIN), and TOPOGRID (a discretised thin plate spline technique available within commercial software ArcInfo version 8.0.1). In order to select the best-fit interpolation method two factors were considered; the number of artefacts presented in the resulting DEM and the time and effort of manual interaction needed to produce the DEM. Based upon these criteria, the best method proved to be TOPOGRID. This interpolation procedure did generate some artefacts at the margins of the ice (sinks), but they were much smaller and less extensive than the generalized linear and triangular artefacts obtained with the other two interpolation methods. A jack-knifing procedure (Lythe and others, 2001) was employed to account for the error added by the selected interpolation method. For that purpose two DEMs were generated and compared; one with all the available information, whilst for the second DEM only 90% of the contour lines were used. The TOPOGRID interpolation method was applied to the whole study area, with contour lines, spot heights and lakes used as topographic information inputs. A 50 m pixel size was selected, with UTM-18S co-ordinates, datum WGS-1984 and mean sea level as altitude reference.

3.1.5 DEM from SRTM data

The SRTM data obtained from JPL/NASA cover the whole SPI, with the exception of many small areas without topographic information due to their rough topography and steep slopes. At the margins of these no-data areas some spurious pixels were identified with altitude values more than 50 m lower than the surrounding pixels. The main explanation for these incorrect elevations is related to the conversion applied by JPL/NASA when reducing the original 30 m pixel size, to the 90 m resolution available in the public domain. These spurious pixels were manually detected and eliminated. Due to the different pixel size with respect to the other data sets the SRTM data was resampled to a 50 m grid size to enable reliable comparison of the different DEMs.

3.2 Errors

3.2.1 Horizontal errors

The horizontal RMS errors for the image rectification, and thus the overall position accuracy of the DEMs generated from the aerial photographs and the ASTER image, were automatically calculated by Socet Set and PCI Geomatica commercial software, yielding 6 and 15 m respectively. These horizontal errors are due to inaccuracies in the location of the GCPs employed in the DEM generation process, errors in identifying the GCPs on the imagery, possible deformations generated by scanning the photographs, or deformations of the aerial photograph edges (Table 3.1).

The horizontal error of the GPS data was calculated automatically using Geogenius commercial software, yielding on average 0.10 m for points measured with geodetic quality GPS receivers, and 4.5 m for points measured with topographic quality GPS receivers. In order to compare these data with the DEMs described above, the GPS data were transformed to a 50 m pixel raster format, and DEMs were generated for each data set. Where more than one GPS point was measured over distances of less than 50 m, an average of these points was used in the rasterization process.

The horizontal error of the DEMs generated from contour lines of the regular cartography of the IGM was calculated to be 15 m. This error is related to contour inaccuracy, datum correction, digitization of contour lines and contour line generation.

Based upon the above discussion, became clear that the horizontal errors are significantly different depending also on the origin of the data. These DEMs obtained from point measurements are much more accurate than the DEMs obtained using remote sensing techniques. In order to compare both DEM types, a pixel size of 50 m was used to cover possible discrepancies between all data sets.

In spite of the above, some data sets (i.e. SRTM) could have higher than 50 m horizontal errors due to the foot print size of the original data, which could be specially important for rough surfaces at the margins of the glaciers or near ice cliffs with significant surface slopes. Up to date, no

report in this issue is available, therefore, will be assumed that the 50 m pixel size used here will cover these possible uncertainties.

3.2.2 Vertical errors

All the GPS measurements were obtained in relatively flat areas away from high mountains, with distances between the kinematic and base measurements no greater than 10 km. Under these conditions, and considering only the lowest Precision Orbit Determination (POD) values, the resulting vertical errors were 7 m for measurements based upon the topographic quality GPS receivers, and better than 0.30 m for the geodetic quality GPS measurements.

The vertical error obtained for the image rectification from GCPs, and thus the overall vertical accuracy of the digital photogrammetric DEMs, was computed by Socet Set, yielding 6.0 m for each of the DEMs. However, when rock outcrops were compared between DEMs derived from aerial photographs from different dates, an average standard deviation of 12 m was obtained, with biases between 1.4 to 1.9 m. The errors have a normal distribution. The 12 m error is related mainly to the inaccuracies of the GCP locations obtained from the regular cartography of the IGM, and is comprised of 8.5 m error for each individual DEM, which is in good agreement with the result obtained automatically by Socet Set.

The elevations of rock outcrop areas were compared between the ASTER DEM and the aerial photograph DEMs, yielding a mean bias of 22 m and a

random error of 24 m. If the random error for the aerial photogrammetric DEMs is taken as 8.5 m, the ASTER derived DEM random error is therefore 22 m. The differences in rock area elevations were spatially distributed with respect to the slope aspect derived from the ASTER DEM, with maximum positive values on western slopes, and maximum negative values on eastern slopes (Figure 3.3). A best-fit curve was calculated to account for these differences, yielding a cosine relation. This systematic deviation is assumed to be due to the ASTER stereo geometry. Compared to the ASTER nadir channel (3N), the 3B stereo sensor is directed backwards by 27.6° from nadir. Thus, compared to the nadir image, northern slopes appear significantly shortened and southern slopes significantly stretched in the backward-looking image. Such perspective distortion could lead to the systematic errors encountered in the automatic ASTER DEM generation (Kääb, 2002).
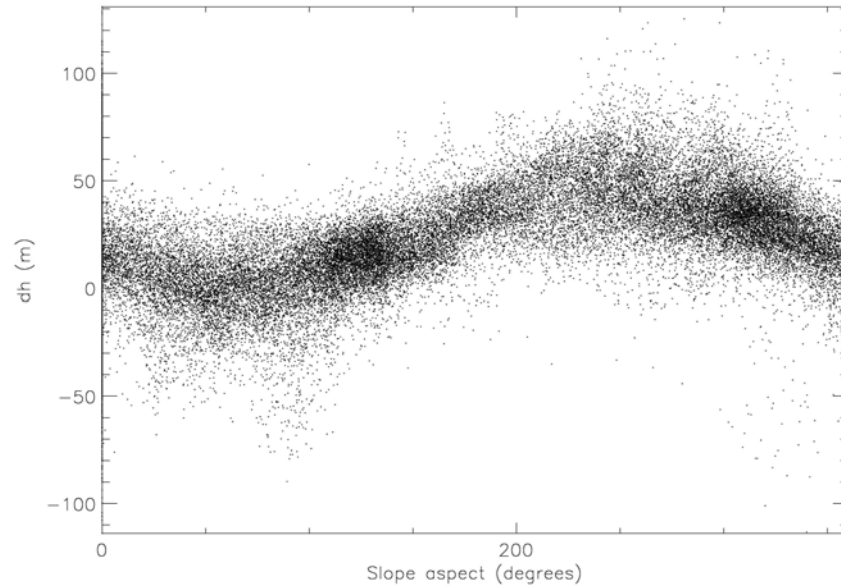
Figure 3.3 Cosine relation between slope aspects derived from the ASTER-DEM (x-axis in degrees) and differences in altitude of rock areas between the 2001 ASTER-DEM and photogrammetric DEM-1975 (y-axis in m).

The cosine relation was applied to the ASTER-DEM to produce an adjusted DEM. The rock area elevations of this adjusted DEM were compared with those of the aerial photograph DEMs, resulting in a mean error of -3.7 ± 19 m. The difference values have a normal distribution. This total random error is comprised of the RMS error of the DEMs derived from aerial photographs (8.5 m), and a final RMS error of the ASTER DEM (17 m). A similar vertical error value was also found by other studies using ASTER DEM derived topography in mountainous terrain (Kääb, 2002).

Table 3.1 Final error estimation for each data set in m.

Data sets	Horizontal error	Vertical error	
		Bias	Random
DEM-1975IGM	15	n/d	19
DEM-1975	6	<2	8.5
DEM-1981	6	<2	8.5
DEM-1995IGM	15	n/d	19
DEM-1997	6	<2	8.5
GPS-1997	4.5	<1	7
GPS-1998	0.1	0	0.30
SRTM-2000	n/d	0	7
GPS-2001	0.1	0	0.30
DEM-ASTER-2001	15	<4	17

n/d, no data

No error estimations for the regular cartography of the IGM were available, however, the regular cartography at 1:50,000 scale is considered to be of class 1 accuracy in terms of the American Society for Photogrammetry and Remote Sensing classification (Falkner, 1995). That means that this cartography is the most stringent, with vertical inaccuracies related to the contour interval possessing a vertical error of 17 m. After applying the jack-knifing procedure, it was estimated that the vertical error added by the interpolation procedure was 9 m. Therefore, the combined vertical error of each DEM generated from contour lines was 19 m.

The SRTM data were processed into continental maps, with GPS control, 7 m vertical precision, and 90 m horizontal posting (Hensley and others, 2000). A comparison of SRTM data with GPS surface reference data on Glaciar Tyndall (Raymond and others, in press) indicates local systematic vertical errors of −3 m, which is consistent with the vertical precision of SRTM, and with negligible biases arising from the penetration of radar signals into snow and ice (Rignot and others, 2001).

Based upon the above discussion, it is possible to conclude that the vertical errors are also related to the origin of the data, with more accurate figures for point data compared with DEMs generated using remote sensing techniques. These last data sets have more intrinsic uncertainties than point data (i.e. GPS data) due to the slope and aspect of the surface topography covered for a wider foot print size sensor.

3.3 Summary

This chapter has described the main methods employed for generation of DEMs for Glaciar Chico based upon different data types. An error assessment has also been carried out, determining the main sources and magnitudes of errors for each model, typically in the range of 0.1 to 15 m horizontally, and 1 to 20 m in the vertical direction. These errors could be considered very high for many purposes, however, the resulting DEMs are sufficiently precise and accurate to allow detailed assessment of the location of geomorphological features and ice elevation changes that will be discussed in Chapter 4.

4. GLACIER CHICO CHARACTERISTICS AND VARIATIONS

4.1 Glacier basin, hypsometry and ELA

4.1.1. Glacier Basin

A previous study by Aniya and others (1996) defined a total ice area of between 243 and 306 km^2 for Glaciar Chico. This large uncertainty was mainly due to difficulties in defining the ice divide at Paso de Los Cuatro Glaciares between Glaciares Chico and Viedma (arising from a lack of regular cartography). Until 2000, the only available topography of the area was generated from GPS points measured in 1997 and 1998, and with these points it was possible to only partially draw the outline of the glacier in the area. Using SRTM data and satellite images of Glaciar Chico it is now possible to delineate the basin of Glaciar Chico more accurately, yielding a total ice area of 192.6 ± 5.3 km^2 in 2001.

The accumulation area of the glacier can be divided into three sub-basins or tributaries; Pirámide (red in Figure 4.1) located between Cordón Pirámide and the ice divide with Glaciar GAEA (labelled A, in Figure 4.1); Hicken (green in Figure 4.1), located to the south where an ice divide separates this glacier from Glaciar Viedma (labelled B in Figure 4.1) and Gorra Blanca (light blue in figure 4.1).

Most of the basin outlines are easily determined when rock outcrops are present, however, there are three ice divides which are more difficult to

define without a full coverage of ice velocities. These are labelled A, B and C in figure 4.1.

Ice divide A is located at 1425 m asl between Glaciares GAEA and Chico, where it is well constrained by the surface topography. Ice divide C is located between Glaciares Chico and Marconi at 1525 m asl, and it too is well constrained by the surface topography.

Ice divide B is located between Glaciares Chico and Viedma, with an altitude range of between 1450 and 1500 m at Corredor Hicken. The eastern portion of the ice divide is well constrained by the surface topography at the lower elevations, and ice velocities determined at the mast installed in 1996 (X in Figure 4.1) corroborate that the ice is flowing toward the north. However, the western, higher altitude portion of this ice divide is more difficult to define without ice velocities, and its location has been determined based only upon ice flow stripes identified on the available satellite images, together with the surface topography of the area.
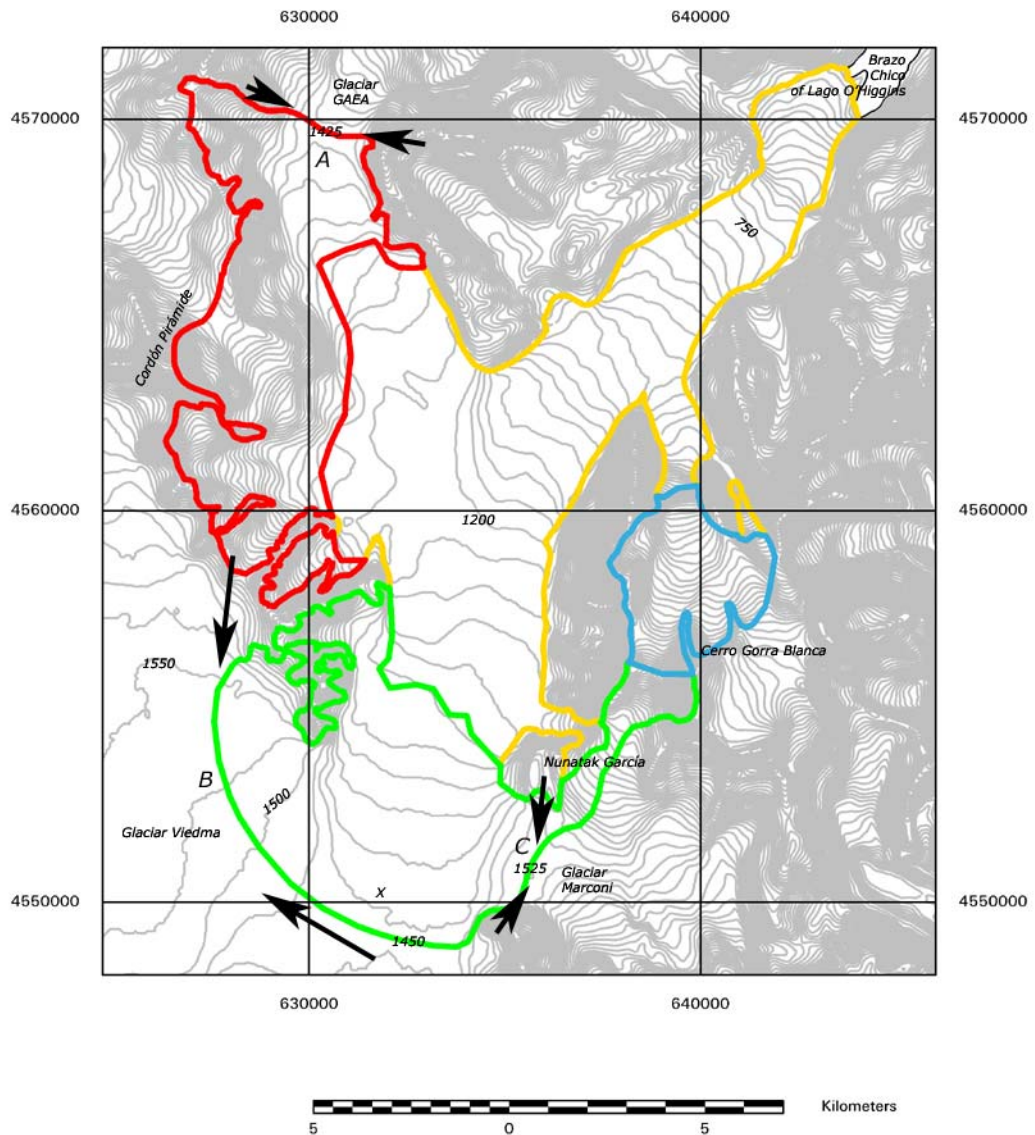
Figure 4.1 SRTM derived contour lines (grey), and the main sub-basins of the glacier; Pirámide (red), Hicken (green) and Gorra Blanca (blue). The arrows show the ice divides where the basin margin is more uncertain. The outline of the ablation area in 2001 is shown in yellow. The mast where ice velocities are available between 1998 and 2001 is labelled "X". UTM-18S co-ordinates in m, WGS 1984.

4.1.2. Hypsometry

The hypsometry of Glaciar Chico was generated from SRTM data collected in 2000 (Figure 4.2), based on a total glacier area of ~193 km^2 (calculated for 2001). This hypsometry shows three distinctive sections; one below 1100 m, where the glacier is steep and is flowing in a narrow valley toward Brazo Chico of Lago O'Higgins; a plateau area with altitudes between 1100 and 1500 m, within which the ELA is located; and a section with altitudes above 1500 m, composed of several steep valleys feeding the main tongue of the glacier, from a maximum altitude of 2810 m at Cerro Gorra Blanca.
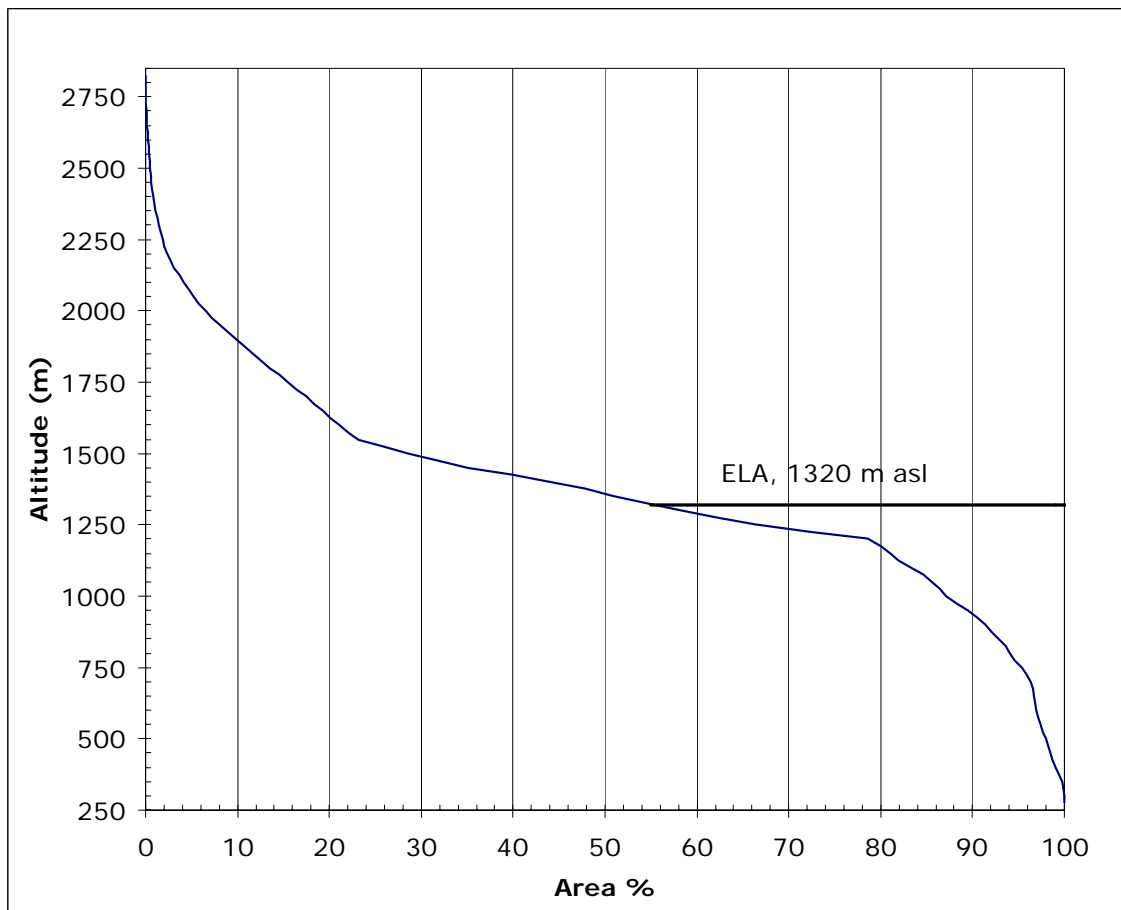
Figure 4.2 Hypsometry curve of Glaciar Chico, based upon SRTM data, showing the estimated ELA in 2001.

4.1.3. ELA

No direct measurements of the position of the ELA for Glaciar Chico are available. One approach to estimating the ELA position is to assume that in Patagonia the snow line in March, at the end of the Southern Hemisphere summer, corresponds to the ELA. This assumption is supported by the fact that temperate ice conditions prevailing across the SPI do not allow the formation of superimposed ice (Warren and Sugden, 1993). The temperate conditions have been widely described for all Patagonian glaciers (Casassa and others, 2002), where ablation is the predominant mass loss process, which is generating huge amounts of melt water in all the ablation areas and also at the lower end of the accumulation areas, where water tables have also been detected up to 1900 m a.s.l. (Shiraiwa and others, 2002). These temperate ice conditions suggest that the ELA has fluctuated widely over time, with the possibility of late summer (or early autumn) snow storms significantly affecting the altitude of the snowline. Such a high degree of uncertainty in its position precludes a precise determination of the ELA from remotely sensed imagery. However, considering the lack of alternative data, the available late summer satellite imagery provides the most reliable method of determining the position of the snowline, and therefore estimating the average ELA, and will be used henceforth.

The first expedition of Kölliker and others (1917), in March 1916, crossed Glaciar Viedma from the eastern margin of the SPI to the northern foot of Cordón Mariano Moreno, approximately 10 km south of the actual ice divide between Glaciares Chico and Viedma. In their book, the explorers described

the glacier surface in detail, locating crevasses which they needed to navigate on their way up the glacier. After leaving Camp VI, at approximately 1300 m asl, they reached snow surfaces and experienced no further trouble with crevasses. This first reference to the snowline of the area can be interpreted as a first approximation of the ELA in Paso de Los Cuatro Glaciares. This historic record indicates an ELA in a place and altitude very similar to the present ELA position of 1250 m asl according to Aniya and others (1996).

Interpretations of the transient snow line from satellite images and aerial photographs are shown in Figure 4.3. These images were acquired between January and March of the respective year (see Tables 2.2 and 2.3 for details), and represent the summer variations in the snow conditions of the glacier. None of the available images were collected at the "nominal" end of the summer at the end of March (Escobar and others, 1992), and therefore, an average value will be assumed based upon the distribution of all the available data.

The spatial distribution of the snow lines shows a horizontal displacement of approximately 2 km between 1945 and 2002. This horizontal displacement has taken place at the confluence of the two main tributaries (Chico and Pirámide, shown in Figure 4.3), where the glacier has a flat surface with slopes of less than 3°, and an altitude range of between 1250 and 1350 m asl. This displacement does not necessarily represent a consistent temporal trend.
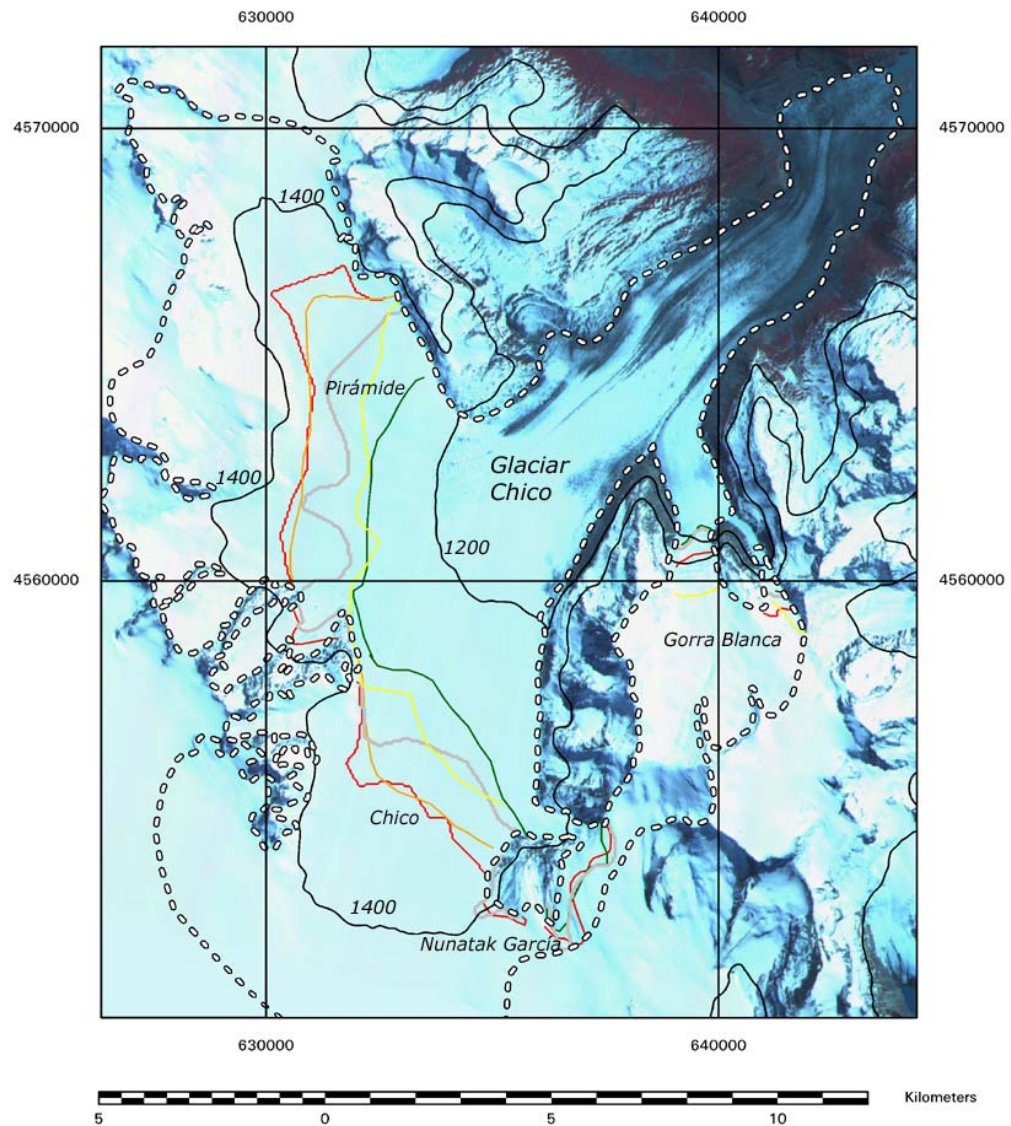
Figure 4.3 ASTER satellite image colour composite (Bands 1, 2 and 3N), showing the snowline estimated for January 1945 (green), March 1975 (grey), January 1981 (red), January 1986 (yellow) and January 2002 (orange). The outline of the glacier in 2001 is shown in dotted white. Contour lines extracted from SRTM data are shown in black (1200 and 1400 m asl). UTM-18S co-ordinates in m, WGS 1984.

In areas where the glacier is more steeply sloping, the snow line was located at higher altitudes, especially around Nunatak García, and at the ice tongue flowing from Cerro Gorra Blanca (Figure 4.3).

Due to the timing of the available data, the snow lines can potentially still move further up the glacier by the end of March. In this sense, the altitude of the snow line obtained from the 1981 aerial photograph could represent an average ELA of the glacier, because it represents the maximum altitude of the snow line from the available observations. The austral summer 1980/1981 was not particularly dry or warm in Patagonia, therefore the snow conditions are presumably representative of a long term average.

The average altitude of the ELA based upon the 1981 snow line is 1320 m asl. This value is mainly controlled by the altitude of the ELA in two of the main tributaries (Chico and Pirámide, Figure 4.3). Based on the more recent SRTM data, the average ELA is only 130 m below the ice divide between Glaciares Chico and Viedma.

From the hypsometry of the glacier shown in Figure 4.2, and assuming that the ELA is located at an average of 1320 m asl, the Accumulation Area Ratio (AAR) of the glacier was calculated to be 55%.

4.2 Glacier variations

4.2.1. General procedure

The frontal and areal variations of Glaciar Chico have been obtained by comparing geo-located and ortho-rectified satellite images (Table 2.3) acquired since 1973. Two classification procedures were applied to account for the glacier extent in each image:

- Colour composite images were produced from Landsat TM and ETM+ bands 1, 4 and 5, with a histogram-equalised stretch; the same procedure was applied to Landsat MSS images, using bands 1, 2 and 3. For ASTER images, the colour composite was generated from bands 1, 2 and 3Nadir.

- Histogram analysis of the ratio of band 4 to band 5 for the Landsat TM and ETM+ images (Paul and others, 2002) was used to classify the study area, in terms of glacier extent, ice-free areas and lakes. To reduce the large number of small pixel areas (speckled noise) unconnected with the main units generated by the histogram analysis, a mode filter was applied.

One set of oblique TRIMETROGON aerial photographs obtained in January 1945 (Table 2.2) was manually interpreted in order to map the approximate position of the glacier at that time.

Ortho-rectified vertical aerial photographs (1975, 1981 and 1997), created during the DEM generation process, were manually analysed on screen, in

order to determine the glacier extent at each date. This analysis was validated by creating a map from the original paper copies of the photographs with a mirror stereoscope (Old Delft Scanning Stereoscope, model ODSS III).

All the datasets were input to a Geographical Information System (GIS) database designed in Idrisi32 commercial software, in order to compare changes in the glacier characteristics over time.

The extent of glacier variations during the late Holocene was revealed by mapping, interpreting and comparing geomorphological features recognizable from the ortho-rectified aerial photographs and remotely sensed satellite images in the region around Glaciar Chico. These features were added to the GIS database, allowing comparison of modern with historic glacier limits. Some of these geomorphological features were also mapped during field campaigns carried out to the area, which were latterly compared with interpretation of remotely sensed imagery.

4.2.2. Variations since the Little Ice Age (LIA)

4.2.2.1. Antecedents

The Quaternary Glaciations of Patagonia were systematised and primarily studied by Caldenius (1932), who, between 1925 and 1928, travelled through the Argentinean and Chilean Pampas, mapping four major moraine systems. These were named in a format analogous to the Swedish system;

Initioglacial, Daniglacial, Gotiglacial and Finiglacial. This last advance was associated with the Northern Hemisphere Younger Dryas cooling period (between 11000 and 10000 years BP), and was subsequently dated by Mercer and Sutter (1982). More recently, the Finiglacial moraine system in the area of Lago O'Higgins/San Martín has been divided in different glacier advances, ranging from 13190 years BP representing the minimum age of the oldest Late Glacial advance moraine system, to 9300 to 9500 years BP signifying the youngest Late Glacial ice advance (Wenzens, 2002).

During the Early-Mid Holocene (10000 to 5000 BP), Wenzens (1999) detected small advances of glaciers located in valleys between Lago Viedma and Lago Argentino, first between 8000 and 7000 BP, and again between 5800 and 5500 BP. These findings concur with Clapperton (1983), who suggested cold climatic spells at ca. 7500 BP, shortly before 6050 BP, and 6000 to 5000 BP. Most of the glacier advances in this period have been considered relatively small, implying that the glaciers were similar in size, or smaller, when compared with those of the present day (Clapperton and Sugden, 1988)

Glacier variations during the Late Holocene were primarily dated and named by Mercer (1965, 1968, 1970), who distinguished three main moraine systems; Neoglaciation I (4500-4000 BP), II (2700-2000 BP), and III (1600-1900 AD, also known as the Little Ice Age, LIA (Grove, 1988)). Neoglaciation has been defined as a geologic-climate unit, rather than a time-stratigraphic unit (Porter, 2000). Clapperton and Sugden (1988) systematize four advances for the Andes Cordillera; Neoglacial I (5000 to

4000 BP), Neoglacial II (3000 to 2000 BP), Neoglacial III (1300 to 1000 BP) and Neoglacial IV (1200 to 1900 AD). This nomenclature has become standard in Patagonia (Aniya and Naruse, 1999). However, Aniya (1995 and 1996) identified four moraine systems based upon dates obtained from moraines located at the eastern margins of Glaciares Upsala, Ameghino and Tyndall; Neoglaciation I (3600 BP), II (2200 BP), III (1600-900 BP) and IV (Little Ice Age, 1600-1900 AD). More recent studies, have increased the number of Neoglaciations up to seven events, the last one being the Little Ice Age (LIA) between 1600 and 1900 AD (Strelin and others, 2002).

In spite of different Holocene advance records for each Patagonian glacier, some synchronicity can be observed. Most of the glacier records show a similar initiation and duration period during the LIA, with a maximum glacier advance during the seventeenth through early twentieth centuries (Luckman and Villalba, 2001). Since the end of the LIA (late 19th Century), most of the Patagonian glaciers have been retreating, with the exception of a few "anomalous" calving glaciers, like Pío XI (Warren and Rivera, 1994).

In the earliest historical records of explorers visiting Patagonian glaciers, as well as in the oldest aerial photographs of the area (1945, Table 2.2), the frontal positions of the glaciers were located very close to, or within a couple of km of, the LIA moraines. This provides further evidence of a small but consistent retreat since the late 19th Century (Aniya, 1995; Casassa and others, 1997; Winchester and others, 2001; Harrison and Winchester, 1998; Marden and Clapperton, 1995; Mercer, 1970).

In the region of Lago O'Higgins, Röthlisberger (1987) detected advances of Glaciar O'Higgins between 6020 and 4675 years BP (see Porter (2000) for a critique of this youngest date) and between 3600 to 3300 years BP. He also analysed nearby Glaciar Huemul, called Mellizo Norte by Aniya and others (1996), located at the eastern margin of the SPI, close to Lago O'Higgins (42 km to the north of the frontal tongue of Glaciar Chico). In this area Röthlisberger (1987) detected four glacier advances, which were dated by means of C14; between 2700 and 2200 BP; 1300 and 1000 BP; 900 and 500 BP, and between 1600 to 1900 AD.

4.2.2.2 Methods

As part of this study, several geomorphological features formed by the glaciers in the area of Lago O'Higgins have been analysed. These features have been manually mapped from aerial photographs (vertical and oblique) as well as from high resolution satellite images, in order to estimate the volumetric changes experienced by the glaciers over recent centuries. This methodology has been widely used to re-construct the extension of glaciations in the Alps (Maisch, 2000), Scandinavia (Haakensen, 1986) and Southern Chile (Clapperton, 1993).

The main geomorphological features identified around Glaciar Chico are:

- Terminal moraines: Prominent cross-valley single or multiple ridges with positive relief. Push moraines have been generated by advances of the glacier, mainly in the lateral valleys, where marginal ice tongues

deposited moraine arcs during several advances. These features are broadly arcuate with winding shapes. At the frontal tongue of the glacier, only the oldest terminal moraines are preserved, the youngest system is probably submerged in Brazo Chico of Lago O'Higgins.

• Lateral moraines: Elongated features that can be identified around most of the glacier, with the exception of the accumulation area. They are generated by the accumulation of morainic material at the margin of the glacier during states of advance or thickening. Generally, when the bedrock is not very rough, these features are ridges with steep sides. In having such steep walls, they are similar to kame terraces, and without direct observations, the two are difficult to distinguish.

• Trim lines: sub-horizontal lines on valley sides separating areas of non-vegetated and vegetated land, or areas covered by different types of vegetation. These features are generally generated following recession of the ice from a stable position, above which vegetation grew for some time. The trim line is associated with a fringe of material abandoned by the ice due to thinning and retreat.

• Kame terraces: Stratified glacial drift deposited between the glacier and adjacent steep valley walls. When the glacier experiences thinning, this material can collapse together with the ice, but it will often partially remain as a terrace along the valley walls.

• Lacustrine features: As lateral valleys are blocked by the glacier, the ice acts as a dam, generating lateral proglacial lakes where fluvial sediments are deposited as laminated layers which can form deltas and terraces along the lake shore lines. After the ice has disappeared or its elevation reduced due to thinning and retreat, former lake shores can be

distinguished as linear features following contour lines, indicating different lake levels.

- Sandurs/fluvial sediments: Some of the lateral valleys are non-glaciated, and therefore contain fluvial sediments, which are commonly dissected by braided stream patterns. At the down-valley side of some terminal moraines, is also possible to distinguish sandurs, or outwash plains, where former glaciers drained and deposited fluvio-glacio lacustrine sediments.

4.2.2.3 Main systems identified around Glaciar Chico

Four independent systems, formed at different times in the region around Glaciar Chico, can be identified according to their characteristic geomorphological features.

System 1

The oldest identified system is composed of a terminal moraine arc and associated sandur, and together they form a peninsula separating Brazo Chico of Lago O'Higgins from main Lago O'Higgins, at 250 m asl. The peninsula (1.2×1.6 km) is bisected through its western margin by a river which connects the Brazo Chico arm with the main lake. The moraines are located along the southern side of the peninsula, and are covered with Lenga trees (*Nothofagus pumilio*). The moraine arc is located 8.5 km to the north of the 1945 position of the glacier. This terminal moraine system is connected to Glaciar Chico by lateral moraines identifiable along the

densely vegetated flanks of the narrow valley, whose bottom is now occupied by Brazo Chico of Lago O'Higgins.

When this system was generated, it is probable that Glaciares Chico and GAEA were connected along "Valle Escondido", a West-East narrow, and presently ice-free, steep valley. Where Glaciar GAEA joined Glaciar Chico in the middle of the valley a common moraine belt was deposited. At that time, Glaciar O'Higgins flowed to the north, occupying the entire bottom of the valley (one arm of the lake), as far as a present day small island in the centre of the lake.

At higher altitudes, small valleys ("B", "D" and "E" in Figure 4.4) were almost completely ice filled by mountain glaciers which fed Glaciar Chico. In valley "A", a separate terminal moraine belt was identified, which was presumably generated at the same time as the "Península" terminal moraine as they are the oldest moraines in their respective valleys. In valley "C", Glaciar Chico deposited a terminal moraine arc.

This oldest system probably represents the maximum Holocene advance of the glacier, and could be assigned to the Neoglacial IV stage of Strelin and others (2002), dated between 2700 and 2000 years BP by Röthlisberger (1987). This assumption is supported by Clapperton (1993) who estimated that maximum advances along the eastern side of the SPI took place at that time. However, further samples from this moraine are necessary to date it by means of c14, dendrochronology or lichenometry.

System 2

This system is not well represented in the study area. No terminal moraine system is evident around the lake, and the lateral moraines are only partially visible at the eastern margin of Brazo Chico of Lago O'Higgins and at the mid-altitude western margin of the glacier. It is likely that in this period, Glaciares GAEA and Chico were disconnected at Valle Escondido as a moraine arc was identified at the bottom of the valley, where both glaciers were separated by a few kilometres.

Terminal moraines of Glaciar Chico were detected in the lateral valleys "A", "C" and "E", whilst in valleys "D" and "B" lateral moraines on the northern flanks were identified, which are presumably in synchronicity with the advance described for Glaciar Chico.
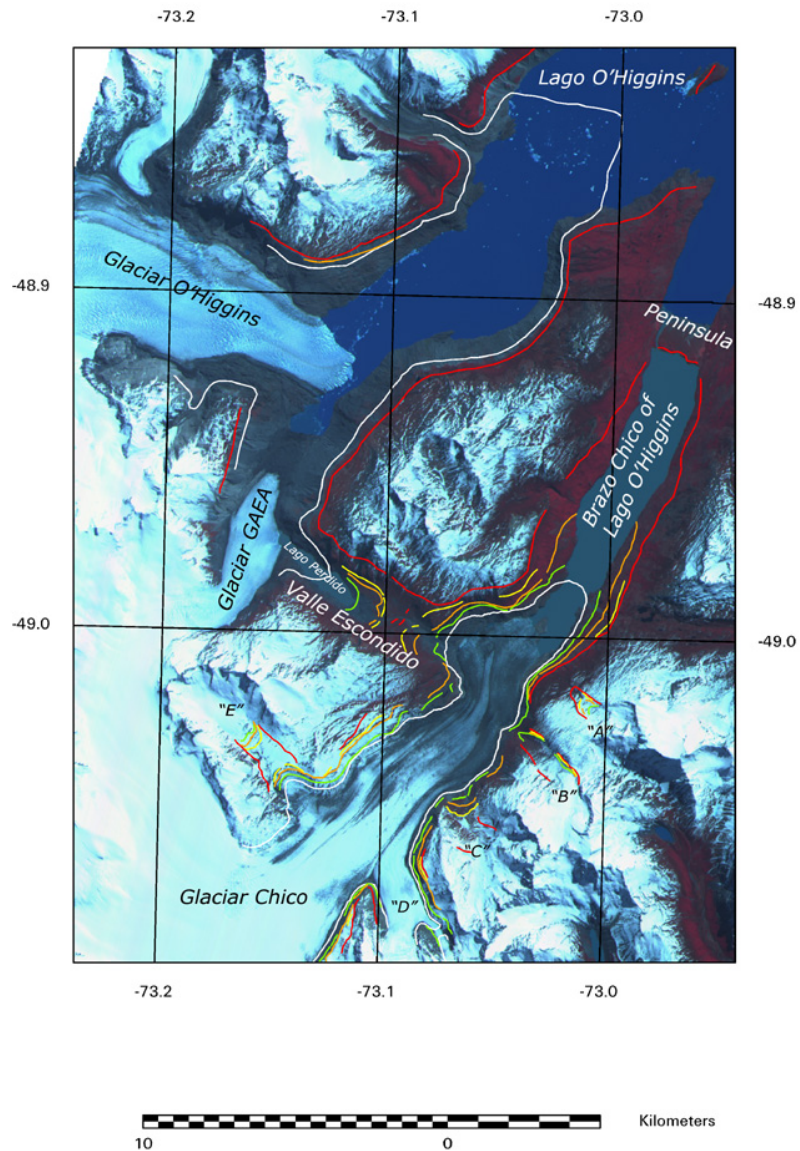
Figure 4.4 Colour composite bands 1, 2 and 3N of an ASTER satellite image acquired on October 14, 2001. The four geomorphological systems described in the text are represented in red (system 1), yellow (2), orange (3) and green (4). The outlines of the glaciers in 1945 are shown in white.

System 3

This system is well represented all around Glaciar Chico, as shown by lateral moraines and trim lines, especially along the eastern margin of the

glacier front. These linear features end at the shore of Brazo Chico of Lago O'Higgins, 2.5 km to the north of the 1945 frontal position of the glacier. No terminal moraines were detected at this site, but it is possible that some underwater depositions have been preserved. To corroborate this assumption it would be necessary to conduct a bathymetry campaign.

At Valle Escondido, two well preserved push moraines were detected, one generated by Glaciar Chico and the second from Glaciar GAEA, which flowed into the valley, but did not join Glaciar Chico. In between the two moraines, fluvio-lacustrine sediments were deposited, indicating that the area was probably partly occupied by a proglacial lake.

A prominent and well preserved lateral kame terrace was detected in valley "D", indicating an ice thinning of approximately 200 m with respect to the present elevation of the glacier in that valley.

In valley "E" (Figure 4.5 and 4.6), two well developed push moraines were detected, one generated from a lateral ice flow of Glaciar Chico, and the second one formed by the mountain glacier flowing from the west. Between both moraine arcs, lacustrine and fluvio-glacial sediments were deposited, indicating that the area was ice free and probably occupied by a proglacial lake. The top of the moraine ridge at the margin of Glaciar Chico in valley "E" was approximately 200 m above the present surface of the glacier.
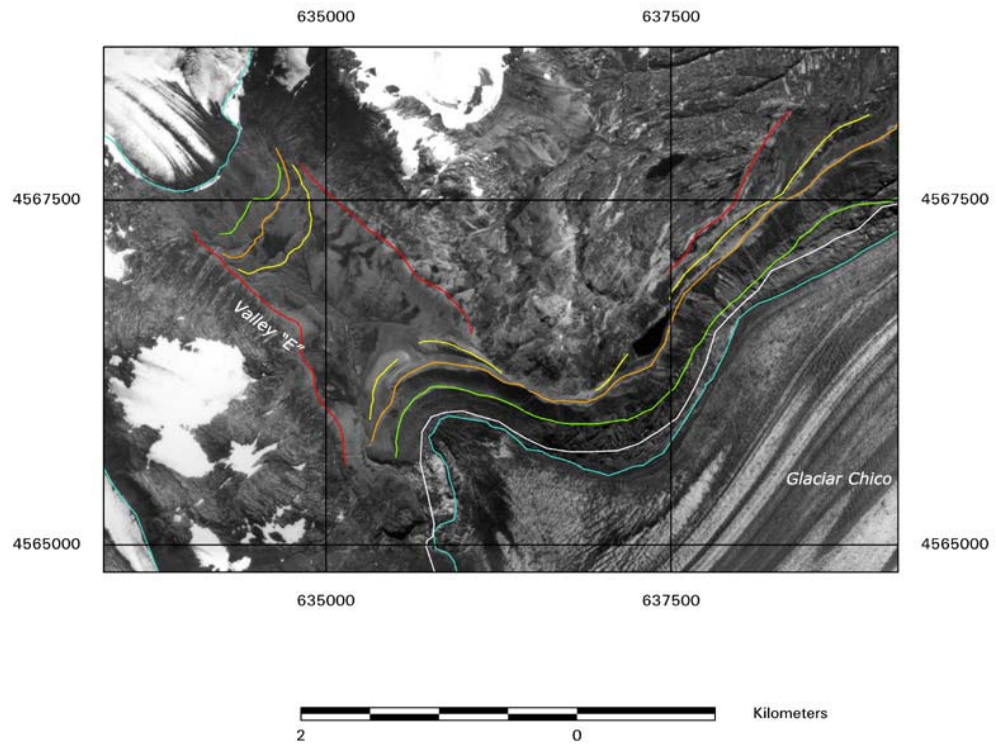
Figure 4.5 Ortho-rectified aerial photographs from 1975, showing details of the geomorphological systems in valley "E". The systems are shown in red (system 1), yellow (2), orange (3) and green (4). The outline of the glaciers are shown in white (1945 position) and blue (1975 position). UTM-18S co-ordinates in m, WGS 1984.
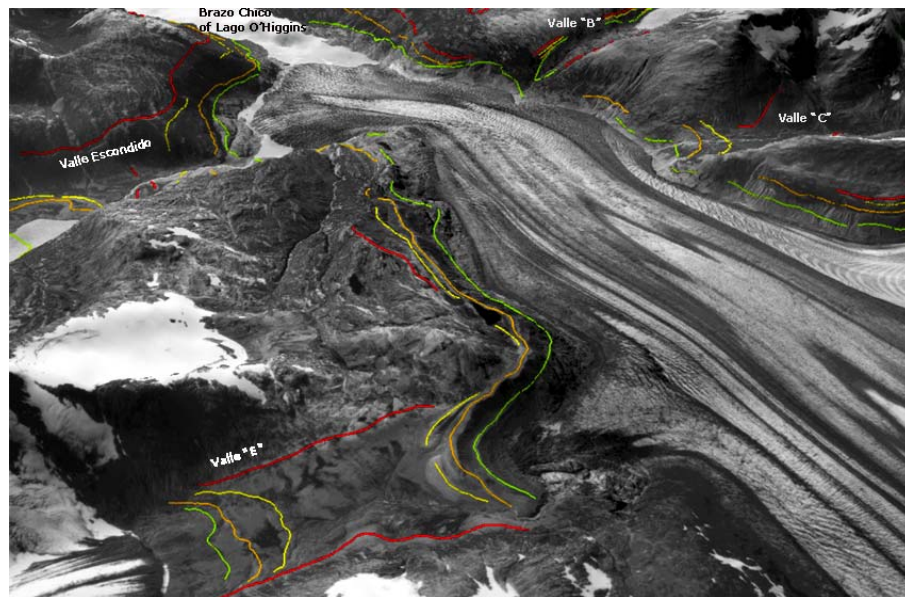
Figure 4.6 3D view of Glaciar Chico based upon DEM-1975 and the aerial photograph of 1975. The geomorphological systems are shown in red (1), yellow (2), orange (3) and green (4).

System 4

This youngest system is mainly represented by a clear trim line visible all around the glacier, as well as some push moraines in the lateral valleys. No terminal moraine was detected at the terminus of the glacier, however, underwater deposition is likely. The lateral moraines and trim line end at the shores of Brazo Chico of Lago O'Higgins, between 500 and 1000 m north of the 1945 glacier front.

At Valle Escondido, two well preserved push moraines were identified, one from Glaciar Chico and the other from Glaciar GAEA. In between, lacustrine and fluvio-glacial sediments were deposited.

In the lateral valleys "A" and "B", push moraines were identified, generated by the advance of the mountain glaciers, and presumably synchronous with the variations of Glaciar Chico. In valley "E", a push moraine formed by an advance of Glaciar Chico was detected a few tens of meters below the previous moraine arc of system 3. The mountain glacier of valley "E" generated a small push moraine, which is also presumed to be synchronous with the last advance of Glaciar Chico.

4.2.2.4 Deglaciation until 1945

Between the last advance of Glaciar Chico (System 4) and 1945, the glacier retreated along all its margins, especially at the glacier front where retreat reached a maximum of -10 m a^{-1}. This process is evident by a trim line that was already visible in 1945.

The frontal tongue of Glaciar Chico in 1945 could be divided into three parts (Figure 4.7). The main one was calving into Brazo Chico of Lago O'Higgins at an altitude of 250 m asl. The second part was calving into a proglacial lake generated at the western end of the glacier in Valle Escondido. The third part, located between the other two sections, where the ice was being forced against the opposite mountain flank, represented the divide between the ice that was deflected towards the north (to the main calving front) and that which flowed to the west through Valle Escondido. In the 1945 aerial photograph it is evident that the Glaciar Chico front at Valle Escondido occasionally experienced dry calving activity, due to the drainage of the proglacial lake into Brazo Chico of Lago O'Higgins.

Between the beginning of the glacier retreat from system 4 and 1945, Glaciar GAEA receded approximately 2 km, leaving a proglacial lake (Lago Perdido), at the bottom of Valle Escondido. This lake was dammed by the push moraine arcs left by the glacier during previous advances. By 1945, Lago Perdido was draining towards the proglacial lake of the western front of Glaciar Chico, and then it was presumably draining subglacially to Brazo Chico of Lago O'Higgins.
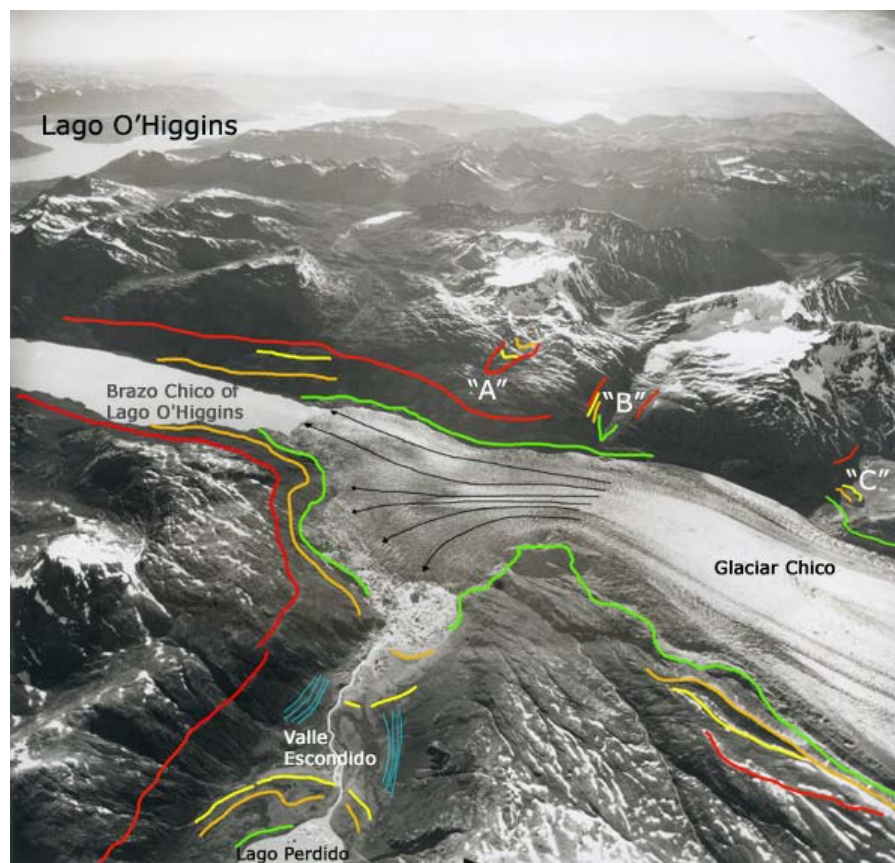
Figure 4.7 Oblique TRIMETROGON aerial photograph acquired on January 23, 1945. The geomorphological systems are shown in red (1), yellow (2), orange (3) and green (4). Paleo shore lake lines are shown in blue. The main flow lines of the glacier are shown in black. Notice the deflected ash bands on the surface of the ice.

4.2.2.5 Discussion of a possible chronology for the LIA

Due to the lack of C14, dendrochronology or lichenometry data from the area around Glaciar Chico, it was not possible to date absolutely the four systems described above. In order to achieve precise dating, new data must be collected from the main moraines, and subjected to analysis. However, a common timing for the last glacier advance in Patagonia has been widely described, and both of the chronologies obtained in the Glaciar Chico region; from Glaciar Huemul (Mellizo Sur in Figure 1.3) by Röthlisberger (1987), and from Glaciar Piedras Blancas (49.20°S, Figure 1.3) obtained by Delgado and others (2002), yielded similar dates for the LIA advances of 1600-1900 AD.

For Glaciar Piedras Blancas, the closest of these two chronologies to Glaciar Chico, the external LIA moraine was dated using dendrochronology by Delgado and others (2002) to between 1640 and 1670 AD. Moreover, the internal moraine, identified with the beginning of the glacier retreat, was dated between 1820 and 1850 AD.

The accuracy of these chronologies could be affected by the presence of material from the active Volcán Lautaro, nevertheless, the LIA advance of Glaciar Piedras Blancas can be used as an analogy for Glaciar Chico, as this glacier is also subject to possible volcanic influences. This deduction is corroborated by the presence of deflected ash bands on its surface (Figure 4.7), which were linked to Volcán Lautaro by Lliboutry (1998).

Initial glacier retreat following the LIA took place during the second half of the 19th Century for most of the glaciers of the NPI and SPI (Marden and Clapperton, 1995; Harrison and Winchester, 2000; Winchester and Harrison, 2000). Therefore, it is realistic to presume that the last advance of Glaciar Chico was synchronous with the LIA advance experienced by the Patagonian glaciers between 1600 and 1900 AD. If this assumption is proven to be true, Glaciar Chico must have begun to retreat in synchronicity with Glaciar Piedras Blancas at around 1850 AD.

4.2.3 Frontal variations between 1945 and 1975

No aerial photographs are available from the period between 1945 and 1975. However, this latter set of photographs (Table 2.2) showed a small retreat around the non-calving terminus since 1945, and more significant changes at the calving front. One of the main changes shown in the aerial photographs of 1975 to be affecting the dynamics of the calving front of the glacier was the appearance of a small island ("La Isla") located at the northeast calving front, in the middle of the Brazo Chico of Lago O'Higgins. This island divided the calving front of the tongue into two small sections flowing either side of "La Isla" (Figure 4.8).

The rate of frontal change of the glacier between 1945 and 1975 was at a maximum at the calving tongue which retreated at rates of between -50 to -60 m a^{-1}.

Apart from a couple of declassified satellite images (Corona) acquired during the 1960s, the oldest satellite image available for the study area was acquired by the Landsat MSS sensor in 1973 (Table 2.2). At this time the frontal position of the glacier was in a very similar position to that shown by the 1975 aerial photograph, but due to the low spatial resolution of the Landsat MSS scene, it was not possible to determine any significant variations.

Other glacier margins retreated at low rates, especially around "Nunatak García" and the glacier tongue flowing to the north from Cerro Gorra Blanca, where a lagoon was first observed in 1945.
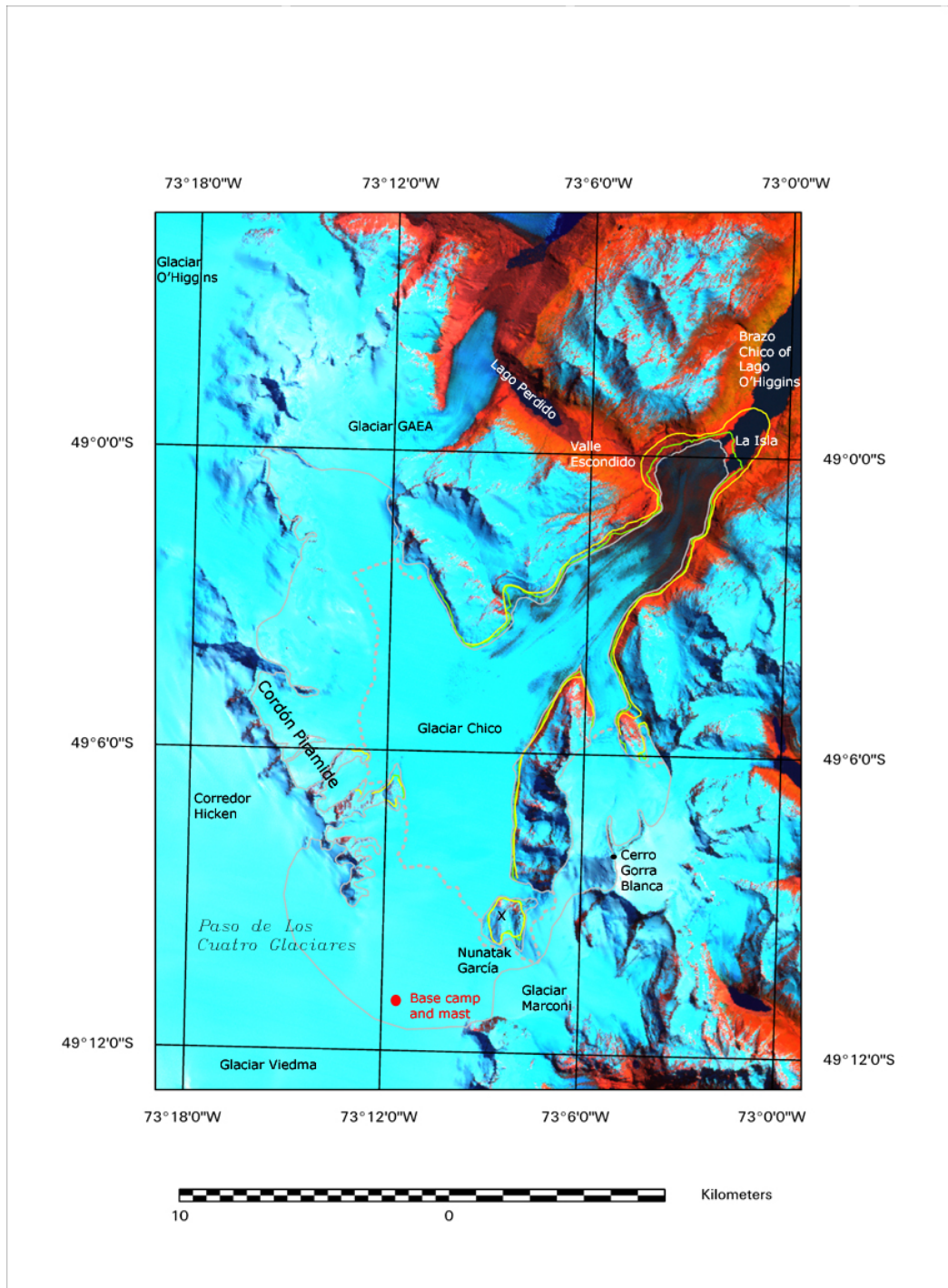
Figure 4.8 Landsat ETM+ false colour composite image (bands 1, 4 and 5) acquired on October 27, 2000. The average ELA of Glaciar Chico is shown by the light grey dotted line. The ice margins of Glaciar Chico in 1945 (yellow), 1975 (green) and 2001 (light grey) are shown. The red dot shows the base camp and mast installed in 1996, where ice velocities are available between 1998 and 2001.

4.2.4 Frontal variations between 1975 and 2001

Since 1975 the glacier has continued to retreat at slower rates compared with the previous 30 years. The main changes took place at the calving front of the glacier, where the ice calved into Brazo Chico of Lago O'Higgins at both margins of "La Isla" (Figure 4.9).
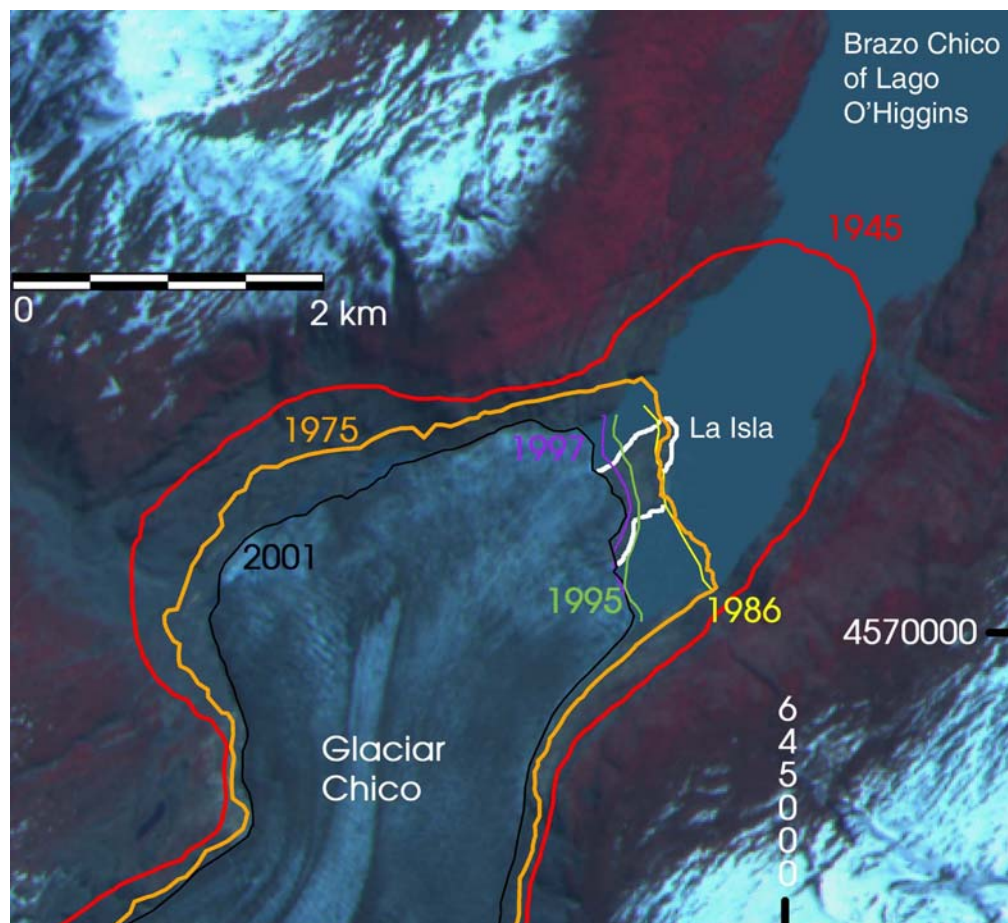
Figure 4.9 ASTER satellite image (colour composite bands 1, 2 and 3N) acquired on October 14, 2001. The terminal fronts of the glacier between 1945 and 2001 are shown. UTM-18S co-ordinates in m, WGS 1984.

Between 1975 and 1986 the glacier front was stable without any significant frontal change. After 1986, the glacier began to retreat until 1995, at rates

of -34 m a^{-1} at the calving front located to the north of "La Isla", and at -57 m a^{-1} at the calving front located to the south of "La Isla". The difference in retreat rates between the two calving fronts could be an indicator of differences in water depth and geometry of the bedrock topography.

Between 1995 and 2001 the calving front located to the north of "La Isla" retreated at a rate of -25 m a^{-1}, whilst the southerly front was more stable without any significant change.

The non-calving front of the glacier on "La Isla" did not show any significant change between 1975 and 1986, however, thereafter it also retreated until 2001 at rates of between -20 and -24 m a^{-1}. The area of "La Isla" has expanded from 0.02 km^2 in 1975 to 0.21 km^2 in 2001.

Ice retreat at moderate rates (4 to 10 ma^{-1}) was also observed all around the ablation area of the glacier between 1975 and 2001. One of the glacier margins which demonstrates considerable evidence of retreat was located at Valle Escondido, where the pro-glacial lagoon observed in 1975 has been replaced by a river draining to Brazo Chico of Lago O'Higgins, partially via a subglacial flow.

4.2.5 Area changes

The total ice area of the glacier between the LIA and 2001 has been determined (Table 4.1, Figure 4.10). Assuming a worst case ice margin delineation error of ± 0.5 pixel size for each data set (25 m), multiplied by

the ice area perimeter length, it was calculated a worst-case under/over-estimation errors of ~5 km^2 for each estimated area (Table 4.1).

The estimation of glacier extent in the LIA was calculated using the outlines of the geomorphological features associated with this period, and proved to be ~213 km^2, with an estimated error of 5.2 km^2 due to outline delimitation plus approximately 1 km^2 of uncertainties in the definition of the geomorphological features.

Table 4.1 Total ice area of Glaciar Chico LIA-2001.

	LIA (1820-1850)	1945 (January)	1975 (March)	1986 (January)	2001 (October)
Total area (km^2)	212.6±6.2	205.3±5.2	199.0±5.2	197.5±5.3	192.6±5.3

Based upon TRIMETROGON aerial photographs, the ice area in 1945 was determined to be ~205 km^2, representing a total area loss of 3.4 ± 2.6 % since the end of the LIA. More than 89 % of this loss corresponds to the terrestrial retreat of all the margins of the glacier, with the remaining loss due to calving into Brazo Chico of Lago O'Higgins, causing the lake to expand by 0.8 km^2 (Table 4.2).

In March 1975, the total glacier area was estimated to be 199 km^2, representing an areal decrease of 3.1 ± 1.4 % with respect to 1945. This areal change was mainly attributable to terrestrial marginal retreat (71%), plus further calving retreat at Brazo Chico of Lago O'Higgins, causing the lake to expand by 1.8 km^2 in 30 years (1975-1945).
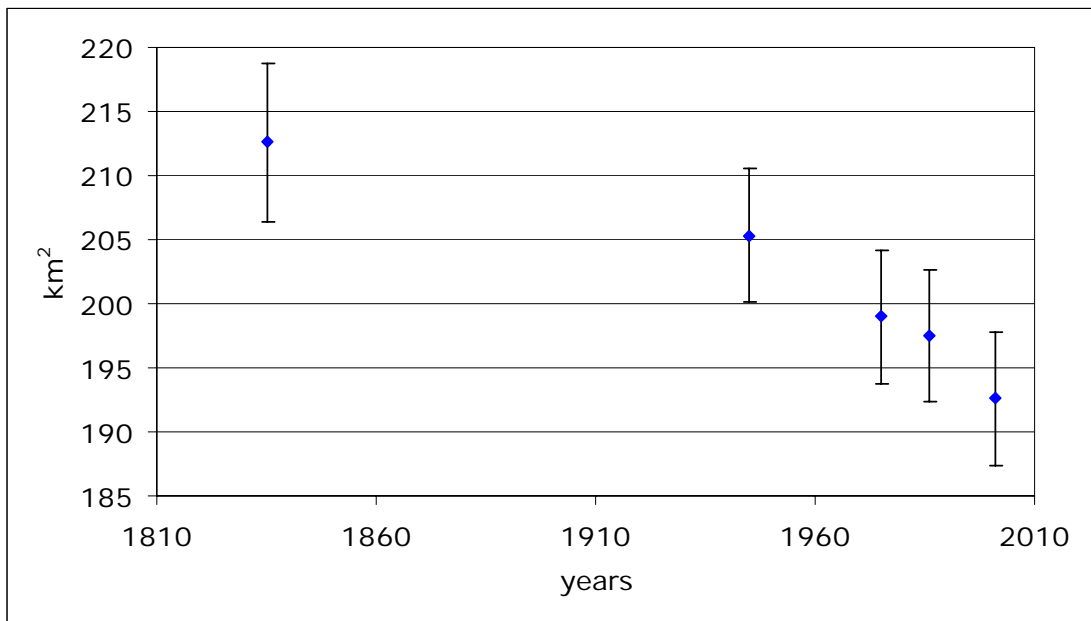
Figure 4.10 Glaciar Chico area changes since the end of the LIA (1835) and 2001.

Table 4.2 Frontal and areal changes LIA-2001.

	LIA*-1945	1945-1975	1975-1986	1986-2001
Frontal retreat (m a^{-1})	-5 to -10	-50 to -60	Stable	-20 to -30
Terrestrial area change (km^2)	-6.5	-4.5	-1.4	-4.4
Area change due to lake expansion (km^2)	-0.8	-1.8	-0.1	-0.5
Rate of total area loss (km^2 a^{-1})	-0.07 ± 0.06	-0.21 ± 0.16	-0.14 ± 0.57	-0.33 ± 0.22

* The date of the end of the LIA was estimated to be 1835 AD

Based upon the 1986 Landsat TM image (Table 2.3) in combination with the SRTM surface topography of the area, a total ice area of ~198 km^2 was calculated for that year. This value is much smaller than the previous

estimation of Aniya and others (1996), due to more accurate definition of the rock outcrops and ice divides. Between 1975 and 1986, the glacier experienced only a small retreat at the calving front, compared with significant terrestrial shrinkage of 1.4 km^2 (Table 4.2).

The most recent assessment of the area of Glaciar Chico of ~193 km^2 was based upon the October 14 2001 ASTER satellite image. This value represents a reduction of 4.7 km^2 (4.2 km^2 of terrestrial area loss plus 0.5 km^2 of lake expansion due to calving retreat) since 1986. This represents the most rapid rate of change since the LIA, at a rate of 0.33 ± 0.22 km^2 a^{-1} between 1986 and 2001 (Table 4.2).

Assuming an ice thickness range between 200 and 400 m for the wasting area (Aniya, 1999), an ice volume loss rate due to area change of -0.071 ± 0.059 km^3 a^{-1} between 1975 and 2001 was obtained.

4.2.6 Ice elevation changes

4.2.6.1 Comparison between different data sets

The ice elevation changes experienced by the glacier were illustrated by comparing DEMs and GPS data from different dates. Boolean masks were generated for each dataset in order to differentiate the areas without data, the rock outcrops, and the accumulation and ablation areas.

Table 4.3 shows the average ice elevation change measured between DEM-1975 and each of the other datasets obtained by comparing the respective DEMs. Analysis of the results reveals ice thinning was occurring over the entire study period, at a lower rate between 1975 and 1981, and more rapidly by 2001. The magnitude of error is greatest between datasets separated by small periods of time, for example between DEM-1975 and DEM-1981, when the thinning rate is lower than the error (although still in agreement with the general trend). The most accurate results were obtained when comparing the geodetic quality GPS measurements of 1998 and 2001 with the 1975 data.

Table 4.3 Comparison of DEM-1975 and the other datasets*.

Data sets	Date	Julian days since DEM-1975	Number of pixels**	Mean Altitude (m)	Ice elevation changes (m a^{-1}) between each data set and DEM-1975***
DEM-1975	15/03/1975	0			
DEM-1981	24/02/1981	2173	35036	1255	-1.2 ± 2.0
DEM-1997	15/03/1997	8036	16176	901	-1.7 ± 0.55
GPS-1997	15/10/1997	8250	440	1332	-1.7 ± 0.49
GPS-1998	23/09/1998	8593	222	1350	-1.7 ± 0.36
SRTM-2000	16/02/2000	9104	49430	1207	-1.7 ± 0.44
GPS-2001	30/09/2001	9696	447	1290	-1.7 ± 0.32

*   The compared areas are not the same

**   A 50 m pixel size was used for all data sets

***   Errors are based upon vertical random values described in Table 3.1.

The differences in altitude between the DEMs are most reliable for the ablation area, where the coverage is more extensive. Figure 4.11 shows the

elevation differences between DEM-1975 and DEM-1997. Over this period the maximum ice thinning was observed at the frontal tongue of the glacier, at both the non-calving (250 - 400 m asl) and the calving front (250 m asl), where a maximum thinning rate of -5.4 ± 0.55 m a^{-1} was measured. Along the central flow line of the glacier, between 500 and 1200 m asl, ice thinning rates were lower, fluctuating between -2.7 to -1.6 ± 0.55 m a^{-1}.
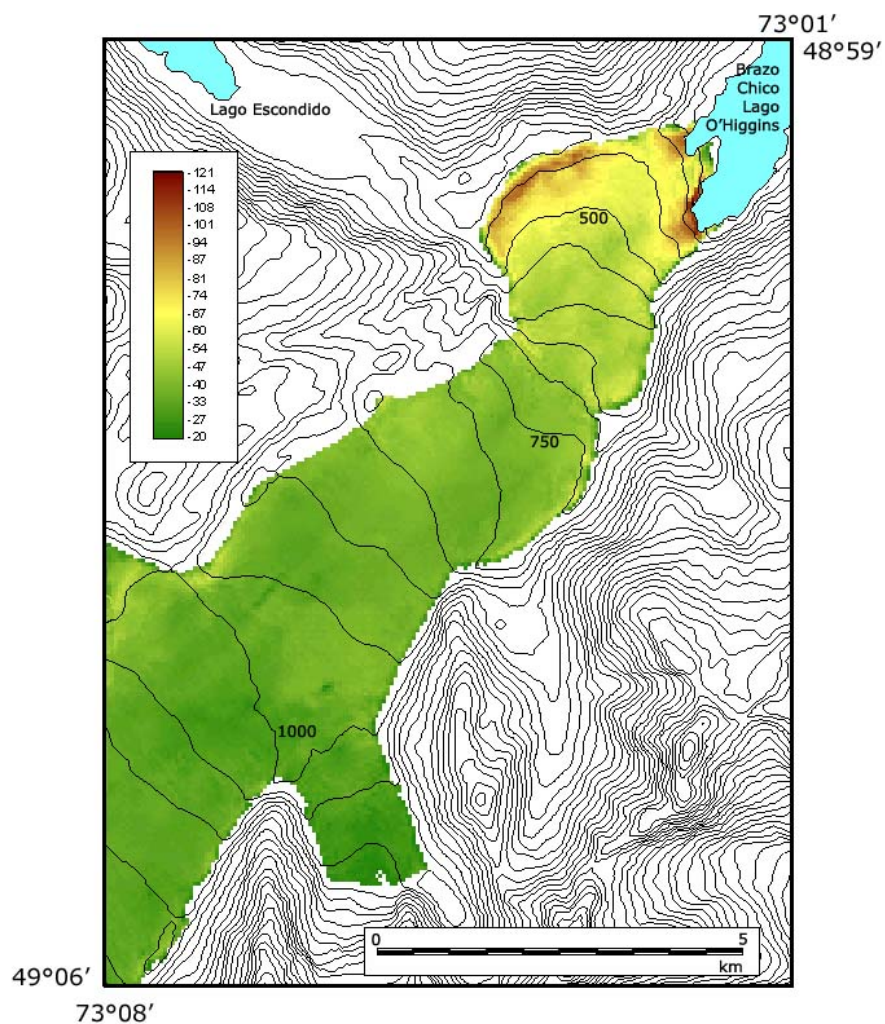
Figure 4.11 Ice elevation changes in m between DEM-1997 and DEM-1975 in the ablation area of Glaciar Chico, between 250 and 1200 m asl. Contour lines derived from DEM-1975 are shown in black.

Over 1100 pixels with GPS altitude values measured between 1997 and 2001, and located between 1100 and 1400 m asl, were compared with DEM-1975, yielding an average thinning rate of -1.7 m a^{-1} (Table 4.3).

Table 4.4 Comparison of DEM-1981 and the other datasets*.

Dataset	Date	Julian days since DEM-1981	Number of pixels in common **	Mean Altitude (m)	Thinning rate (m a^{-1}) between each dataset and DEM-1981***
DEM-1981	24/02/1981	0			
DEM-1997	15/03/1997	5863	9648	1102	-1.6 ± 0.75
GPS-1997	15/10/1997	6077	180	1274	-1.8 ± 0.66
GPS-1998	23/09/1998	6420	88	1302	-1.8 ± 0.48
SRTM-2000	16/02/2000	6931	40089	1278	-1.7 ± 0.58
GPS-2001	30/09/2001	7523	291	1257	-1.8 ± 0.41

*   The compared areas are not the same

**   A 50 m pixel size was used for all data sets

***   Combined errors are based upon vertical random values described in Table 3.1.

Similar results were obtained when DEM-1981 was compared with the other datasets (Table 4.4). The thinning rate is slightly higher than the results obtained when comparisons were made with DEM-1975. These higher values are a possible indication of the acceleration in thinning since 1981. The lower thinning rate obtained between DEM-1981 and DEM-1997, is possibly related to the small area in common between these datasets, and its position in the mid-altitude region of the glacier, where the tributary flowing from Cerro Gorra Blanca joins the main glacier. This tributary

appears to be thinning below the local ELA, but at higher altitudes the data are noisy, with a random distribution of pixels showing thickening and thinning (Figure 4.12).
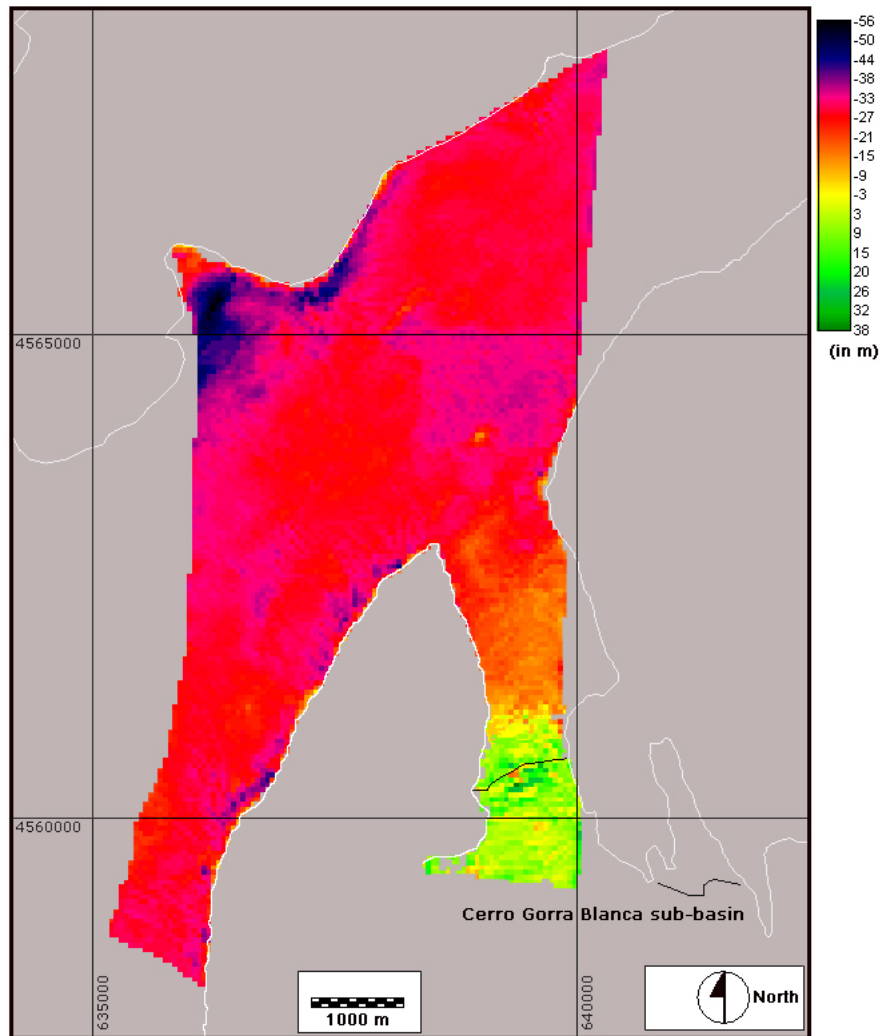
Figure 4.12 Ice elevation changes in m between DEM-1997 and DEM-1981 for Glaciar Chico, between 750 and 1750 m asl. The ELA is shown in black. The 1975 outline of the glacier is shown in white. Co-ordinates in m, UTM-18S, WGS-1984.
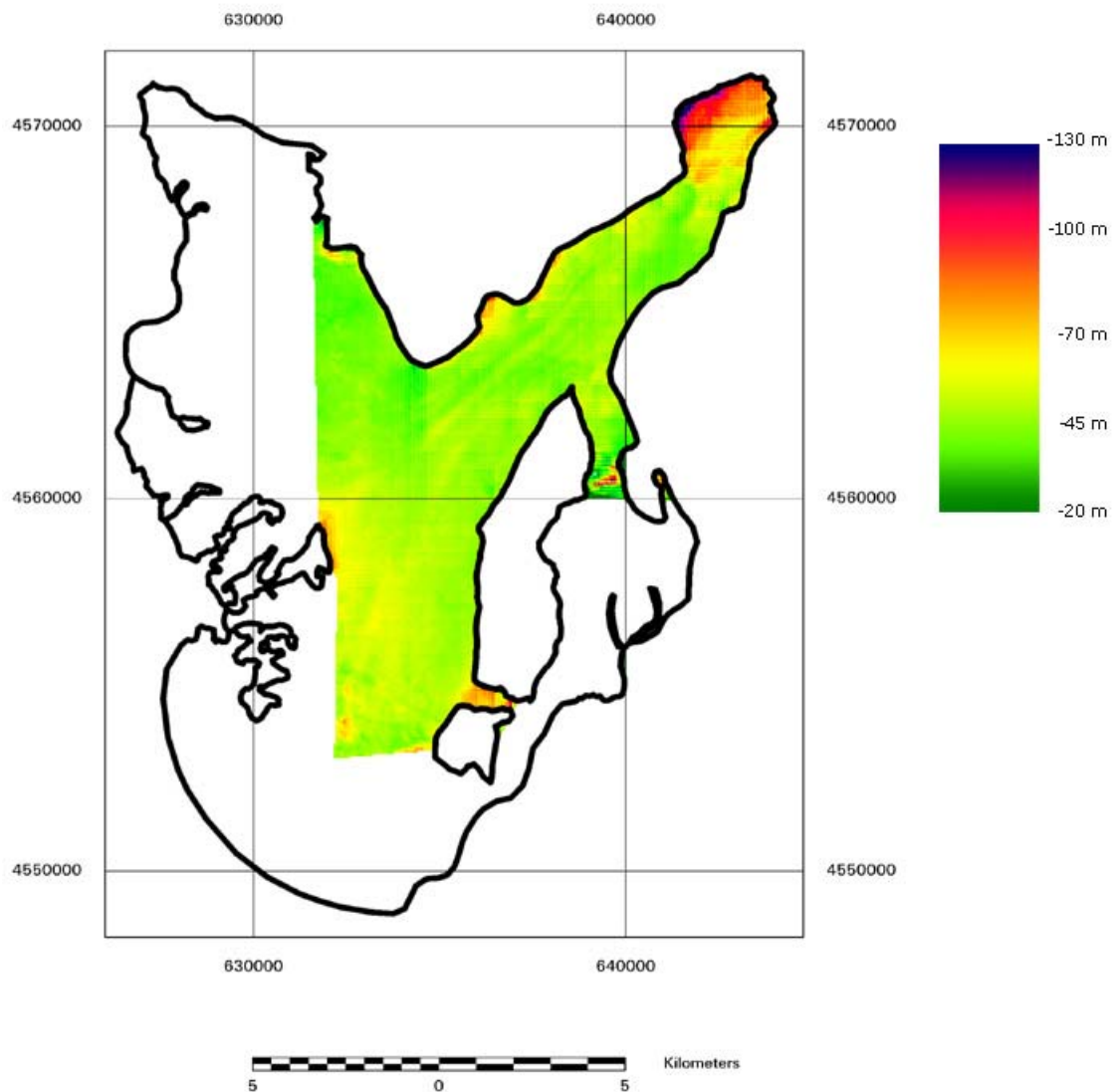
Figure 4.13 Ice elevation changes (in m) between SRTM and DEM-1975 for Glaciar Chico. The 2001 outline of the glacier is shown in black. Co-ordinates in m, UTM-18S, WGS-1984.

When SRTM and DEM-1975 were compared (Figure 4.13), a similar result was obtained, with maximum thinning of up to 130 m at the terminal front, and no spatial trend over the rest of the glacier with average values of

around -40 m across most of the area, equating to an annual thinning rate of -1.6 to -1.7 $\pm$ 0.44 m a^{-1}.

The ASTER-DEM was also compared with the other datasets, resulting in the same pattern of thinning rate for the ablation zone of the glacier (Table 4.5). Over the shortest time period the thinning is less than the error, but for a longer-term analysis the ASTER-DEM results are consistent with the thinning rates of Tables 4.3 and 4.4. Comparison with GPS data was not possible because the datasets did not overlap. Neither was it useful to compare the ASTER-DEM with SRTM, due to the short time interval between these datasets.

Table 4.5 Ice elevation change between ASTER and selected other DEMs*.

	DEM-1997		DEM-1981		DEM-1975	
	Mean altitude	m a^{-1}	Mean altitude	m a^{-1}	Mean altitude	m a^{-1}
ASTER	898	-2.2 $\pm$ 4.2	1371	-1.6 $\pm$ 0.9	1190	-1.7 $\pm$ 0.7

* The compared areas are not the same

Analysis of 13 rapid-static points, measured with geodetic quality GPS receivers in the 1998 and 2001 campaigns in the ablation area of the glacier between 1100 and 1320 m asl (Figure 3.1), revealed an average thinning rate of -1.5 $\pm$ 0.14 m a^{-1}. The differences were normally distributed, with a minimum rate of -1.3 m a^{-1}, and a maximum of -1.9 m a^{-1}.

For 12 geodetic quality rapid-static GPS measurements made in the accumulation area of the glacier between 1320 and 1450 m asl in 1998 and 2001, a mean thinning rate of -1.9 ± 0.14 m a^{-1} was calculated. This ranged between -2.3 and -1.4 m a^{-1}, but showed no apparent altitudinal or spatial pattern.

One of the higher altitude GPS sites on the glacier was the mast installed at 1440 m asl in January 1996 (Base camp and mast, in Figure 4.8). Between October 1, 1998 and October 3, 2001, when the top of the mast was measured with geodetic quality GPS receivers, the structure moved to the north with a horizontal velocity of 53 m a^{-1}, and with a total downward vertical displacement of the mast of -10 m. Considering the surface slope in this area (1.4°), the downward vertical displacement due to ice advection was estimated to be -3.8 m, resulting in a total ice thinning of -6.2 m (-2.0 ± 0.14 m a^{-1} or -1.8 m a^{-1} of w. eq. considering that the changes are due to ice thinning with a density of 0.9 gr cm^3). Analysing snow densities and the height of the mast above the snow surface, an average snow accumulation of 0.57 ± 0.21 m a^{-1} of w. eq. was estimated between 1994/95 and 2001/02 (see Section 6.3.2.1). Thinning is therefore three times the annual accumulation estimated for this location, suggesting that in addition to climate, ice dynamic factors might be responsible in forcing the thinning at the lower end of the accumulation area, as will be discussed in Chapters 6 and 7 of this thesis.

In order to determine possible acceleration/deceleration trends in ice elevation changes, two sections of the glacier were analysed in more detail.

The first one was located at the lower end of the glacier (between 400 and 500 m asl) where different trends were observed; between 1975 and 1995 when an average thinning rate of -1.9 ± 1.0 m a^{-1} was measured, and between 1995 and 2000 when a 2.5 times higher thinning rate of -4.6 ± 3.4 m a^{-1} was estimated (Figure 4.14). In spite of the higher thinning rate during the last period, the great involved errors avoid to reach any conclusive trend. The second section was located at mid altitude of the glacier between 950 and 1050 m asl (Figure 4.15), showed an acceleration trend with an average thinning rate of -1.9 ± 0.6 m a^{-1} between 1981 and 2000, almost 2 times higher than the thinning measured between 1975 and 1981. At higher altitude, there are not enough data to estimate a long time series trend (25 years).
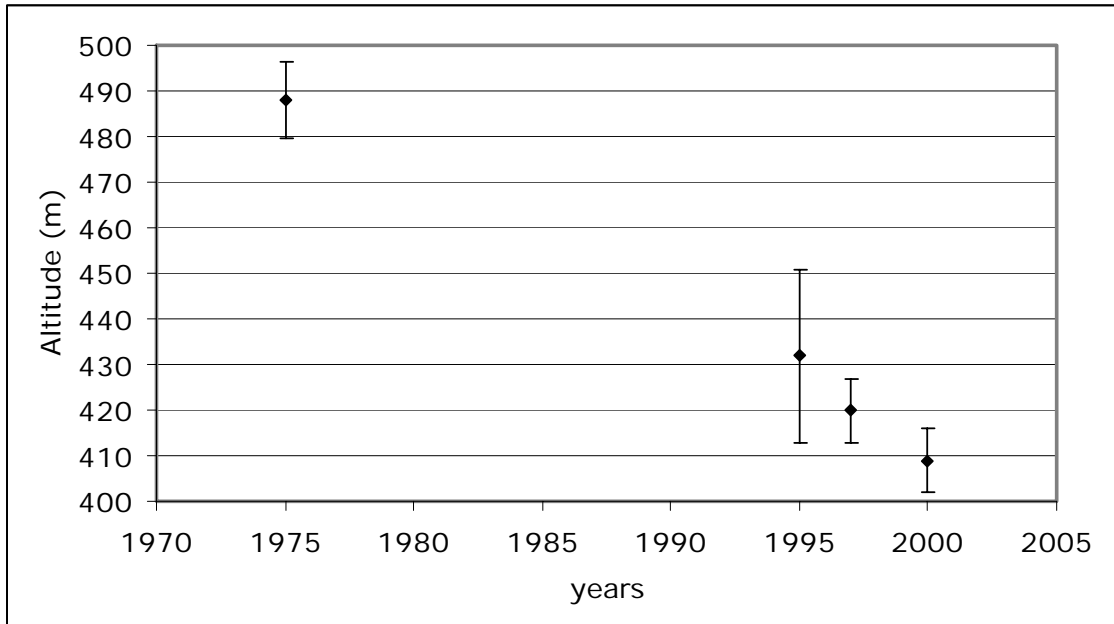
Figure 4.14 Ice elevation changes 1975-2000 at low altitude of Glaciar Chico. Error bars are referred to values described in Table 3.1.
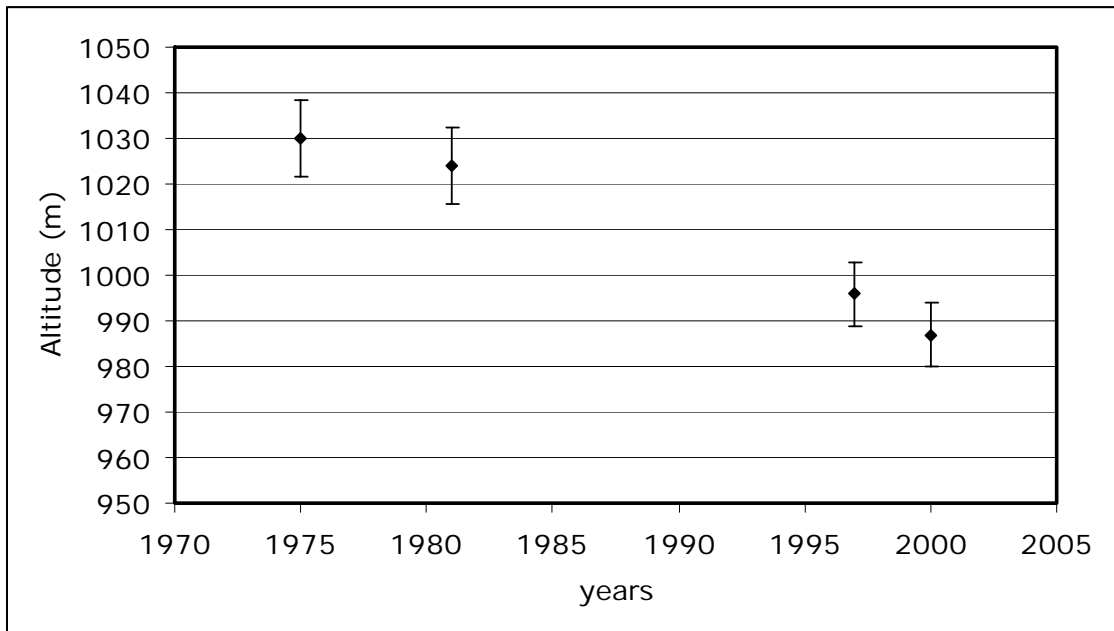
Figure 4.15 Ice elevation changes 1975-2000 at mid altitude of Glaciar Chico. Error bars are referred to values described in Table 3.1.

4.2.6.2 Ice elevation changes versus altitude

Ice thinning was observed in all the ablation area between 250 and 1320 m of altitude. At the lower part of the accumulation area between 1320 and 1440 m asl were also observed thinning, however, above this altitude the thinning is reduced almost to null and in the area between 1900 and 2860 m asl no change or even thickening could have taken place if the lower altitude values are extrapolated. Based upon the mean thinning rates per altitude range measured between 1975 and 2000 on Glaciar Chico (Figure 4.16) and considering no changes at higher altitude (> 1900 m), an average ice thinning rate of -1.3 ± 0.44 m a^{-1} for the whole glacier was obtained (Figure 4.16).
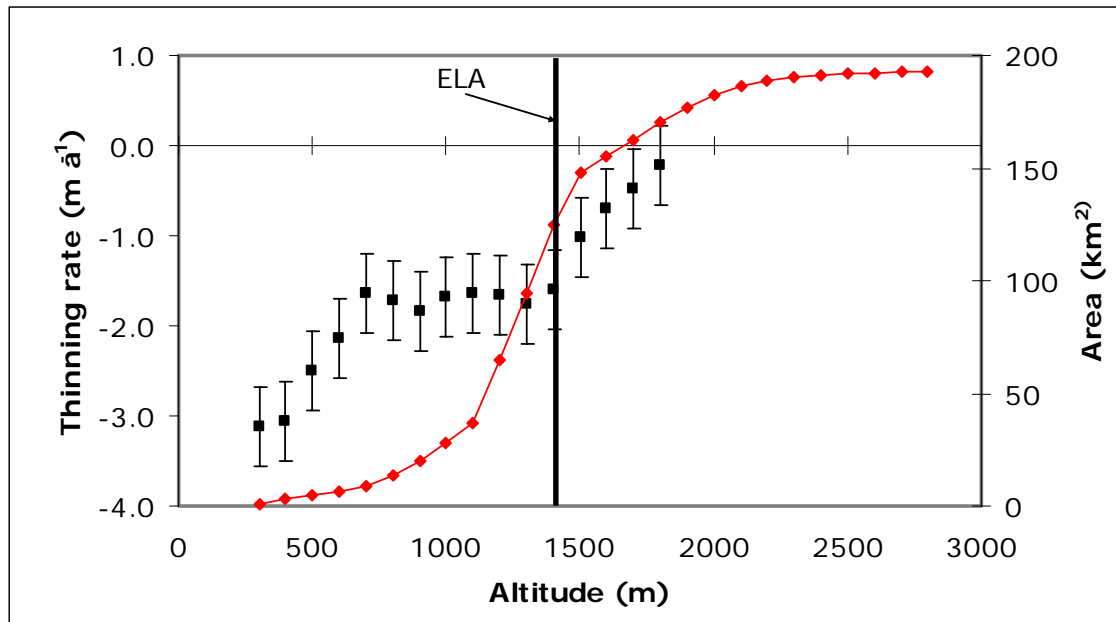
Figure 4.16 Mean ice elevation change (1975-2001) per altitude (black squares, left hand y-axis in m a^{-1}), compared with the cumulative area of the glacier (red curve, right hand y-axis).

In order to compare the altitude variations of the ice elevation change, several topographic profiles were defined (Figure 4.17). These profiles were mainly located in the ablation area of Glaciar Chico, where the topographic coverage was more complete. The longitudinal profile was defined as following the ice flow of the glacier from the Hicken sub-basin (Figure 4.1) to the approximate location of the LIA terminal position.

The LIA surface topography was assumed to follow the same shape as the DEM-1975 profile, but displaced toward the north in order to match the start of the profile with the LIA terminal position (Figure 4.18). A similar procedure was applied in Norway to calculate the surface topography of glaciers during the LIA (Haakensen, 1986). A 50 m vertical random error has been assumed for this LIA surface topography, based upon the

uncertainties in the definition of the trim lines and possible variations in the slope of the surface topography.

The assumption that the surface slope of the glacier in 1975 could be used to calculate the LIA topography is supported by the fact that in 1975 the glacier was almost totally calving into Brazo Chico of Lago O'Higgins, i.e. in the same way as the glacier was calving during the LIA. Since 1975, the shape of the glacier tongue has been modified due to the appearance of "La Isla", however, comparing the surface topography of 1975, 1981 and 2000 shows that the overall change in shape is only slight (Figure 4.18 and 4.19). Considering the vertical random error introduced by this change in morphology, it was possible to estimate the surface topography for the LIA only for elevations between 250 and 1300 m asl.

The transverse profiles were calculated based upon the LIA moraines or trim lines detected at the glacier margin. In the centre of the valley for each transverse profile, the LIA topography matches the estimated altitude obtained from the longitudinal profile. Between these three points (two trim line/moraine elevations at the margins of the glacier, and the altitude of the longitudinal profile in the centre) the estimated LIA topography follows the shape of the DEM-1975 topography in a semi-convex shape. The bi-cubic spline procedure was applied in order to interpolation the surface topography between these three points.

In Figure 4.18 it is possible to appreciate the resulting ice surface topography along the longitudinal profile. The LIA topography was

estimated only to the ELA of the glacier at that time, however, is likely that the accumulation area has also suffered thinning since then. The maximum altitude of the LIA geomorphological evidence was recorded at approximately 1300 m, at a site located only 2 km to the north (downstream) of the present location of the ELA.

Figure 4.19 shows in more detail the ice elevation changes experienced by the glacier between 900 and 1400 m asl. This area of the glacier was covered by almost all the datasets, and is further evidence that thinning has been a trend since the LIA.
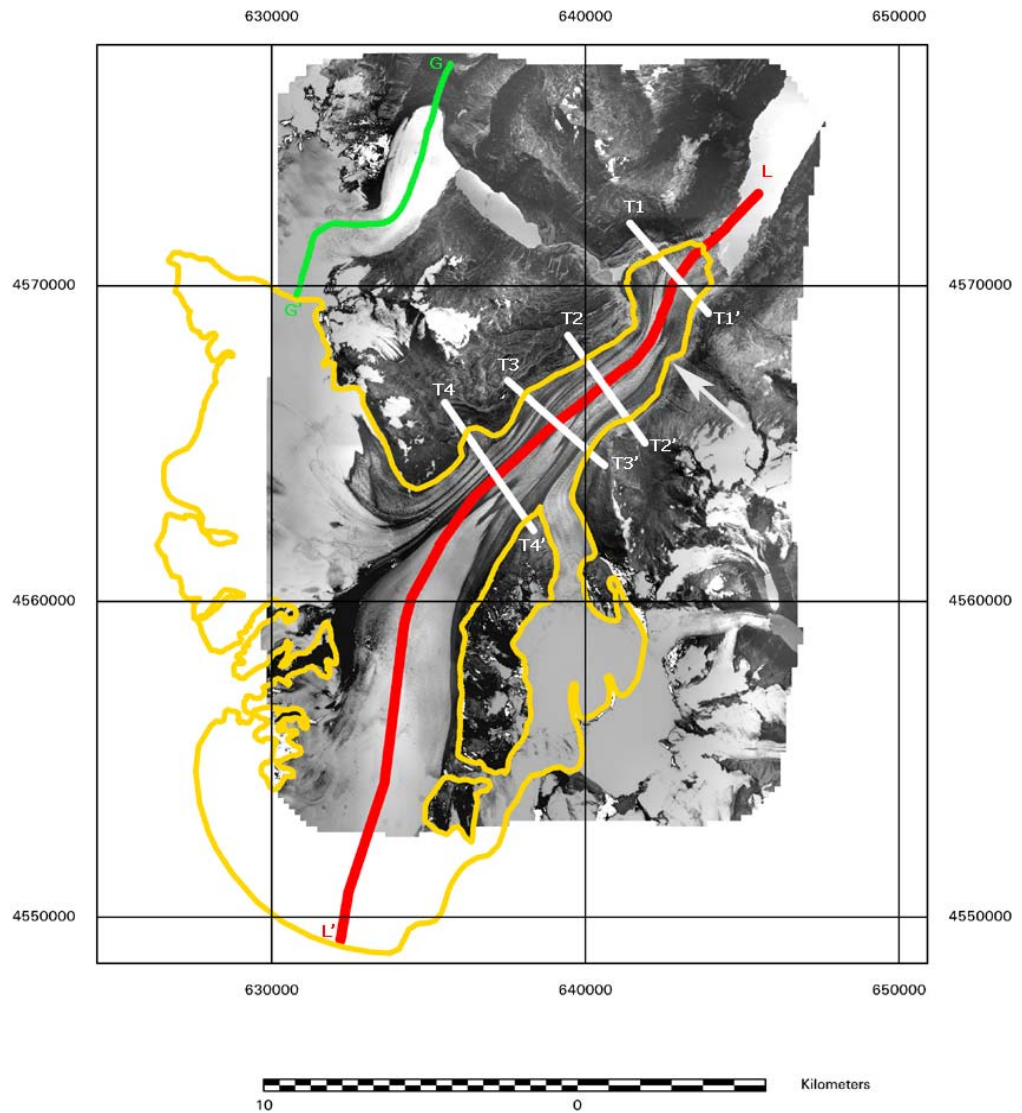
Figure 4.17 Ortho-rectified 1975 aerial photograph mosaic of Glaciar Chico showing the location of the topographic profiles discussed in the text. In red, the longitudinal profile of Glaciar Chico (L-L′). In green, the longitudinal profile of Glaciar GAEA (G-G′). The transverse profiles of Glaciar Chico (T1-T1′, T2-T2′, T3-T3′ and T4-T4′) are shown in white. The outline of Glaciar Chico basin in 2001 is shown in yellow. UTM-18S co-ordinates in m, WGS 1984.

The transverse profiles (Figures 4.20 to 4.22) show the thinning experienced by different sections of the glacier. Traverse 1 (Figure 4.20), was located at the terminal front of the glacier, only 1.4 km away from the present calving front. This profile presents an average thinning rate of -1.3 0.36 m a^{-1} between the end of the LIA (assumed to be at 1835 AD) and 1975. Between 1975 and 2000 (SRTM), the thinning rate increased to an average of -3.4 ± 0.44 m a^{-1}.

Transverse profile 2 (Figure 4.21) exhibits an average thinning rate of -0.7 ± 0.36 m a^{-1} between the LIA and 1975, and -1.8 ± 0.44 m a^{-1} between 1975 and 2000 (SRTM). Transverse profile 3 (Figure 4.22) shows an average thinning rate of -0.7 ± 0.36 m a^{-1} between the LIA and 1975, and an average thinning rate of -1.9 ± 0.44 m a^{-1} between 1975 and 2000. Transverse profile 4 (Figure 4.23), shows an increase in the thinning rates from -0.8 ± 0.36 m a^{-1} for the period between the LIA and 1975 to -2.0 ± 0.44 m a^{-1} between 1975 and 2000. These higher values for profile 4 are induced by the lateral tongue of the glacier, which has been occasionally covered by a lateral pro-glacial lake, which could accelerate mass losses by higher melting at the water/ice contact, and occasional calving.
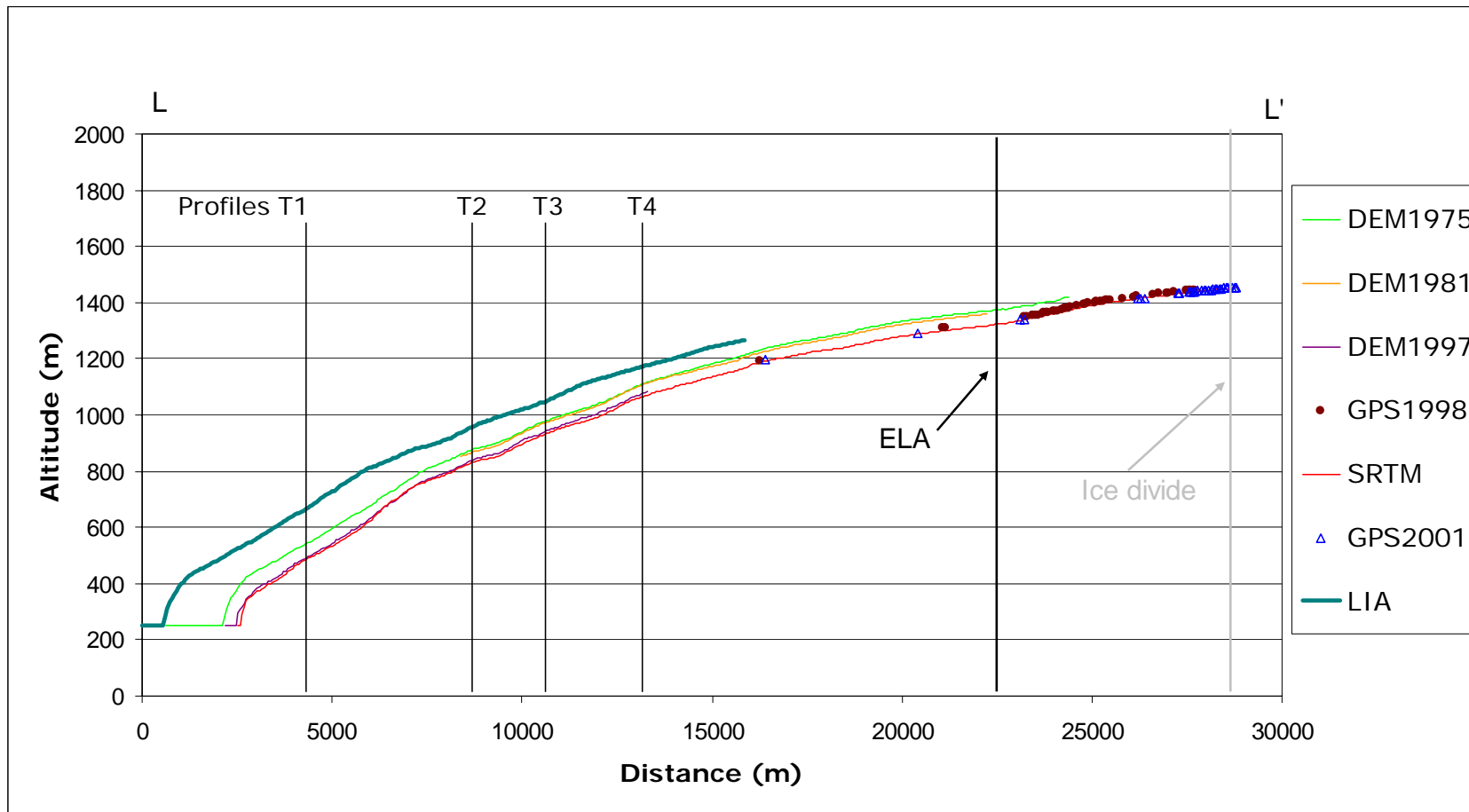
Figure 4.18 Topographic longitudinal profile of Glaciar Chico for different dates. The location of the profile is shown in Figure 4.17. The average ELA is shown in black and the ice divide between Glaciares Chico and Viedma in grey.
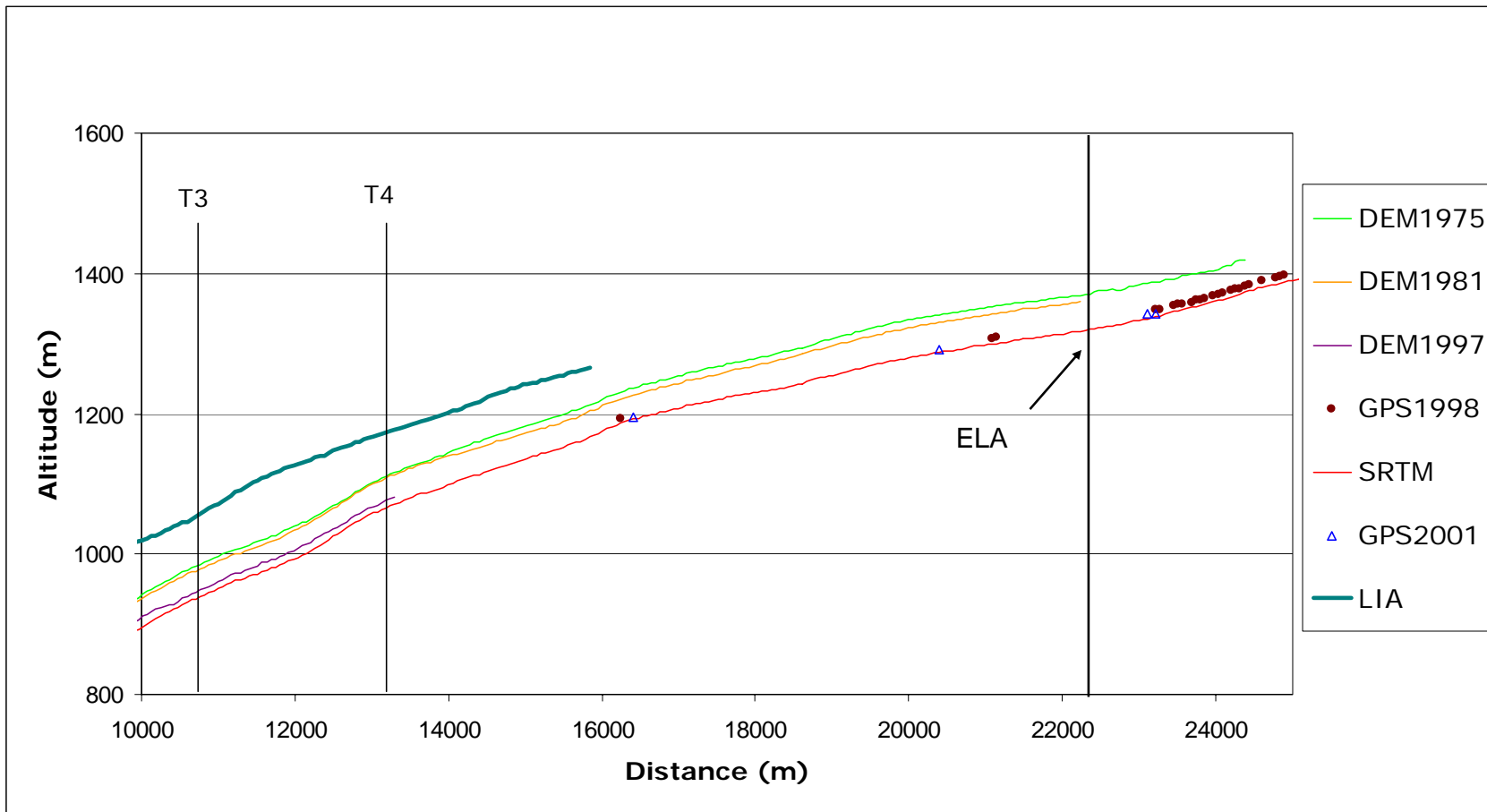
Figure 4.19 Section of longitudinal profile L-L' showing mid-altitude ice elevation changes since the LIA.
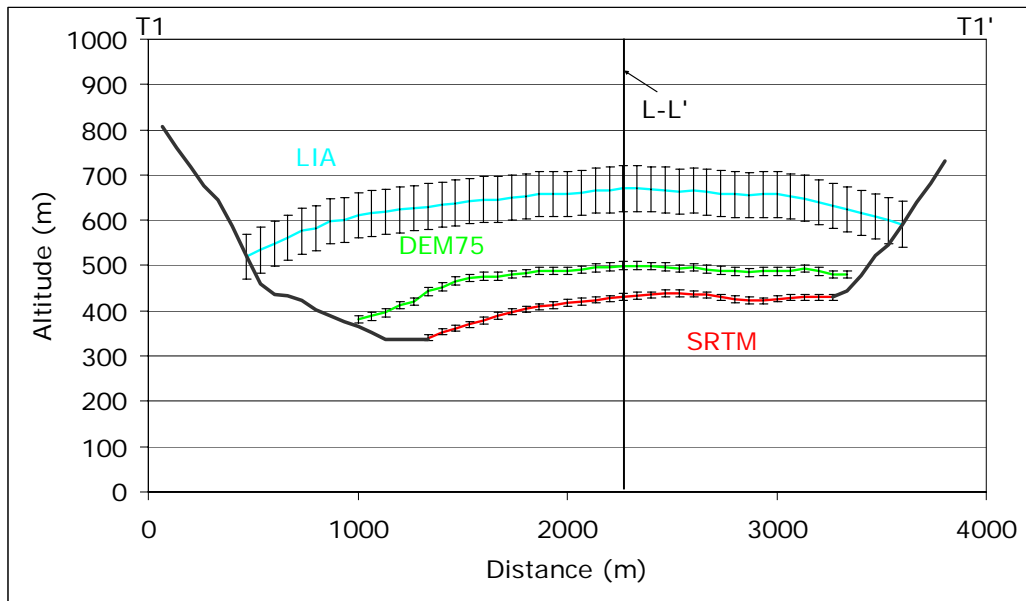
Figure 4.20 Transverse topographic profile T1-T1', showing ice elevation change between the LIA and 2000 (see Figure 4.17 for the location of the profile). The elevation error bars are indicated in black.
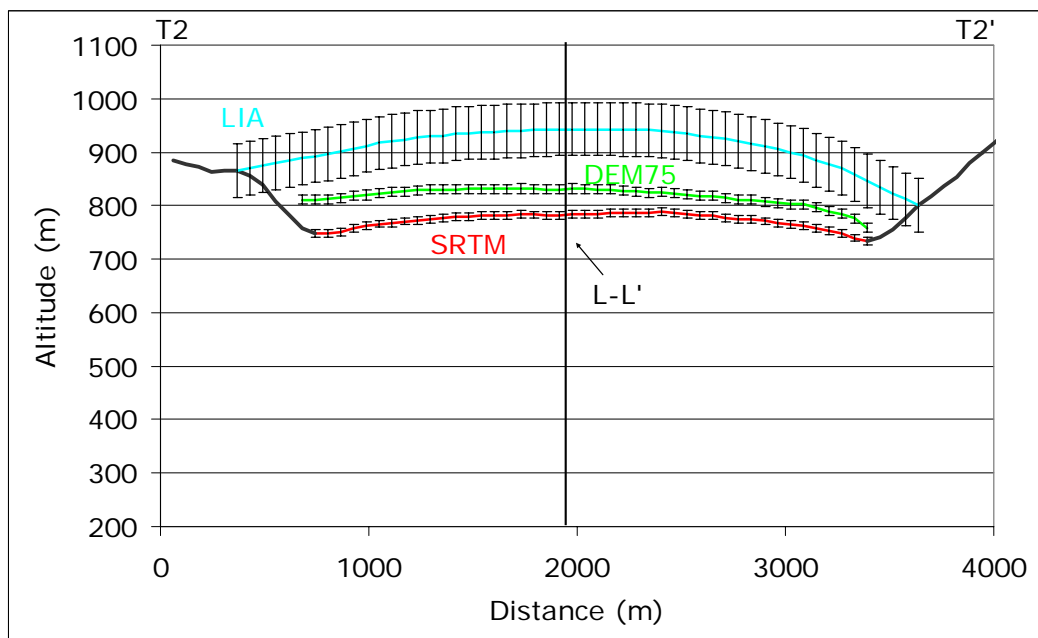
Figure 4.21 Transverse topographic profile T2-T2', showing ice elevation change between the LIA and 2000 (see Figure 4.17 for the location of the profile). The elevation error bars are indicated in black.
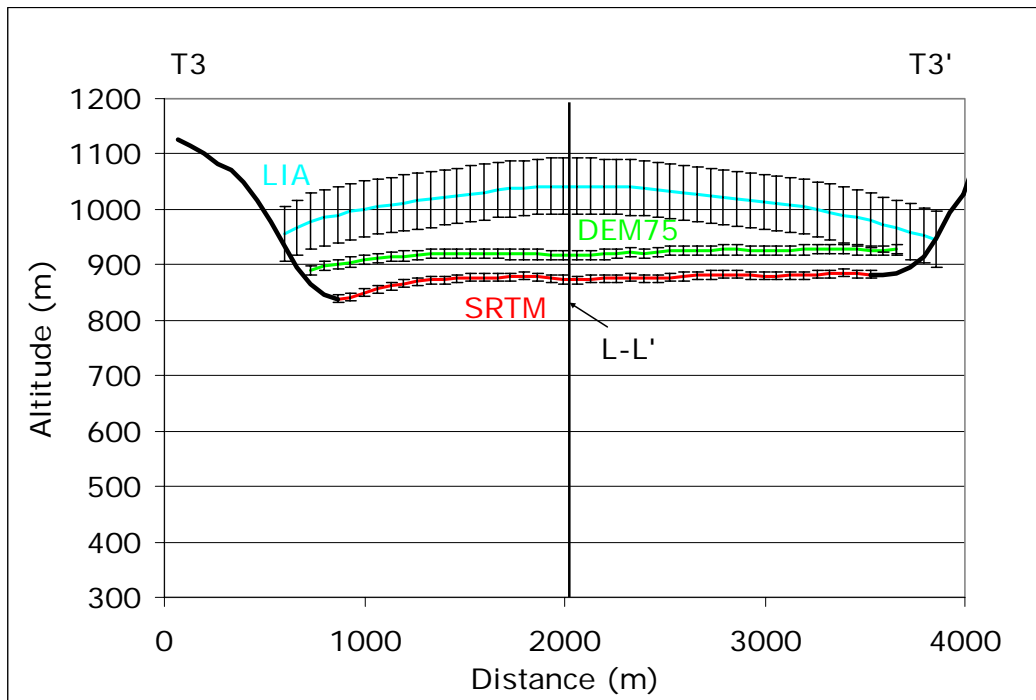
Figure 4.22 Transverse topographic profile T3-T3′, showing ice elevation change between LIA and 2000 (see Figure 4.17 for the location of the profile). The elevation error bars are shown in black.
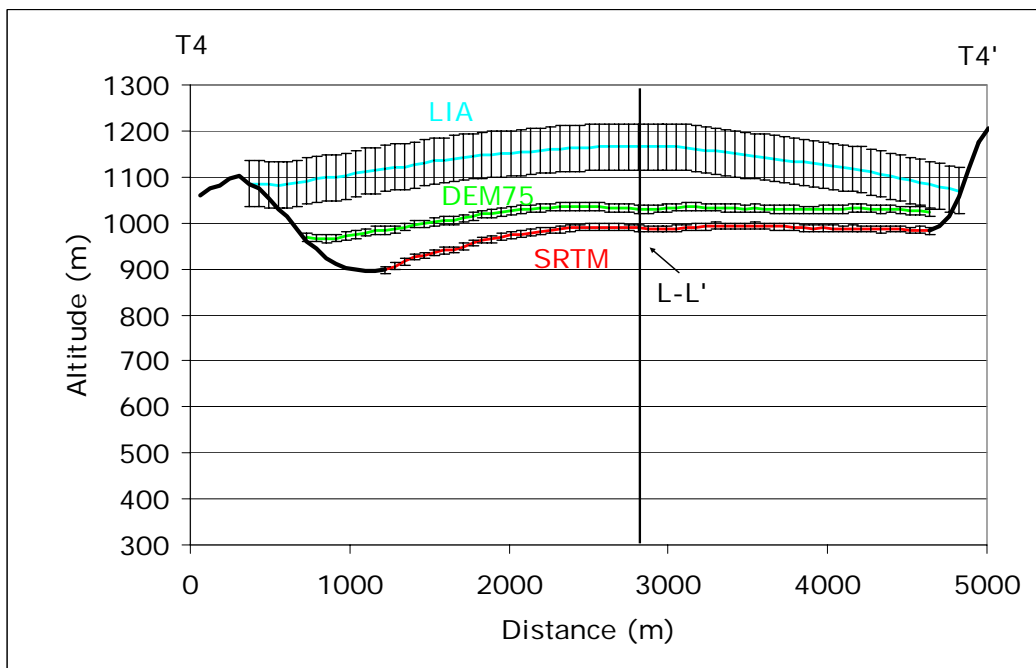
Figure 4.23 Transverse topographic profile T4-T4′, showing ice elevation change between LIA and 2000 (see Figure 4.17 for the location of the profile). The elevation error bars are shown in black.

The general trend of thinning along the central flow line profile L-L' is shown in Figure 4.24. The maximum thinning was observed, as expected, at the lower end of the glacier, where the thinning rates peaked at -1.5 ± 0.36 m a^{-1} between the LIA and 1975, and at -4.7 ± 0.44 m a^{-1} between 1975 and 2000.
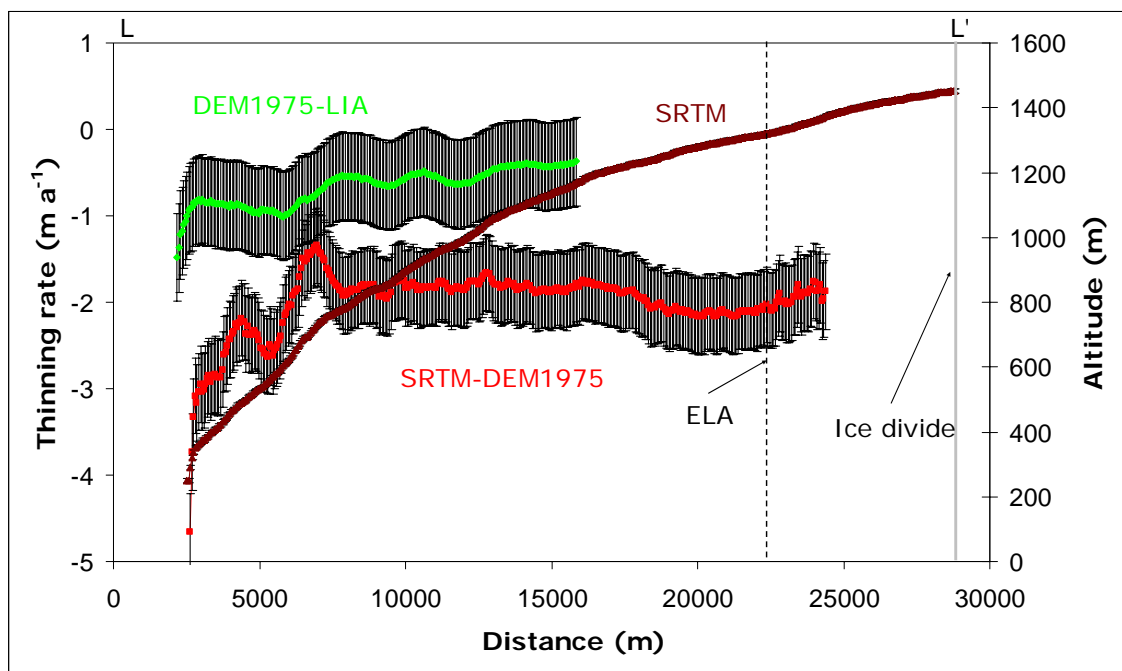
Figure 4.24 Longitudinal profile (L-L') showing SRTM topography (right hand y-axis in m) and ice elevation change rates (left hand y-axis in m a^{-1}). The average ELA is shown by the dashed line (1320 m asl), and the ice divide between Glaciares Chico and Viedma is shown in grey (1450 m asl). The location of the profile L-L' is shown in Figure 4.17. The vertical error bars for each dataset are shown in black.

At higher altitudes, the estimated thinning between the LIA and 1975 decreases with distance until the combined error exceeds the thinning (at approximately 1200 m asl). Between 1975 and 2000, the thinning also decreases with altitude, however, between 800 and 1400 m asl, the thinning has no altitudinal trend, with an average value of -1.9 ± 0.44 m a^{-1}.

Comparing both curves of ice elevation change (Figure 4.24), it becomes clear that along the entire length of the glacier thinning rates have been much higher (by a factor of three) in recent years compared with the period following the LIA (-0.5 ± 0.36 m a^{-1} between the LIA and 1975 versus -1.3 ± 0.44 m a^{-1} between 1975 and 2000 for the glacier as a whole). The one exception is the area between 600 and 800 m asl, where between 1975 and 2000 (SRTM) the thinning rates approached the values experienced in the earlier period. This area is steep (between 6 and 25°) and narrow (only 1.5 km wide), indicating a threshold in the subglacial topography (shown by the arrow in Figure 4.17).

4.2.7 Mass balance of the glacier based upon the geodetic method

Considering the mean ice elevation change rates per altitude range and the respective area of each altitude range (Figure 4.16), a mean volume of ice loss due to thinning of -0.25 ± 0.09 km^3 a^{-1} was calculated between 1975 and 2001. Adding an estimated ice volume loss due to area change of -0.071 ± 0.059 km^3 a^{-1}, the total ice volume loss by Glaciar Chico between 1975 and 2001, yielded -8.64 km^3 (-0.32 ± 0.11 km^3 a^{-1}).

Conversion of a surface elevation change in the accumulation area to a change in ice thickness depends on the what these changes are representing: if they represent a short-term change in snowfall, it should be multiplied by the ratio of the density of near-surface snow to the density of ice, but if it represents long-term changes in ice flow, no conversion is necessary (Paterson, 1994:47). Therefore, in order to calculate the volume of water equivalent loss by the glacier during the 27 years, a mean density of 0.9 g cm^3 for ice was assumed, yielding an average volume loss of -0.226 ± 0.081 km^3 a^{-1} of w. eq. due to ice thinning between 1975 and 2001. This assumption is supported by the fact that most of the ablation is taking place in the ablation area and at low altitude of the accumulation area of the glacier, where the observed elevation changes at the mast installed in 1996 represent a long-term change in ice flow, because they are almost three times higher than the specific mass balance measured at the mast (Section 6.3.2.1), therefore the thinning of almost -2 m a^{-1} measured between 1998 and 2001 represent a long-term change on the glacier and not inter annual snowfall variations.

Adding an average volume loss of -0.064 ± 0.059 km^3 a^{-1} of w. eq. due to area change, the total volume loss by the glacier, based upon the geodetic method yielded -7.83 km^3 of w. eq. (-0.290 ± 0.097 km^3 a^{-1} of w. eq.) between 1975 and 2001.

4.2.8 Other glacier variations related to Glaciar Chico

4.2.8.1 Glaciares O'Higgins and GAEA

The frontal and areal variations of nearby Glaciares O'Higgins and GAEA (Figure 4.25) are not the main topic of this thesis, however, their variations during the 20th Century could affect the dynamics of Glaciar Chico, and therefore it is useful to analyse them in more detail.

In terms of areal and frontal changes, the variations experienced by these nearby glaciers are much greater than those of Glaciar Chico. The changes appear to be closely related to the calving activity of Glaciar O'Higgins, which was presumably mainly controlled by the water depth at the calving front (Casassa and others, 1997). This assumption was recently confirmed by bathymetric measurements from a joint Chilean and German field campaign, which measured an average of 700 m and a maximum of 836 m of water depth (Casassa personal communication) in the middle of the lake arm at a position between the 1973 and 1975 terminus of Glaciar O'Higgins (labelled B in Figure 4.25). Under conditions of similar, and shallower water depths, the terminal tongue of other freshwater calving glaciers of Patagonia have been known to suffer major calving events, for example Glaciar Upsala (Figure 1.2) experienced a total ice area loss of 4.76 km^2 between 1996-2000 (Skvarca and others, 2002). At this glacier, one single day calving event produced icebergs with a combined area of 0.3 km^2 of ice (Aniya and others, 2000), confirming that the ice front was probably very close to its buoyancy point in the lake.

The frontal tongue of Glaciar O'Higgins retreated at high rates between 1945 and 1986, after which time the terminal front became more stable, with only small changes between this date and 1995 (Casassa and others, 1997). Since 1995, an important change has been taking place south of the frontal tongue of the glacier, where a valley previously occupied by a lateral ice tongue and moraines of Glaciar O'Higgins has been partially transformed into a new arm of Lago O'Higgins (Figure 4.26).

In 1960, the British explorer Eric Shipton led an expedition to Glaciar O'Higgins together with Chilean mountaineers to look for an "elusive" active volcano, wrongly linked by Lliboutry (1956) to Nunatak Viedma (Figure 1.3). During the expedition, the Chilean mountaineer Eduardo García took a photograph of Glaciar O'Higgins, whose terminal position is reproduced in Figure 4.25. After a couple of days of trekking, they reached the lateral valley between Glaciares O'Higgins and GAEA. In 1945, Glaciar GAEA flowed from the SPI toward the east, where it calved into Lago Perdido (Figure 4.26), but Shipton (1963) noted that in this place (Labelled X in Figure 4.25), Glaciar GAEA was making a vigorous thrust over dead ice to form a tributary of Glaciar O'Higgins.

This phenomenon was clearly an indication that Glaciar GAEA was advancing toward the north, altering the main direction of the ice flow observed in 1945. The primary explanation for this change must be associated with the thinning and rapid collapse experienced by Glaciar O'Higgins whilst its lower tongue was lying on a deep fjord of Lago

O'Higgins (at depths of more than 700 m at a position between the 1975 and 1945 glacier front, Casassa personal communication). Therefore, initially Glaciar O'Higgins acted as a barrier for Glaciar GAEA, deflecting its ice flow toward Lago Perdido in 1945. However, as the lower tongue of Glaciar O'Higgins started to collapse into the lake, the deep subglacial topography of the valley encouraged Glaciar GAEA to push north. In 1975 (Figure 4.26) Glaciar GAEA showed retreat at the eastern arm that was calving into Lago Perdido, but showed advance to the north (Figure 4.25). At the same time, the lateral tongue of Glaciar O'Higgins, in the valley visited by Shipton, was much more debris/moraine covered than in 1945, presumably because the glacier was increasingly unable to evacuate the lateral moraines near the terminus. Evidence from the 1973 Landsat MSS image and 1975 aerial photographs indicates that the glacier tongue was collapsing and retreating at rates of between 2500 and 2700 m a^{-1}; representing one of the maximum retreat rates observed in Patagonia.
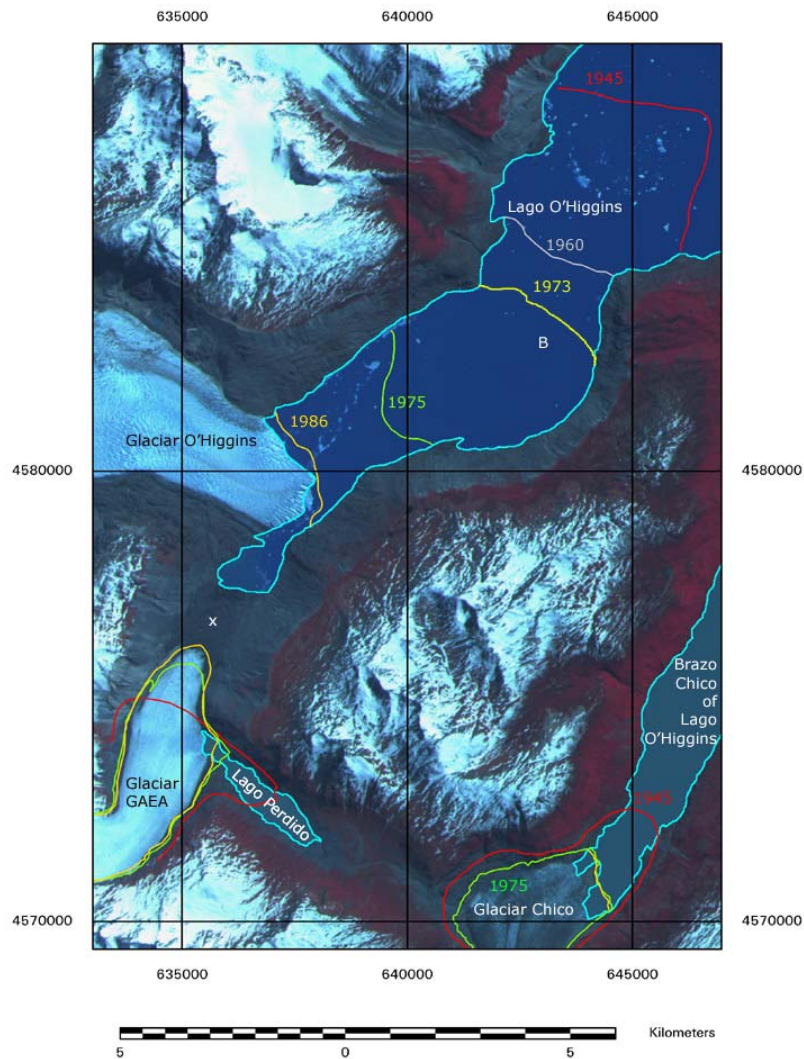
Figure 4.25 ASTER satellite image (October14, 2001) false colour composite (bands 1, 2 and 3N). Frontal variations are shown in red (1945), grey (1960), yellow (1973), green (1975) and gold (1986). The margin of Lago O'Higgins in 2001 is in light blue. See Tables 2.2 and 2.3 for details of each dataset used. The 1960 position was copied from Casassa and others (1997). "B" is the location of measured point with maximum water depth as described in the text. UTM-18S co-ordinates in m, WGS 1984.
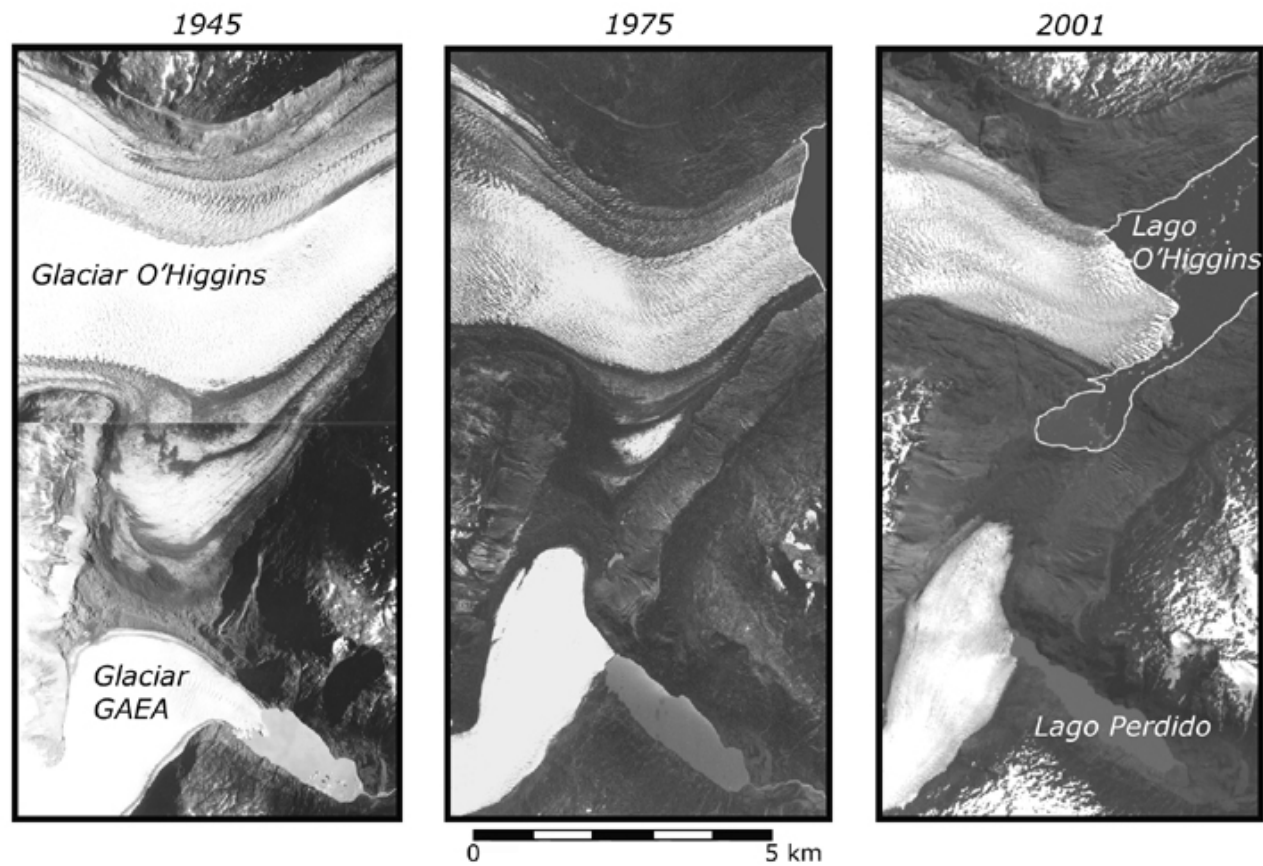
Figure 4.26 Sequence of aerial photographs (1945 and 1975) and band 2 of the ASTER image acquired on October 14, 2001, showing Glaciar GAEA and its confluence with Glaciar O'Higgins. The scale is an approximation. North is to the top of the images, but the orientation between each varies slightly.

Between 1975 and 1986, Glaciar GAEA advanced further north to the maximum recent position of its bare ice surface, reforming previously deposited moraines in this sector into an arcuate band. Between 1986 and 2001, the bare ice front of the glacier has been stable (Figure 4.25), but it has however shown a significant thinning and lateral shrinkage. The debris/moraine covered lower tongue of the glacier began to retreat more rapidly after 1998/1999, when the new bay of Lago O'Higgins was created (Strelin personal communication).
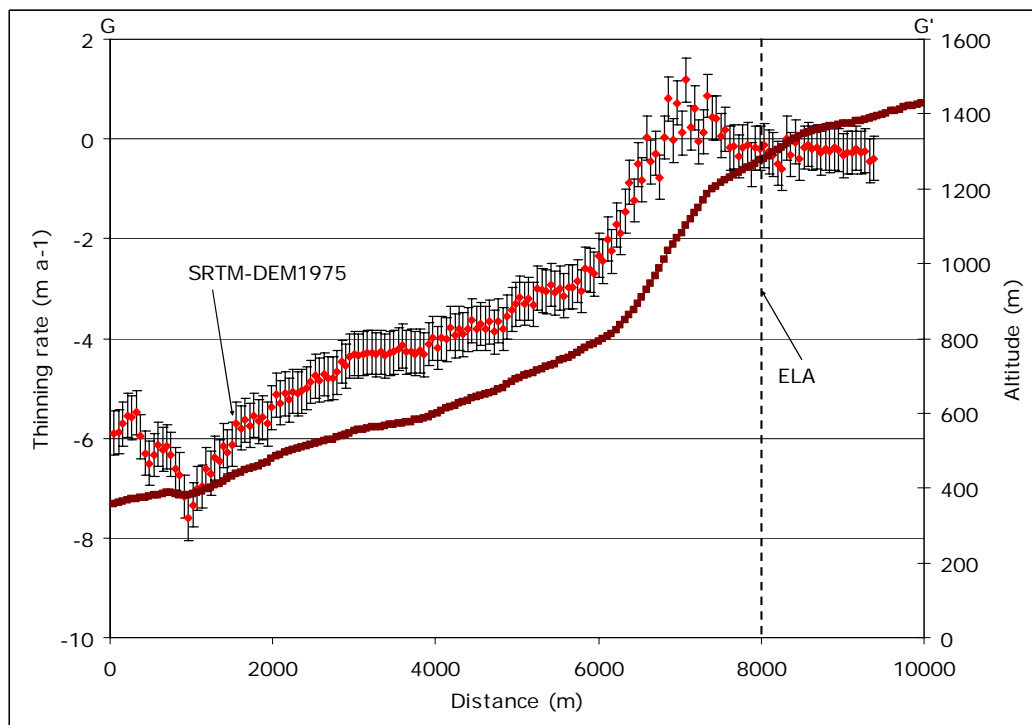
Figure 4.27 Longitudinal profile (G-G') of Glaciar GAEA showing topography (SRTM, right hand y-axis in m) and ice elevation change rates (left hand y-axis in m a^{-1}). The average ELA is shown by a dashed line (1290 m asl). The location of the profile is shown in Figure 4.17. The vertical elevation error bars are shown in black.

The ice elevation changes of Glaciar GAEA were established by comparing SRTM and DEM-1975 data (Figure 4.27). These two datasets covered the entire ablation area of the glacier, but the accumulation area was only partially surveyed. The mean average thinning rate measured for the ablation area of Glaciar GAEA was -3.16 ± 0.44 m a^{-1}. The maximum thinning rates were observed for the debris/moraine covered ice (between 0 and 2 km in Figure 4.27) that is currently calving into the new arm of Lago O'Higgins (Figure 4.28), where the average thinning rate was 5.8 ± 0.44 m a^{-1}.

Figure 4.28 Panoramic hand-held photograph of Glaciares GAEA (left) and O'Higgins (centre-right), obtained in April 2003 by Alvaro Giannini.

At higher altitudes, the ice elevation changes of Glaciar GAEA become progressively smaller, reaching positive values for the steep and heavily crevassed area of the glacier (km 7 in Figure 4.27). Above the ELA of the glacier, no significant change was observed between 1975 and 2000.

The ice elevation changes of Glaciar O'Higgins were analysed by comparing SRTM and DEM-1975IGM data (Figure 4.29). This latter dataset only covered the ablation area of the glacier, and has the highest vertical error

of this study (Table 3.1), however, the observed thinning rates are much larger than the errors, at an average of -4.6 ± 0.81 m a^{-1}.

The ice elevation changes with respect to the altitude of Glaciar O'Higgins along the longitudinal profile H-H' are shown in Figure 4.30. The first section of the profile (between km 0 and 2.5 in Figure 4.30) represents the glacier area described above as having now been replaced by a lake, and consequently the observed thinning is underestimated, due to the unknown thickness of the ice.

Above the present terminal front of the glacier (km 2.4 in Figure 4.30), the thinning rates decrease with altitude, to a minimum thinning rate of -2.0 ± 0.81 m a^{-1} at approximately 900 m asl. This trend is interrupted at the steepest section of the glacier (approximately km 6 in Figure 4.30), where the thinning rates are lower than the general trend.
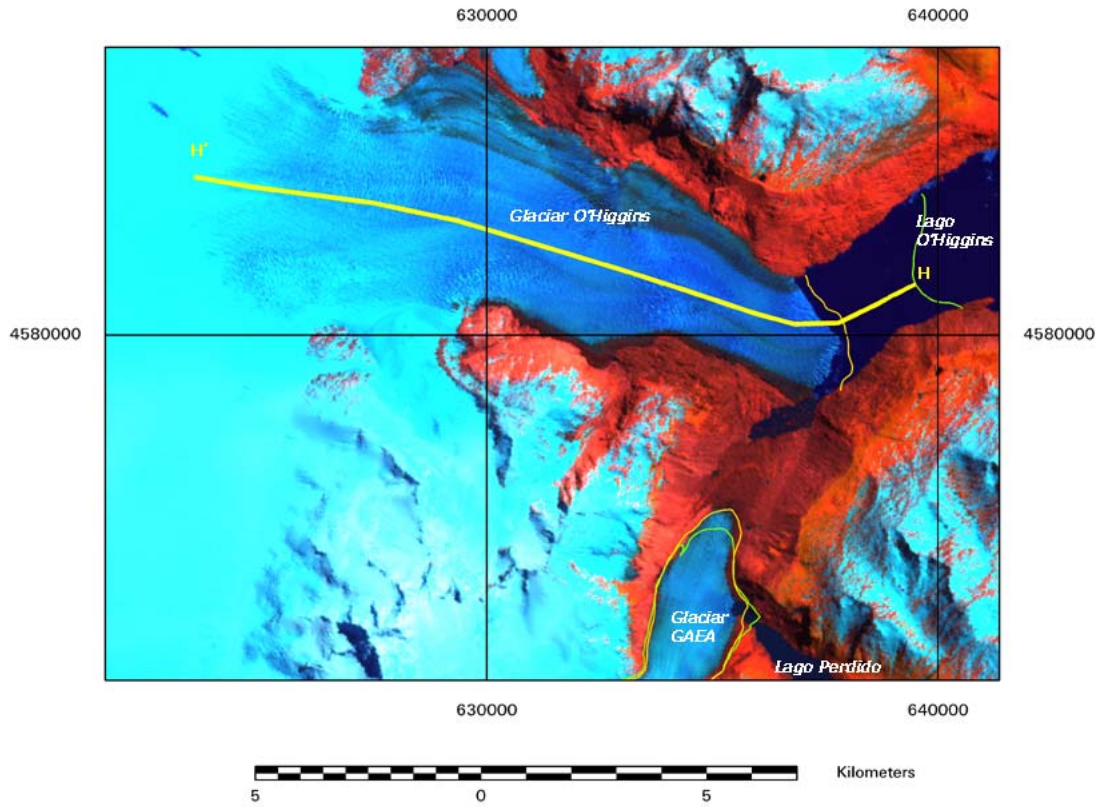
Figure 4.29 Landsat ETM+ false colour satellite image acquired on October 27, 2000 showing the location of the topographic profile of Glaciar O'Higgins discussed in the text (H-H' in yellow). Terminal positions of the glaciers are shown in green (1975) and orange (1986). UTM-18S co-ordinates in m, WGS 1984.
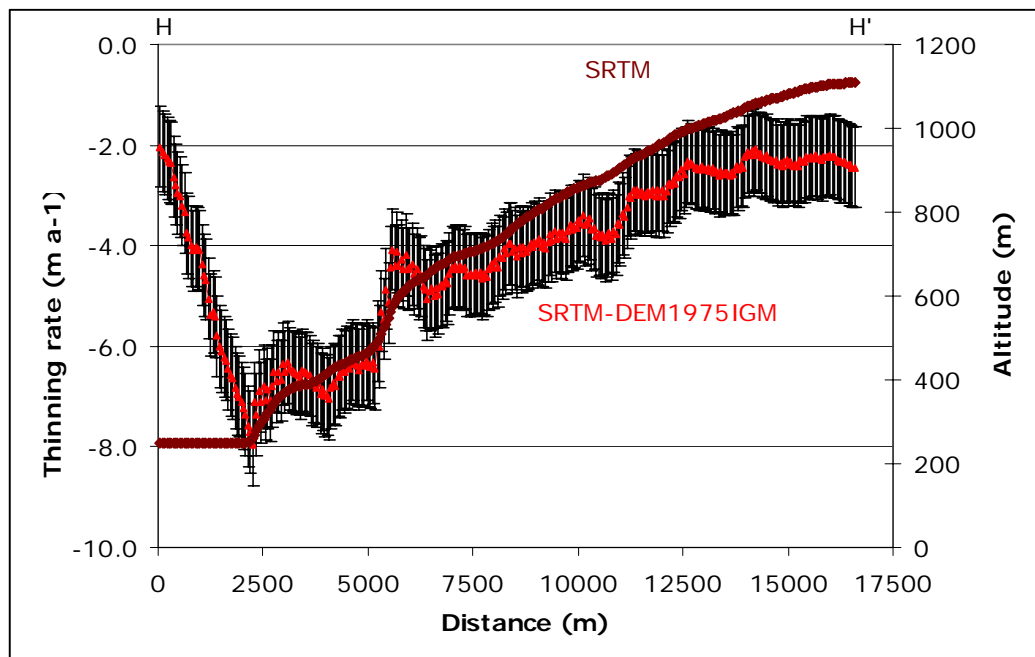
Figure 4.30 Longitudinal profile of the ablation area of Glaciar O'Higgins (H-H') showing surface topography (SRTM, right hand y-axis in m) and ice elevation change rates (left hand y-axis in m a^{-1}). The location of the profile is shown in Figure 4.29. The vertical elevation error bars are shown in black.

The changes experienced by Glaciares O'Higgins and GAEA have been closely related to each other in the past, with the main driving factor behind these observed changes being the calving dynamics of Glaciar O'Higgins. The main implication of these changes for the dynamics of Glaciar Chico could be for a possible migration of the ice divide between Glaciares GAEA and Chico. Similar processes have been reported for glaciers of the USA (Waddington and Marriott, 1986) and Antarctica (Nereson and others, 1998), and it was also quoted as a possible explanation for the anomalous fluctuations of Icelandic glaciers during the Holocene (Dugmore and Sugden, 1990).

In order to test this possibility, a new surface topography must be generated in the region of the ice divide between the two glaciers, either by means of direct geodetic quality GPS, or airborne or satellite laser altimetry measurements. A comparison of these new data with SRTM and the older datasets available for the area (1995 and partially in 1975), would allow an estimation of the magnitude and direction of a possible migration. In the absence of such data however, a hypothesis about the possible direction of the migration can be formulated. As Glaciar GAEA has thinned and advanced during recent decades, the most probable direction of ice migration is toward the south, where part of the accumulation area of Glaciar Chico would be captured. Glaciar GAEA is smaller (only 28 km^2 versus 191 km^2 for Glaciar Chico) and shorter than Chico (~10 km versus 23 km from the ice divide along the central flow line to the calving front), but it is much steeper than Chico (~20° versus ~1° of surface slope around the ELA). Therefore, it is likely that the dynamics of the lower tongue of Glaciar GAEA are subject to a higher longitudinal stretching rate near the terminus (Figure 4.31), which would be propagated upstream with an unknown lag time, affecting the position of the ice divide, and forcing its migration toward the Glaciar Chico basin. A key unknown factor in this process is the subglacial topography of Glaciar GAEA. If the bedrock is consistently deep, as was measured in the nearby lake (Casassa, personal communication), the glacier will continue to retreat, and the ice will probably thin further south and upstream toward the ice divide.

Figure 4.31 Terminal front of Glaciar GAEA after the new bay of Lago O'Higgins was opened in 1998/99, initiating calving of the glacier into Lago O'Higgins. Notice the transverse crevasses near the front of the glacier denoting extension flow near the terminus. Photograph obtained by Alvaro Giannini, February 2002.

4.2.8.2 Glaciar Viedma

Glaciar Viedma is the other glacier that shares an ice divide with Glaciar Chico. This is one of the largest glaciers of the SPI with an ice area of 945 km^2 (Aniya and others, 1996). The position of the terminal front of the glacier has varied only slightly since 1968, with a total area loss of 1.34 km^2 between 1986 and 1997 (Aniya and others, 2000). Rignot and others (2003) detected a small area of thinning (calculated from total volume loss divided by area) with an average rate of -0.01 ± 0.28 m a^{-1}, but peaking at -4.4 m a^{-1} between 1975 and 2000, with a maximum thinning rate measured at the lower front of the glacier between 1969 and 2000, yielding -2 to -10 m a^{-1}.

The frontal variations in the position of the terminal tongue of this glacier since 1916 are shown in Figure 4.32, based on the map published by Kölliker and others (1917) and recent Landsat MSS and TM satellite imagery.
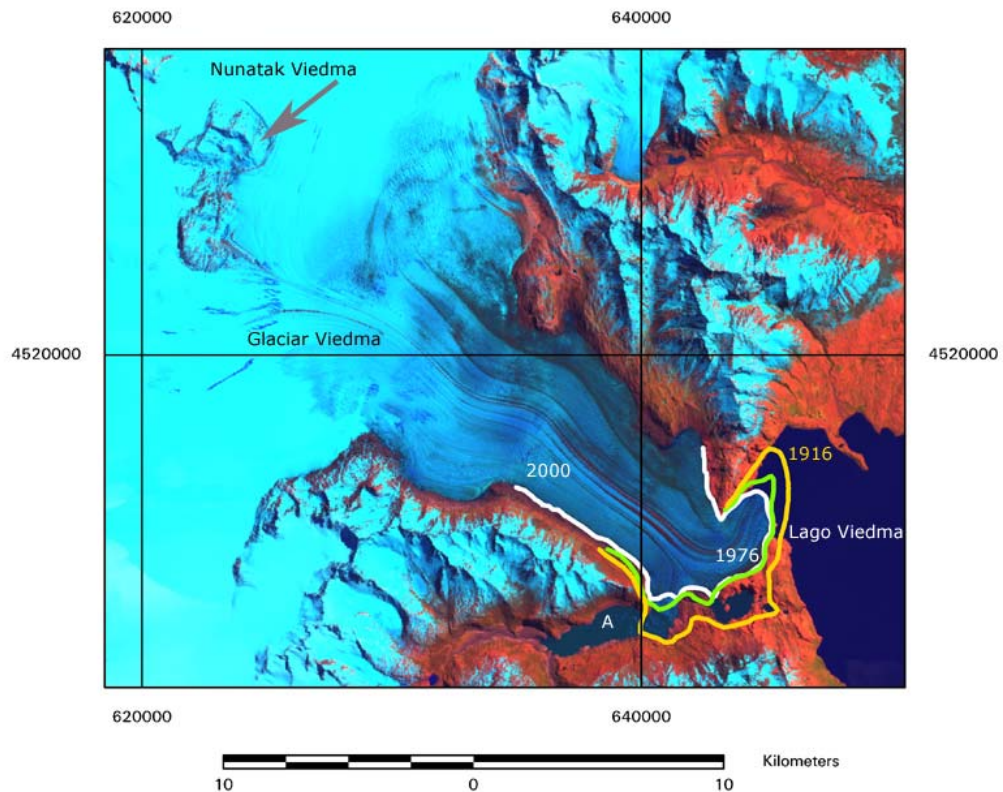
Figure 4.32 Landsat ETM+ false colour composite image (bands 1, 4 and 5) acquired on October 27, 2000. The ice margins of Glaciar Viedma of 1916 (gold), 1976 (green) and 200 (white) are shown. UTM-18S co-ordinates in m, WGS1984 datum.

Between 1916 and 1976 the frontal tongue of the glacier retreated by an average of 550 m, at a retreat rate of -8 m a^{-1}. The most significant changes took place at the southern margin of the glacier, where there are

several proglacial lagoons. These lagoons have been observed since at least 1976, and the biggest one (labelled A in Figure 4.32) was initially mapped in 1916 by Kölliker and others (1917). Between 1976 and 2000, the Lago Viedma calving front of the glacier retreated between 300 and 500 m (-13 to -21 m a^{-1}); one of the smallest retreat rates measured across the SPI during this time.

At P4G where Glaciares Viedma and Chico share a common ice divide, very little surface topography data have been collected, and therefore, even the glacier basins that have been mapped contain high uncertainties (Aniya and others, 1996). However, due to the low relief conditions of the area, a possible migration of the divide could not be totally discounted, especially if one, or both, glaciers undergo collapse retreats in the future, like that observed at Glaciar O'Higgins. In order to evaluate and monitor possible changes of the ice divide, a new field campaign must be carried out in this area, using geodetic quality GPS receivers or laser altimetry systems.

4.3 Summary

In this chapter the glacial history of Glaciar Chico and its neighbouring glaciers since the LIA have been analysed. All the glaciers have been retreating since the LIA, but with different retreat rates. Glaciar O'Higgins has shown the maximum retreat, presumably due to the high calving rate at Lago O'Higgins. Glaciar Chico retreated at higher rates between 1945 and 1975 when the frontal tongue was calving into Brazo Chico of Lago O'Higgins, but since 1975, and the appearance of "La Isla" at the glacier

front, calving activity has been reduced, and the retreat process slowed. Ice elevation changes have been also measured since 1975 at Glaciar Chico, based on field data, vertical aerial photographs and satellite images. A maximum ice thinning of -5.4 ± 0.55 m a^{-1} was observed at the glacier front between 1975 and 1997. GPS data were used in the accumulation area of the glacier to infer a thinning rate of -1.9 ± 0.14 m a^{-1} between 1998 and 2001. An acceleration thinning trend was observed in recent years, compared with a long term changes since the end of the LIA. Comparing the recent records of ice elevation changes, a even higher acceleration trend was observed since 1995 at the ablation area of the glacier, compared with the previous period 1975 and 1995. These changes could be related to increases in temperature and a reduction in precipitation in Patagonia, however in order to further investigate this explanation, the next chapter will analyse climatic changes observed at several stations around the SPI.

5. REGIONAL CLIMATOLOGY

5.1 Introduction

Regional climatology in the context of this thesis refers to the mean temperature and precipitation conditions observed between 1960 and 1991 for all stations located between 45 and 53°S, near (~200 km) the main axe of the Patagonian Andes mountain range (Figure 4.1). This regional concept is similar to the one used by IPCC (2001), but smaller in terms of the involved area.

5.1.1. Precipitation

The SPI is located in southern Chile at a latitude where high precipitation occurs during winter and summer, amounting to an estimated annual average precipitation of 7000 mm on the higher plateau of the SPI (Escobar and others, 1992). The east and west margins of the SPI are characterized by a strong contrast in climatic behaviour due to the presence of the Andes mountain range, which acts as a large barrier to the prevailing westerly winds (Warren and Sugden, 1993).

The western margin of the SPI consists of a labyrinth of fjords and channels, surrounded by rough mountainous terrain. The great majority of days during a normal year are rainy and cloudy; for example in Evangelistas (-52.4°S, Figure 5.1) precipitation has been recorded on up to 322 days per year (Carrasco and others, 2002). Consequently, the

western side of the SPI receives a high annual precipitation, ranging from a minimum of 2000 mm at Cabo Raper (-46.83°S) to more than 7000 mm at Isla Guarello (-50.35°S, Figure 5.2). This typical maritime environment is mainly a product of the location of semi-permanent cold fronts that are associated with migratory low pressure systems embedded in the mid-latitude westerlies coming from the Pacific Ocean (Montecinos and Aceituno, 2003).
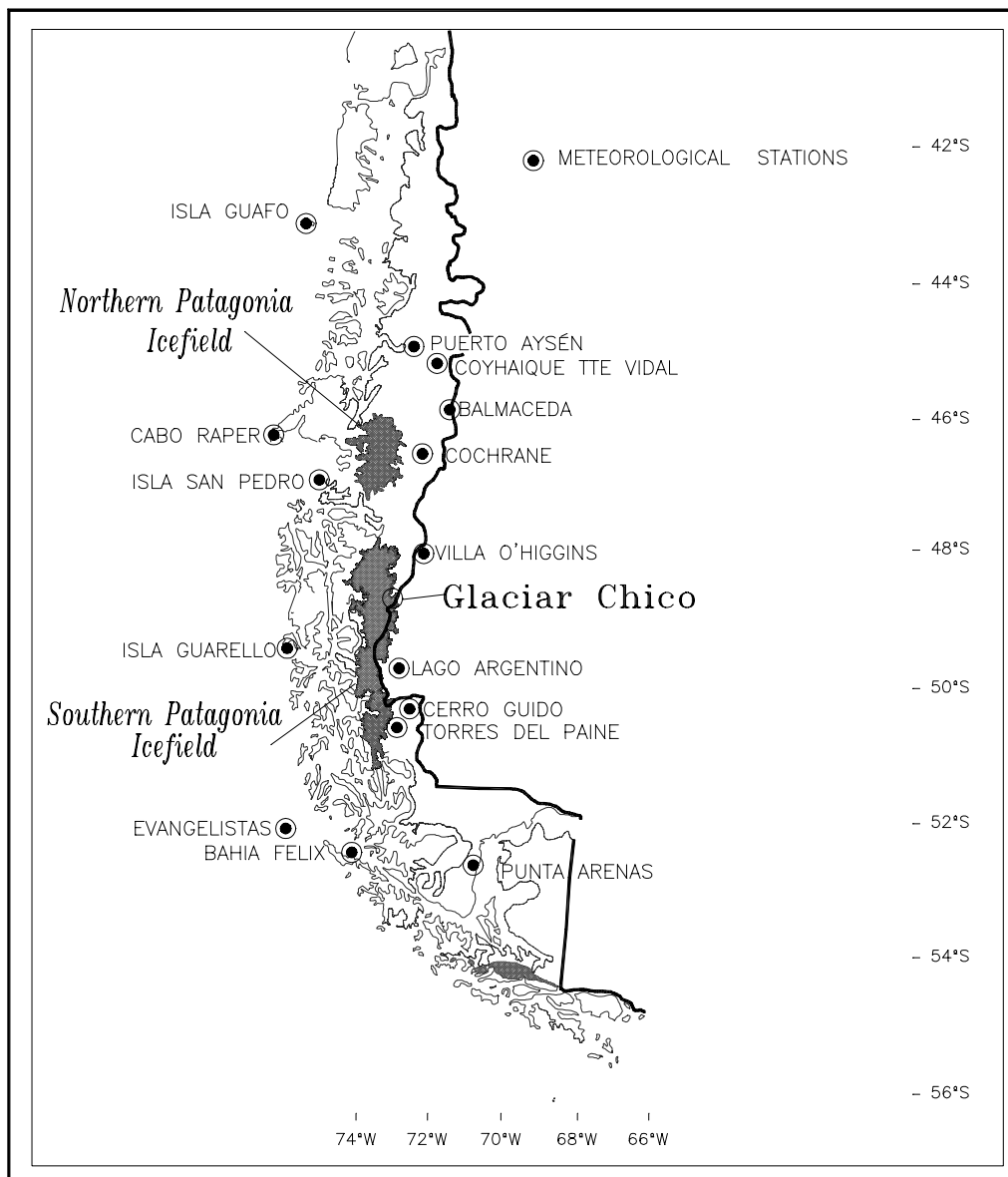
Figure 5.1 Location of meteorological stations described in the text.

In contrast, the eastern margin (Figure 5.2) is characterised by dry and cold steppes, interrupted by lakes of glacial origin generated during the Quaternary, and with some small mountain ranges associated with the main Andes chain (Clapperton, 1993). Climatically, this margin of the SPI exhibits more continental conditions, with fewer precipitation days per year compared with the western margin (for example, only 147 days of rainfall were registered at Punta Arenas (-53°S) in 2000, Buturovic (2001)). The annual precipitation across the eastern margin of the SPI is sharply reduced when compared with the amounts in the west, from an estimated maximum average of 6400 mm at the eastern side of the SPI (Escobar and others, 1992) to 800 mm at Villa O'Higgins (-48.47°S, Figure 5.1) located 34 km east of the SPI, and a minimum of 205 mm at Lago Argentino (-50.33°S), located 58 km east of the calving front of Glaciar Perito Moreno (Figure 5.1). This rain shadow effect of the Andes range is associated with strong and dry föhn winds in the east (Endlicher and Santana, 1988).

Precipitation series across western Patagonia have been analysed for several stations (Figure 5.1), with a secular decreasing trend observed at Isla Guafo (-43.57°S), Cabo Raper (-46.83°S) and Isla San Pedro (-47.72°S, Figure 5.1). This general trend is, however, interrupted by cycles of years with higher than normal precipitation recorded during the 1940s and 1950s, and most significantly, during the 1970s (Rosenblüth and others, 1995; Rivera and Casassa, 1999; Carrasco and others, 2002). Further south between Evangelistas (-52.4°S) and Bahía Felix (-52.97°S),

Rosenblüth and others (1995) detected a monotonic decrease in precipitation during most of the twentieth Century prior to the mid-1980s, with rainfall reductions of between 20 and 25%. Since 1983, Evangelistas station has registered a sharp increase in precipitation, which must be analysed with caution before further validation of the data (Carrasco and others, 2002).

On the eastern side of the SPI (Figure 5.2), the time series for Lago Argentino (-50.33°S) showed high inter-annual precipitation variability, with a weak decreasing trend during the second half of the last Century. More significantly, a cycle of years with higher than average precipitation was recorded during the 1960s, and a cycle with lower than average precipitation measured during the 1980s (Ibarzabal y Donángelo and others, 1996).
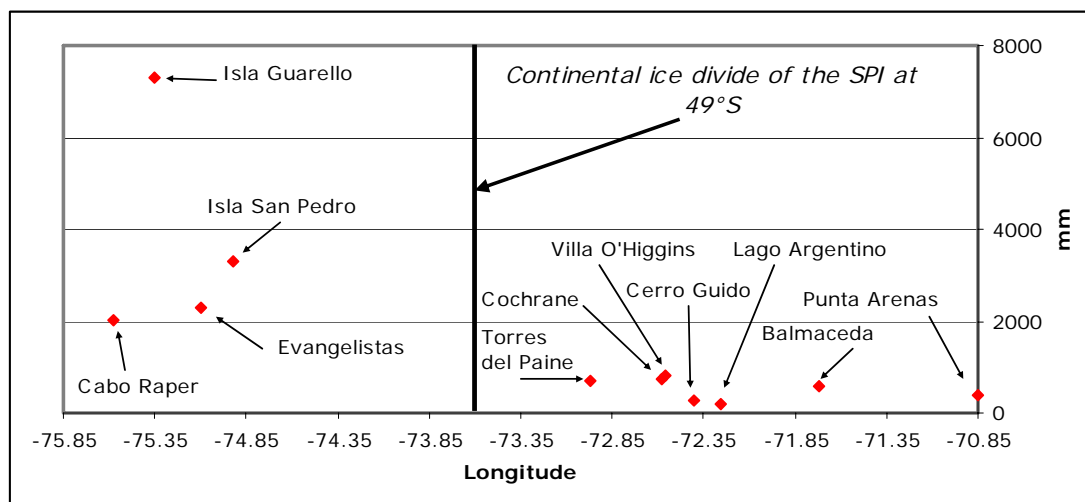
Figure 5.2 Annual precipitations on both sides of the SPI.

5.1.2. Temperature

The temperatures on both sides of the SPI also exhibit contrasting behaviour, with the maritime influence on the western margin of the SPI generating small seasonal oscillations. But the more continental environment of the eastern side ensures larger seasonal oscillations with colder winters and warmer summers (Carrasco and others, 1998).

Historical records of air temperature measured in Southern Patagonia during the twentieth Century show higher warming trends among eastern stations than the trends observed among western stations (Rosenblüth and others, 1997).

On the western side of the SPI two warming patterns have been described; one characterised for the area north of Puerto Aysén (-45.41°S, Figure 5.1) with no significant increase in annual mean temperature and only a weak minimum temperature increase between 1960 and 1992, specially during summer months (Rosenblüth and others, 1997), and the second pattern observed south of 46° S, where an undisputed warming appears in the records of Isla San Pedro (-47.22°S) and Evangelistas (-52.4°S) (Rosenblüth and others, 1995).

Most of the stations on the eastern side of the SPI showed warming trends of different rates. The most significant is the warming trend measured at Punta Arenas (-53°S, Figure 5.1), with a rate of 0.013 °C a^{-1} between 1933 and 1992, but accelerated warming between 1962 and 1992 when

the annual mean temperature increased by 0.021 °C a^{-1} (Rosenblüth and others, 1997). At other stations on the eastern margin of the SPI, for example Lago Argentino (-50.33°S, Figure 5.1), temperatures show only a weak warming trend of 0.01 °C a^{-1} between 1937 and 1990 (Ibarzabal y Donángelo and others, 1996).

Following analysis of temperatures at the 850 hectopascal (hPa) geopotential height at Punta Arenas (-53°S) from grid points of the National Center for Environmental Prediction / National Center for Atmospheric Research (NCEP/NCAR) 40 years reanalysis data, Carrasco and others (2002) estimated an overall warming trend of 0.98 °C between 1958 and 1998. The most significant period of this increase was between 1958 and 1985. This warming trend was mainly explained by an increase in winter temperatures at 850 hPa of 0.0455 °C a^{-1} between 1977 and 1998. During the same period, summer temperatures at 850 hPa showed a weak cooling trend of -0.0224 °C a^{-1}. Using NCEP-NCAR 40 years reanalysis project data obtained at grid points equally spaced between -42.5°S and -55°S and between -70°W and -77.5°W, Rasmussen and others (In press) also detected a warming trend at 850 hPa of ~0.5°C over 40 years between 1960 and 1999 at both, winter and summer months.

5.1.3. Macroscale climate

The temperature and precipitation series' obtained from Patagonian stations can be associated with large scale oceanic-atmospheric

phenomena present in the Pacific Ocean. These phenomena have been described by different indices, including the Pacific Decadal Oscillation (PDO) and the Southern Oscillation Index (SOI). The PDO is defined as the leading mode of October-March sea surface temperature variability across the Pacific Ocean poleward of 20° N (Mantua and others, 1997), and the SOI is defined as the twice-normalized Tahiti minus Darwin pressure anomalies (Trenberth and Shea, 1987).

These two indices are intrinsically related in their origin (the temperature anomalies of the tropical Pacific Ocean and their associated atmospheric changes), but have different time scales. The SOI is an inter-annual event, widely associated with changes in sea surface temperature caused by the El Niño Southern Oscillation (ENSO) oceanic-atmospheric phenomenon (Trenberth and Hurrell, 1994), whilst the PDO is a decadal event, also associated with sea surface temperatures in the tropical Pacific Ocean, but not well understood in its timescale and long-term dynamics (Biondi and others, 2001). Both the SOI and PDO have been correlated, such that warm (cold) phase ENSO-like conditions tend to coincide with the years of positive (negative) polarity in the PDO (Mantua and others, 1997). One of the best expressions of the interdependence between both indices is the change in sea surface temperatures recorded in the eastern tropical Pacific Ocean during recent decades, changing from cooler than normal to warmer than normal after the 1976 climate shift (Giese and others, 2002), and the increased number of El Niño-like events in recent years.

The PDO has been shown to modulate ENSO teleconnections in North America (Gershunov and Barnett, 1998), but very little is known about possible southern hemisphere teleconnections, in spite of evidence of significant decadal oscillations in the temperature series recorded at South American stations during last Century. These oscillations are characterised by two big changes around 1936 and 1976, namely the occurrence of negative temperature anomalies before 1936, and of positive temperature anomalies values after 1976 (Jones and others, 1994).

Several studies have also related higher than normal precipitation in central Chile (30° to 38°S) with negative phases of the SOI during warm events of El Niño years, whilst rainfall deficits were typically observed between 38° and 41°S during the same SOI phase (Rutlland and Fuenzalida, 1991; Montecinos and Aceituno, 2003). These years with warm ENSO phases are characterised by positive glacier mass balances at Glaciar Echaurren Norte in central Chile (33°S), whilst during the opposite phase of SOI in the so-called "La Niña" years, negative glacier mass balances have been observed (Escobar and others, 1995).

Analysing monthly mean records of climate data obtained from the NCEP/NCAR 40 years reanalysis project, Schneider and Gies (2004), detected a positive correlation (r=0.4) between SOI and precipitation rate anomalies at the western coast of southern Chile between 45°S and 55°S, with precipitation decreases by 15% during strong El Niño years. At the eastern side of the Andes, no significant correlation was found using NCEP-NCAR data.

Significant negative correlations between the SOI and mean annual temperature were found among stations located between 18°S and 33°S in Chile, with non-significant correlations among stations located further south. However, when a seasonal decomposition was applied to these more southerly stations, a weak positive correlation was found between winter and spring maximum temperatures and the SOI in the Patagonian area of Puerto Aysén-Punta Arenas between 1960 and 1992 (Rosenblüth and others, 1997).

For the period 1948-1983, Aceituno (1988) detected a significant mean temperature cooling at Punta Arenas (-53°S) during September and October months of El Niño years, mainly as a result of lower maximum temperatures. One explanation for this phenomenon has been its association with the presence of a blocking anticyclone over the Bellinghausen sea (90°W) during El Niño years, causing cold air to be advected over the Patagonian region (Rutllant and Fuenzalida, 1991). Garreaud (1995) considered a second possibility, related to a blocking effect over the northeast sector of the Weddell Sea (around -55°S, -40°W), that favours the occurrence of quasi-stationary fronts over Central Chile and low temperatures in southern Patagonia.

In synthesis, the ENSO and PDO indices could play an important role in the climate variability experienced within Patagonia, and therefore, they could be important for the glacier mass balance of the SPI. However, the

lack of detailed, systematic and validated climatic data from the region make it difficult to establish an accurate relationship.

In this chapter, the climatic series' obtained from selected stations located close to the SPI will be analysed in terms of their seasonal and inter-annual variations. They also will be compared with PDO annual values, in order to investigate possible teleconnections between the tropical Pacific Ocean and the Patagonian region at a decadal scale.

5.2 Data and methods

Records are available from several meteorological stations in southern Patagonia (Table 5.1), but most of them lack continuity and contain many gaps.

All the stations on the western side of the SPI are located along the coast, and are operated by the Chilean Navy Hydrographic Service (SHOA), who maintain lighthouses all around the fjords and channels of southern Chile. Some of these stations were installed at the beginning of the 20th Century, but most of the datasets are only available until the 1980s and have numerous gaps.

Two Chilean governmental agencies are in charge of the eastern stations; the Chilean Meteorological Office (DMC) and the Public Works Ministry (DGA). The DMC has been responsible for providing meteorological information to the airports of the region since the 1950s, and thus has the

most complete and systematic meteorological data series. Since the 1980s the DGA has been operating meteorological stations, many of which have been installed in remote places like Villa O'Higgins (-48.47°S, a small town of 300 inhabitants, Figure 1.3 and 5.1) and at a police station in Cerro Guido (-50.88°S, Figure 5.1). These stations are closer to the SPI than the stations operated by DMC and SHOA, however, the series are the shortest and contain many gaps in the data.

One of the stations used here is located at the airport of Calafate in Argentina (Lago Argentino, -50.33°S, Figure 5.1, Table 5.1). The precipitation and temperature data for this station were downloaded from the NASA Goddard Institute for Space Studies (GISS), USA (http://www.giss.nasa.gov/data/). Some months without data in the GISS data set were completed with data provided by Jorge Strelin, (CADIC, Ushuaia, Argentina). No data filling procedure was applied to the precipitation series of this station.

Table 5.1 Meteorological stations discussed in the text.

Name of Station	Latitude (S)	Longitude (W)	Height (m)	Operator	Margin of the Ice fields	Distance to Glaciar Chico* (km)
Isla Guafo	-43.57	-74.75	140	SHOA	West	635
Puerto Aysén	-45.41	-72.70	11	SHOA	West	420
Coyhaique Tte Vidal	-45.60	-72.10	310	DMC	East	405
Balmaceda	-45.90	-71.72	520	DMC	East	382
Cabo Raper	-46.83	-75.58	40	SHOA	West	318
Cochrane	-47.26	-72.58	182	DMC	East	218
Isla San Pedro	-47.72	-74.92	22	SHOA	West	206
Villa O'Higgins	-48.47	-72.56	260	DGA	East	93
Lago O'Higgins en tenencia	-48.88	-72.74	300	DGA	East	48
Lago Argentino	-50.33	-72.26	220	Argentina	East	145
Isla Guarello	-50.35	-75.35	15	SHOA	West	201
Cerro Guido	-50.88	-72.40	82	DGA	East	196
Torres del Paine	-51.18	-72.97	46	DGA	East	222
Evangelistas	-52.40	-75.10	55	SHOA	West	381
Bahía Félix	-52.97	-74.07	15	SHOA	West	426
Punta Arenas	-53.00	-70.85	37	DMC	East	457

Notes:

* With respect to base camp used at the accumulation area (Figure 2.2).

Argentina, Servicio Meteorológico Argentino.

DGA, Dirección General de Aguas del Ministerio de Obras Públicas, Chile.

DMC, Dirección Meteorológica de Chile.

SHOA, Servicio Hidrográfico de la Armada de Chile.

5.2.1. Completion of partial data series

The stations used in this thesis can be separated into four groups based on the procedure used to complete and homogenise the data series:

1. The Punta Arenas (-53°S) precipitation and temperature series and the Puerto Aysén (-45.41°S) temperature series were completed and homogenised by Rosenblüth and others (1995).

2. Several precipitation series (Table 5.2) were filled and homogenised by means of time-series modelling and correlation with nearby stations by the DMC (Jorge Carrasco, personal communication).

3. No homogenisation or gap filling was performed on the precipitation series of the other stations because of the lack of nearby long term records.

4. The monthly temperature series of Coyhaique Tte Vidal (-45.6°S), Cochrane (-47.26°S) and Lago Argentino (-50.33°S) were completed in this thesis.

Table 5.2 Available precipitation data series.

Meteorological Station	Record duration		Method of filling data gaps	Annual average 1961-1991 (mm)*
	From	To		
Isla Guafo	January, 1908	December, 2000	DMC	1604
Puerto Aysén	January, 1931	December, 2000	DMC	2645
Coyhaique Tte Vidal	January, 1950	December, 2000	DMC	1353
Balmaceda	February, 1961	December, 2002	No data gaps	600
Cabo Raper	January, 1914	December, 1983	Not completed	2033
Cochrane	January, 1950	March, 2002	DMC	700
Isla San Pedro	January, 1933	September, 1989	Not completed	3305
Villa O'Higgins	October, 1993	October, 2002	Not completed	800
Lago Argentino	January, 1937	December, 1999	Not completed	205
Isla Guarello	January, 1949	June, 1963	Not completed	7313
Cerro Guido	January, 1984	January, 2003	Not completed	261
Torres del Paine	May, 1982	January, 2003	Not completed	716
Evangelistas	January, 1899	December, 1984	Not completed	2280
Bahía Félix	June, 1913	April, 1986	Not completed	4061
Punta Arenas	January, 1911	December, 1991	*Rosenblüth and others (1995)*	371

the exact period used between 1961 and 1991 varies for each station depending on data availability

In order to complete the temperature series of the stations listed in Table 5.3, the following procedure was adopted, based upon Rosenblüth and others (1995):

1. A regression analysis was carried out between all the stations. The stations with high correlations (r^2 greater than 0.95) were grouped and compared.

2. The regression equation obtained between stations with the highest correlation was used to generate a modelled series.

3. A residual analysis was carried out in order to estimate the errors of the modelled and observed series.

4. The best fit regression equation was used to fill the gaps of the series.

One of the most complete and reliable stations of southern Patagonia is Balmaceda (-45.9°S), which is operated on a daily basis by professional personnel working at the main airport of the region. Data collected at Balmaceda were analysed in comparison with the other stations located on the eastern side of the SPI in order to fill their gaps, yielding correlation coefficients higher than 0.95 in all cases (Tables 5.4 to 5.6). The resulting regression equations were applied to the observed data, generating a random distribution of residuals ranging from -2 to +2°C, with higher errors for the minimum temperatures and lower errors for the maximum temperatures.

Table 5.3 Available temperature data series.

Meteorological Station	Temperature		Method of filling data gaps
	From	To	
Puerto Aysén	January, 1932	December, 1992	Rosenblüth and others (1995)
Coyhaique Tte Vidal	January, 1961	December, 2001	This study
Balmaceda	January, 1961	December, 2001	No gaps
Cochrane	July, 1969	March, 2002	This study
Lago Argentino	January, 1961	December, 2001	This study
Punta Arenas	January, 1905	December, 1992	Rosenblüth and others (1995)

Note: All the data gaps are non contiguous months were some isolated instrumental or personnel problem avoided data collection.

Table 5.4 Parameters used to fill the gaps of Cochrane.

Regression parameters	Independent station: Balmaceda	
	Dependent station: Cochrane (January 1969 to March 2002)	
	Minimum monthly temperatures	Maximum monthly temperatures
Number of gaps (months)	14	16
Constant	0.985	0.295
Standard error of dependent estimation (Y)	0.992	0.955
Correlation coefficient	0.956	0.986
Number of Observations	381	379
Degrees of Freedom	379	377
X Coefficient	0.949	1.093
Standard error of X Coefficient	0.015	0.010

Table 5.5 Parameters used to fill the gaps of Coyhaique Tte Vidal.

Regression parameters	Independent station: Balmaceda Dependent station: Coyhaique Tte Vidal (January 1961 to March 2001)	
	Minimum monthly temperatures	Maximum monthly temperatures
Number of gaps (months)	2	3
Constant	2.239	1.729
Standard error of dependent estimation (Y)	0.756	0.507
Correlation coefficient	0.972	0.994
Number of Observations	441	440
Degrees of Freedom	439	438
X Coefficient	0.928	0.972
Standard error of X Coefficient	0.011	0.005

Table 5.6 Parameters used to fill the gaps of Lago Argentino.

Regression parameters	Independent station: Balmaceda Dependent station: Lago Argentino (January 1961 to March 2002)
Number of gaps (months)	22
Constant	0.196
Standard error of dependent estimation (Y)	1.009
Correlation coefficient	0.976
Number of Observations	470
Degrees of Freedom	468
X Coefficient	1.0658
Standard error of X Coefficient	0.011

The completed temperature and precipitation series were visually interpreted using an exponential filter smoothing function described by Rosenblüth and others (1995). By applying this filter twice, once forward and once backward in time, the phase is preserved and the inter-annual variability reduced. The filter is described by the following equations:

$$y_t = cx_t + (1 - c)y_{t-1} \qquad t=2,3,\ldots\ldots\ldots\ldots\ldots N \qquad \text{Eq. 5.1}$$

$$z_t = cy_t + (1 - c)z_{t+1} \qquad t=(N\text{-}1),\ (N\text{-}2),\ldots,3,2,1 \qquad \text{Eq. 5.2}$$

Where x_t is the original data value at time t,

y_t is the intermediate smoothed value at time t,

z_t is the output of the filter at time t,

c is a coefficient determining the degree of smoothing, ranging between 0 (maximum smoothing) and 1 (no smoothing).

The filtering process needs to be initialized in both directions, therefore in the forward stage, the first smoothing value (y_1) is taken to be the average from a number of years of the series. Rosenblüth and others (1997) used five years, whilst Carrasco and others (2002) used seven. Here, five years will be used to calculate "y_1" in order to make the completed series compatible with the longer series of Rosenblüth and others (1997). In the backward stage, z_N was taken as the final value of y, therefore, the final value in the output inherits the previous value from the intermediate variable (Rosenblüth and others, 1997).

Rosenblüth and others (1997) used a value of 0.11 for c, whilst Carrasco and others (2002) used a value of 0.25 for c. In this thesis a value of 0.25 will be applied, because when this value was used by Rosenblüth and others (1995), it resulted in an acceptable level of high-frequency smoothing but without excessive filtering that removed important multi-

annual variations. This latter requirement is necessary as the subject of this thesis is more concerned with decadal variations and how they affect the mass balance of the Patagonian glaciers, rather than general trends of temperature or precipitation variation.

The general trends of precipitation and temperatures were achieved based upon regression analysis of the completed unfiltered monthly data. The errors of these trend rate were also obtained from the regression analysis, after analysing the standard deviation of the series. In order to calculate the significance of the temperature and precipitation series trends, a two-tail Student t test was applied to each data set. This calculation has some limitations specially regarding autocorrelation in the time-series when the number of effectively independent observations is not well accounted using the residuals of the regression (Vaughan and others, 2003), however, the approach used here has been widely applied to climatic data (Rosenblüth and others, 1997).

5.2.2. Derivation of comparable indices

The monthly PDO values were downloaded directly from http://jisao.washington.edu/pdo/PDO.latest, a web site maintained and frequently updated by Nathan Mantua of the University of Washington, Seattle, USA. In order to calculate an annual index based upon the monthly values, the average monthly October-March values will be used, as proposed by Biondi and others (2001).

To compare the climatic series' obtained from the different stations, an index was calculated for each station, defined as

$$I = \frac{(x_a - x_{med})}{\sigma}$$

Eq. 5.3

where I is the annual anomaly,

x_a is the observed annual value,

x_{med} is the inter-annual average and

σ is the standard deviation of x_{med}.

5.3 Regional precipitations

5.3.1 Seasonality

For the purposes of this discussion, winter is taken to be June, July and August (JJA) and summer to be January, February and March (JFM).

The highest annual average precipitation along the western margin of Patagonia was recorded at Isla Guarello (-50.35° S) between 1949 and 1963, with a total of 7313 mm a^{-1} (Table 5.1 and Figure 5.1). Toward the north and south of Isla Guarello (-50.35° S), the precipitation totals are smaller and exhibit a regional seasonal pattern (Figure 5.3), with predominant winter precipitation to the North (Isla Guafo, -43.57°S, Figure 5.3). There appear to be no seasonal differences at Cabo Raper (at -46.83°S, between Isla Guafo and Isla Guarello), but a degree of seasonality further south with minimum winter precipitation in

Evangelistas (-52.4°S, Figure 5.3). The three stations discussed above are located on islands on the western side of Patagonia, representing the first topographic barrier to the western frontal systems. Further inland, between the fjords and the SPI, a second line of stations show a similar pattern of seasonality, but with higher total amounts of precipitation (Figure 5.4). The spatial distribution of the precipitation along the western side of the SPI is thus mainly controlled by orographic uplift of the predominant westerlies, with a positive linear trend between altitude and precipitation (Carrasco and others, 2002).

The observed seasonality is mainly explained by the north-south displacement of the axis of the westerlies in the southern hemisphere. This is a function of the position of the Jet stream and the subtropical anticyclone cell of the south-eastern Pacific Ocean, which reaches its northernmost position during the austral winter, and its southernmost position during the austral summer (Montecinos and Aceituno, 2003; Rutllant and Fuenzalida, 1991).
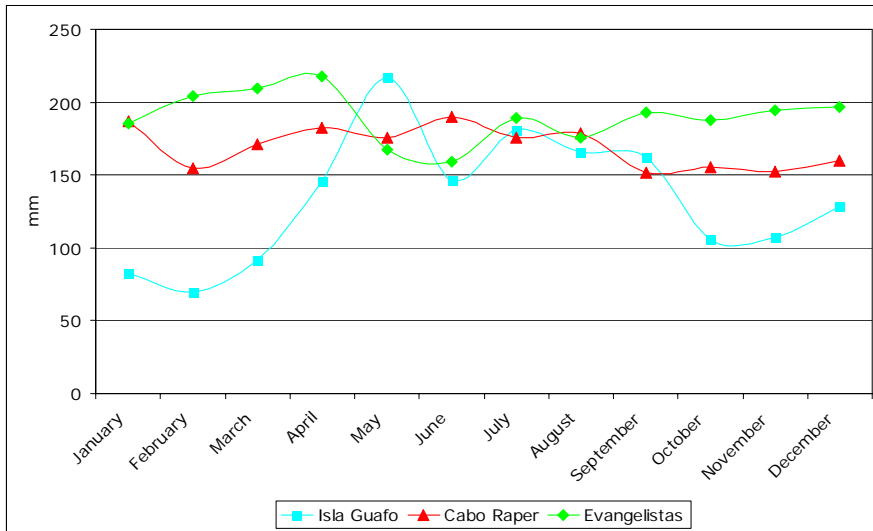
Figure 5.3 Average monthly precipitation at selected stations along the western margin of Patagonia, using available data recorded between 1961-1990.
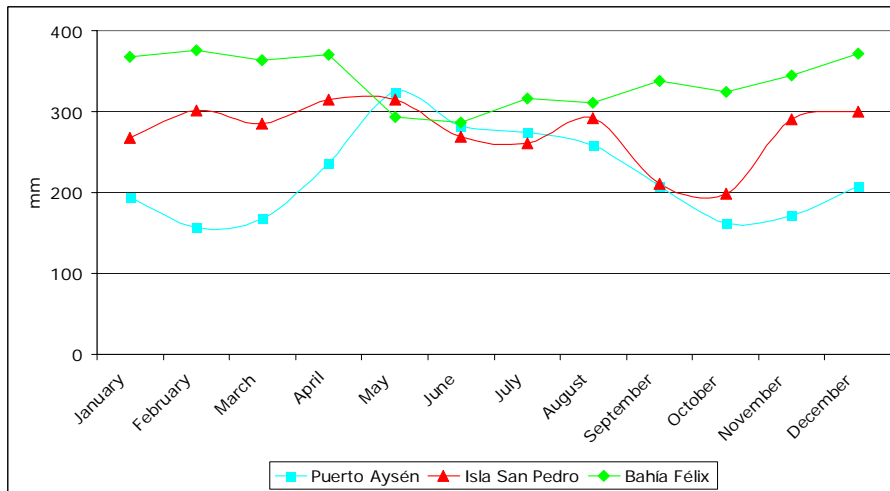
Figure 5.4 Average monthly precipitation of selected stations inland from those shown in Figure 5.3 using available data recorded between 1961-1990 (note the different scale on the y-axis).

A similar pattern of seasonality is also observed among the eastern stations (Figure 5.5), with a maximum winter precipitation in Cochrane (-47.26°S), a predominant but not significant winter precipitation in Lago Argentino (-50.33°S), and no clear seasonality in Punta Arenas (-53°S).
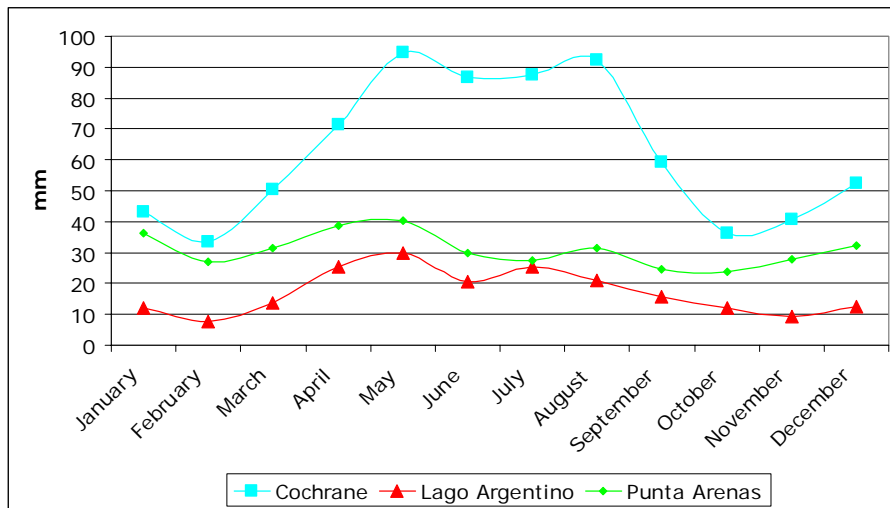
Figure 5.5 Average monthly precipitation of selected stations using available data registered between 1961-1990. Punta Arenas data obtained from Rosenblüth and others (1995).

The spatial distribution of total precipitation along the eastern side of the SPI is mainly controlled by the distance to the main mountain chain of the Andes, with maximum precipitation occurring at the highest summits of the SPI and a sharp decrease toward the east, reaching a minimum only a few km away from the terminal positions of the glaciers.

5.3.2 Precipitation series

5.3.2.1 Western stations

Station Puerto Aysén (-45.41°S, Table 5.1 and 4.2, Figure 5.1) is located at the eastern end of the Homonymous Fjord, in a glacial valley surrounded by mountains up to 2000 m asl. Precipitation has been recorded at this station since 1931 (Figure 5.6), and shows a general trend of decline in annual values, only interrupted during the early 1960s when a cycle of years with precipitation higher than average was registered. Since then, the precipitation has decreased until 2000. The average reduction of precipitation between the periods 1931-1960 versus 1961-1990 is approximately 300 mm, representing 10% of the 1931-1960 annual average precipitation (Table 5.7).

Table 5.7 Precipitation trends.

Station	Precipitation trend	Period
Puerto Aysén	-27 ± 6 mm a^{-2}**	1961-1990
Coyhaique Tte Vidal	-25 ± 6 mm a^{-2}**	1961-1990
Balmaceda	-8 ± 3 mm a^{-2}*	1962-1990
Cochrane	-6 ± 4 mm a^{-2}	1961-1990
Lago Argentino	-7 ± 2 mm a^{-2}**	1965-1990

Notes: * Significant at the 5% level, ** Significant at the 1% level

As described in Section 5.3.1, the seasonality in precipitation at Puerto Aysén between 1961 and 1990 shows a clear winter maximum (Figure

5.4). However, when compared with the seasonal values recorded between 1931 and 1960 it was evident that an important change had occurred in summer precipitation totals (Figure 5.7), with a reduction of 22% over the 1931-1960 precipitation. This decrease in summer precipitation could be an indicator that the average axis of the westerlies has shifted south in recent decades, causing the blocking anticyclone typically observed in Central-South Chile (33-45°S) to increase in area and extend further south.

Figure 5.6 Annual precipitation series of Puerto Aysén 1931-2000. The thick curve represents the smoothed exponential trend and the squares are the annual precipitation values.
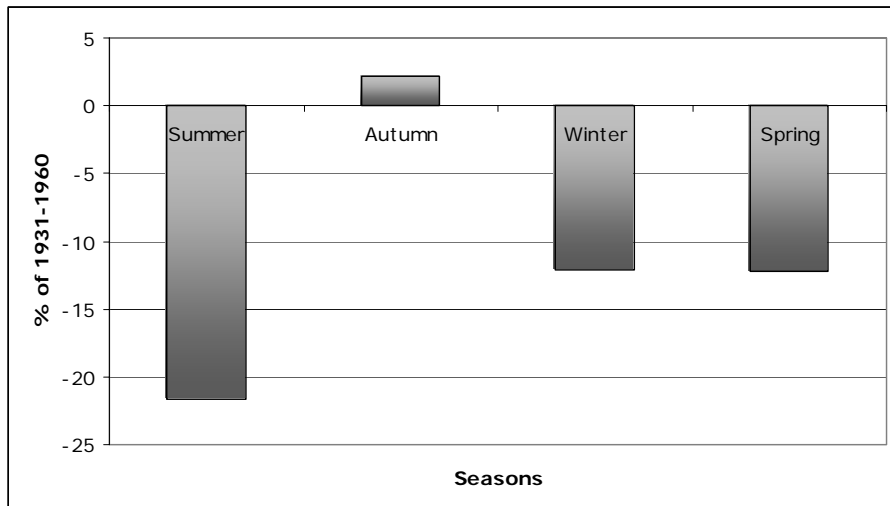
Figure 5.7 Average precipitation per season at Puerto Aysén for the period 1961-1990 compared with the period 1931-1960.

When the PDO values were compared to the index of precipitation anomalies for Puerto Aysén (based upon Equation 5.3), no conclusive relationship could be established for the whole series (Figure 5.8). However, the cycle of maximum precipitation recorded during the 1960s is well correlated to negative values of the PDO. The 1976 shift in the PDO to positive temperature anomalies is also well correlated with a significant reduction in precipitation, and, during the recent decades that have been characterised by negative precipitation anomalies, the PDO has shown a general positive predominance. These relationships suggest a general trend of lower than normal precipitation during periods with frequent El Niño years, and higher than normal precipitation during periods with a higher frequency of La Niña years.
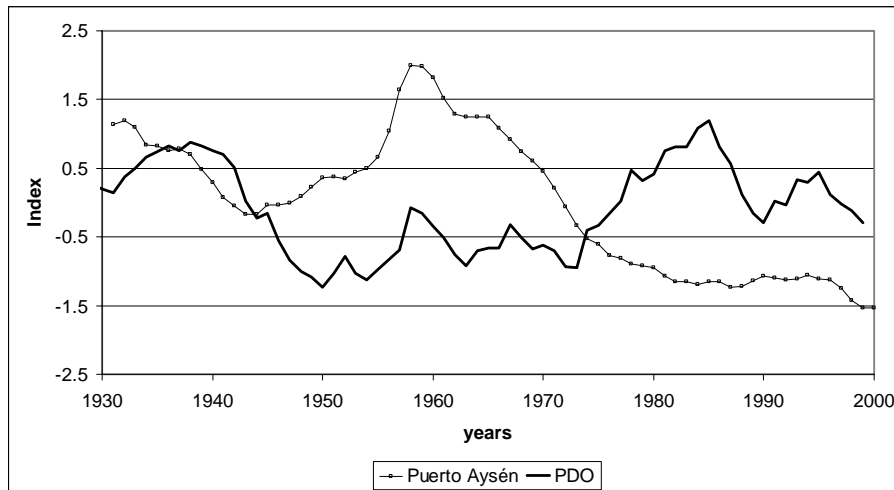
Figure 5.8 Index of Puerto Aysén annual precipitation anomalies and PDO index values in the period 1931-2000.

5.3.2.2 Eastern stations

Coyhaique Tte Vidal station (-45.6°S) is located at the city airport of the regional capital (Coyhaique), more than 400 km to the north east of Glaciar Chico. The precipitation series from this station shows two distinctive patterns, firstly a cycle of years with higher than average precipitation records between 1950 and 1980, reaching a maximum of 2242 mm in 1966, and secondly, between 1980 and 2000 characterised by lower annual values than the previous period, but with no trend of change. Overall, the annual precipitation recorded during the 1990s is approximately 130 mm less than the 1950-2000 average (Figure 5.9).
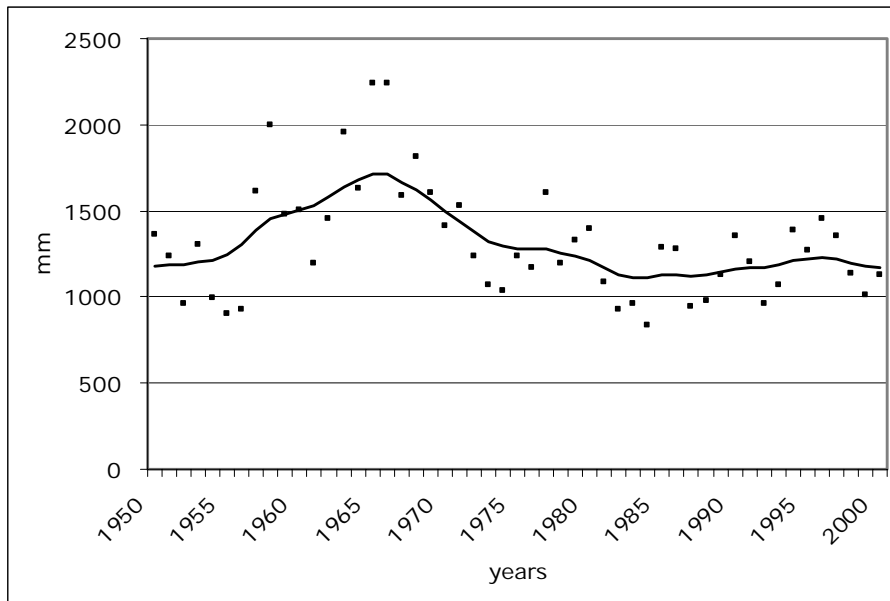
Figure 5.9 Coyhaique Tte Vidal precipitation series between 1950 and 2000. The squares show the mean annual value. The thick line shows the values produced by the exponential smoothing filter.

Balmaceda station (-45.9°S) is located 2 km from the border with Argentina, at the western edge of the Argentinean pampas. Precipitation records at this station are available since 1962, and the general trend shows a reduction in the total annual values (Table 5.7). This was most significant between 1962 and the mid 1980s, after which no general trend is apparent (Figure 5.10).
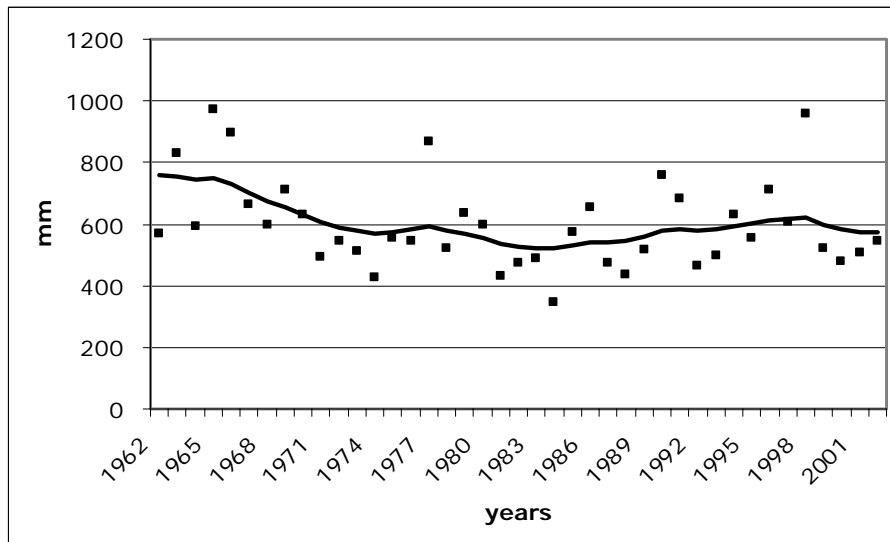
Figure 5.10 Balmaceda precipitation series between 1962 and 2001. The squares show the mean annual value. The thick line shows the values produced by the exponential smoothing filter.

Cochrane station (-47.26°S) is located at the eastern margin of the NPI, and therefore, could be considered to be representative of the rain shadow effect generated by the Patagonian icefields of the Andean mountains. Two distinctive patterns are observed in the precipitation series, firstly, a cycle with higher than average precipitation between 1950 and the mid-1970s, with a maximum record of 1215 mm in 1965, and secondly, a succession of years with lower than average precipitation during the 1980s but no clear trend of change (Figure 5.11).
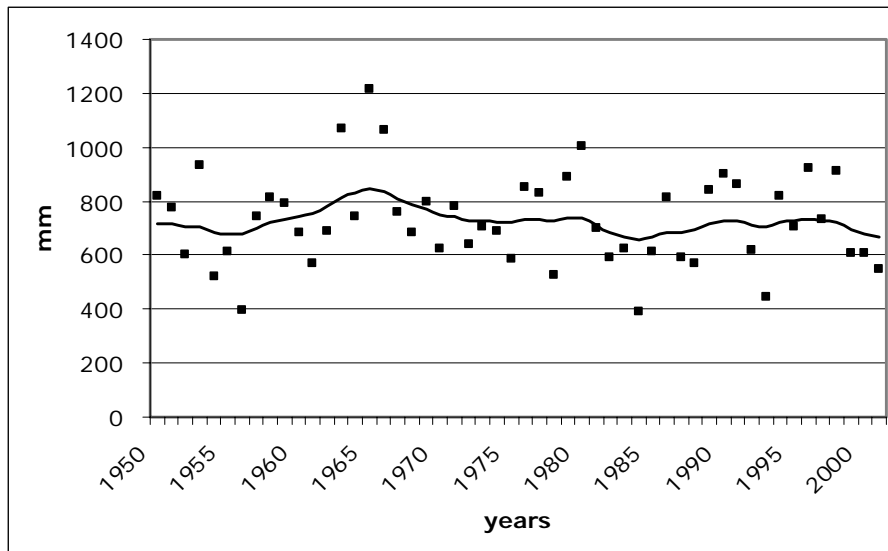
Figure 5.11 Cochrane precipitation series between 1950 and 2001. The squares show the mean annual value. The thick line shows the values produced by the exponential smoothing filter.

The records from the station at Lago Argentino (-50.33°S) were originally analysed by Ibarzabal y Donangelo and others (1996) who detected many data gaps in the series which were not filled. Here the series have been updated to 1999 and no data gap filling procedure has been applied (Figure 5.12). No general trend was observed in the overall period, but between 1965 and the early 1990s, a reduction in precipitation was clearly visible (Table 5.7). Over the last ten years, the annual precipitation values have increased to totals similar to those observed during the previous cycle of high precipitation in the 1960s.
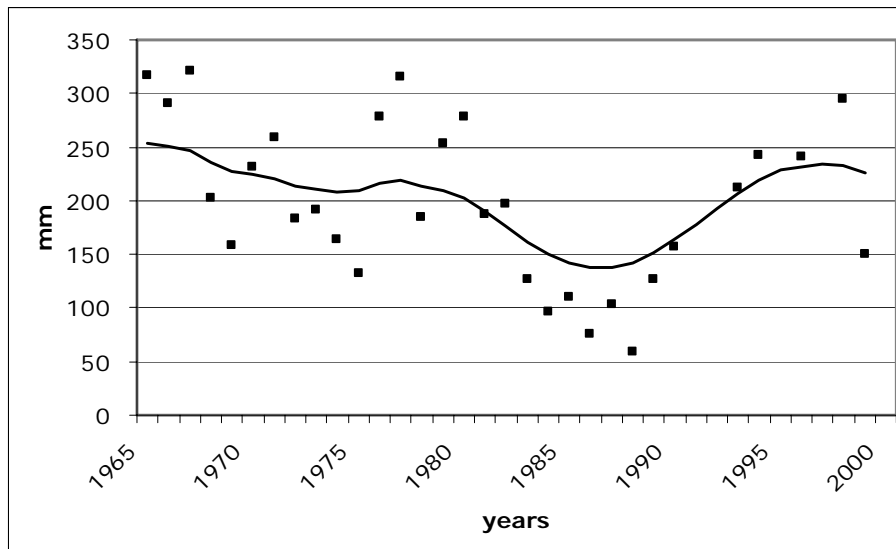
Figure 5.12 Lago Argentino annual precipitation series 1965-1999. The squares show the mean annual value. The thick line shows the values produced by the exponential smoothing filter. The series present several data gaps especially during the 1990s.

5.3.3 Comparison with PDO values

In Figure 5.13, the index of precipitation anomalies (based upon Equation 5.3) calculated for the eastern stations are compared with the PDO values between the years 1950 and 2000. The first temporal pattern previously described for each station, i.e. a positive period with high precipitation between the 1950s and 1970s seems to be well correlated with lower than average PDO values. The second pattern, of a general reduction in precipitation at all the stations around the mid-1970s, could be associated with the positive PDO cycle initiated after the 1976 climate shift. During this cycle, the maximum PDO value was recorded in 1985, synchronous with some of the lowest precipitation anomalies for all the stations. During the 1990s, the PDO values have fluctuated around zero without a

significant trend, whilst the precipitation totals are in general higher than during the 1980s, but, with the exception of Lago Argentino which shows a significant increase in precipitation, without a noticeable trend.
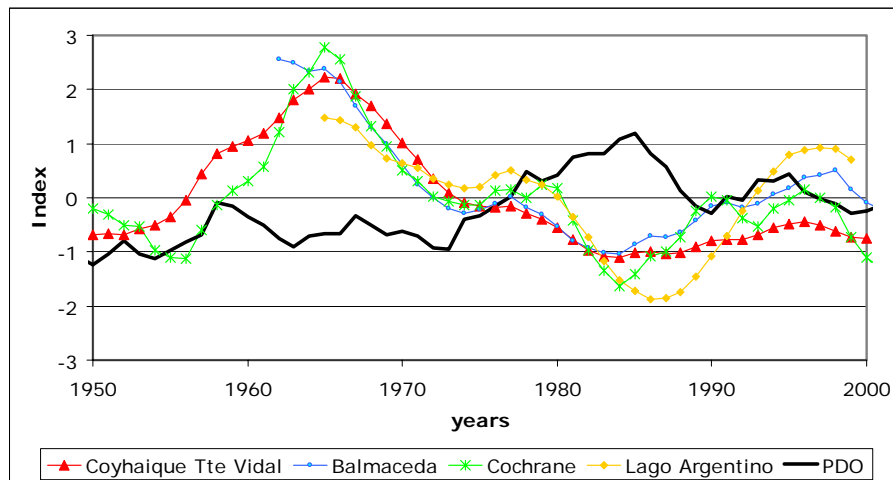
Figure 5.13 Eastern station index of precipitation anomalies between 1950 and 2000, compared with PDO index values.

The relationships shown in Figure 5.13, suggest that higher precipitation occurs during more frequent La Niña years, with this pattern reversed during periods with more frequent El Niño events. This trend is consistent with the precipitation pattern observed in central-south Chile, where it is well known that during El Niño years, the eastern Pacific Ocean anticyclone is displaced north of its normal position, thus allowing frontal systems from the west to penetrate central and northern Chile, generating higher than average precipitation between -26° and -38°S (Rutllant and Fuenzalida, 1991). In this context, it is therefore probable that the Patagonian region experiences less than normal precipitation during El Niño years, especially if the high pressure cell located around the Bellinghausen sea has migrated north, blocking and displacing the

western frontal systems to central-southern Chile, as described by Rutlland and Fuenzalida (1991). Conversely, during La Niña years, the axis of the westerlies is displaced towards the south due to a stronger and more southerly eastern Pacific Ocean anticyclone cell, thus generating drought conditions in central-southern Chile (-26 to -41°S), and, possibly, higher precipitation in southern Patagonia.

5.4 Regional temperatures

5.4.1 Seasonality

The mean annual temperature measured at the stations surrounding the SPI is between 6°C and 9°C, with a regional lapse rate of 6°C km^{-1} (DGA, 1987). A similar lapse rate value (6.5°C km^{-1}) was estimated for the region including the SPI by Kerr and Sugden (1994), in spite of the complex variability in temperatures observed over glaciers and different land-cover types. Along the eastern margin of the SPI, Stuefer (1999) calculated a higher temperature lapse rate of 8°C km^{-1}, while on the western side of the NPI, Sessions (1975) measured an average lapse rate of 5 °C km^{-1}. These differences between the east and west slopes of the ice fields are consistent with the contrast in maritime and continental climatic behaviour across the SPI.

The seasonal variations in the annual temperature of selected stations, can be observed in Figure 5.14. These stations have been selected, because they have the longest temperature records of the region and they

are the closest to Glaciar Chico. To permit the comparison of records obtained at different altitudes, a regional temperature lapse rate of 6.5 °C km^{-1} was applied to all stations in order to calculate the mean monthly temperatures at sea level.

The most westerly station with available temperature data (Puerto Aysén, Figure 5.14), shows the smallest seasonal range with relatively higher temperatures during the winter and lower temperatures in the summer. All the other stations, located on the eastern margin of the SPI, show a higher winter-summer amplitude. The coldest month recorded by all the stations is July, and the maximums are typically observed during January.
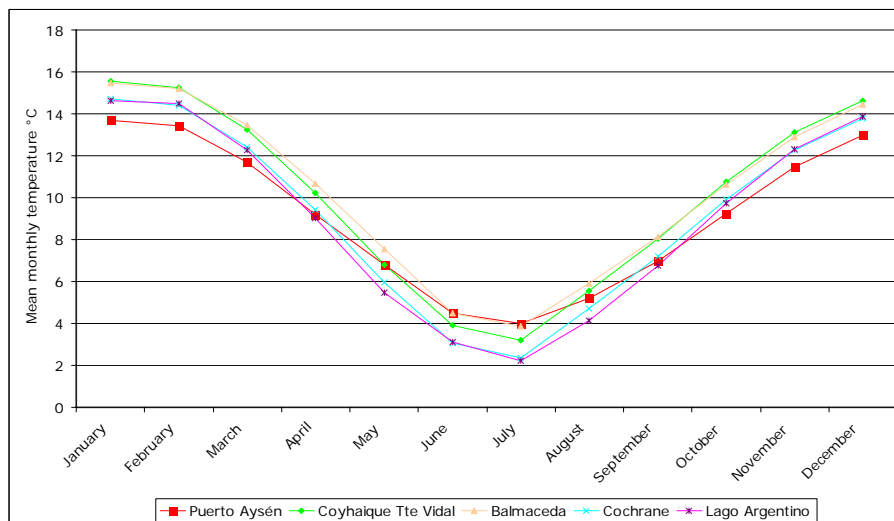
Figure 5.14 Mean monthly temperatures (°C) between 1961 to 1990. For ease of comparison, the values have been converted to sea level altitude for each station, using a temperature lapse rate of 6.5 °C km^{-1}.

5.4.2 Temperature series

5.4.2.1 Western station

The only station on the western side of the SPI with available temperature data is Puerto Aysén (-45.41°S, Figure 5.1). This dataset was analysed by Rosenblüth and others (1997), but they did not identify any significant inter-annual trend for either the mean, maximum or minimum temperatures (Figure 5.15 and Table 5.8). However, a decadal oscillation was obtained after applying the exponential smoothing filter, resulting in three cycles, around 1945, 1965 and 1985 (Figure 5.15).
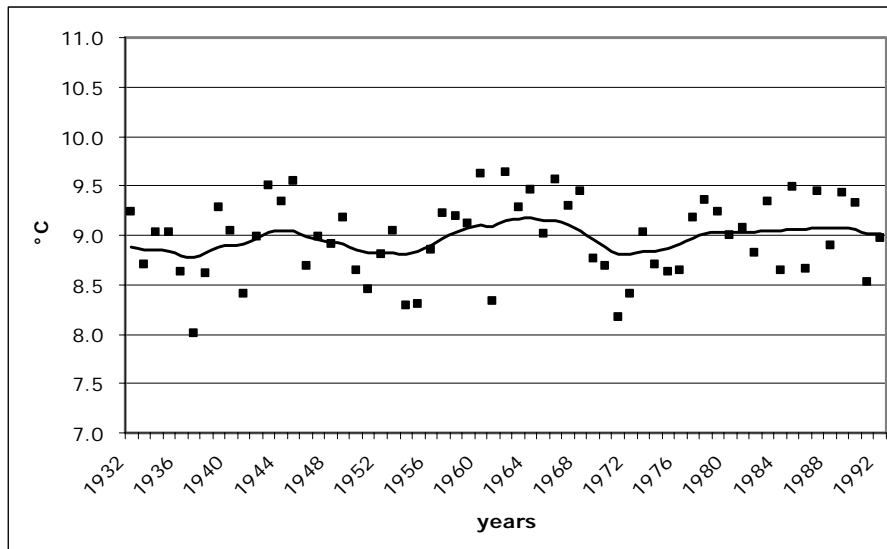
 Figure 5.15 Mean annual temperatures at Puerto Aysén between 1932 and 1992. The squares show the mean annual value. The thick line shows the values produced by the exponential smoothing filter. No significant trend was observed in this record.

Table 5.8 Temperature trends 1961-1990 (°C a^{-1}).

Station	Minimum Temperature	Mean Temperature	Maximum Temperature
Puerto Aysén[1]	0.006	-0.004	-0.006
Coyhaique Tte Vidal	-0.012 ± 0.010	0.001 ± 0.001	0.014 ± 0.012
Balmaceda	0.012 ± 0.011	0.019 ± 0.011	0.026 ± 0.012*
Cochrane (1969-1990)	0.029 ± 0.013*	0.033 ± 0.013 *	0.040 ± 0.016*
Lago Argentino	n/a	0.028 ± 0.011*	n/a
Punta Arenas[1]	0.039**	0.021*	-0.004

[1]   Period 1960-1992 based upon Rosenblüth and others (1997)
*   Significant at the 5 percent level
**   Significant at the 1 per cent level

5.4.2.2 Eastern stations

Coyhaique Tte Vidal station (-45.6°S) also appears to have no significant temperature trends in any of the analysed series (Table 5.8). The mean annual temperature at this station (Figure 5.16) does show some decadal oscillation, with a decrease in the 1960s to a minimum in 1973, and an increase from 1976 to 1982, but no significant trend during the 1990s. The other stations located along the eastern side of the SPI do show some significant trends (Table 5.8) between 1961 and 1990, most notably the maximum temperatures of Balmaceda (Figure 5.17), the mean temperatures of Cochrane (Figure 5.18), and the mean temperatures of Lago Argentino (Figure 5.19). Further south, Rosenblüth and others (1997) also reported significant warming trends in the minimum and mean temperatures of Punta Arenas. However, when the temperature series are analysed up to year 2000, the warming trends are much

weaker due to the higher inter annual variability observed during the 1990s.
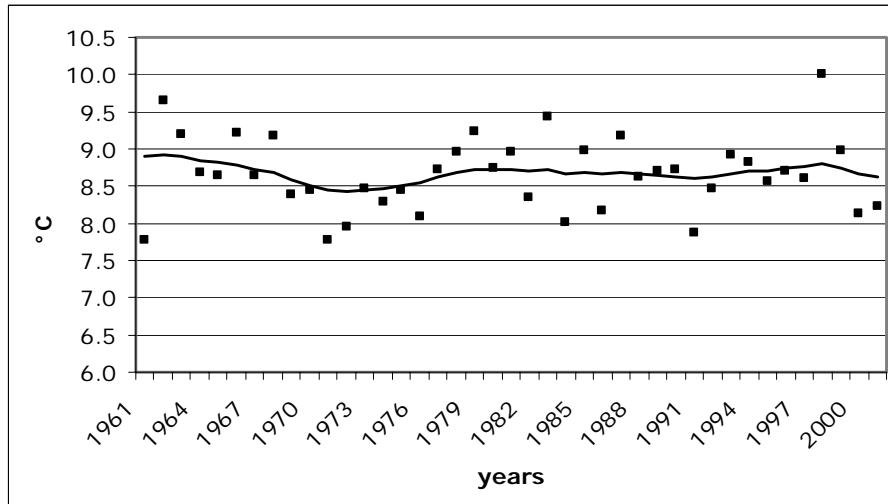
Figure 5.16 Mean annual temperatures at Coyhaique Tte Vidal between 1961 and 2001. The squares show the mean annual value. The thick line shows the values produced by the exponential smoothing filter. No significant trend was observed.
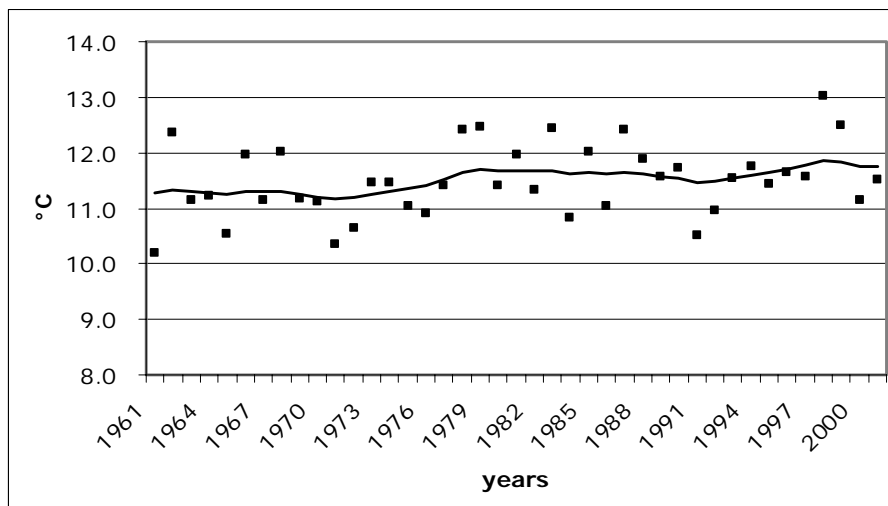
Figure 5.17 Maximum mean temperatures at Balmaceda between 1961 and 2001. The squares show the mean annual value. The thick line shows the values produced by the exponential smoothing filter. A significant warming trend at the 5% level was observed between 1961 and 1990.
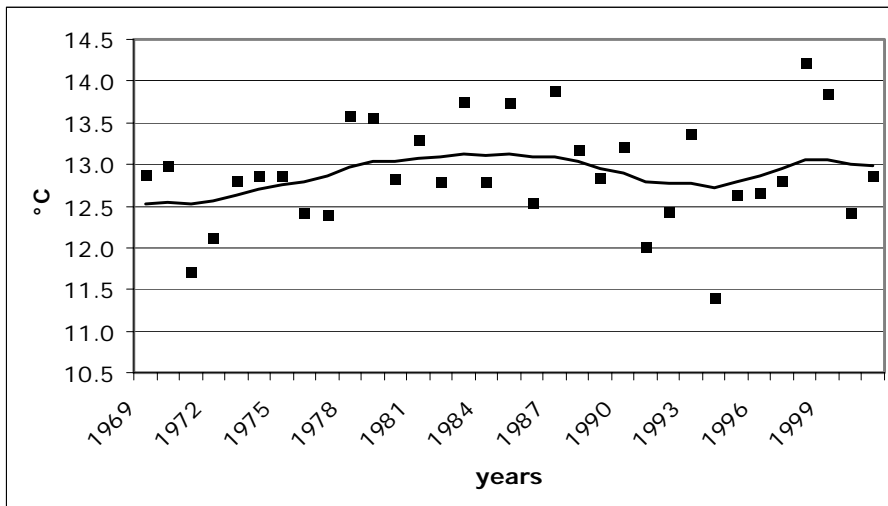
Figure 5.18 Maximum annual temperatures at Cochrane between 1969 and 2001. The squares show the mean annual value. The thick line shows the values produced by the exponential smoothing filter. A significant warming trend at the 5% level was observed between 1969 and 1990.
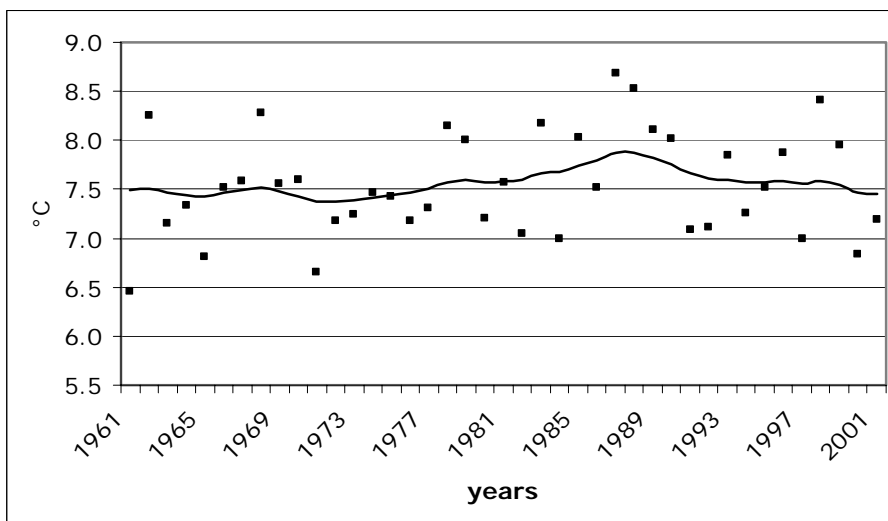
Figure 5.19 Mean annual temperatures at Lago Argentino between 1961 and 2001. The squares show the mean annual value. The thick line shows the values produced by the exponential smoothing filter. A significant warming trend at the 5% level was observed between 1961 and 1990.

5.4.3 Comparison with PDO values

A common pattern observed in all the station records is the 1976 climate shift. Figure 5.20 shows the index of mean annual temperature anomalies (based upon the annual values calculated using Equation 5.3) for all the eastern stations, compared with the annual PDO values. During the 1960s, the Coyhaique Tte Vidal series shows some discrepancies with respect to the other stations, but since the beginning of the 1970s, all the stations show a similar pattern of increasing temperature anomalies, which is coincident with an increase of PDO values since the beginning of the 1970s. This cycle of positive temperature anomalies seems to reach a maximum in the early 1980s, after which most of the series began to show a cooling trend which lasted for about 10 years. In recent years, the temperature anomalies have been fluctuating around the long-term average values. The Lago Argentino records showed a maximum in temperatures at the end of the 1980s, but afterwards a decrease in temperatures was observed.
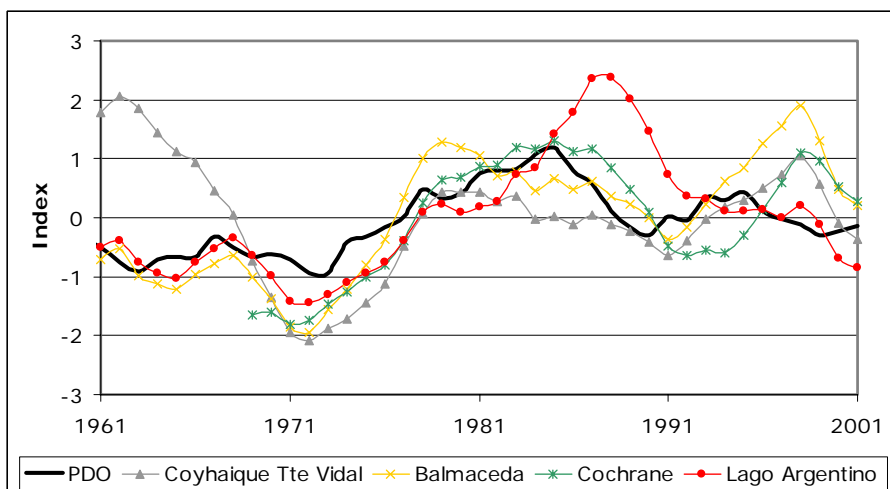
Figure 5.20 Index of mean annual temperature anomalies between 1961 and 2001, compared to the PDO index values.

The above description, suggests that during periods with more frequent El Niño events (for example, the years after 1976), the temperatures of most of the eastern stations are higher than normal, and conversely when La Niña is the most frequent phenomena (prior to 1976) the temperatures are lower than normal. However, no conclusive relationships can be established at the regional level because the particular trends at each station are a response to the influence of large scale atmospheric-oceanic phenomena such as ENSO.

5.5 Summary

The precipitation and temperature series of several stations located around the SPI have been analysed. The majority of stations showed a cycle of positive rainfall anomalies during the 1960s, followed by a decrease of total annual precipitation, yielding in some cases a reduction of 20 – 30% with respect to the 1931-1960 records. A general and significant warming trend was observed at several stations on the eastern side of the SPI, although no trend was observed on the western side. No direct or clear relationship was found between either climatic series and the PDO values. However, some general relationships were observed, specifically the 1976 shift in both temperature and precipitation, and the lack of any trend during the 1990s. The trends described here for the eastern stations are the closest and longest available records in relationship to Glaciar Chico and its neighbouring glaciers, therefore, these trends and data sets will be used as input to the mass balance degree-day model that will be developed in the following chapter.

6.- Mass balance

6.1 Introduction

Ice elevation, frontal and areal changes experienced by Glaciar Chico between 1975 and 2001 (Chapter 4) seem to be in synchronicity with climatic changes registered in recent decades at nearby stations located on the eastern side of the SPI (Chapter 5). However, the magnitude of these combined climate changes, and their implications for glacier dynamics are unknown. To analyse the significance of changes in the temperature and precipitation records, and estimate the extent to which variations in the glaciers of the SPI can be explained by them, a mass balance model written in Matlab 5.0 commercial language was run over 27 hydrological years (April-March) between 1975/76 and 2001/02. The model is based upon the degree-day factor concept constrained by temperature records, snow accumulation that is forced by precipitation series and field data, and, estimations of calving at the glacier front. Similar models have been applied to glaciers in Norway (Laumann and Reeh, 1993) Iceland and Greenland (Jóhanneson and others, 1995). These models have been run using data from reference meteorological stations and a limited number of parameters necessary to determine annual mass balance, and they have been calibrated with direct measurements of inter- annual mass balance. These authors also tested the model under different climatic change scenarios in order to determine the sensitivity of each glacier and their possible future responses.

As described in Chapter 1, no systematic long-term direct mass balance programme is available for the SPI, therefore the calibration of the model presented here will be based upon restricted mass balance measurements carried out in the accumulation area of Glacier Chico, and from ablation measurements available from a number of glaciers of the SPI. The model benchmarks and the parameters used in the model are described and discussed below.

6.2 Model description

The mass balance of a calving glacier, like Glaciar Chico, can be defined as the annual algebraic sum of the total accumulation, ablation and ice export due to calving (Equation 6.1),

$$B_n = B_a + B_b + B_c \qquad \text{Eq. 6.1}$$

where, B_n is the net mass balance

B_a is the net accumulation

B_b is the net ablation

B_c is the ice export due to calving

The mass balance at the end of the balance, or hydrological, year, defined for Patagonia between April and March (Escobar and others, 1992), is the net mass balance for that year. This annual change in mass is expressed as an equivalent volume of water per unit area relative to the previous

summer surface (Paterson, 1994). The average net balance of a glacier is defined by Equation 6.2,

$$\overline{b_n} = B_n/S$$

Eq. 6.2

where, $\overline{b_n}$ is average net balance for the whole glacier and

S is the total area of the glacier

The area of the glacier is calculated from the 50 m resolution DEM described in Chapter 3. The DEM is the initial input to the mass balance model, and all calculations are based on this grid, with each pixel defined by UTM coordinates (*x,y*), and altitude (*z) in metres*. The climatic forcing parameters are obtained from a reference station, which was selected based upon the following criteria;

- the location of the station must be representative of the general climatic conditions prevailing on Glaciar Chico on the eastern-continental margin of the SPI;
- the quality and continuity of the data;
- the length of the temporal series of precipitation and temperature.

Due to the lack of more detailed temporal data, monthly mean values of precipitation and temperature are used to calculate the accumulation and ablation, as described below. The use of monthly data adds a significant degree of uncertainty to the model as it is possible for the mean monthly temperature to be above 0°C, yet the mean daily temperature on some

days may be below 0°C. Conditions on these days, therefore, do not permit ablation, but they could be counted as contributing to ablation in the model. In order to correct this perturbation Reeh (1989) and Huybrechts and others (1991) used the standard deviation (σ) of daily temperatures for each month, then, they assumed a Gaussian distribution of these values around the mean temperature and therefore they estimated the probability of having days with positive temperatures, even if the mean value was negative.

The above correction could be applied to the monthly data used here, however, no daily data were available and therefore a σ must be assumed, contributing with higher uncertainties to the model. Huybretchts and others (1991) used a σ value of 5°C, however, when considering average over several years, the contribution from σ around monthly average could become zero (Van der Veen, 1999), therefore, due to lack of daily data and avoiding excessive assumptions, in this model will be used the average temperature per month without correction, as the main interest of this thesis is the inter-annual variation of the mass balance and not short-term perturbations.

6.2.1 Net Accumulation

Net accumulation (B_a) is defined as the total gain of snow and ice by a glacier during the time interval of a year. Due to the lack of direct measurements on the glacier, the snow accumulation is assumed to be related to the temporal distribution of precipitation recorded at a reference

station. A regional precipitation lapse rate gradient is used to extrapolate the reference precipitation values to each pixel of the glacier. This gradient is based upon the relationship between altitude and precipitation obtained from available meteorological stations and field data in the region surrounding the SPI. A critical value (*tt*), defined as a temperature threshold determining the proportion of precipitation falling in solid form on the glacier was also defined; below this critical value it is assumed that all precipitation falls as snow (Equation 6.3),

If $tm_t < tt$ then, $$B_{an} = \sum_{t=1}^{12} ppm_t + (z - z_p)g$$

If $tm_t \geq tt$ then, $B_a = 0$ Eq. 6.3

Where, B_{an} is the net snow accumulation per pixel during a year

                  tm is the mean monthly temperature estimated for each pixel on the glacier (*x,y*)

                  tt is the critical temperature value that defines whether the precipitation falls as snow

                  ppm is the monthly precipitation at a reference meteorological station

                  z is the altitude of each pixel on the glacier (*x,y*)

                  z_p is the altitude of the reference meteorological station

                  g is the regional precipitation lapse rate gradient

                  t is the month of the hydrological year (*t*=1:12 where April =1 and March =12)

Thus, the total accumulation of the glacier (B_a) is the sum of the snow accumulation of the individual pixels multiplied by the total surface area of the glacier (Equation 6.4),

$$B_a = S \sum\nolimits_{1}^{n} B_{an}$$ Eq. 6.4

Where n is the total number of pixels of the glacier derived from the DEM

The average net accumulation of the glacier is defined by Equation 6.5,

$$\overline{b_a} = B_a/S$$ Eq. 6.5

where, $\overline{b_a}$ is average net accumulation for the whole glacier and

S is the total area of the glacier

6.2.2 Net Ablation

Net ablation (B_c) is defined as the total ice and snow lost due to melting occurring during a period of one hydrological year over the total glacier area. Due to the lack of ablation measurements on Glaciar Chico, a degree-day factor model (Braithwaite, 1995) is used. This model has been widely applied (Hock, 2003), and several improvements have been added to the basic formula (Hock, 1999). The model is based on the empirical relationship between the ablation of snow/ice, and the mean daily air

temperatures above 0°C, which has been recognised as an important factor in long term analyses of glacier ablation. This relationship varies with surface albedo and due to the effects of the sky view factor on potential direct solar radiation (the shadowing effect of rough topography on the spatial/temporal distribution of radiation over the glacier), and the failure of the model to account for spatial variation of ablation due to distribution of direct solar radiation is a significant weakness. Despite this, and the fact that the accuracy decreases with increasing time resolution (Lang, 1986), the simplicity of its application and the reduced number of parameters required to run the model makes it a powerful tool for application to glaciers that have a lack of direct measurements, like Glaciar Chico.

The first step in the application of the degree-day model is the determination of the mean monthly air temperature (*tm*) for each pixel of the glacier (*x,y*), based upon the registered value at the reference station and the regional adiabatic lapse rate (Equation 6.6),

$$tm = tm_r - (z - z_p)j \qquad\qquad \text{Eq. 6.6}$$

Where tm_r is the mean monthly temperature registered at the reference station

j is the regional adiabatic lapse rate

The melting generated by the cumulative positive temperatures calculated per pixel per month depends primarily on a factor (*k*), which is function of the surface type covering each pixel of the glacier at the time of

measurement, namely snow, debris-covered ice or bare ice. The resulting meltwater will percolate into the snow cover where it is possible that a refreezing could take place especially during winter seasons. In many models, runoff is assumed not to start until the amount of refrozen melt exceeds a certain fraction (*Pmax*) of the winter accumulation (Van der Veen, 1999). For instance, on the Greenland ice sheet Reeh (1989) determined a *Pmax* of 0.6, however, for temperate glaciers where superimposed ice is not important and where the potential freezing of the winter-snow cover is much lower than Greenland, *Pmax* could be neglected (Lauman and Reeh, 1993). Accordingly, in the model presented here, *Pmax* will be considered a minor factor and will be set equal to zero.

By definition, above the ELA only snow is covering the glacier, therefore all melting is generated by a degree-day factor for snow surfaces (k_s), as described by Equation 6.7.

If *z* > ELA, then

$$B_{bs} = k_s \sum_{t=1}^{12} tm^+ * dpm \qquad\qquad \text{Eq. 6.7}$$

Where, B_{bs} is the net ablation above the ELA per pixel (x,y)

k_s is the degree-day factor for snow surfaces (see Table 6.6)

tm^+ is the value of the mean monthly temperature above 0°C per pixel (*x,y*)

dpm is the number of days per month

At the beginning of the hydrological year the surface of the ablation area is mainly bare ice, however, through the year the glacier surface can be covered by snow, therefore, each pixel will have a different degree-day factor (k) depending on the temperature and the amount of solid precipitation (ppm) per pixel.

The potential situations below the ELA are:

      A. Pixels located below the ELA and where there is solid precipitation during a month. Due to the monthly temporal resolution of the model, it is impossible to divide the month into smaller periods, therefore, it will be assumed that if there is snowfall in any one month, melting will affect only the snow, and a degree-day factor for snow surfaces will be applied (Eq. 6.8),

If $z \leq$ ELA, and, if $ppm_t > 0$ then,

$$B_{bis} = k_s \sum_{t=1}^{12} tm^+ * dpm \qquad\qquad \text{Eq. 6.8}$$

Where B_{bis} is the annual net ablation per pixel (x,y) located in the ablation area and experiencing snow coverage

      B. In the absence of solid precipitation below the ELA during the hydrological year, the surface of the glacier could be snow or ice, depending on the transient mass balance (B_{nt}). This is calculated as the sum of the difference between solid precipitation (ppm) and ablation of the

snow coverage (B_{bs}) between the respective month and the beginning of the hydrological year, as described by Equation 6.9,

$$B_{nt} = \sum_{t=1}^{t} ppm - B_{bis}$$

Eq. 6.9

Therefore, the net ablation of each month is described by Equation 6.10,

If $z \leq$ ELA; and, if $B_{nt} \leq 0$, then

$$B_{bi} = k_i \sum_{t=1}^{12} tm^+ * dpm$$

Eq. 6.10

Otherwise, if $z \leq$ ELA and, if $B_{nm} > 0$, then $B_{bi}=0$.

Where B_{bi} is the monthly net ablation per pixel (x,y) located below the

            ELA with transient snow coverage

            k_i is the degree-day factor for ice surfaces (see Table 6.6)

            dpm is the number of days per month

The annual net ablation for each pixel of the glacier is therefore the sum of all the ablation components (Eq. 6.11),

$$B_{bn} = B_{bs} + B_{bi} + B_{bis}$$

Eq. 6.11

The annual net ablation for the whole glacier is calculated with Equation 6.12,

$$B_b = S\sum_{1}^{n} B_{bn}$$
<div align="right">Eq. 6.12</div>

Where n is the total number of pixels of the glacier area derived from

the DEM

Finally, the average net ablation of the glacier is defined by Equation 6.13,

$$\overline{b_b} = B_b/S$$
<div align="right">Eq. 6.13</div>

where, $\overline{b_b}$ is average net ablation for the whole glacier and

S is the total area of the glacier

6.2.3 Calving

Calving is the process whereby a glacier that terminates in deep water loses ice by the breakaway of icebergs during a hydrological year (B_c). The process is controlled by the dynamics of the terminal section of the glacier, where the stress regime is very high due to the typically rapid ice flow associated with basal water pressure, which can approach the ice pressure (Meier, 1989). Under these conditions, most of the fast motion near the terminus of a temperate glacier may be realised through sliding, with flotation of the ice tongue unable to occur, except locally and transiently, because of the low tensile strength of temperate ice containing abundant englacial water (Warren, 1992). Consequently, the catastrophic collapse of

the lower tongue of Patagonian glaciers has been generated when high ice thinning rates and ice velocities near the ice front have brought the glacier to a near buoyancy point (Warren and others, 2001; Skvarca and others, 2003).

Calving is a complex process which has only recently been analysed in more detail for Patagonian glaciers (Warren and Aniya, 1999). These authors concluded that there is a strong positive linear correlation between calving rates and water depth, however, for any given depth of water, the calving speeds of tidewater glaciers are about an order of magnitude greater than those of freshwater glaciers (Funk and Röthlisberger, 1989).

In Patagonia, this enhanced speed was confirmed by Warren and others (1995a and b; 2001), who analysed freshwater calving from Glaciares Upsala, San Rafael and Nef.

The behaviour of some of the Patagonian calving glaciers has been defined as out of phase with both climate changes and regional glacier variation trends (Warren, 1992, Rivera and others, 1997a). In Patagonia, the majority of the calving glaciers were retreating during most of the 20th Century, albeit at varying times and rates (Aniya and others, 1997, Aniya, 2001). These general trends suggest that climate change is the driving background force, but specific responses are much more complicated and depend on local factors, including calving rates, hypsometry and geometry (Warren and Rivera, 1994).

In order to calculate the ice export due to calving, Van der Veen (1996) related the glacier terminus position change with the along-flow ice speed and calving speed. An alternative approach focuses on the role of near-terminus stretching, retreating and thinning, indicating that ice thickness decreases during glacier retreat because of an increase in the stretching rate (Venteris, 1999). Also of importance is the presence of crevasses at temperate glacier fronts which can accelerate the calving process (Warren and others, 1995b). Venteris (1999) also concluded that variations in calving rate and terminus retreat are better linked to differences in ice flow and terminal buoyancy than to the composition of the terminal water body.

In this sense, the basic parameters needed to calculate the calving rates of temperate glaciers are; ice thickness and velocity near the glacier front, water depth, and composition/temperature of the fjord or lake that the glaciers are calving into (Van der Veen, 2002). Unfortunately, none of these parameters are available for Glaciar Chico, therefore only a theoretical approximation of the process is presented.
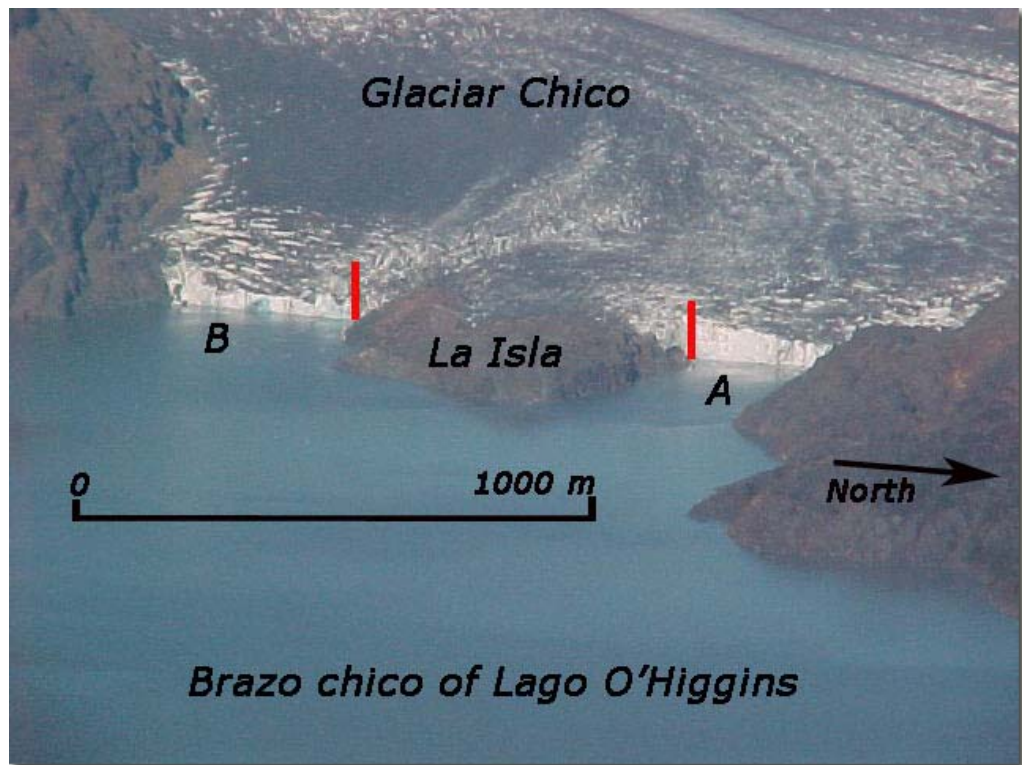
Figure 6.1 Glacier Chico calving front in 2001. A and B are the two branches discussed in the text. The red bars represent a height of approximately 50 m. Photograph from http://www.camposdehielo.cl

As described in Chapter 4, Glaciar Chico is partially calving into one arm of Lago O'Higgins. The frontal tongue of the glacier is divided into two branches, one of 300 m long at the northern side of "La Isla", and the other of 390 m long to the south of La Isla (A and B respectively on Figure 6.1). Since 1975, both calving fronts have been very stable, displaying only minor retreat and area changes (Table 4.2).

In order to estimate the calving rates of the glacier, the number of icebergs on the satellite images and aerial photographs available for this study were analysed as a measure of possible calving events taking place into Brazo Chico of Lago O'Higgins in recent decades. This lake has a total area of

15.6 km^2, and is connected to Lago O'Higgins through a narrow river at the northern margin of a moraine belt (Peninsula) deposited during the Holocene (Chapter 4, Fig. 4.4). As Table 6.1 shows, the area and number of icebergs observed in the lake Brazo Chico of Lago O'Higgins since 1973 are both very small. These datasets only represent snapshots of the glacier history, and therefore seasonal variations are to be expected. However, if the relationship between the calving process and ice velocities at the glacier terminus as described above is accepted, the small seasonal variations measured by Rott and others (1998) at Glaciar Upsala where ice velocities were only 7% higher during summer compared with winter seasons, suggests that the calving process must also be similar through the year. None of the observed icebergs have a tabular form, and their sizes are generally small, therefore it is possible to presume that they were generated by calving of grounded ice.

Table 6.1 Icebergs on Brazo Chico of Lago O'Higgins 1973-2001.

Year	Surface (km^2)	Number of icebergs
1973	0.018	1
1975	0.013	7
1981	0.0040	4
1984	0.0041	2
1986	0.030	9
1995	0.0090	7
1997	0.0010	3
2001	0.0020	2

Note. See Tables 2.2 and 2.3 for details about each data set.

The low level of calving activity observed at the glacier front of Glaciar Chico could be related to the shallow water depths of the lake near the front. The bathymetry has never been measured, however, the glacier front is located in a narrow valley, and the presence of "La Isla" indicates that water depths are not sufficient to allow the glacier to approach a buoyancy point. The heights of the ice walls at the calving sections of the glacier front are approximately 30 to 40 m at A, and 10 to 20 m at B (Fig. 6.1). If the glacier terminus is in hydrostatic equilibrium, the water depth at the glacier front (hw_f) can be estimated from the thickness of the ice above the waterline (h_0), yielding a water depth range of between 90 and 360 m (Eq. 6.14) at the calving front of Glaciar Chico.

$$hw_f = 9h_0 \qquad\qquad\qquad \text{Eq. 6.14}$$

The frontal ice walls of Glaciar Chico have been visited several times since 1996. On none of these visits have thermo-erosional notches been inferred (Warren and others, 2001), which could indicate significant changes in the lake level, or more importantly, possible raising of the ice due to buoyancy-driven upward displacement of the glacier terminus.

Taking into account the above discussion, and the fact that the mass balance model will be applied between 1975 and 2001 (after the appearance of "La Isla" at the glacier front), calving processes at the frontal

tongue of Glaciar Chico will be initially considered as a negligible component of the mass balance model.

6.3 Parameterization

6.3.1 DEM

The model is initiated with the DEM generated from the aerial photographs acquired in March 1975 (Chapter 3.1.2). This DEM covered all the ablation area, and part of the accumulation zone of the glacier. In order to complete the 1975 surface topography for the whole glacier, the most up-to-date and complete DEM of the region based upon 2000 SRTM data was used.

As described in Section 4.2.6.2, ice elevation changes between 1975 and 2000 were detected at elevations between 250 and ~1900 m asl, but above this altitude, no changes or even thickening were observed. Therefore using SRTM data to complete the surface topography of these areas will not introduce substantial errors. The topography of the rest of the glaciated areas without data, in the elevation region between approximately 1400 m and 1900 m, was determined from a linear regression equation based upon the relationship between DEM-1975 and SRTM data (r=0.99).

The resulting DEM was smoothed using a mean filter in order to preclude breaks in the margins of the overlapping areas, resulting in a DEM called MODEL-DEM-1975. When compared to the SRTM DEM, this model showed

an average thinning of -1.3 ± 0.44   m a^{-1} for the glacier as a whole between 1975 and 2000.

The initial area parameters of the model were defined by the glacier area measured in 1975 (199 km^2), and the ELA position was estimated from the snowline observed on aerial photographs acquired in March 1975 (Section 4.1.3 and Figure 4.3).

6.3.2 Accumulation

Very few direct snow accumulation measurements are available from Glaciar Chico, and no precipitation records are available above ~300 m asl, the elevation of the highest meteorological station near the SPI (Table 5.1).

Consequently, most of the precipitation estimations are based on a regional hydrological model designed by Escobar and others (1992), who calculated a mean precipitation of 7 m a^{-1} w. eq. for the SPI as a whole, with an average of 7.4 m a^{-1} on the western side of the SPI and 6.4 m a^{-1} on the eastern side. In the national hydrological balance published by DGA (1987), the SPI appears to have an annual mean precipitation of up to 8 m a^{-1} at an altitude of approximately 2000 m, however no absolute maximum values are given for the tops of the mountains.

The snow accumulation estimations in Patagonia have been obtained from ice cores drilled from Glaciar Moreno of the SPI (50°38'S, 73°15'W, 2680 m asl) where a mean accumulation of 1.2 m a^{-1} of w. eq. was estimated by

Aristarain and Delmas (1992); from Glaciar Tyndall of the SPI (50°59'S, 73°31', 1756 m asl) where Shiraiwa and others (2002) estimated an annual accumulation of 17.8 m a^{-1} w. eq. between 1998 and 1999, whereas that of 1999/2000 was expected to be 11.0 m a^{-1} w. eq.; from Glaciar San Rafael of the NPI (46°56'S, 73°32'W, 1292 m asl) where Yamada (1987) estimated a net accumulation rate of 3.45 m a^{-1} w. eq. and from Glaciar Nef of the NPI (45°56'S, 73°19'W, 1500 m asl) where Matsuoka and Naruse (1999) calculated 2.2 m a^{-1} w. eq.

The above estimations of accumulation indicate the high spatial and temporal variability, depending on the location of each drilling site and the year of drilling. However, one common characteristic obtained from these ice cores was the presence of a water saturated firn-ice layer, at 42.5 m in Glaciar Tyndall, 19.7 m in San Rafael and 13.3 m in Glaciar Nef. A similar aquifer was also observed at 10 to 20 m depth in Glaciar Tyndall at an altitude of between 1300 and 1500 m by Casassa and others (2001), when they surveyed the glacier and measured the ice thickness by means of a helicopter-borne radar system.

These water saturated firn-ice layers suggest the presence of meltwater in the accumulation areas, which could originate from a summer heat wave causing the surface snow temperature to rise to melting point. The resulting water could percolate to the aquifer, and perhaps also drain slowly downslope, effectively feeding englacial and subglacial water conduits leaving the accumulation area. Considering this ablation, the total precipitation could easily be higher than 20 m a^{-1}, at least on the western

side of the continental ice divide, for example at the Glaciar Tyndall drilling site. This value is well beyond the maximum range predicted by Escobar and others (1992), confirming the poor current understanding of the mass balance of the area.

6.3.2.1 Mass balance at base camp (1440 m) of Glaciar Chico

The direct measurements of mass balance available for the study area were collected from several snow pits dug in the accumulation area of Glaciar Chico since 1996. Details of the methods and equipments used in these campaigns are described in Chapter 2.

Table 6.2 shows the snow densities measured in each snow pit dug at approximately 1440 m in the surroundings of the mast installed in 1996 on Glaciar Chico. In all the snow pits ice pipes and abundant ice lenses with thickness of up to 4 cm were found (Figure 6.2). The height of each snow pit surface was measured with respect to the top of the mast. These measurements could be affected by the tilt of the tower (generated by the ice flow), however consistency is maintained as the measurements have always considered the vertical distance between the top of the tower and the snow surface. Considering that the snow densities obtained from snow pits are sampled every 20 cm, the height of the snow surface and position of the end-of-summer layer is considered to be accurate to 0.2 m.

Table 6.2 Snow pit densities at base camp, Glaciar Chico (1440 m).

Snow Depth	1996, January 14	1997, October 15	1998, October 3	2001, September 21	2002, October 7
	Density	Density	Density	Density	Density
Cm	g cm^3	g cm^3	g cm^3	g cm^3	g cm^3
20	0.29	0.4	0.23	0.41	0.33
40	0.48	0.36	0.38	0.45	0.3
60	0.5	0.43	0.4	0.41	0.38
80	0.52	0.41	0.37	0.41	0.4
100	0.53	0.43	0.43	0.4	0.33
120	0.55	0.44	0.42	0.39	0.4
140	0.54	0.46	0.41	0.44	0.42
160	0.56	0.48	0.42	0.45	0.38
180	0.54	0.44	0.42	Ice layer	0.44
200	0.54	0.48	0.46	0.45	0.44
220	0.55	0.49			
240	0.53	0.54			
260	0.52	0.54			
280	0.57	0.52			
300	0.57	0.52			
320		0.58			
340		0.53			
360		0.53			
380		0.5			
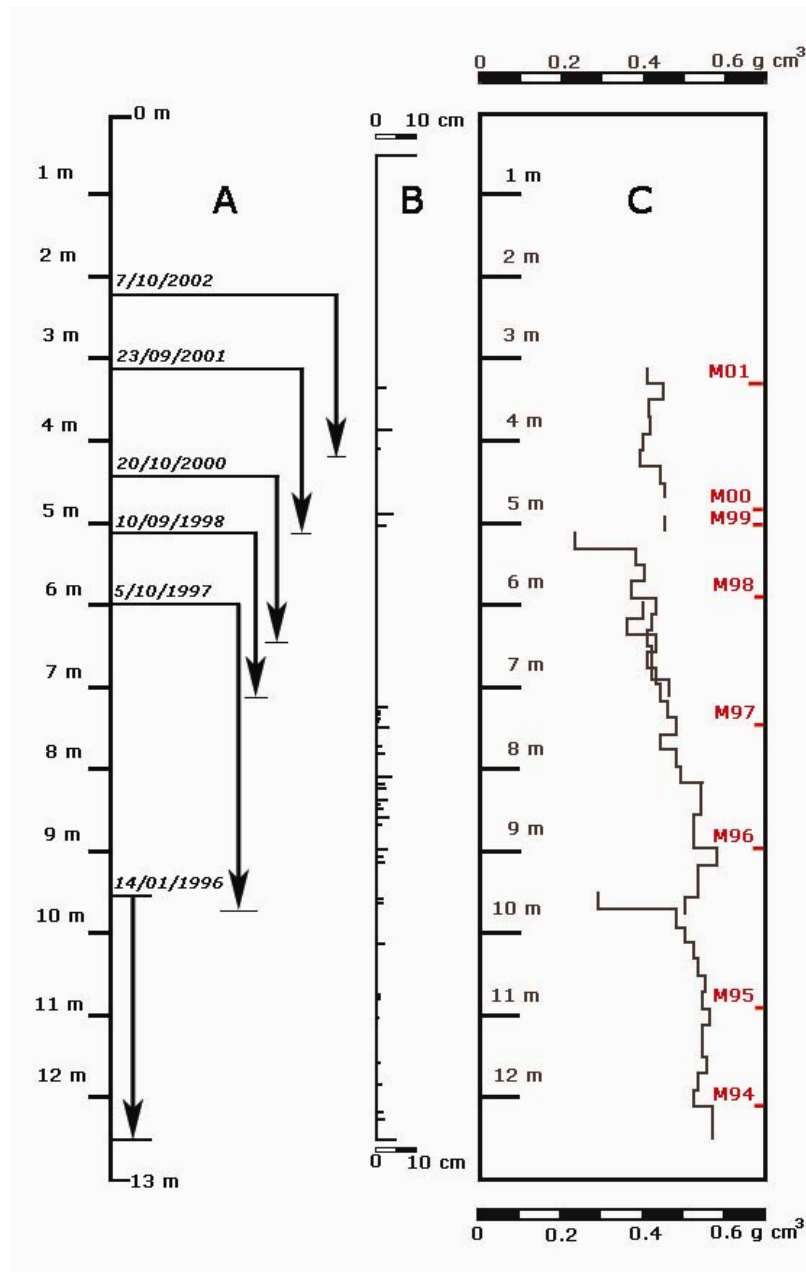
Figure 6.2 Results from snow pits dug in the accumulation area of Glaciar Chico. The vertical scale (m) is with respect to the top of the mast installed in 1996. Panel A indicates the date of each snow pit and the height of the snow surface with respect to the top of the mast and depth of the snow pit. Panel B indicates the presence of ice lenses and their thickness in cm. Panel C shows the snow densities obtained from each snow pit in g cm^3. An estimate of the end of each hydrological year between 1994 and 2001 is shown in red.

The snow densities are lower at the surface of the snow pits due to more recent snowfalls, therefore the first layer of each snow pit represents daily variations in meteorological conditions. Below this layer, densities are progressively higher until the end of the previous summer layer is reached, characterised by a sequence of higher density ice lenses and usually with some deposition of dust. Below these layers, densities are slightly reduced indicating the surface from the previous winter. On the right hand side of Figure 6.2 (in red), the position of the end of each hydrological year is shown, based upon analysis of the snow stratigraphy, snow densities, height of the snow surface with respect to the top of the mast, and in situ observations of the continuity of ice lenses and dust deposition.

Most of the snow density profiles versus snow depth (Figure 6.3) show similar trends and values, the exception being the 1996 snow pit which has slightly more dense snow between a depth of 80 and 220 cm. Analysis of all the snow density profiles (Figure 6.2) reveals a general trend of low accumulation and lower densities in more recent snow pits.
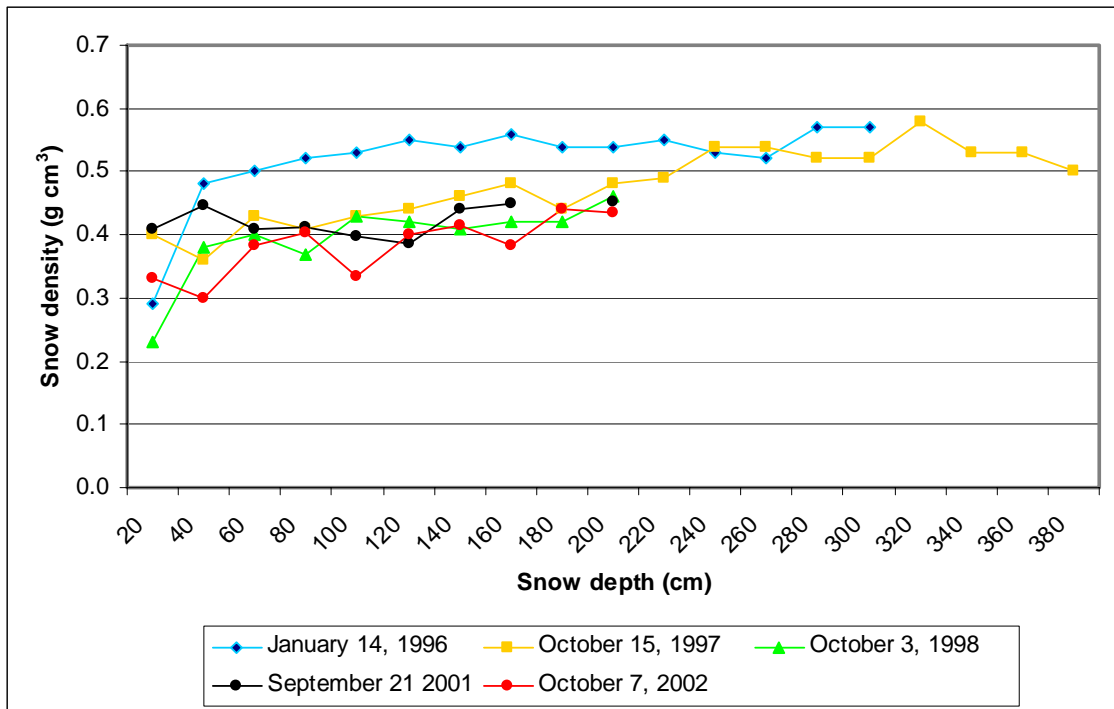
Figure 6.3 Snow densities and snow depth for each snow pit. Errors (not shown) are considered to be 10% for each measurement.

The snow temperatures were also measured in each snow pit, yielding values close to 0°C at the bottom of the pits and negative values at the surface of the snow pack (Figure 6.4), confirming the temperate conditions prevailing in the area. These measurements are considered to be accurate to the order of ± 0.5 °C due to uncertainties of the instrument.
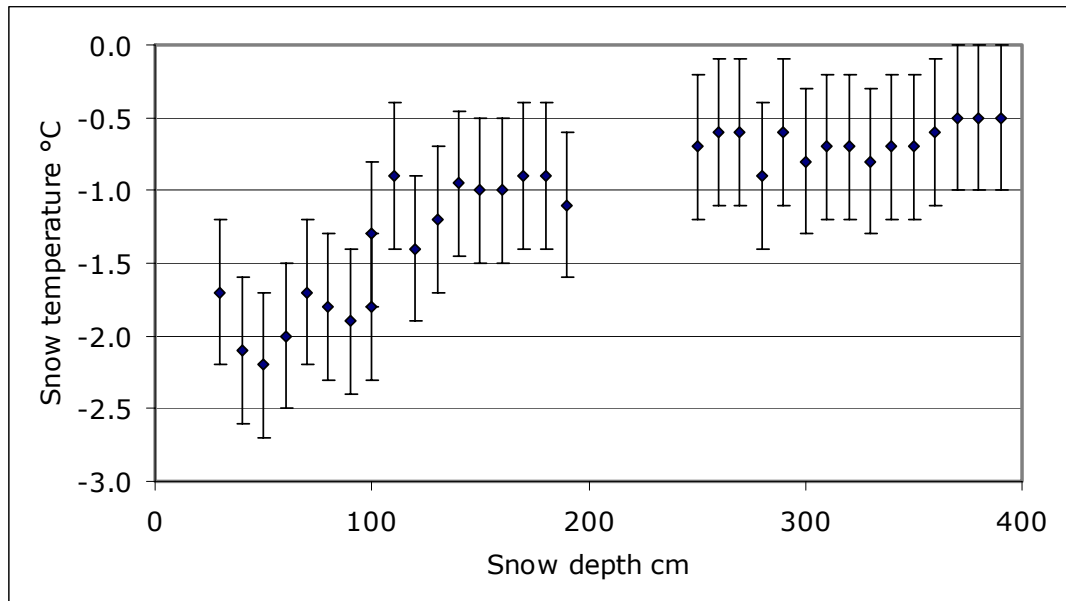
Figure 6.4 Snow temperatures (°C) from the snow pit dug at Glaciar Chico on October 5, 1997. The error bars represent ± 0.5°C.

Snow densities were also obtained during each field campaign from the area around the base camp using a Mt. Rose Federal sampler model 3600 (a professional grade snow sampler based on the United States Forest Service design criteria). Snow densities obtained using the Mt. Rose equipment represent the average densities of the surface snow layer, including ice lenses, pipes and soft snow at shallow depth, whilst snow pits provide a detailed measurement of snow densities and stratigraphy every 20 cm. The snow densities obtained using the Mt Rose sampler were compared to the results obtained from the snow pits in order to calculate the errors and possible biases in the snow density estimations introduced by the averaging process.

Table 6.3 shows the snow densities of the upper snow layer (snow depth in cm) using both methods, resulting in a linear relationship with an average

difference of ~0.05 g cm³ lower densities from the snow pits compared to Mt. Rose results. This difference could be explained by local spatial variations of the snow accumulation or some bias in the methods. Snow density measurements using samplers (especially cylinder tubes) commonly have errors to the order of 10% (Harper and Bradford, 2003), therefore the differences between both methods could be considered the result of the random sampler error.

Table 6.3 Snow densities measured using different samplers.

	Base Camp, Glaciar Chico 1440 m asl		
	1996, January 14	**1998, October 3**	**2001, September 21**
	Density (g cm³)	**Density (g cm³)**	**Density (g cm³)**
500 cm³ tube	0.50	0.37	0.41
Mt. Rose	0.54 (10 samples)	0.43 (1 sample)	0.47 (8 samples)
Mean snow depth (cm)	154	122	97

Based upon the snow depth determined for each hydrological year and the respective snow density of each annual layer, it was possible to estimate the mass balance at the location of the mast, yielding an average of 0.57 ± 0.21 m a^{-1} of w. eq. between 1994/95 and 2001/02. The error is comprised of the uncertainties in the snow depth measurements (0.2 m) and the estimated error of the density measurements (10% or ~0.05 g cm³). This average accumulation rate is much smaller than any previous estimation of snow accumulation obtained from the SPI, which could be explained by the fact that it was measured at relatively low altitude within the accumulation

zone and on the eastern margin of the SPI, where it is well known that precipitation rates are much lower than on the western margin.

A general trend of reduction in the snow accumulation can be seen for the series as a whole over the measurement period, with the exception of 2000/2001 when the accumulation was higher than the previous year. The maximum accumulation of 1.06 m a^{-1} w. eq. was observed in 1994/95, whilst the minimum was observed in 1999/00 when only 0.15 m a^{-1} w. eq. accumuated (Figure 6.5). Shiraiwa and others (2002) also observed a notable difference in accumulation between 1998/99 and 1999/2000, the latter experiencing only 62% of the former.
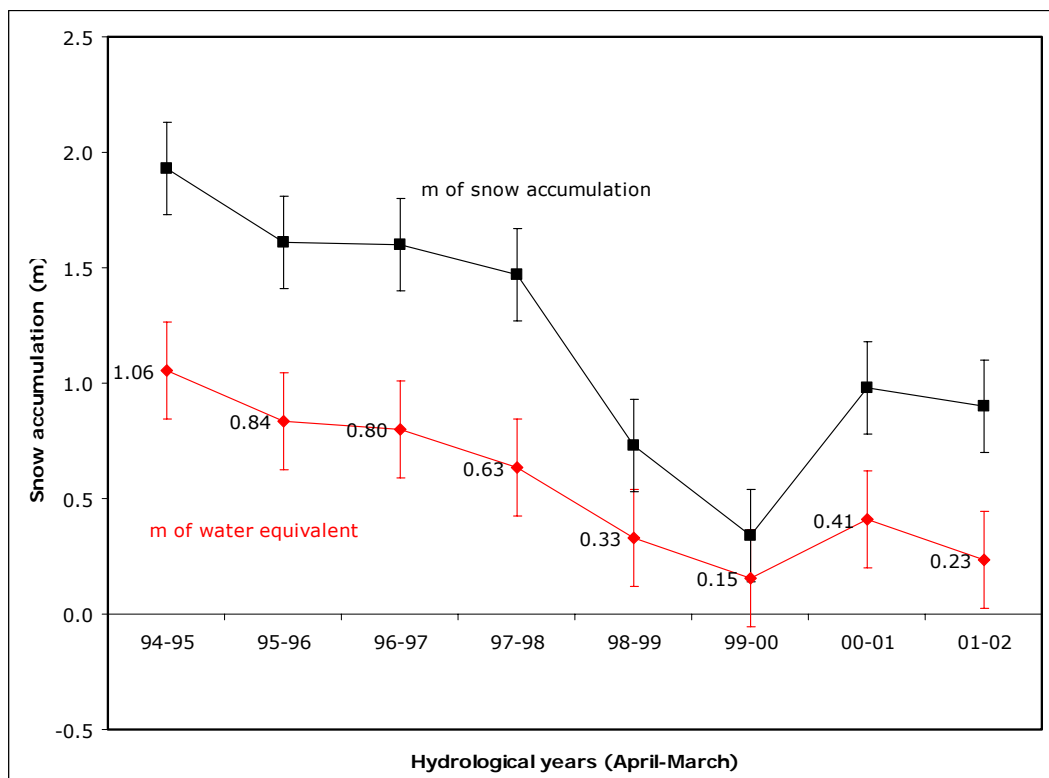
Figure 6.5 Annual mass balance (in m a^{-1}) between hydrological years 1994/95 and 2001/2002, estimated for the base camp at 1440 m, Glaciar Chico, SPI.

The specific mean mass balance obtained at the mast between 1994 and 2002 is one of the main parameters that will be used in Section 6.4.1 to test the mass balance model.

6.3.2.2 Vertical distribution of precipitation

In order to determine the regional precipitation lapse rate, the records from several stations located along the eastern side of the SPI and close to the glacier were analysed (Tables 5.1 and 5.2). To date, no permanent meteorological station is located in the accumulation area of the SPI. Therefore to estimate precipitation totals at higher altitudes three stake networks located on ice plateaux away from surrounding mountains installed during field campaigns carried out in recent years were used (Table 6.4, Figure 6.6). At all of these stake network sites snow variations were measured daily, allowing a preliminary estimation of precipitation after applying snow densities obtained from snow pits and discrete measurements carried out in each site.

Table 6.4 Stake networks measured at the SPI.

Station	Latitude (degrees)	Longitude (degrees)	Altitude (m)	Distance to base camp, Glaciar Chico (km)
Base camp Glaciar Chico	-49.18	-73.19	1445	0
HPS-F	-49.60	-73.45	1577	50
HPS-I	-49.89	-73.54	1833	83

The measurements took place in spring (between September and October) over periods of 14 to 34 days. These short periods of time are assumed to be representative of the whole year, in order to allow comparison with the annual average precipitation values obtained from the meteorological stations located in the surroundings of the SPI. This assumption is based upon the lack of seasonality in the rainfall on both sides of the SPI described in Chapter 5, however this assumption does add an important uncertainty to the annual estimation, and therefore must be considered as a preliminary estimate of the precipitation at the summits of the SPI. Another problem is posed by the high inter-annual variation in the precipitation totals. As these measurements are based upon a single observation they therefore do not represent the inter-annual variability observed at the lower altitude meteorological stations. However, these measurements are the only direct observations of accumulation from this area of the SPI and can thus be considered a first approach to the problem.
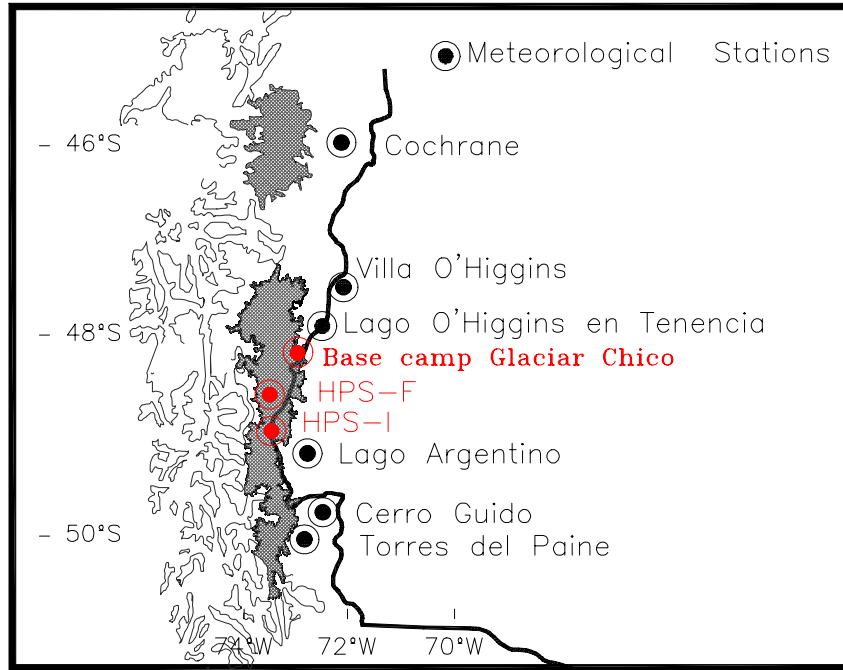
Figure 6.6 Meteorological stations and stake measurements (in red) used to estimate annual precipitation on the eastern side of the SPI.

The snow densities used to calculate the precipitation from snow accumulation recorded at each stake network were derived from measurements of the upper 20 cm snow layer observed in each snow pit, representing a general indication of the prevailing snowfall conditions at each site. The densities vary widely between sites due to the differences in altitude and longitude, with the snow observed at higher altitude and further west (nearer the continental ice divide) being less dense.

The annual precipitation calculated for each stake network is shown in Table 6.5. The errors have been calculated based upon a 10% possible monthly variability in snowfall, plus uncertainties in total snowfall measurements and snow density measurements. The maximum value obtained at Altiplano Italia (HPS-I) seems to be very high when compared

with the estimations of Escobar and others (1992), however this value is smaller than the annual accumulation estimated at lower altitude by Shiraiwa and others (2002). Thus the estimated value of 9.63 m a^{-1} could be representative of the variability encountered at different locations across the SPI. The value obtained at the base camp on Glaciar Chico is similar to the annual precipitation of 4.5 m a^{-1} estimated by DGA (1987) for this site.

Table 6.5 Estimated precipitation from stake networks.

Stake network	Days of Measurement	Snowfall (cm)	Density (g cm^3)	Precipitation (m a^{-1})
Base camp, Glaciar Chico	34	115	0.33	4.07± 0.54
HPS-F	20	178	0.23	7.37 ± 0.96
HPS-I	14	229	0.16	9.63 ± 1.36

Figure 6.7 shows the distribution of annual precipitation recorded at meteorological stations located within ~250 km of Glaciar Chico along the eastern side of the SPI (Table 5.1 and 5.2), and the estimations obtained from the stake networks located in the accumulation area of the SPI. The vertical distribution of precipitation follows an exponential trend, with maximum values found at the higher altitudes of the SPI.
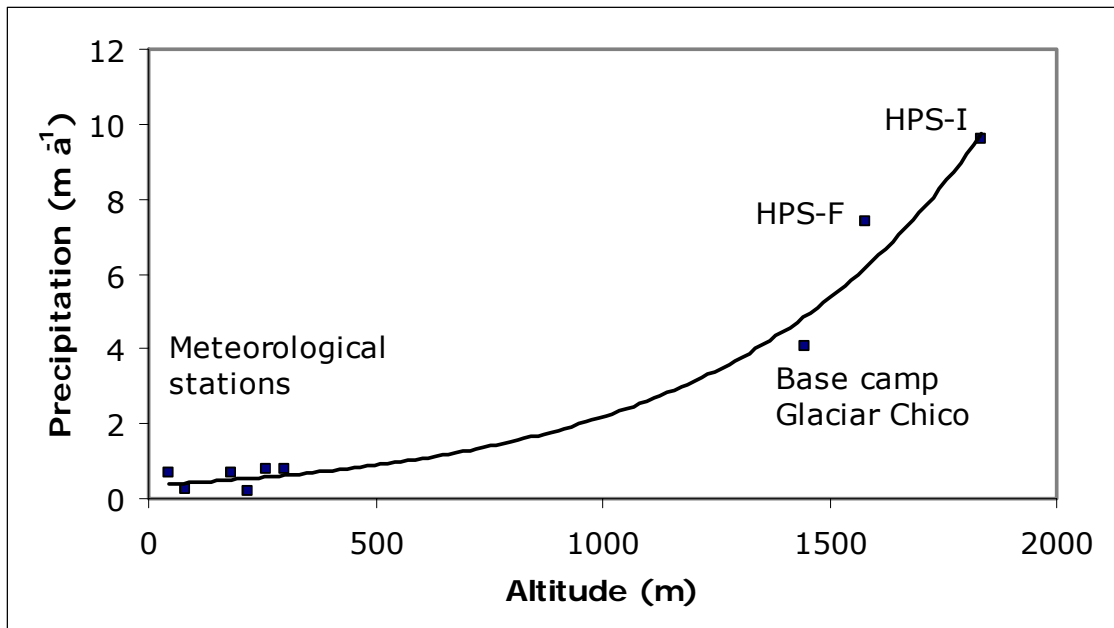
Figure 6.7 Distribution of annual precipitation with altitude along the eastern side of the SPI, in m a^{-1}.

Due to the large uncertainties in the precipitation estimates at higher altitudes, the exponential relationship must be carefully evaluated before applying the resulting equation to the glacier as a whole. According to such an exponential curve, the top of the mountains near Glaciar Chico ($\sim$2800 m) could receive a maximum of 33 m a^{-1} of precipitation. This value far exceeds the maximum precipitation predicted by Escobar and others (1992) for Patagonia, and so must be considered with caution. Given that the mountains surrounding Glaciar Chico are located to the east of the continental watershed divide, it is likely that the mountain summits do receive a high annual precipitation. However, it is unlikely to be greater than that estimated for Glaciar Tyndall (10-17 m a^{-1}) located on the western side of the continental watershed divide. Therefore, it may be more reliable to assume that the vertical distribution of precipitation in the region is represented by two linear trends; one between the lowlands and the

plateaux of the SPI, and a second at higher altitudes where the sharp increment in figure 6.7 was observed. Moreover, instead of a unique regional gradient, a range of possible values appears to be more realistic and representative of the contrasting distribution of precipitations, in the range from 3 to 4 mm m^{-1}.

The above range of potential regional vertical precipitation gradients will be used for tuning the mass balance model, as will be described in more detail in Section 6.4.1.

Precipitation on the glacier is assumed to fall as snow only if the temperature at the altitude of each pixel of the glacier is below a specific threshold (*tt* in °C). Typically, values used in mass balance models are in the range from +1 to +2 °C. For example, Jóhannesson and others (1995) used a value of +1°C when modelling glaciers in Iceland and Norway following reports from Laumann and Reeh (1993) of snowfall in Norway at temperatures up to +1°C. A similar value was used by Verbunt and others (2003), whilst Gustafsson and others (2001) estimated that a mix of snow and rain is possible up to +2°C. In the model presented here a threshold value of +2°C will be used to take account of the temperate conditions prevailing on the SPI and the possibility of other solid precipitation (hail and sleet), as was also described for Blue Glacier in the USA (Rasmussen and others, 2000).

6.3.2.3 Reference station for precipitation

As has already been shown, precipitation in the region is highly variable in both temporal and spatial distribution, therefore, the selection of a reference station for the mass balance model based upon the criteria enunciated in Section 6.1.1, results in two possibilities; Cochrane and Lago Argentino. These stations are located on the eastern side of the SPI under the precipitation shadow effects of the icefields (Cochrane is ~50 km east from Glaciar Colonia of the NPI, whilst Lago Argentino is ~60 km east from Glaciar Moreno of the SPI). Both stations have been operating for more than 30 years, however, the Lago Argentino precipitation series exhibits many gaps in data collection during the 1990s (Section 5.2, Figure 5.12). Conversely, Cochrane has been operated by professional personnel of DMC, and presents no data gaps between 1975 and 2001, therefore this station will be used as a reference in the mass balance model for calculating the precipitation series on Glaciar Chico.

6.3.3 Ablation

6.3.3.1 Degree-day factors

Very few direct measurements of ablation are available from the Patagonian icefields. Most of the estimates were obtained after applying a degree-day factor model based upon limited ablation measurements carried out on ice in the ablation areas of Patagonian glaciers. These measurements are commonly obtained from stakes drilled into ice and monitored on a daily

basis for a couple of weeks. Only the Glaciar Moreno (Figure 1.2) stake networks have been surveyed and re-installed over a period of several years during the 1990s to allow a long term estimation of ablation.

The first stake network on Glaciar Moreno was installed in November 1993 by Naruse and others (1995) at an altitude of approximately 350 m and 4.5 km upstream from the calving front. The stake was resurveyed 110 days later in March 1994, during which time 7 m of ice had been lost (6.3 m w. eq. assuming an ice density of 900 kg m^3). The cumulative positive temperature of this period was determined from the daily temperature obtained from the Lago Argentino meteorological station and a local automatic weather station installed on site, yielding a degree-day factor for ice (k_i) of between 6.9 and 7.1 mm °C d^{-1} of w. eq. Using this factor, and considering the annual positive cumulative temperatures measured at the automatic weather station located at 180 m asl near the glacier front, the annual ablation for the hydrological year 1993/94 was calculated to be 12.8 m w. eq. (Takeuchi and others, 1996). Using monthly mean temperatures obtained at the Lago Argentino station between 1962 and 1994, Naruse and others (1997) estimated the inter-annual variation of ice ablation at this site to be on average 13 ± 2 m w. eq. a^{-1}, with maximum values of 14 ± 2 m w. eq. a^{-1} and a minimum of 11 ± 2 m w. eq a^{-1}. Based upon data acquired at the Lago Argentino station, a similar calculation was applied to Glaciar Upsala at 250 m asl (Figure 1.2), with a mean annual ablation estimate of 15 ± 2 m w. eq. a^{-1}, ranging from a maximum of 16 ± 2 to a minimum of 13 ± 2 m w. eq. a^{-1} between 1964 and 1994 (Naruse and others, 1997).

On December 1 1995 a stake was drilled (Stake D) using a steam driller (Heucke, 1999) at an altitude of ~230 m near the margin of Glaciar Moreno. This was re-surveyed several times until April 30 1996, yielding a total ablation of 10.99 m, which corresponds to a k_i of 7.3 mm °C d^{-1} w. eq. (Stuefer, 1999).

At an elevation of ~380 m on Glaciar Moreno, Stuefer (1999) installed a stake network (profile A) which was measured several times between 1995 and 1998, resulting in a mean k_i for the winter season (April-October) of 2.9 mm °C d^{-1} w. eq. at the centre of the glacier and 3.9 mm °C d^{-1} w. eq. at the margin of the glacier. During the summer season (November-March) they calculated higher k_i values, with an average of 6.5 mm °C d^{-1} w. eq. at the centre of the glacier and 7.6 mm °C d^{-1} w. eq. at the margin. These values were used by Rott and others (1998) to estimate mean ablation values of 44.9 mm d^{-1} w. eq. for the summer season, and 10.3 mm d^{-1} w. eq. for the winter season, giving an estimated total annual ablation of 10.1 m a^{-1} w. eq. for Profile A.

Ablation rates have also been measured at an altitude of ~700 m on Glaciar Tyndall, where Koisumi and Naruse (1992) obtained a mean k_i of 11.8 mm °C d^{-1} w. eq. based upon 8 days of measurements carried out in December 1990. During 7 days of December 1993, Takeuchi and others (1995) resurveyed the same area of Glaciar Tyndall (~700 m), and obtained an average k_i of 12.4 mm °C d^{-1} w. eq.

At Glacier Soler of the NPI, Fukami and Naruse (1987) measured smaller k_i values of 5.48 mm °C d^{-1} w. eq. for bare ice surfaces, whilst on the debris covered ice surface of the glacier they calculated a k_i of 7 mm °C d^{-1} w. eq.

The above measurements demonstrate the wide variability in the degree-day factor for ice surfaces depending on the altitude, albedo of the surface and the reference temperature series used. Therefore a range of k_i values of between 6 and 7.5 mm °C d^{-1} w. eq. will be used in the model in order to determine the best-fit result, especially considering that the ablation area of Glaciar Chico is not necessarily homogeneous bare ice, as some of its surface is dirty with ash bands and some debris and other morrenic materials (See Figure 6.1).

Table 6.6 summarises the best-fit degree-day factors obtained after applying mass balance models in the Northern Hemisphere to several temperate glaciers of Norway and Iceland. These models are based upon temperature and precipitation records from a reference station which are extrapolated to the glacier in a similar way to that used in the model presented here. Due to the lack of snow ablation measurements from Patagonian glaciers, the range of values presented in Table 6.6 for snow ablation (k_s) will be tested in the model in order to obtain the best-fit result.

Table 6.6 Best-fit parameters obtained from degree-day factor models applied to glaciers in the Northern Hemisphere.

Location	Degree-day factors mm °C d^{-1} w. eq.		References
	Snow	**Bare ice**	
Nigardesbreen (southern Norway)	4.4	6.4	Jóhannesson and Sigurdsson (1995)
Sátujökull (Iceland)	5.6	7.7	Jóhannesson and Sigurdsson (1995)
Alfotbreen (southern Norway)	4.5	6	Laumann and Reeh (1993)
Nigardesbreen (Southern Norway)	4.0	5.5	Laumann and Reeh (1993)
Hellstugubreen (Southern Norway)	3.5	5.5	Laumann and Reeh (1993)

6.3.3.2 Reference station for temperature

The spatial distribution of temperatures in Patagonia has been described to be linearly distributed with respect to altitude (DGA, 1987). However, different saturated lapse rate temperature gradients have been estimated for the region based upon direct measurements and available temperature records. For example, at Glaciar Benito located on the western side of the NPI, Sessions (1975) measured a lapse rate of 5.0 °C km^{-1}. Peña and Gutiérrez (1992) estimated a slightly higher value of 5.3 °C km^{-1} for Torres del Paine located on the eastern side of the SPI. Also on the eastern side of the SPI, Takeuchi and others (1996) calculated a lapse rate of 8 °C km^{-1} at the lower end of Glaciar Moreno, whilst DGA (1987) estimated a regional average lapse rate of 6 °C km^{-1}. Considering that the model will be

representative of the wider region, and that no measurements exists for Glacier Chico, a lapse rate range between 6 and 6.5 °C km^{-1} will be tested.

Only two meteorological stations on the eastern side of the SPI provide useful reference records for running the mass balance model, based upon the criteria enunciated in 5.1. These stations (Cochrane and Lago Argentino) exhibited a small number of data gaps, which were filled in Section 5.2.1. Both stations present a high correlation (r=0.98), with slightly higher (0.36°C) monthly average values at Cochrane due to its more northerly location. Glaciar Chico is located at 49°S, at a similar distance from both stations, therefore it is reasonable to estimate an average temperature series based upon both stations in order to define the reference record. For this purpose, a regional lapse rate of 6 °C km^{-1} was applied to both station's records in order to calculate the temperature series at 250 m, corresponding to the minimum altitude of the glacier. Then the mean monthly temperature was calculated, based upon each monthly value of the series 1975 – 2001 obtained from both altitudinally corrected stations, yielding the temperature of the reference record (*tmr*).

6.4 Results of the model

6.4.1 Calibration and best-fit parameters

The best-fit values were obtained initially by comparing the mass balance measured at the mast located at the Glaciar Chico base camp with the resulting mass balance obtained from the model for the same location. The second consideration was based upon a comparison of the ablation rates measured from nearby glaciers of the SPI at different altitudes and the ablation determined by the model at the same altitude. Finally, the precipitation obtained from the model at Glaciar Chico's base camp was compared with the estimated precipitation for the same location based upon stake measurements.

After applying the fixed parameters given in Table 6.7, and experimenting with different values for the other parameters listed in Table 6.8, the best-fit values were obtained.

Table 6.7 Fixed model parameters.

Parameter	Name	Value	Unit
Elevation of reference station for temperature	z_{pt}	250	m a.s.l.
Elevation of reference station for precipitation	z_{pp}	182	m a.s.l.
Snow/rain threshold	tt	2	°C

Table 6.8 Best-fit parameter values determined from the model.

Parameter	Name	Tested range	Best-fit value	Unit
Degree-day factor for ice	k_i	0.006 to 0.0075	0.0065	m °C d^{-1} w. eq.
Degree-day factor for snow	k_s	0.0035 to 0.0045	0.004	m °C d^{-1} w. eq.
Precipitation/ Elevation gradient below 1400 m	g_l	0.003 to 0.0035	0.003	m m^{-1}
Precipitation/ elevation gradient above 1400 m	g_h	0.0035 to 0.004	0.0037	m m^{-1}
Temperature lapse rate	j	0.006 to 0.0065	0.006	°C m^{-1}

Table 6.9 shows the comparison between selected parameters (modelled versus observed/estimated). The precipitation estimated in the model for the area surrounding the base camp of glacier Chico is very similar to the estimated value obtained from stake measurements and snow pits. However, the ablation rates obtained in the model are slightly higher than those estimated by Naruse and others (1997). The ablation rates at 250 m from Glaciares Upsala and Chico are within the error range described by Naruse, but the difference at 370 m is significantly higher than the combined mean value and error estimated for Glaciar Moreno. The main reason for these higher values could be related to the higher temperatures at Glaciar Chico due to its more northerly location compared with the other two glaciers used for reference purposes.

Table 6.9 Model results for Glaciar Chico versus observed parameters from specified locations.

Parameter	Modelled (m a^{-1} w. eq.)	Observed (m a^{-1} w. eq.)	Reference for observed values
Precipitation at base camp Glaciar Chico (1440 m a.s.l.)	3.94*	4.07 ± 0.54	This study
Ablation at glacier front (250 m a.s.l.)	16.1*	14.5 ± 2**	Naruse and others (1997)
Ablation at ~350 m a.s.l.	15.7*	12.6 ± 2***	Naruse and others (1997)
Mass balance at base camp Glaciar Chico (1440 m a.s.l.)****	0.58	0.54± 0.21	This study

average value 1975-2001

** estimated for Glaciar Upsala based upon ice density of 900 kg m^3

*** estimated for Glaciar Moreno based upon ice density of 900 kg m^3

****estimated between 1994/95 and 2001/02 with the exception of 2000/01

In spite of the above differences between modelled and observed/estimated values, the most important source of calibration data for the model were the balances obtained at the base camp of Glaciar Chico between 1994/95 and 2001/02. Figure 6.8 shows the modelled series and the observed balance at this location. In most years the modelled values are close to the observed series, with the significant exception of 2000/2001, when the modelled balance is 4 times higher than the observed value. This difference could be related to particular meteorological conditions at the reference stations during this period which did not affect the glacier (or vice versa). After a preliminary analysis of the temperature series of this year, become

clear that the mean temperatures of September where one of the most peculiar of the whole series with the lowest mean values at Lago Argentino and the second lower at Cochrane between 1975 and 2001. Regarding precipitation, the record from both stations are within normal values.
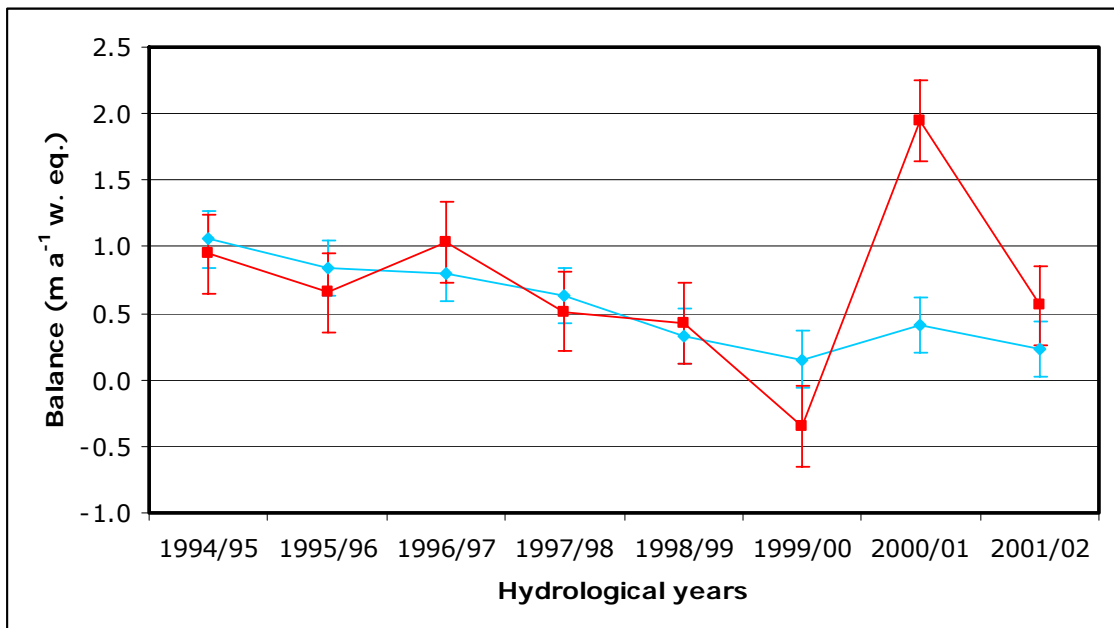
Figure 6.8 Modelled mass balance (red) and measured mass balance at the mast (light blue) in m a^{-1} of w. eq. The error bars represent 0.2 m a^{-1} of w. eq. for the measured series and 0.3 m a^{-1} of w. eq. for the modelled series.

In the light of the above, it is reasonable to assume, therefore, that the measurements at the base camp represent a smoothed record of a complex accumulation process taking place on the main plateaux of the SPI, with extreme years not necessarily well characterised. This could be especially true for years when dry and/or warm conditions prevent any accumulation, resulting in a negative mass balance at altitudes higher than normal. In these cases it will be impossible to accurately assign annual mass balances from snow pits or ice cores. However, between 1994/95 and 2001/02 the

snow pits and the height of the mast above the snow surface have been measured on a near annual basis, therefore, it is unlikely that a year with negative mass balance at this location occurred unnoticed.

In order to improve the inter-annual variations of the modelled mass balance, other variables could to be included (i. e. wind direction and speed at different altitudes acquired at radiosonde stations), however, the main problem will remain until an automatic weather station (AWS) is installed on the glacier (o nearby) in order to better represent the local meteorological conditions affecting the glacier.

Considering the series between 1994/95 and 2001/02 with the exception of 2000/01, the mean difference between the observed and modelled values is 0.04 ± 0.26 m a^{-1} w. eq.; this being equal to one standard deviation between both series (Table 6.9). The modelled values in general seem to replicate well the balance and precipitation observed at the base camp of Glaciar Chico, however the uncertainties are high, as revealed by the extreme accumulation modelled for 2000/01. Estimating errors for the modelled values is difficult because of the lack of data for calibration, however a mean error estimate of 0.3 m a^{-1} w. eq. will be assumed for the modelled data based on the differences obtained by comparing balances at the base camp, plus other uncertainties not accounted for here. Considering that the observed mass balance at the base camp has an error of 0.21 m a^{-1} w. eq., all but one (2000/01) modelled annual mass balances are statistically similar to the measured values.

The best-fit degree-day factors obtained from the calibrated model (Table 6.8) are similar to those values obtained from model runs applied in the Northern Hemisphere (Table 6.6), and within the range of measurements acquired in Patagonia. Nevertheless, some degree-day factors measured in Patagonia, especially those obtained during short periods during the summer (Takeuchi and others, 1996), are much higher than the best-fit values yielded by the model. This could be explained by the fact that during the summer degree-day factors are 2 times higher than during the winter (Rott and others, 1998), and therefore an annual degree-day factor must be smaller than the summer observation in order to represent the conditions during the whole year.

Two best-fit precipitation gradients were obtained (Table 6.8), representing the shallow gradient observed at lower altitudes (below 1400 m), and the steeper gradient at high altitudes where the main plateaux of the SPI are located. The boundary between these gradients (1400 m) was also tested, and the best result obtained after calibrating the values with the precipitation measurements from the mast installed at Glaciar Chico's base camp. The use of two linear gradients, in spite of the exponential function described in Figure 6.7, is supported by the fact that the exponential function resulted in extremely high modelled values of precipitation on the mountain tops. With the two best-fit gradients used here, the maximum modelled precipitation yielded an average of 12.2 m a^{-1} at an elevation of 2800 m, which is higher than Escobar and others (1992), but within the range of maximum precipitation estimated by Shiraiwa and others (2002) for a location exposed to wind and to the west of the continental ice divide.

6.4.2 Modelled mass balance 1975-2001

The mass balance model calculates total accumulation and total ablation, and therefore the mass balance at the specified elevation of each pixel of the glacier surface between the given dates of April 1975 and March 2002.

Two DEMs (MODEL-DEM-1975 and SRTM) were used to account for the effect of the elevation feedback on the mass balance of the glacier generated by the ice elevation change between 1975 and 2002. The same parameters (Tables 6.7 and 6.8) were used for both DEMs and a linear ice thinning rate between 1975 and 2002 was assumed (-1.3 m a^{-1}). The differences between the resulting mass balances from both DEMs were proportionally subtracted in order to obtain the final mass balance of the glacier (Figure 6.9).
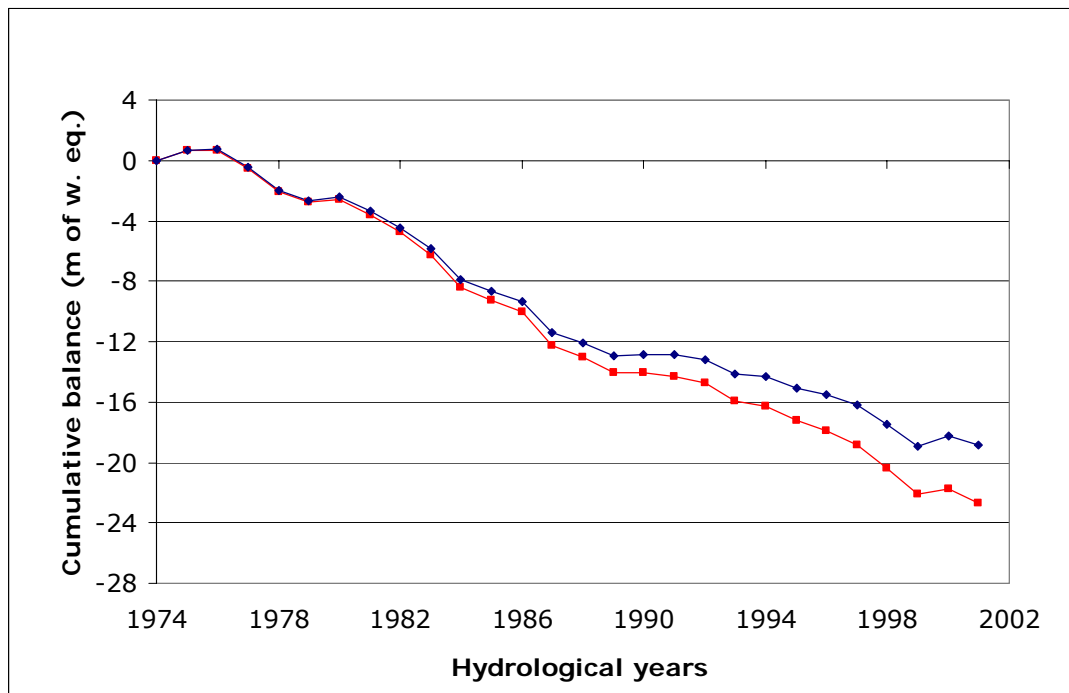
Figure 6.9 Cumulative mass balance of Glaciar Chico between 1975 and 2001 in m a^{-1}. The blue line shows the modelled mass balance without allowing for altitudinal changes on the glacier. The adjusted mass balance to acknowledge the ice elevation changes experienced by the glacier during this period is shown in red.

Both modelled cumulative mass balances can be seen in Figure 6.9. Both curves begin with the same mass balance value in 1975, however the differences are progressively greater as the ice elevation difference increases between both DEMs. At the end of the modelling period there is an average difference of -0.14 ma^{-1} between the non-adjusted DEM versus the adjusted DEM due to ice thinning observed between 1975 and 2001. That means that ~17% of the modelled mass balance of Glaciar Chico could be explained only by elevation changes, representing the elevation feedback effect.

Table 6.10 Main components of the modelled mass balance of Glaciar Chico.

Hydrological Year	Glacier Area (km^2)	$\overline{b_a}$ (m a^{-1})	$\overline{b_b}$ (m a^{-1})	$\overline{b_n}$ (m a^{-1})	B_n (km^3 a^{-1})
1975	199.0	3.98	-3.31	0.66	0.13
1976	198.9	3.82	-3.78	0.04	0.01
1977	198.7	3.71	-4.93	-1.22	-0.24
1978	198.6	3.37	-4.92	-1.55	-0.31
1979	198.5	3.73	-4.45	-0.72	-0.14
1980	198.3	3.99	-3.81	0.18	0.04
1981	198.2	3.53	-4.51	-0.99	-0.20
1982	198.0	3.47	-4.63	-1.15	-0.23
1983	197.9	3.41	-4.90	-1.49	-0.29
1984	197.8	3.30	-5.45	-2.15	-0.42
1985	197.6	3.57	-4.45	-0.88	-0.17
1986	197.5	3.59	-4.38	-0.79	-0.16
1987	197.2	3.17	-5.35	-2.18	-0.43
1988	196.8	3.52	-4.29	-0.76	-0.15
1989	196.5	3.53	-4.58	-1.05	-0.21
1990	196.2	3.94	-3.95	-0.01	0.00
1991	195.9	3.82	-4.08	-0.25	-0.05
1992	195.5	3.73	-4.17	-0.45	-0.09
1993	195.2	3.27	-4.45	-1.18	-0.23
1994	194.9	3.77	-4.09	-0.32	-0.06
1995	194.6	3.56	-4.52	-0.96	-0.19
1996	194.2	3.67	-4.34	-0.67	-0.13
1997	193.9	3.58	-4.53	-0.95	-0.18
1998	193.6	3.53	-5.06	-1.53	-0.30
1999	193.3	3.23	-4.98	-1.75	-0.34
2000	192.9	3.84	-3.47	0.37	0.07
2001	192.6	3.56	-4.55	-0.99	-0.19
Average		3.6±0.3	-4.44±0.3	-0.84±0.3	-0.165±0.059

Considering the glacier area changes determined in Section 4.2.5, and assuming a linear trend between the observed dates, the resulting net mass balance of the glacier and each of the main components is shown in Table 6.10. The average modelled annual mass balance between 1975 and 2001 was -0.84 ± 0.3 m a^{-1}, equivalent to a total volume loss of -4.46 km^3 (an average of -0.165 ± 0.059 km^3 a^{-1}) during the 27 year period of the model run.

The majority of years (23 out of 27) exhibited negative mass balances, with an extreme negative balance of -2.18 calculated for 1987/88, and the greatest positive balance of 0.66 calculated for 1975/76 (Figure 6.10). Between 1975 and 1981 the average mass balance of the glacier was negative, although 3 years were indicated to have a positive values. Between 1982 and 2000 every year presented negative mass balances, only interrupted in 1991 when the balance was almost zero. The cumulative curves present a negative linear trend for the net mass balance, especially after the series of positive years at the beginning of the analysis period (Figure 6.11).
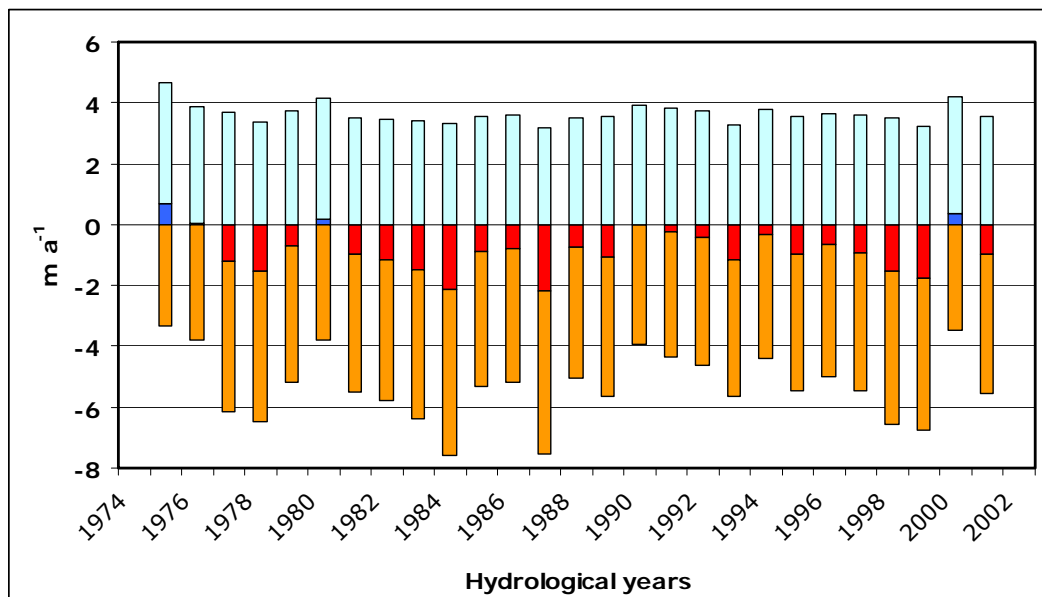
Figure 6.10 Annual modelled mass balance calculated for Glaciar Chico between 1975 and 2001 in m a^{-1}. The light blue bars represent the net accumulation. The orange bars represent the net ablation, and the resulting mass balance is represented in red for years with negative values and blue for years with positive net mass balances.
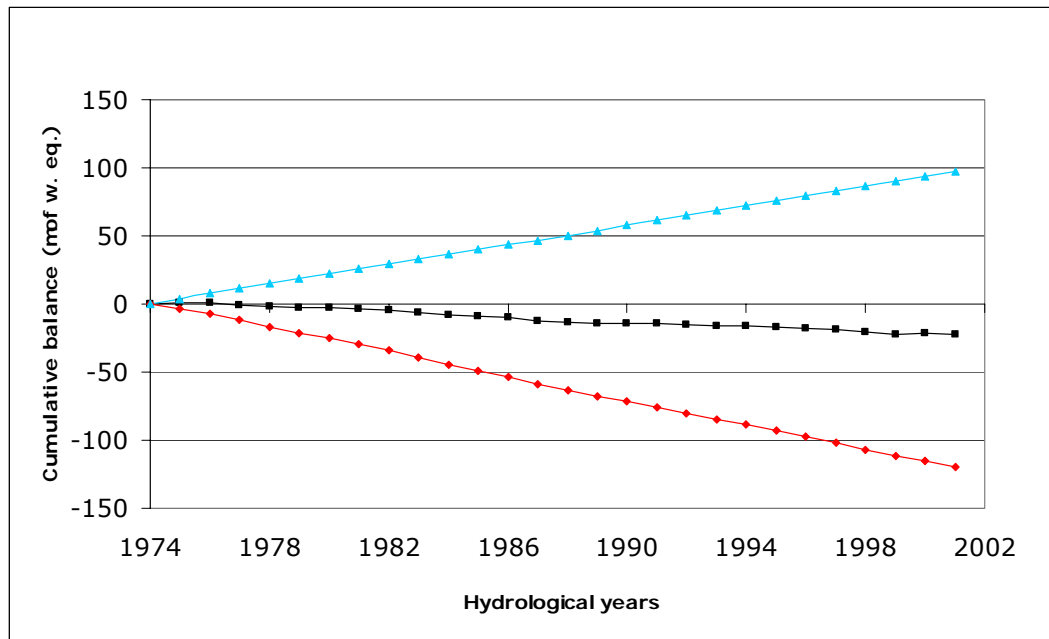
Figure 6.11 Cumulative net balance (black line), accumulation (light blue line) and ablation (red line) between 1975 and 2001 in m a^{-1}.

In spite of this generally negative trend, a high inter-annual variability was observed during the study period (Figure 6.12), which was more significant at the beginning of the series when positive and negative mass balance years were observed alternately. During the 1980s the net mass balance showed some variability, but the values were consistently negative, however by the end of this decade the rate of mass balance loss had declined. During the 1990s, the mass balance series demonstrated a smaller inter-annual variability within a negative trend, reaching a minimum balance in 1999. The most recent years of the series present a similar pattern to that observed at the beginning of the series, with increased inter-annual variability fluctuating above and below zero. The modelled mean net mass balance at the location of the mast between 1975 and 2001 was 0.69 ± 0.3 m a^{-1}, which is higher than the mean value

observed between 1994 and 2001 at the mast ($\sim 0.6 \pm 0.21$ m a^{-1}), but within the error range of both data sets.
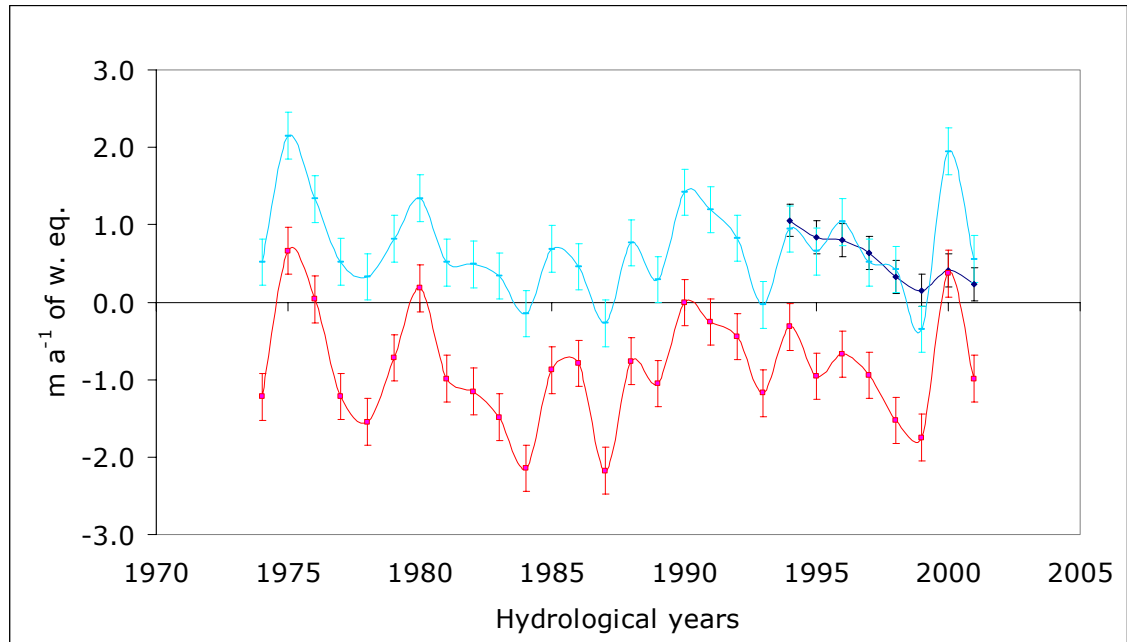
Figure 6.12 Mass balance measured at the mast between 1994 and 2001 (dark blue line), modelled for the mast (light blue line) and modelled for the glacier as a whole (red line) in m a^{-1}. The error bars represent 0.3 m a^{-1} w. eq. for the modelled series and 0.2 m a^{-1} w. eq. for the measurements at the mast.

The mass balance series modelled for the mast installed at 1440 m asl showed a similar pattern of inter-annual variability to that of the glacier as a whole, but appears to be much smoother. During the first part of the series between 1975 and 1980, the area surrounding the mast showed positive accumulation, however during the 1980s the values were progressively smaller, with negative balances at this altitude during 1984/85 and 1987/88. During the 1990s the modelled data for the mast showed positive balances, with the exception of 1993/94 and 1999/2000.

This last year is well correlated with the minimum observed accumulation registered from snow pits and direct observations at the mast.

Considering the resulting mean mass balance between 1975 and 2001 with respect to altitude (Figure 6.13), it is possible to appreciate a semi-linear trend. Minimum balances are evident at lower altitudes (-16 ma^{-1} at ~250 m), a mean modelled ELA at approximately 1415 m, and positive values at higher altitudes with a maximum of 12 m a^{-1} at the top of the mountains (~2800 m).
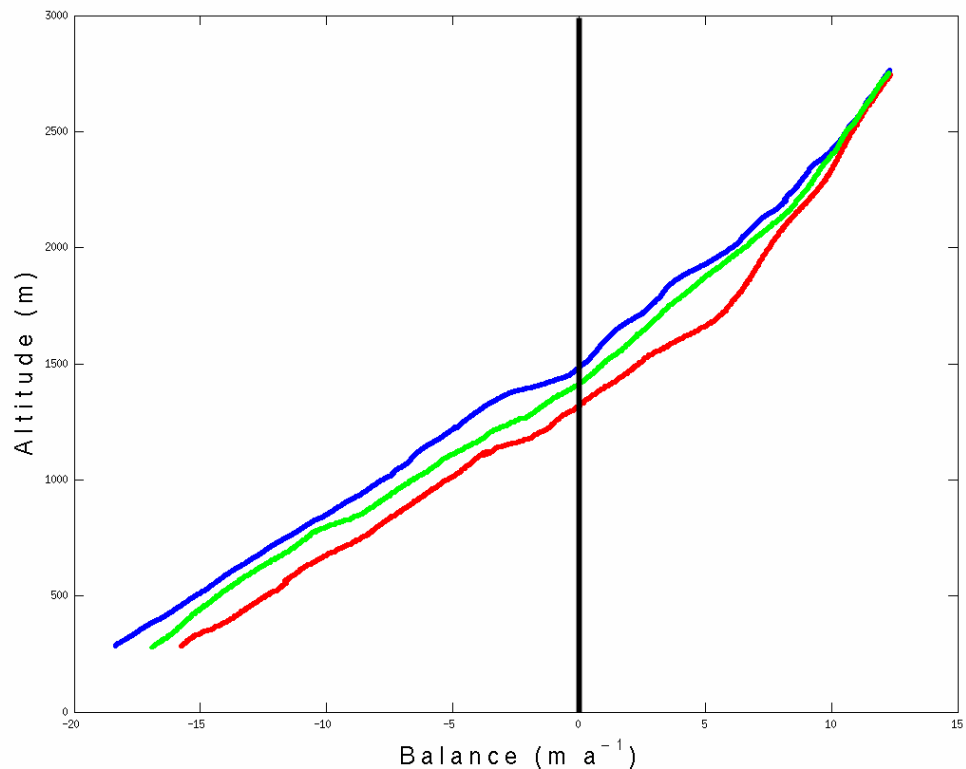
Figure 6.13 Modelled mass balance (m a^{-1}) of the whole glacier versus altitude (m). The most positive mass balance of the series (1975/76) is shown in red and the most negative mass balance of the series (1987/88) is in blue. The mean mass balance between 1975/76 and 2001/02 is shown in green.

The average mass balance gradient of the glacier is modelled to be 0.0132 a^{-1}, which is within the range of between 0.010 and 0.015 a^{-1} calculated by Naruse and others (1995) for Glaciares Moreno and Upsala.

The curves obtained for hydrological years with extreme balances (positive in 1975/76 and negative in 1987/88) have almost the same shape as the average curve at higher altitudes (>2000 m), probably meaning that this area permanently experiences temperatures below +2°C (the precipitation/snow threshold). This suggests that there is no significant ablation in this region, a fact which is corroborated by Figures 6.14 and 6.15 of the modelled accumulation and ablation gradients for the glacier. Below 2000 m the differences between the modelled mass balances for these extreme years are more significant, particularly at the altitudes of the main plateaux of the SPI (1400 to 2000 m), where, during 1975/76, a higher accumulation was modelled (Figure 6.14). During 1987/88, the year of the series with most negative modelled mass balance, the estimated ELA reached a maximum altitude of ~1500 m, which is above the ice divide between Glaciares Chico and Viedma (~1450 m). This indicates that most of the main plateaux of Paso Cuatro Glaciares flowing into Glaciar Chico experienced ablation. Below the altitude of the modelled ELA the differences are linearly distributed around the mean value.

The accumulation gradient (Figure 6.14) shows no significant variation between the mean, maximum and minimum curves in areas located below 1000 m and at altitudes higher than 2300 m. But significantly, all the

differences between the extreme years occur around the ELA and in the main plateaux of the SPI. Below 2300 m the mean accumulation curve is similar to the exponential distribution of precipitation described in Figure 6.7. However, at higher altitudes, the extrapolated precipitation value generates a maximum accumulation value of 12 ma^{-1}, which is much smaller than the predicted value of 33 m a^{-1} if the exponential curve is used.
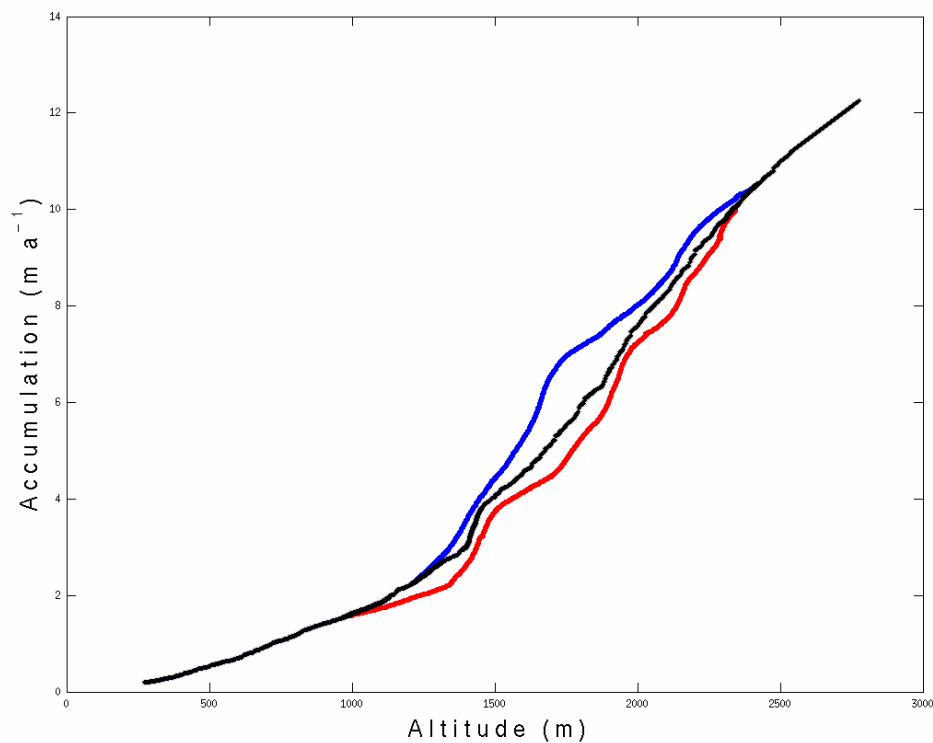
Figure 6.14 Modelled accumulation (m a^{-1}) of the whole glacier versus altitude (m). The highest accumulation year of the series (1975/76) is shown in blue and the lowest accumulation year of the series (1987/88) in red. The mean accumulation between 1975/76 and 2001/02 is shown in black.

The modelled ablation gradient for the whole glacier is shown in Figure 6.15. All curves (mean, maximum and minimum ablation) present a linear trend between 250 and ~2000 m. Above this altitude the ablation approaches zero for all the curves.
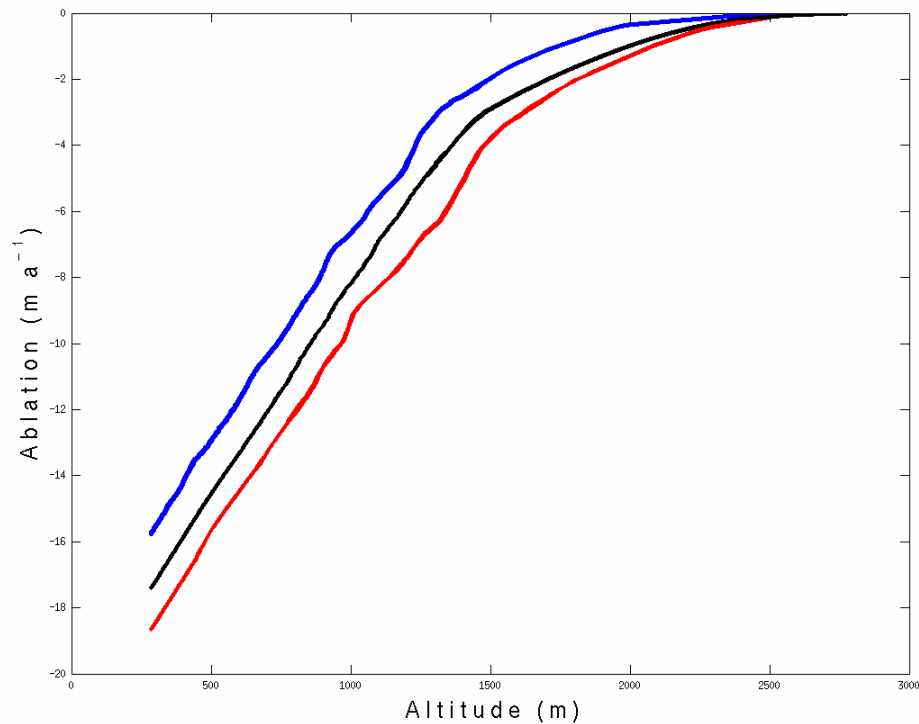
Figure 6.15 Modelled ablation (m a^{-1}) of the whole glacier versus altitude (m). The smallest ablation year of the series (1975/76) is shown in blue and the highest ablation year of the series (1987/88) in red. The mean ablation between 1975/76 and 2001/02 is shown in black.

The spatial distribution of the mean modelled accumulation between 1975 and 2001 is shown in Figure 6.16, with minimum values indicated at the lower end of the glacier, where some snow accumulation can occur only during the winter. At mid-altitudes, near the ELA of the glacier, the total accumulation rises to 2 to 3 m a^{-1}, with a gentle gradient up to the base

camp in the accumulation area of the glacier, where the accumulation is approximately 4 m a^{-1}. The upper areas of the glacier show a sharp increase in the accumulation gradients, especially at the flanks of the two main mountain ranges of the area, Gorra Blanca in the east and Pirámide in the west.
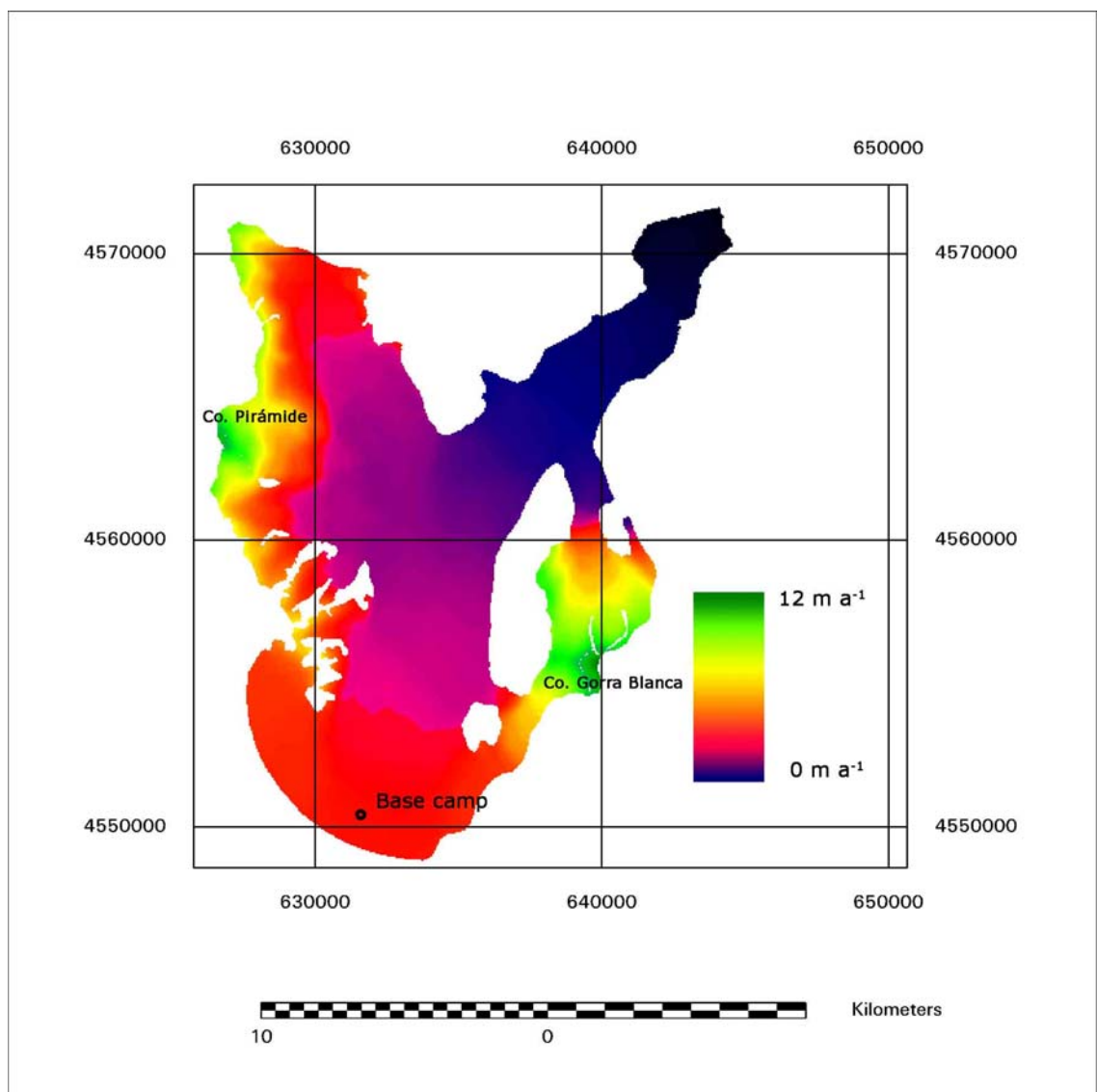
Figure 6.16 Mean modelled accumulation between 1975 and 2001 across Glaciar Chico in m a^{-1}. UTM co-ordinates in m datum WGS1984.

The spatial distribution of mean modelled ablation between 1975 and 2001 is shown in Figure 6.17. As described above, the areas higher than 2000 m present almost no ablation, whereas at the lower end of the glacier maximum mean ablation rates of -16 m a^{-1} were modelled at the calving front of the glacier into Brazo Chico of Lago O'Higgins. The area surrounding the ELA of the glacier has a modelled ablation rate of -4 m a^{-1}, whilst at the mast in the accumulation area there is an ablation rate of -3 m a^{-1}.
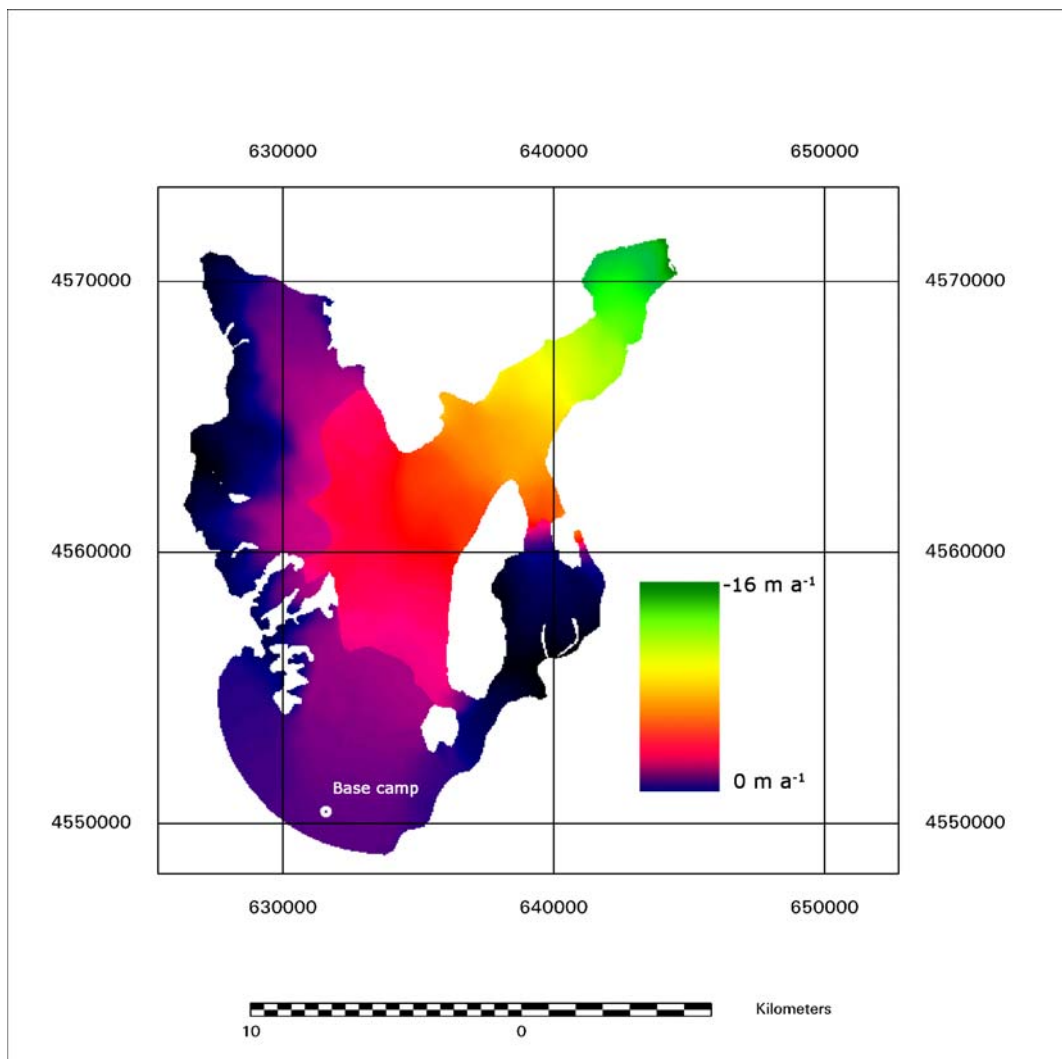
Figure 6.17 Mean ablation between 1975 and 2001 across Glaciar Chico in m a^{-1}. UTM co-ordinates in m datum WGS1984.

The spatial distribution of the mean modelled mass balance of the glacier is shown in Figure 6.18. The approximate location of the ELA for different years is also included in order to estimate possible changes in its position. The initial ELA used in the model (ELA-1975) is located at the lowest altitude of the series (1300 m). The mean ELA obtained from the model for the period 1975 – 2001 is located at approximately 1400 m, at a higher position with respect to the average ELA obtained between 1981 and 2001 (1320 m) as described in more detail in Section 4.1.3. The area between the mean modelled ELA and ELA-1975 is very flat, therefore the horizontal migration is greater than the vertical change. This migration of the ELA is much larger than the changes observed at the steep glacier tongues flowing from Cerro Gorra Blanca where the ELA has been more stable (Figure 6.18).
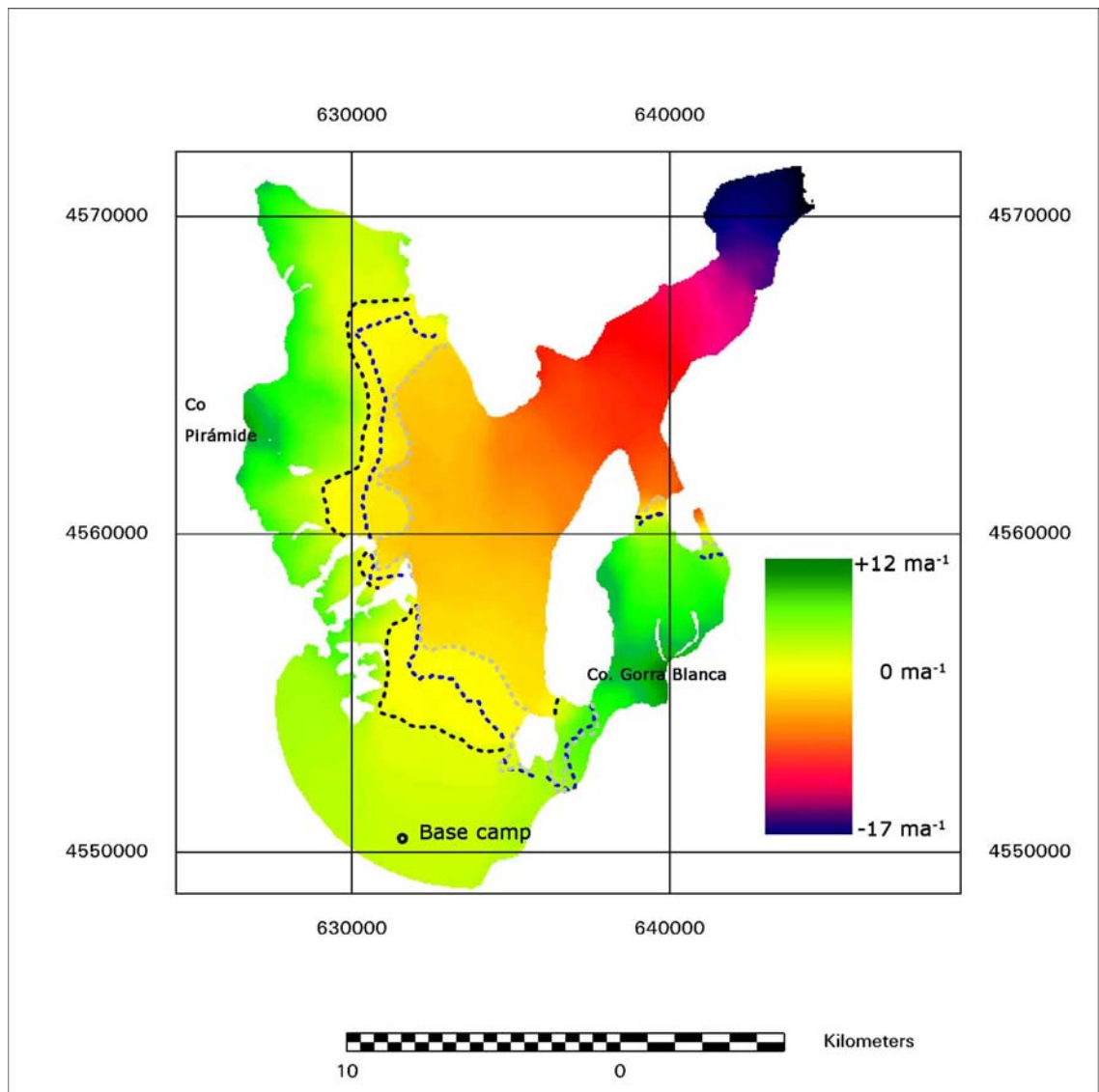
Figure 6.18 Mean mass balance of the glacier in m a^{-1}. The grey dotted line represents the estimated ELA in 1975. The blue dotted line is the ELA in 2001. The black dotted line is the mean ELA obtained from the model. UTM co-ordinates in m datum WGS1984.

6.4.3 Sensitivity analysis based upon different climate scenarios

The mass balance model described here was run several times using different climate change scenarios described by the Intergovernmental Panel for Climate Change (IPCC, 2001) for the Southern South America

(SSA) region. These simulated projections are based upon an increase in atmospheric CO_2 of 1% a^{-1}, both with and without sulphate forcing using different coupled Atmosphere-Ocean General Circulation models (AOGCMs). These models have different spatial and temporal scales, varying from 300 to 500 km for the horizontal atmospheric resolution and centennial to millennial time scales.

The spatial resolution of all these models is very coarse, therefore southern Chile is poorly represented, and the spatial climatic variations described in Chapter 5 for Patagonia are not indicated at all. Thus the projected changes in temperature and precipitation described by the IPCC (2001) for SSA are here considered only to be a general approximation.

The climatic changes for the SSA region vary widely between AOGCMs, however a general trend of temperature increases of between +2°C and +3°C per Century appear to be typical of the region. Regarding precipitation, most of the AOGCMs estimate an increase in winter precipitation of between 10 and 20%, and a reduction of summer precipitation of between 0 and 20% for the period 2071 to 2100 compared with the mean for the period 1961 to 1990.

The projected temperature increases described by the IPCC fall within the observed range of climatic changes described in Chapter 5 for Patagonia (see Table 5.8), where temperature trends fluctuated between 2.1 and 3.3 °C per 100 years among the stations located along the eastern side of the SPI. The observed range of changes in precipitation in Patagonia (Table

5.7) are much higher than the values predicted by the IPCC (2001), and all of the significant annual precipitation trends currently observed in Patagonia are negative. However, if these precipitation trends are maintained in the future, Patagonia will be a desert by the end of the 21st Century with precipitation totals close to zero at most of the stations. This scenario is very unlikely because the precipitation trends observed in Patagonia between 1961 and 1990 were significantly affected by the cycle of positive precipitation anomalies observed during the 1960s. Based on the assumption that in the future there will be oscillation patterns similar to that described for the 1960s, a change in annual precipitation of between -30% and +20% over the next hundred years will be applied in the mass balance model. These climatic scenarios will be testing without consideration of possible seasonal variability, assuming that the climatic perturbations will be homogeneously distributed trough the year. This assumption simplify the calculations of possible glacier responses, but could induce to high uncertainties. For instance, if all forecasted reduction in precipitation is taking place during winter season, the effects on snow accumulation will be much more dramatic than predicted.

The temperature and precipitation records observed at the reference station (which acts as the main climatic input for the model) were re-calculated using the forcing parameters described for each climate change scenario. The resulting series of temperature and precipitation were tested individually and then combined. The same fixed and best-fit parameters defined in Tables 6.7 and 6.8 were used for each climatic scenario. DEM-

1975-MODEL and ELA-1975 were used as the initial conditions for running the model.

6.4.3.1. Model run with no elevation feedback effect

The model was run only for one DEM (DEM-MODEL-1975) in order to compare results without the influence of elevation feedback on the mass balance. The magnitude of the elevation feedback was originally calculated by comparing the model results from two DEMs (1975 and SRTM), which were generated based upon ice elevation changes observed on the glacier during the period between 1975 and 2001. Ice elevation changes due to the different forcing climatic scenarios described are unknown, and it is unlikely that the observed thinning will be similar for each of the forcing scenarios, for example the elevation feedback effect will be probably enhanced with a warming trend of +3°C. Therefore, in order to resolve only the changes in the mass balance the same initial topography is applied for all scenarios. The impact and magnitude of a possible elevation feedback effect will be discussed further in Section 6.3.3.2.

Table 6.11 shows the mass balance components obtained using the observed data and DEM-MODEL-1975, as well as the results obtained by running the model with each future climatic scenario considered here. The climate change scenarios have been divided into three groups (Table 6.11):

- No changes in temperature, and a precipitation decrease of -30% per Century.

- A warming trend of +2°C per Century, with different precipitation scenarios ranging from -30% to +20% per Century.

- A warming trend of +3°C per Century, with different precipitation scenarios ranging from -30% to +20% per Century.

The results presented in Table 6.11 show the mean accumulation ($\overline{b_a}$), ablation ($\overline{b_b}$) and mass balance ($\overline{b_n}$) per year (over a 27 year period) for the glacier as a whole, and the mean balance for the location of the mast installed at Glaciar Chico's base camp.

Table 6.11 Results of the mass balance model for different scenarios without elevation feedback.

Scenario	$\overline{b_a}$ (m a^{-1})	$\overline{b_b}$ (m a^{-1})	$\overline{b_n}$ (m a^{-1})	$\overline{b_n}$ at mast (m a^{-1})
Model with observed data and without elevation feedback	3.66	-4.36	-0.70	0.93
No change in T°C and precip. -30%	3.65	-4.37	-0.72	0.91
+2°C and -30% precip.	3.54	-4.69	-1.15	0.53
+2°C and -20% precip.	3.54	-4.68	-1.14	0.54
+2°C and -10% precip.	3.55	-4.68	-1.13	0.54
+2°C and no change in precip.	3.56	-4.68	-1.12	0.55
+2°C and +10% precip.	3.56	-4.68	-1.12	0.56
+2°C and +20% precip.	3.57	-4.68	-1.11	0.56
+3°C and -30% precip.	3.49	-4.85	-1.36	0.35
+3°C and -20% precip.	3.49	-4.84	-1.35	0.36
+3°C and -10% precip.	3.50	-4.84	-1.34	0.37
+3°C and no change in precip.	3.51	-4.84	-1.33	0.37
+3°C and +10% precip.	3.51	-4.84	-1.33	0.38
+3°C and +20% precip.	3.52	-4.84	-1.32	0.39

Note. The climate change scenarios are expressed as changes per 100 years for temperature (T°C) and precipitation (precip.). For example, +2°C is equivalent to +0.02 °C a^{-1}, -10% precip. is equal to -0.1% a^{-1}.

The first climate change scenario, defined as having an unchanged temperature and a decrease in precipitation of -30% over a Century, shows only small differences (<3%) with respect to the results obtained using the model based upon observed data. The differences are not only restricted to accumulation, which was reduced at the mast and the glacier as a whole, but also affected ablation, which slightly increased, presumably in response to reduced snow cover on the surface of the glacier, causing increased ice ablation due to the higher degree-day factors used for ice surfaces.

The second climate change scenario group, based upon a warming trend of 2°C per Century, generated a significant reduction (~60%) in the mean mass balance of the glacier, ranging from a minimum of -1.15 to a maximum of -1.11 m a^{-1}. Interestingly, different precipitation scenarios did not significantly affect the final result, with the difference between a decrease of -30% and an increase of +20% being only 0.04 m a^{-1}. The average balance at the mast showed a reduction of only ~40% with respect to the modelled value obtained using observed data, indicating that with this warming trend (+2°C), the ablation area experiences the most change, which is confirmed by the greater change in ablation compared with that in accumulation.

The last climate change scenario group, based upon a warming of +3°C per Century, resulted in a reduction of 90% of the average mass balance of the glacier, ranging from a minimum of -1.36 m a^{-1} under the scenario of a -30% precipitation decrease, to -1.32 m a^{-1} under the scenario of an increase of 20% in precipitation. The main changes are evident in the

ablation component, which reached -4.85 m a^{-1} during the most extreme climate change scenario of +3°C and -30% precipitation. At the location of the mast the average mass balance showed a reduction of ~60% with respect to the modelled data without climatic change forcing, indicating that the accumulation area responds at a lesser rate to predicted climate change scenarios.

6.4.3.2 Model run with elevation feedback effect

As described before, the estimated effect of the ice elevation change feedback on the mass balance of the glacier is ~17%. Assuming that this proportion is applicable to the scenarios of climate change described here, the following net mass balance results are obtained (Table 6.12).

Table 6.12 Results of the mass balance model for different scenarios including elevation feedback.

Scenario	$\overline{b_n}$ (m a^{-1})
Model result with observed data including elevation feedback	-0.84
No change in T°C and precip. -30%	-0.87
+2°C and -30% precip.	-1.41
+2°C and -20% precip.	-1.40
+2°C and -10% precip.	-1.39
+2°C no change in precip.	-1.38
+2°C and +10% precip.	-1.37
+2°C and +20% precip.	-1.36
+3°C and -30% precip.	-1.68
+3°C and -20% precip.	-1.67
+3°C and -10% precip.	-1.66
+3°C no change in precip.	-1.65
+3°C and +10% precip.	-1.64
+3°C and +20% precip.	-1.63

The effects of the elevation feedback were proportionally added to each year of the new modelled series, resulting in a cumulative increase in the mass balance (Figure 6.19) from -22.7 m w. eq. (the model results including elevation feedback and observed climate data) to -44.5 m w. eq. obtained using the climate scenario of +3°C and no change in precipitation.
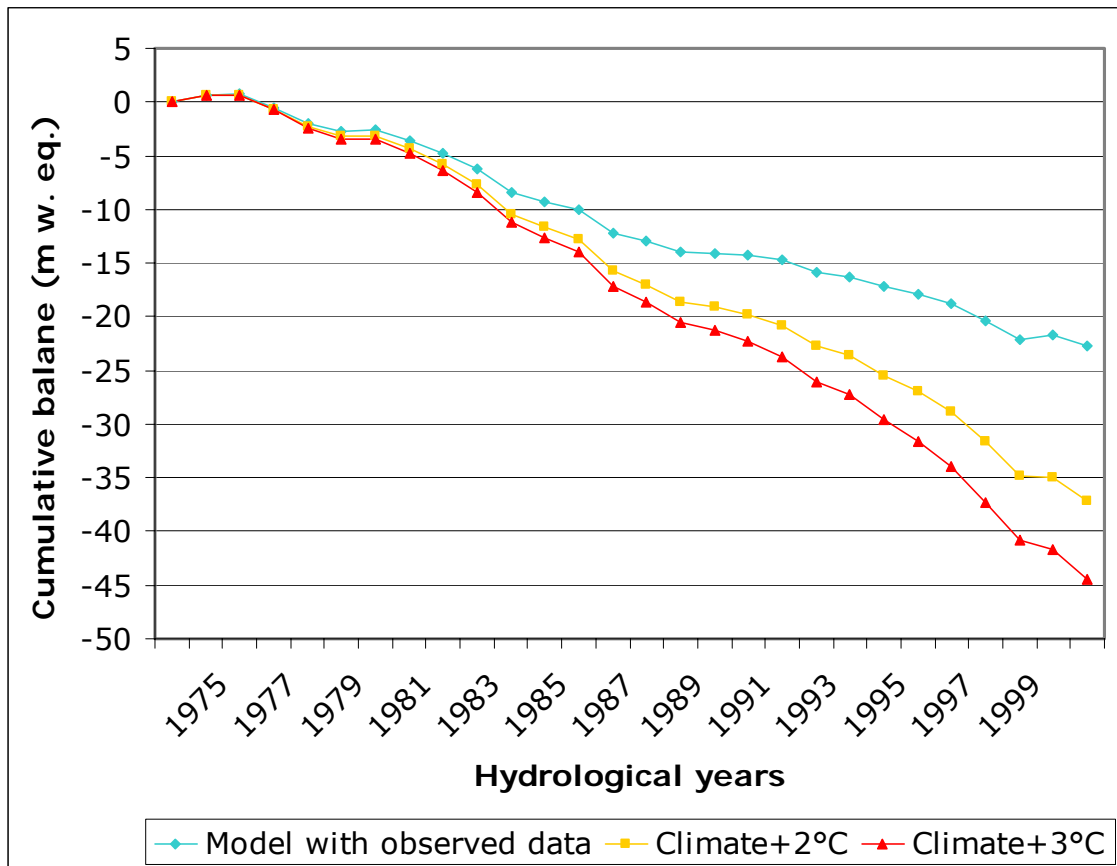
Figure 6.19 Cumulative average mass balance (m w. eq.) obtained by running the model including elevation feedback with observed data and under temperature increases of +2°C and +3°C per Century.

A very different result was obtained for the scenario of unchanged temperature and a precipitation decrease of 30%. The cumulative average mass balance obtained with this scenario is only slightly smaller than the model result using observed data, yielding an average difference of < 3% at the end of the 27 year period.
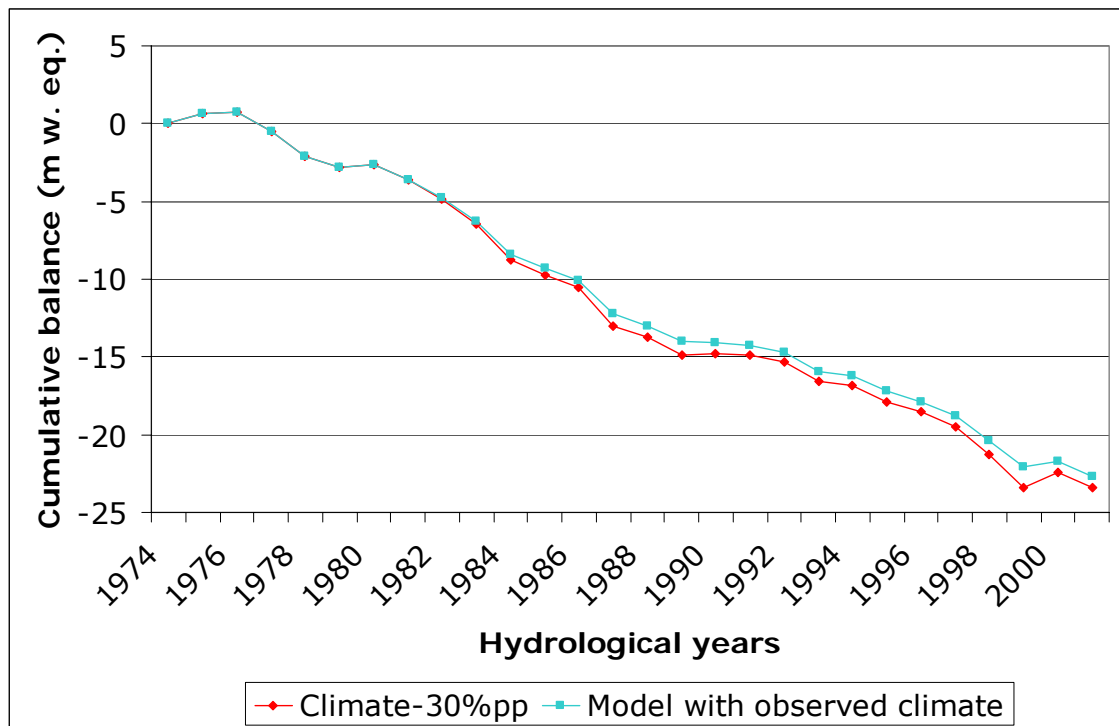
Figure 6.20 Cumulative average mass balance (m w. eq.) obtained by running the model including elevation feedback, with observed data and a climate change scenario of unchanged temperature and a precipitation reduction of -30%.

The mean balance obtained from increasing temperature by +3°C per Century and no change in precipitation plotted versus altitude is shown in Figure 6.21. The curve is very similar to the one obtained by running the model using observed climatic data, however, an average vertical displacement of -50 m was obtained in the ablation area, where the balance under the climate change scenario is more negative. At higher altitudes, the differences between both curves are progressively smaller, indicating that above ~2000 m, no significant changes take place under these conditions of climate change.
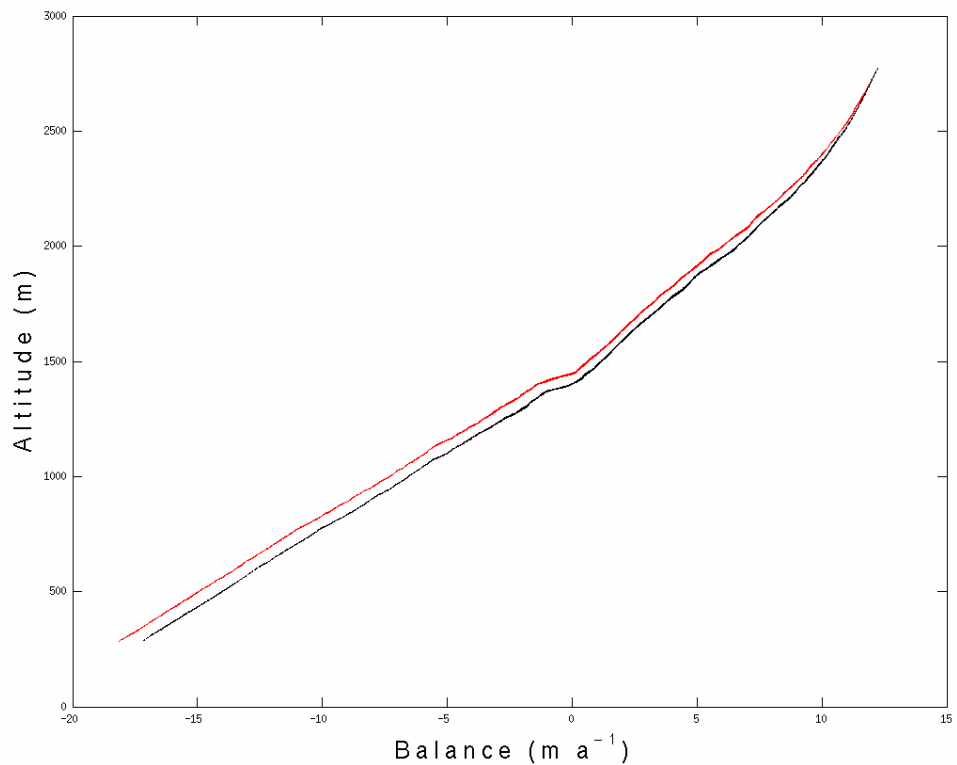
Figure 6.21 *Modelled mean mass balance (m a^{-1}) versus altitude (m), obtained for the whole glacier by running the model based upon observed climate data (black line), compared with results obtained using a +3°C warming trend and no change in precipitation (red line).*

Considering that the modelled mass balance of the glacier proved to be much more sensitive to temperature than precipitation changes, the model was also tested with more extreme climatic change scenarios including warming trends up to +5°C per Century in order to verify the response of each mass balance component. Figure 6.22 shows the resulting gradients, characterized by linear reductions in all components, the largest gradient of change being predicted for the net mass balance of the glacier, and the smallest being the gradient of accumulation.
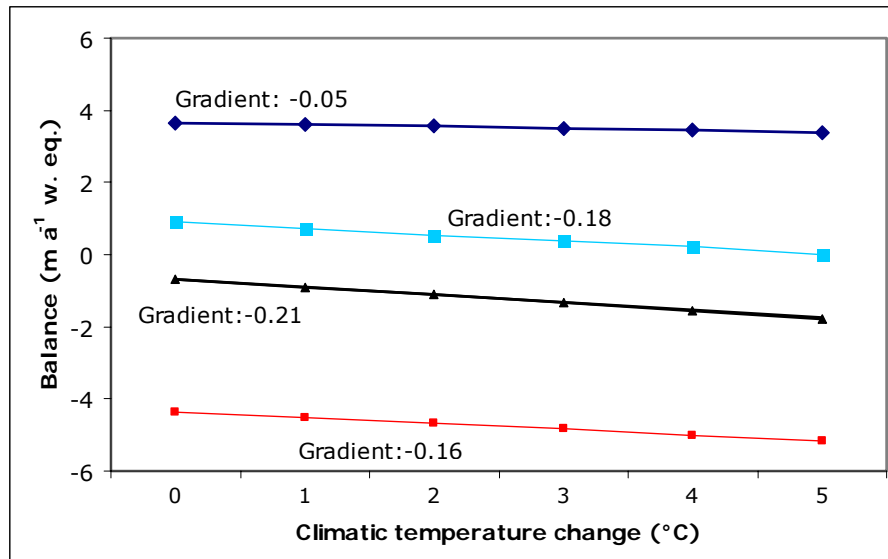
Figure 6.22 Sensitivity of the mass balance model components to warming trends defined as climatic scenarios with warming trends between 0 (observed) and +5°C per 100 years. The blue line shows the net accumulation for the whole glacier, the light blue line shows the net balance at the mast, the black line shows the net balance for the glacier as a whole and the red line shows the net ablation for the whole glacier.

The reduction observed in the net mass balance is therefore a primary response to higher ablation rates, affecting the ablation area as well as the lower altitudes of the accumulation area, where the mast site also shows an significant decrease in net accumulation.

6.5   Comparison with results obtained by the geodetic method

The results obtained from the degree-day model and the geodetic method were compared, as both datasets were obtained during the same period of time between the hydrological years 1975 and 2001. Table 6.13 shows the average mass balance (in km^3 a^{-1} of w. eq.) obtained using both methods,

indicating that the final result of the mass balance model is within the error margin estimated for the observed ice elevation changes. However, the difference between modelled and observed mass balance results could be considered significant, as the model represents approximately three quarters of the mass balance change measured by comparing DEMs (geodetic method), suggesting that the climate changes observed at the reference stations used in the mass balance model are not sufficient to account for all the elevation changes measured on the glacier, and therefore, a dynamic component must by included in order to fully understand all the variations taking place at Glaciar Chico. A similar conclusion was reached by Rignot and others (2003) when analysed the ice elevation changes of the SPI as a whole, explaining that calving was the main dynamic component affecting most of the glaciers.

Table 6.13 Volume loss by the glacier between hydrological years 1975 and 2001.

	Geodetic measurements (km^3 a^{-1} of w. eq.)	Mass balance Model (km^3 a^{-1} of w. eq.)
Average volume loss	-0.226 ± 0.081	-0.165 ± 0.059
Average volume loss due to area and frontal retreat (km^3 a^{-1} of w. eq.)	-0.064 ± 0.053	
Total volume loss (km^3 of w. eq.)	-7.83 ± 2.62	-6.18 ± 2.13

In Figure 6.23 it is possible to appreciate the differences with altitude between the modelled average net mass balance based upon climatic forcing data and the average ice elevation changes between 1975 and 2001. At the glacier front (250 to 500 m) both curves are similar, and thus

a further indication that calving does not significantly affect the balance of the glacier. At approximately 700 m, the observed thinning is less than the modelled mass balance. This part of the glacier was described in Section 4.2.6.2 as the narrowest and steepest part of the glacier, suggesting a subglacial threshold. Between 1200 and 1500 m, actual ice elevation changes are greater than the modelled mass balance, which suggests a dynamic component. From 1900 m to the mountain summits, the modelled mass balance is increasingly positive, however, no observations of ice elevation changes are available for this region, and the extrapolation of the curves from lower altitude suggest no change or only limited thickening.
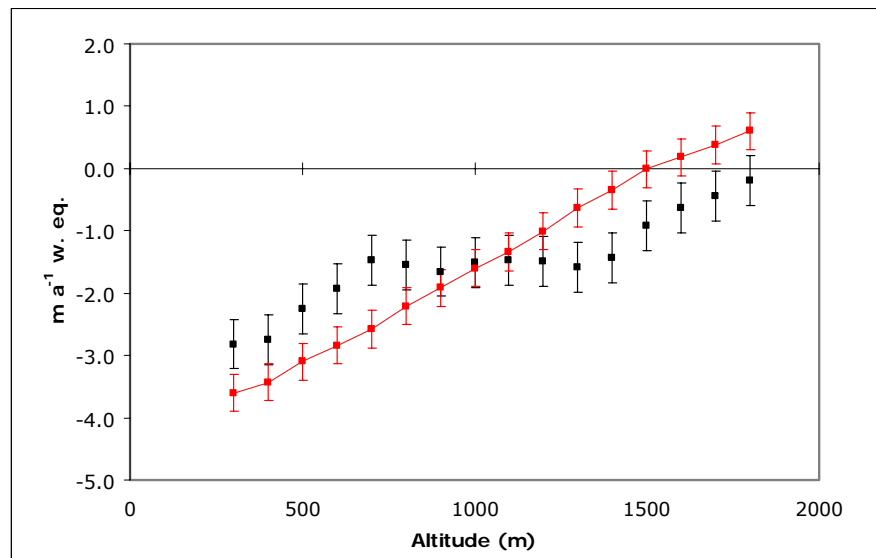
Figure 6.23 Modelled average net mass balance (red line) and measured average ice elevation change rates (black line) in m a^{-1} of w. eq. between 1975 and 200,1 versus altitude. The error bars represent 0.3 m a^{-1} of w. eq. for modelled mass balance data and 0.4 m a^{-1} of w. eq. for ice elevation changes.

To conclude therefore, most of the potential dynamic thinning takes place above the ELA of the glacier at ~1300 m, and below 1900 m. This area is mainly a plateau, shared by two basins and partially delimited by ice divides located at approximately 1450 m separating Glaciar Chico from Glaciares GAEA and Viedma respectively (Section 4.1.1).

6.6 Summary

A mass balance model has been presented, calibrated and tested in this Chapter in order to estimate the effects of temperature and precipitation variations observed along the eastern margin of the SPI on Glacier Chico. These effects are mainly associated with the accumulation and ablation processes taking place on the glacier during the last 27 years.

The ablation component of mass balance was based upon a degree-day factor model which has been forced with monthly data of temperatures obtained from two meteorological stations. The accumulation component was based upon data observed at Cochrane station, as well as some measurements of snow accumulation and precipitation obtained from the accumulation area of the SPI. Calving has been primarily considered to be a minor non-contributable component.

The calibration of the model was based upon direct measurements of mass balance carried out at a mast installed in 1996 in the accumulation area of the glacier, where measurement from several snow pits and stakes are available. The measured net balance for this specific point yielded an

average of 0.57 ± 0.21 m a^{-1} w. eq. between the hydrological years 1994/95 and 2001/02. A total annual precipitation of 4.07 ± 0.54 m a^{-1} was also estimated.

An average mass balance for the glacier as a whole of -0.84 ± 0.3 m a^{-1} was obtained by running the model between 1975 and 2001, with an average accumulation of 3.60 m a^{-1} and an average ablation of -4.44 m a^{-1}. The modelled mass balance of the glacier during these 27 years yielded a total volume loss of -4.46 km^3 of w. eq. In spite of the errors involved in the model calculation, the final result is considered to be significantly different when compared with the observed ice elevation changes experienced by the glacier, concluding that dynamic components must be considered to fully understand the recent glacier responses. These possible dynamic components are discussed in next chapter, together with an overview of the main findings of the thesis and possible future research.

7. Discussion and conclusions

7.1 Discussion

The climatic changes observed at several stations located around the SPI confirm that the region experienced a significant trend of warming, as well as a decrease in precipitation between 1961 and 1990 (Chapter 5). These climatic changes have been credited as the main background force behind the glacier retreat and shrinkage observed in Patagonia during recent decades (Aniya and others, 1996). However, it is naive to attribute all the glacier variations to the observed climate change, without considering the role played by dynamic components within the glacier system. Dynamic components have been quoted as playing and important role in explaining ice elevation changes in several glaciers, especially on the Greenland ice sheet (Abdalati and others, 2001), where during recent years dynamic thinning has increased, expanding the thinning zone to higher altitudes (Thomas and others, 2003).

The history of fluctuations of Glaciar Chico has been described in detail in Chapter 4. All these data indicate that the glacier started to retreat at a slow rate (Table 4.2) from the end of the last glacial maximum during the Little Ice Age (LIA), around 1835 AD. Since 1945, the rate of frontal retreat and area shrinkage accelerated until 1975, when an island appeared at the glacier front and effectively reduced the calving activity (Section 4.2.3). Subsequently, the glacier has experienced two frontal and areal change trends, one between 1975 and 1986 when the frontal tongue of the glacier

did not experience major changes, and a second between 1986 and 2001 when the frontal retreat and area wasting again accelerated, achieving the maximum rates of decline apparent during the past 165 years.

The ice elevation changes observed on the glacier showed a long-term thinning rate of -0.5 ± 0.36 m a^{-1} between the end of the LIA and 1975. Between 1975 and 2000 the average rate of thinning across the whole glacier was -1.3 ± 0.44 m a^{-1}, with evidence between 1995 and 2001 of an accelerated thinning rate at the glacier front of -4.6 ± 3.4 m a^{-1}; 2.5 times higher than during the previous 20 years. This trend of accelerated thinning was also detected at mid-altitudes (950 to 1050 m asl) between 1981 and 2001, when the surface elevation decreased by -1.9 ± 0.6 m a^{-1}; twice the observed elevation change for this section of the glacier between 1975 and 1981.

Across the accumulation area of the glacier there are insufficient data to estimate widespread ice elevation change trends, however, all measured points located between altitudes of 1300 and 1500 m showed high thinning values, with an average rate of -1.9 ± 0.14 m a^{-1}.

One point on the glacier which deserves specific attention is the mast installed at an elevation of 1440 m in 1996, where a thinning rate of -2.0 ± 0.14 m a^{-1} was measured between 1998 and 2001. This rate is more than three times higher than the mean net mass balance observed at the mast between 1994 and 2001 (0.57 ± 0.21 m a^{-1} of w. eq.), indicating that thinning does not reflect snowfall inter annual variations, but rather a

strong advection of ice. At approximately the altitude of the mast, the NCEP-NCAR 40 year re-analysis data collected at 850 hPa geopotential height showed a significant warming trend between the 1950s and 1985 (Section 5.1.2). As this must necessarily have enhanced ablation of snow and ice, there is the possibility that the observed thinning could also be related to snow densification or high snow accumulation/ablation variations. Similar processes affecting the surface snow layer have been discussed as a possible explanation of differential ice elevation changes observed on the Greenland ice sheet (McConnell and others, 2000).

As a result of higher temperatures at higher altitude (1440 m), it is reasonable to expect that some ablation could take the form of sublimation, however this would mainly occur under clear sky conditions, which are unusual in this area. It is therefore more probable that ablation due to warming would take place as melting. Such a sequence of melting and refreezing events is evident from the number of ice layers observed at snow pits in the area (Figure 6.2), suggesting that some melt water is present in the lower part of the accumulation area, increasing the densification rate of the snow/firn. However, the snow pits dug at this location between 1996 and 2001 indicate that surface snow density has decreased during recent years (Figure 6.2). Densification of the surface snow layer at the mast could have taken place in a long-term time scale without notice in recent snow pits, however such a process is unlikely to account for a total ice elevation change of ~40 m in 25 years as suggested by the observed measurements. Therefore, another possibility could be enunciated; the higher temperatures in the accumulation area of the glacier

generate melt water which percolates into the glacier, leaving the accumulation area through a water table as has been observed for several Patagonian glaciers (Section 6.3.2). The presence of such a water table is confirmed by the temperate condition of the Patagonian glaciers, where melt water could easily percolate to the bed, contributing to enhanced basal sliding and melting. A similar process of ice flow acceleration due to the combination of ice thinning, higher melt rates and enhanced basal sliding was reported for Glaciar Soler of the NPI, where velocities measured in 1998 were much higher than previous measurements obtained in 1985, when the glacier was approximately 40 m thicker (Yamaguchi and others, 2003).

The ice elevation changes observed at Glaciar Chico show similar altitudinal patterns to those of other glaciers of Patagonia (Naruse and Skvarca, 2000), with maximum thinning at lower altitudes in the ablation area, and minimum values in the accumulation areas. However, the thinning rates measured at lower altitudes of Glaciar Chico are two to three times smaller than the thinning observed at the majority of glaciers in Patagonia, where maximum values of up to -14 m a^{-1} have been reported for some calving glaciers (Naruse and others, 1995). Higher thinning rates were also observed on nearby Glaciares O'Higgins and GAEA where calving has proved to be a much more important control on the glacier dynamics (Section 4.2.8). As a consequence, it is possible to presume that calving is not a major factor in the dynamic system of Glaciar Chico; a conclusion that is corroborated by the lack of icebergs and calving events observed from remotely sensed imagery (Section 6.2.3).

The changes which have taken place at mid-altitudes of the glacier are in agreement with a normal temperature lapse rate gradient (linear regression between elevation and ice thinning), indicating that the thinning is probably driven by an increase of temperature with elevation. Nevertheless, the estimated warming trends observed in the region (Table 5.8) are not large enough to fully account for the total magnitude of ice elevation change measured on the glacier. This assertion is based upon the results of the mass balance model, which has been forced by temperature and precipitation series observed in the region, where a mean net mass balance of -0.84 $\pm$ 0.3 m a^{-1} of w. eq. was calculated, representing approximately three quarters of the estimated thinning of -1.2 $\pm$ 0.4 m a^{-1} of w. eq. experienced by the glacier as a whole between 1975 and 2001.

In spite of the above, both mass balance estimations (geodetic versus degree-day model) are within the respective errors, and the difference could be mainly related to uncertainties in the model and the observed elevation changes. One of the parameters in the model that could partially account for this difference is the use of monthly climatic data, which is presumably underestimating the ablation taking place during months where the mean temperature are negative but some days within this month could have positive temperatures. In order to test this factor, and considering the lack of daily data, the model was run using an estimated standard deviation of 5°C as proposed by Huybrechts and others (1991) and temperature steps of 0.1°C up to 20°C, assuming that temperatures have a normal distribution around the mean monthly temperature value. As

presumed, the ablation rates increased, therefore, the best-fitted parameters were re-tuned in order to validate the model results when compared with the ablation rates observed at glacier fronts in Patagonia, and with the specific mass balance observed at the mast. The new best-fitted parameters were within the range postulated in Table 6.8 resulting in a mean average mass balance of -0.89 ± 0.3 m a^{-1} w. eq. which is similar to the previous estimation (-0.84 ± 0.3 m a^{-1} w. eq.). This more negative balance is not strong enough to account for the all the differences with respect to the observed ice elevation changes on the glacier (-1.2 ± 0.4 m a^{-1} w. eq.).

Therefore, if calving is not the main dynamic component, and the differences between modelled and observed mass balance are not related to uncertainties in the estimations, a further explanation has to be offered to account for the approximately one quarter of thinning observed on the glacier, which is presumably not directly related to the climatic changes observed in Patagonia. These dynamic factors were mainly associated with possible changes taken place at the lower part of the accumulation area (Section 6.5), where Glaciar Chico is sharing a plateaux with Glaciares Viedma and GAEA.

As described in Section 4.2.8.1 Glaciar GAEA suffered significant changes in response to the collapse of the lower tongue of Glaciar O'Higgins, resulting in high thinning rates across most of the glacier. Unfortunately, no data were obtained for the plateau where the ice divide with Glaciar Chico is located, therefore it is not possible to determine the extent of any ice divide

migration. However, as the longitudinal stretching affecting the front of Glaciar GAEA has generated high thinning rates as well as a limited advance of the tongue, it can be hypothesised that the thinning is propagating upstream. If this process is proven to be true, the ice divide could migrate into Glaciar Chico, effectively reducing its accumulation area. This process could have been affecting Glaciar Chico for several decades as the first recorded changes taking place on Glaciar GAEA, as a consequence of Glaciar O'Higgins collapsing and retreating, date from 1960 (Shipton, 1963).

The second basin that is possibly affected by dynamic thinning shares part of Corredor Hicken at Paso de Los Cuatro Glaciers, a plateau that mainly belongs to Glaciar Viedma (Section 4.1.1). The ice divide between Glaciares Chico and Viedma seems to have been relatively stable since 1916 when the area was first visited (Kölliker and others, 1917). However, as the accuracy of the survey carried out in this campaign was very rudimentary, the observations must be considered as only an approximation. There are not enough GPS or DEM data points to allow an estimate of ice elevation trends or possible migrations of this ice divide, however, it is possible to speculate that the stability showed by the frontal tongue of Glaciar Viedma during most of the 20th Century (Section 4.2.8.2), also extends to the divide. In the event of possible future scenarios where Glaciares Viedma and/or Chico could undergo collapsing retreats triggered by further warming trends, the location of this ice divide will probably alter. A systematic programme of surveying will be necessary to monitor this process, particularly as, in addition to glaciological reasons, the area is

highly sensitive from a political point of view as the border between Chile and Argentina in the area has not been definitively mapped, but partially depends on the location of the continental watershed divide between basins draining to the Pacific and the Atlantic oceans. From a glaciological standpoint, it would also be very interesting to monitor any possible migration of this ice divide as a proxy of other significant changes taking place in the area.

Another dynamic component proposed as a possible cause of the thinning observed in Patagonia is related to excess creep (Rignot and others, 2003). A similar process was described for Greenland, where the dynamic thinning was related to two components: a change in vertical ice creep and a change in ice advection, which was associated to higher horizontal velocities, which were thickening parts of the glaciers by bringing additional thicker ice from upstream (Thomas and others, 2003). Unfortunately, very limited ice velocity measurements are available on Glaciar Chico in order to test this theory. Attempts to derive ice velocities from InSAR analysis (Interferometric Synthetic Aperture Radar) based upon tandem European Remote-sensing Satellite images (ERS-1 and ERS-2) were unsuccessful due to many factors, including the small number of available images, image acquisition during the summer when high rates of ablation are common, the relatively short baselines and, the rough topography of the area with many layovers within the InSar scenes (Baldwin, 2003).

One possible explanation for the differences observed between ice elevation changes and modelled mass balance illustrated in Figure 6.23, could be

related to changes in ice advection from the accumulation area. The section of the glacier at ~1400 m of altitude (where thinning was stronger than modelled mass balance) could be affected by higher ice advection resulting in lowering the surface topography, whilst the glacier section located at ~700 m of altitude (where the elevation changes are smaller than modelled mass balance) could be receiving these ice excess coming from upstream resulting in smaller ice elevation changes. Most of the glacier is thinning in response to negative mass balances, but the spatial differences of thinning could be related to this dynamic adjustment.

The possible ice velocity acceleration affecting Glaciar Chico could also be indirectly related to the activity of Volcán Lautaro, located at the ice divide between Glaciares Viedma and O'Higgins (Figure 1.2 and 1.3). This volcano was only discovered in 1960 during Shipton's expedition to the SPI (Shipton, 1963), but has a long history of eruptions, including observations in the mid-1860s which were attributed to a then unknown volcano (Martinic, 1999). During the 20th Century the volcano erupted in 1933, 1960, 1972, 1978 and 1979, as summarized by Lliboutry (1998). The possible connection between the volcanic activity and the dynamics of Glaciar Chico could be through enhanced subglacial geothermal activity in the vicinity of the volcano, as well as albedo alteration through the deposition of ash and tephra layers.

The volcanic geothermal contribution to subglacial melting and sliding was considered as a possible explanation for the surging type of advance experienced by Glaciar Pio XI (Figure 1.2 and 1.3) during the 1970s and

1990s by Rivera and others (1997a). During recent decades the volcano appears to have been inactive, however, during field campaigns carried out in the area in November 1998, the author of this thesis observed evidence of volcanic activity on the eastern flank of the volcano in Corredor Hicken, with streams of melt water observed at several places at altitudes above 1800 m. This melt water was brown and turbid, presumably due to a geochemical process taking place on the flanks of the volcano, or simply because of ash entrainment, therefore the streams were most probably generated by geothermal activity and not simply from surface ablation, which is unlikely at ~800 m above the transient snow line at the time of observation. If this geothermal activity occurs even in the absence of recent eruptions, it is possible to speculate that a significant volume of melt water must be semi- permanently generated in the area, contributing to the creep deformation and basal sliding of nearby Glaciares Pío XI, O'Higgins and Viedma. Given that this last glacier is affected by such processes, it is also probable that the accumulation area of Glaciar Chico, which is directly connected to Glaciar Viedma at Corredor Hicken, is also affected.

The second possible influence of Volcán Lautaro could be related to the deposition of ash layers on the accumulation area of the SPI during volcanic eruptions, which are subsequently buried by snow fall and transported downstream to appear on the surface of the ablation areas as ash bands. This process was first described by Lliboutry (1957) for several glaciers of the SPI in the surroundings of Paso Cuatro Glaciares. These ash bands are still clearly visible in the ablation area of Glaciar Chico (Figure 4.6), where the dark, thin ash layers reduce the albedo of the ice surface and increase

potential ablation. In the mass balance model used in Chapter 6 a degree-day factor for ice was selected without definition of albedo, therefore it is viable to expect locally higher ablation rates which were not considered in the model.

In summary of the possible dynamic components discussed here, it is possible to conclude that the most likely processes affecting the glacier are related to higher ice velocities at the lower altitudes of the accumulation area (the main plateau), in response to enhanced creeping and basal sliding due to the increased amount of melt water produced in response to higher temperatures at higher elevations. These positive feedbacks can be reinforced by two factors, namely the long-term change of the glacier since the end of the LIA, and intermittently enhanced basal melting due to geothermal activity related to Volcan Lautaro.

That the accumulation area of the glacier has been shrinking due to migration of the ELA (Section 4.1.3) is not in doubt. This process was confirmed by the mass balance model which produced an average ELA at a much higher altitude than the estimated ELA for the period 1981-2001, indicating that higher ablation rates and a negative mass balance are more likely to affect the plateaux of the glacier close to the ice divides (Section 6.4.2), particularly during warmer hydrological years such as 1987 and 1999. The modelled mass balance for 1999/2000 showed ablation up to the altitude of both ice divides (~1450 m), however the specific net balance estimated for that year from snow pits dug at the mast (1440 m), showed a small but positive balance of 0.15 ± 0.21 m a^{-1} w. eq. This balance was the

minimum obtained at the mast between 1994 and 2001. As the error of this observation is higher than the balance of this year, it is possible that the negative mass balance modelled for this hydrological year is statistically similar to the observed value, and therefore it is conceivable that the ice divides were losing mass. Notably, in this year the AAR of the glacier reached a minimum of 35% (Figure 7.1), compared with an average of 55% between 1981 and 2001.
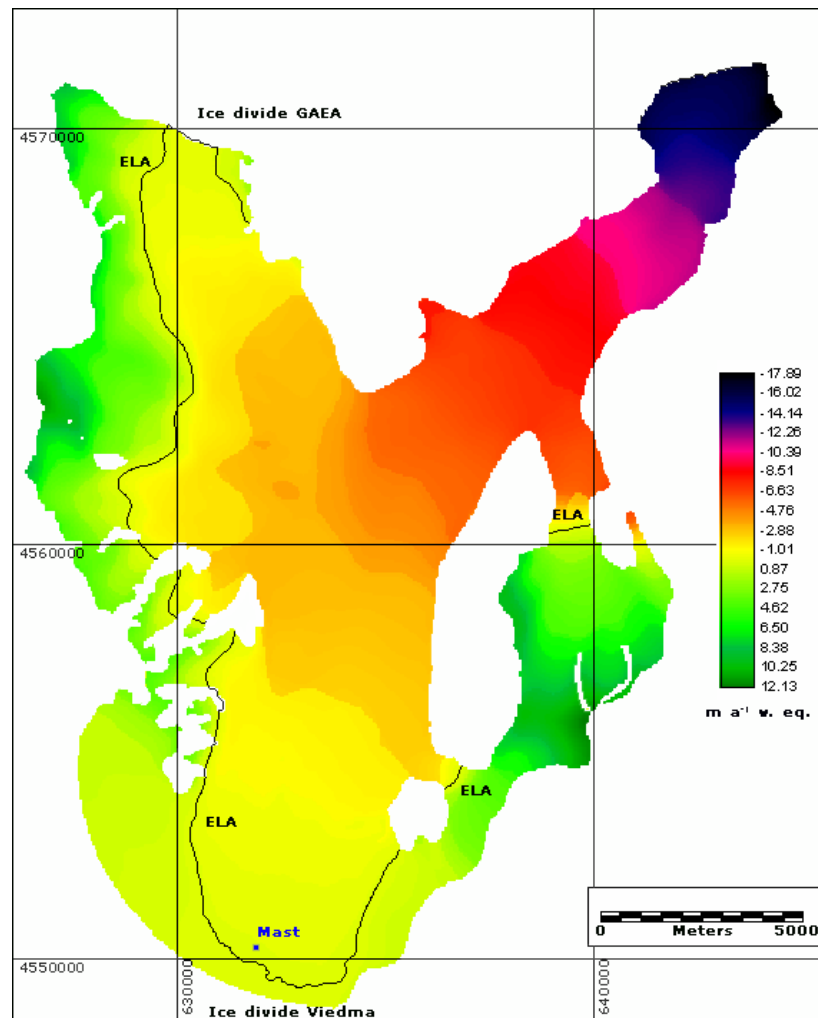
Figure 7.1 Modelled mass balance for hydrological year 1999/2000 in m a^{-1} of w. eq. The black line represents the modelled ELA for the year. UTM co-ordinates in m, WGS1984-18S.

As discussed in Section 6.4.3, the mass balance of Glacier Chico is very sensitive to changes in temperature, confirming the continental condition of the glacier previously described by Warren and Sugden (1993). In this context, if warm years like 1999/2000 are more frequent in the future, as is predicted by scenarios of climate change with warming trends of up to 3°C per Century, the AAR will experience further reduction, and therefore the viability of the glacier will be jeopardized, until further retreats of the frontal tongue will reduce the ablation area bringing the glacier to a new steady-state condition. Table 7.1 illustrates the changes of AAR experienced by the glacier since 1945 based upon the transient snowline described in Section 4.1.3, and predicted by the mass balance model results for different climate change scenarios.

Table 7.1 AAR changes

Year / climate change scenario	Accumulation-Area ratio AAR (%)
1945	64
1975	60
Estimated average 1981-2001	55
Model mean AAR based upon observed climate 1975-2001	49
Model mean AAR under climate change scenario of +2°C	48
Model mean AAR under climate change scenario of +3°C	45
Model mean AAR under climate change scenario of +3°C and -30 % precipitation	44

A wide range of AAR values between 50 and 80% have been described for steady-state glaciers at different latitudes and regions (Hawkins, 1985), with typical values lying between 55 and 65% (Porter, 1975). Comparing the AAR values presented in Table 7.1 for different climate scenarios with this range described for steady-state glaciers, it becomes clear that Glaciar Chico is approaching a point where the size of the accumulation area is less than the ablation zone, and therefore if the present trend of warming is maintained or accelerated in the future, an expected unbalance glacier could undergo a collapsing retreat of the lower tongue until reaching a new steady-state condition.

The mass balance model produced mass balance gradients similar to those estimated for other Patagonian glaciers. However, when different climate change scenarios were applied, an increase in the net balance gradient was observed, from an average of 0.013 a^{-1} between 1975 and 2001 to a maximum of 0.014 a^{-1} during the scenario characterized by a warming of 3°C per Century and a 30% decrease in precipitation. The steeper gradient indicates that the mass turnover will increase, and therefore lead to further acceleration of the ice flow.

The mass balance model used here could be considerably improved to include other important factors such as potential radiation, albedo, wind, and a more realistic reference station. A closer, more representative reference AWS measuring the parameters defined above, together with daily temperatures and more systematic measurements of ablation and

accumulation would definitely reduce the uncertainty within the model, allowing a better estimation of the mass balance of the glacier and region. Meanwhile, Glaciar Chico has proved to be a very suitable target for mass balance studies, with a dynamic component that is important, but not as dominant as for the majority of calving glaciers in the SPI, where any response to a climatic signal could be significantly reinforced or obscured. The model employed here to account for the mass balance is a first attempt, that could be useful for other glaciers in order to estimate the importance of dynamic components, or the sensitivity to precipitation or temperature changes. A better understanding of this topic for the whole area requires more complex and comprehensive models, however the spatial variability and contrasting behaviour described for the western maritime margin compared with the eastern one, indicates that a basin, or at least common basins, approach is preferable to a single model for the SPI as a whole.

Table 7.2 summarizes the main components of the mass balance model run for Glaciar Chico compared with results for other Patagonian glaciers. The accumulation rate values for these other glaciers are typically much greater than the results obtained for Glaciar Chico. Nevertheless, the results obtained by Schwikowski and others (2002) from a shallow ice core drilled from nearby Cerro Gorra Blanca (Table 7.2), confirms that this area of the SPI is suffering a drastic reduction in the amount of annual accumulation.

Table 7.2 Mass balance components in Patagonia (Summary)

Net Ablation (m a^{-1})	Net Accumulation (m a^{-1})	Net Balance (m a^{-1})	Period	Site (altitude, Lat/Long)	Reference
		+3.45	1984/85	HPI-west (1296 m, 46°44′S/ 73°32′W)	Yamada (1987)
-3.4	5.6	+2.2	1996	HPI-east (1500 m, 46°56′S/ 73°19′W)	Matsuoka and Naruse (1999)
-4.44 ± 0.3	3.6 ± 0.3	-0.84 ± 0.3	Average 1975/ 2001	Glaciar Chico-eastern side SPI	This study
		+0.57 ± 0.2	Average 1994/ 2001	Mast Gl. Chico (1440 m, 49°00′S/ 73°04′W)	This study
		+1	2000/200 1	Gorra Blanca-easter (2300 m, 49°07′S/ 73°03′W)	Schwikowski and others (2002)
	6 ± 1*		Mass flux model result	Glaciar Moreno eastern side SPI	Michel and Rignot (1999)
	5.54 ± 0.5*		Mass flux model result	Glaciar Moreno eastern side SPI	Rott and others (1998)
		+1.2	Average 1980/ 1985	Gl. Moreno eastern side (2680 m, 50°38′S/ 73°15′W)	Aristarain and Delmas (1993)
	14.4		Average 1998/ 1999	SPI-west (1756 m, 50°59′S/ 73°31′W)	Shiraiwa and others (2002)

* indicates balance accumulation

Ice cores have been widely used for determining glacier mass balance based upon measurements of net accumulation estimated from the identification of annual layers and the use of density measurements (Alley

and others, 1997; Isaksson and Melvold, 2002). Several ice core parameters can aid in identifying annual layers (for example from stable isotopes, algal biomass, visual stratigraphy and seasonal cycles of chemical species), however the main difficulty of applying these techniques in Patagonia is the high level of melt water production which can wash out such signals and thus prevent an accurate mass balance interpretation.

At the drilling site of Cerro Gorra Blanca, Schwikowski and others (2002) estimated that no significant melting was taking place based upon the observed variations of the isotopic records (δ^{18}O). This assertion is confirmed by the results of the mass balance model, which yields a mean net ablation of -0.3 ± 0.3 m a^{-1} w. eq. for the drilling site. However, the net accumulation of 1 m a^{-1} w. eq. estimated by Schwikowski and others (2002) for the drilling site is only ~15% of the calculated accumulation for the drilling site obtained with the mass balance model. One possible explanation for this large discrepancy is the effect of wind on the snow accumulation, with the mass balance model used here neglectful of wind re-distribution and wind erosion of the snow. This factor must be important in the area as westerlies affect the region on a semi-permanent basis, driving snow that fell on the western side of the SPI towards the eastern side where Glaciar Chico is located. However, not all the western glaciers will necessarily suffer snow losses due to wind erosion, with their aspect and the protection they receive from the surrounding topography potentially allowing the glacier to eventually benefit from windborne re-distribution of snow. The drilling site at Cerro Gorra Blanca (Figure 1.3) is probably affected by strong winds due to its location on a high altitude

plateau, therefore wind erosion could be a very important determinant on the accumulation rate. Meanwhile, the basin located at the foot of Cerro Pirámide (Figure 1.3) is well protected by Cordón Pirámide, and therefore it is possible that some of the westerly snow deposition could be trapped within this basin. Thus, it is possible to conclude that wind is an important factor in the distribution of snow accumulation, with a trade-off between areas with gains versus losses, a process that should be acknowledged by the model.

Apart from the possible dynamic component discussed above affecting the glacier during recent decades, the main glacier variations are driven by climate change. As described before, more than three quarters of the ice elevation changes can be explained by the mass balance model enforced with climatic observations. However, not all this percentage is a direct response to warmer/drier conditions due to the important role played by feedbacks triggered by climatic changes. Among these feedbacks, the ice surface elevation and glacier length responses are the most important.

In order to test these feedbacks, an equation (Equation 7.1) proposed by Raymond and others (in press) will be used to account for the contribution from climate change described in terms of ELA changes (first term on the right side); the elevation feedback caused by the ice elevation changes (second term); the glacier area feedback caused by the area changes (third term); and the lake area feedback expressed as the glacier area change due to lake expansion (fourth term). The first three contributions are a standard consideration for all glaciers (Elsberg and others, 2001), but the

fourth contribution could be of particular importance for Glaciar Chico as it is calving into a freshwater lake.

$$\Delta\langle b\rangle = G(-\Delta ELA + \Delta h - H\frac{\Delta Ag}{Ag} - EH\frac{\Delta Al}{Ag})$$ Eq. 7.1

Where, Δ<b> is the average change in mass balance rate per unit area of glacier Ag, measured relative to a reference climate and geometry (Ag, Al and h)

G is a scaling factor with time (unit $^{-1}$) associated with effective vertical gradients in ice equivalent thickness balance rate

Δh is the average ice elevation change experienced by a glacier relative to a reference geometry

H is the difference in elevation between the ELA and terminus of the glacier

ΔAg is the terrestrial margin area change experienced by the glacier

E is a scaling factor related to the melting that would be caused by net heat absorbed per unit area of the lake surface

ΔAl is the lake area change experienced by the lake into which the glacier terminates

In spite of the simplification of several parameters used in this equation, especially with regard to potential melting in the lake, Raymond and others

(in press) considered that the relative sizes of the distinctly different terms were correctly accounted for when applied to Glaciar Tyndall of the SPI.

Table 7.3 Main parameters used for Equation 7.1

Parameter	Glaciar Tyndall	Glaciar Chico****
Ag (km^2)	319*	199
ΔAg (km^2)	-11.4*	-5.8
Al (km^2)	10*	15.6
ΔAl (km^2)	3.1*	0.6
ΔELA (m)	-50**	-50
Δh (m)+	-86**	-35
H (m)	850**	1020
E	1.6**	1.6**
G (a^{-1})	0.015***	0.013
$\Delta <b>$ (m a^{-1})	-1.7**	-0.72

Sources:* Rivera and Casassa (2004), ** Raymond and others (in press), *** Naruse and others (1995), **** This study

Notes:+ the Δh value for Glaciar Tyndall was estimated at a profile measured repeatedly since 1985, whilst for Glaciar Chico it represents the mean value for the glacier as a whole.

Table 7.3 shows the main parameters input to Equation 7.1 for Glaciares Chico and Tyndall in order to estimate the controlling factors driving retreat in both glaciers. The reference climate and geometry for both glaciers were based on observations in 1975, and the parameters correspond to the variations measured between 1975 and 2001. The calculated values for

Δ<b> indicate the acceleration in shrinkage rate with reference to 1975, resulting in negative values for both glaciers. The *Δ<b>* value obtained for Glaciar Tyndall is comparable to the increase in thinning rate from -2 m a^{-1} measured in 1975, to about -4 m a^{-1} in 2002 measured by Raymond and others (in press). The *Δ<b>* value obtained for Glaciar Chico is also comparable to the increase of thinning observed since 1975, with a thinning rate prior to 1975 of -0.5 m a^{-1}, increasing between 1975 and 2001 to an average thinning rate of -1.3 m a^{-1}.

The main conclusion that can be drawn from applying Equation 7.1 to Glaciar Chico is that the most probable dynamic force affecting the glacier is the long-term change of the glacier, reflected in the thinning measured before 1975. The observed component inputs to Equation 7.1 indicate that climate changes have been the main driving factor since 1975, with changes in the glacier reinforced by the altitude feedback. The area changes have not been sufficient to compensate for the ice thinning and ELA rise, and the lake melting is almost insignificant, but the elevation feedback calculated here is very strong. It is also more significant than thought following previous estimations obtained in this thesis by comparing the results of mass balance model runs with and without elevation changes. For a mountain glacier with a terrestrial terminus, negative climate driving forces are stabilized by area feedbacks due to ablation area shrinkage (Raymond and others, in press). But the strong elevation feedback observed on Glaciar Chico can be explained as a result of the altitude of the terminus of the glacier, which, between 1975 and 2001, has remained at ~250 m where the ice is calving into Brazo Chico of Lago O'Higgins, forcing

a substantial lowering of the upstream surface profile of the glacier. A similar conclusion was reached by Rignot and others (2003), who ascertained that climate forcing (warmer and drier conditions) including topographic feedbacks for the SPI as a whole, are not sufficient to explain the observed glacier thinning.

In spite of the elevation feedbacks and the possible dynamic thinning discussed for Glaciar Chico, the change in the mass balance of the glacier primarily represents the climate changes experienced by the region (Chapter 6). It is well known that mountain valley glaciers with large areas and a large altitude range, present a strong and efficiently smoothed signal of secular trends, with a delay of several decades with respect to climate changes as compared with smaller cirque glaciers (Haberli, 1995 and 1998). In the light of this, when the cumulative mass balance modelled for Glaciar Chico is compared with observed mass balance observations available from across the Andes (Figure 7.2), it becomes clear that Glaciar Chico is showing a significant long-term trend. Conversely, Glaciar Echaurren Norte in Central Chile (33°35'S, 70°08'W, area 0.4 km^2, length 1.2 km) presents a much more noisy cumulative balance that reflects high inter- annual variations which have been closely related to the ENSO phenomenon (Escobar and others, 1995). Measurements were made for a couple of years on Glaciar Los Tres (49°20'S, 73°00'W, area 0.976 km^2, length 1.5 km), on the eastern side of the SPI and only 17 km to the southeast of the base camp at Glaciar Chico, however, due to its small size these are more likely to represent inter-annual changes rather than long-term responses to climate change.
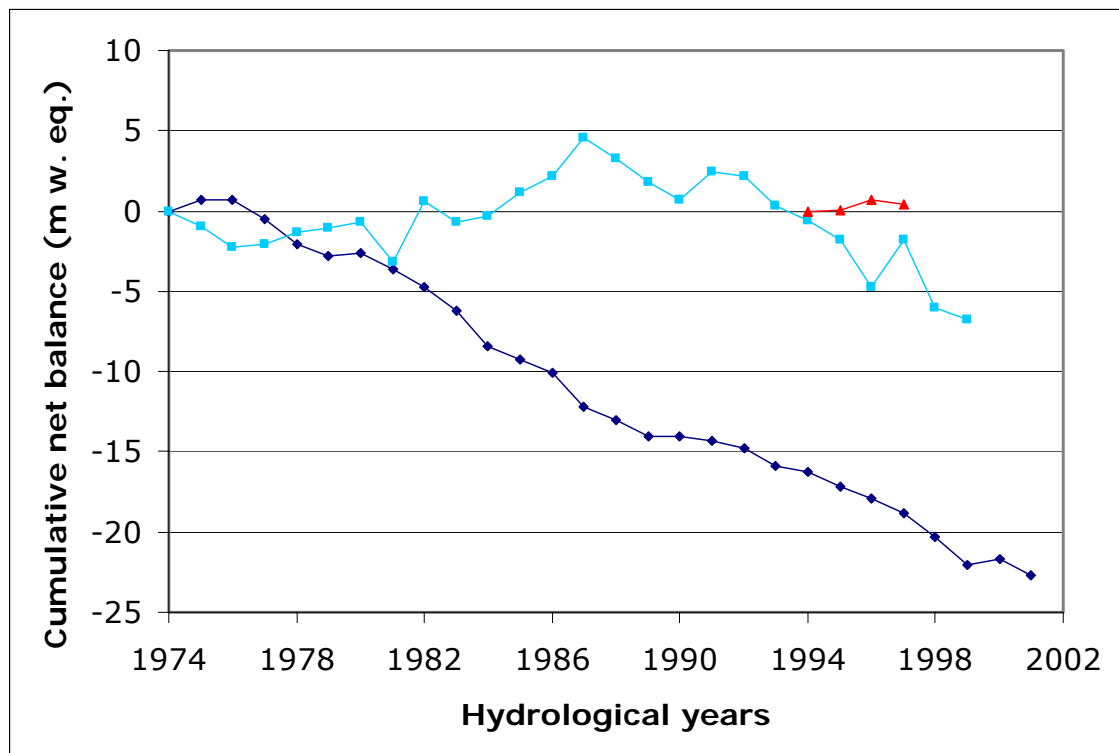
Figure 7.2 Net cumulative mass balance of Glaciares Echaurren Norte in light blue (IAHS/UNESCO, 2001), Chico in dark blue (this thesis) and Los Tres in red (IAHS/UNESCO, 2001).

The background climatic changes observed in Patagonia have been most significant between 1961 and 1990. During the 1990s the high inter-annual variability of temperatures reduced the warming trends recorded at all the meteorological stations in the region. These climatic oscillations were compared with PDO indices, but only weak relationships were shown. Of these, only the 1976 shift in the climate system was clearly visible in the climatic data obtained in Patagonia, although the more frequent ENSO years after 1976 were only generally correlated with lower precipitation. Conversely, before 1976, precipitation reached a maximum during the more frequent La Niña years (negative PDO values). Temperatures seem to follow PDO and ENSO years more closely, with generally higher

temperatures after 1976 coincident with positive PDO values (more frequent El Niño years). However, individual meteorological station records do exhibit out of phase changes when compared with PDO values, especially Coyhaique Tte Vidal before 1976, and Lago Argentino during the late 1980s.

Based upon the warming trends recorded in Punta Arenas, Lago Argentino and Cochrane stations between 1961 and 1990, it is possible to characterize the area as suffering recent rapid regional warming, similar to the observed changes experienced on the Antarctic Peninsula (Vaughan and others, 2003). However, based on the available data collected in Patagonia, it is unsafe to draw a conclusive causal relationship with ENSO, or any other atmospheric-oceanic interactions. Villalba and others (2003) described the surface temperature changes experienced during recent decades by the Patagonian region between 46° and 55°S as "remarkable, more intensive during the summer seasons and affecting predominantly minimum temperatures". These patterns of change are compatible with the teleconnections described by Karoly (1989) for the Southern Hemisphere during El Niño years, with the abrupt change toward warmer sea surface temperatures in 1976 the clearest decennial-scale oscillation mode over the Pacific ocean during the past 130 years (Villalba and others, 2001). In this context, and considering all the dendrochronological evidence obtained in Patagonia by Villalba and others (2003), it can be concluded that the warming trends observed from instrumental data in Patagonia during recent decades represent an unprecedented warming in long term climatic variations since the end of the LIA during the mid-19th Century.

This assertion is confirmed by the retreat of the majority of glaciers in Patagonia, with the peculiar exception of a few calving glaciers which are well known to respond to non-climatic driving forces. Consequently, the long-term variations of Glaciar Chico are almost certainly a response to this long-term warming trend, and they have been enhanced during recent decades by positive feedbacks including elevation changes and ice dynamic responses to a rise in the ELA, with a subsequent increase in ablation, basal sliding and creeping.

The response time of a glacier to mass balance changes can be related to the ratio between its maximum thickness and its annual ablation at the terminus (Paterson, 1984). The problem with applying this estimation to Glaciar Chico is the lack of ice thickness measurements for the glacier as a whole. Rivera and Casassa (2002) described the available ice thickness profiles obtained using a low frequency radio echo sounding system, which measured up to 800 m of ice thickness, before losing signals from deeper ice due to the prevailing temperate conditions. Nonetheless, if the maximum thickness of Glaciar Chico is assumed to be 800 m, and with an average annual ablation of 16 m a^{-1} at the glacier front, the glacier time response will be approximately 50 years, which is much slower than the 10 to 25 year response estimated for nearby Glaciar Pío XI based upon climatic anomalies versus frontal variations (Rivera and Casassa, 1999). Thus, it can be speculated that the observed negative mass balance of Glaciar Chico will be amplified and have a more significant effect on the glacier frontal

position over the next few decades in response to the warming trends between 1960 and 1991, and especially following the 1976 climatic shift.

The contribution of the Patagonian Icefields (NPI and SPI) to global sea level rise was estimated to be 0.042 ± 0.002 mm a^{-1} between 1968/75 and 2000, and doubling between 1995 and 2000 to 0.105 ± 0.3 mm a^{-1} (Rignot and others, 2003), indicating that an important, and significant, acceleration of ice thinning and area shrinkage had taken place in recent years. This acceleration is confirmed by this work, with Glaciar Chico having shown evidence of higher thinning and areal change in recent years. However, the estimates of the contribution of the Patagonian glaciers to sea level rise described by Rignot and others (2003), Rivera and others (2002) and Aniya (1999) did not consider the significant ice elevation change taking place in the accumulation area of the icefields. The thinning rates measured in the accumulation area of Glaciar Chico (average of -1.9 ± 0.14 m a^{-1}) fall far out of the range of changes estimated by Aniya (1999) of between -0.5 and -1 m a^{-1}, and are much higher than the no-change or small thinning assumption of Rignot and others (2003). Therefore it is possible to conclude that these generic sea level change calculations may be underestimating the total volume of melt water contributed by the icefields.

The Patagonian icefields are though to account for ~9% of the global eustatic sea level rise contribution from mountain glaciers (Rivera and others, 2002; Rignot and others, 2003), however the SPI and NPI represent only ~3 % of the global area of mountain glaciers. This indicates that a

disproportionately large contribution is generated from Patagonia, presumably due to its temperate conditions, as well as high mass turnover, relatively low altitude of the ELAs and high proportion of calving glaciers.

7.2 Conclusions

This study has presented a combined method for determining the mass balance of Glaciar Chico of the SPI using remote sensing techniques, direct measurements of ice elevation changes and a mass balance degree-day factor model. Using this combined method it has been possible to detect the main factors affecting the glacier variations, leading to the conclusion that the glacier has been experiencing negative mass balances as well as accelerated trends of ice thinning and area shrinkage since at least 1975, which can be mainly and primarily attributed to an increase in temperatures and a reduction in precipitation. These climatic triggering factors have been amplified by a positive altitude feedback generated by a progressive lowering of the ice topography due to thinning. The climate changes observed in the area surrounding the glacier are, however, not sufficient to account for all the ice elevation changes measured on the glacier and, therefore, a dynamic component is probably partially responsible for controlling ice thinning. Having considered other possibilities, it was concluded that the most likely dynamic process to be affecting the glacier is the enhanced creeping and basal sliding due to an increase of melt water at progressively higher altitudes. A long-term response of the glacier to the climate changes observed since the end of the LIA is also a possible cause of some of the ice thinning. In spite of the potential effects of these

dynamic components on the glacier, it was also concluded that due to the lack of calving activity at the glacier terminus, the glacier is a suitable candidate for a mass balance programme to monitor the direct effects of climate changes on the glacier behaviour.

Methods

Several DEMs were generated and compared for Glaciar Chico, based upon GPS and SRTM data, as well as aerial photographs and a satellite image. An error assessment was carried out in order to determine vertical and horizontal errors, concluding that the most accurate dataset was based upon geodetic quality GPS receivers, which was unfortunately, the spatially least extensive. The altitudes of the most extensive dataset of SRTM data proved to be accurate to the order of 7 m. One of the least accurate results was obtained using ASTER images, which generated vertical errors of 17 m and a patchy spatial coverage due to the lack of contrast within snow covered areas. In spite of the high degree of errors associated with some of the datasets used, the thinning signals retrieved from the DEMs were much higher than the noise, validating both the data and the method.

Glacier variations

Glaciar Chico has been retreating since the end of the LIA with thinning and area change rates that have been accelerating during recent years. The area changes mainly, but not uniquely, affect the ablation zone of the glacier, with an estimated total volume loss of 1.73 ± 1.43 km^3 of w. eq.

between 1975 and 2001. The great majority of these area changes (91%) were explained by the retreats of terrestrial margins, illustrating the minor importance of calving as a driving factor controlling the glacier. Ice elevation changes were observed in the glacier below an altitude of 1900 m, with maximum thinning rates of -5.4 ± 0.55 m a^{-1} at the glacier terminus, -1.9 ± 0.14 m a^{-1} in the vicinity of the ELA, and -2.0 ± 0.14 m a^{-1} at 1440 m asl in the accumulation area of the glacier. The glacier as a whole exhibited an average thinning rate of -1.3 ± 0.44 m a^{-1} between 1975 and 2000. The total volume loss by the glacier due to thinning was calculated to be -6.1 ± 2.19 km^3 of w. eq. between 1975 and 2001.

Climate change

Trends of warming temperatures, as well as a decrease in annual precipitation, were observed at most meteorological stations in Patagonia. A maximum warming trend of 0.033 °C a^{-1} was observed at Cochrane between 1969 and 1990, whilst a maximum decrease in precipitation of -27 mm a^{-2} was observed at Puerto Aysén between 1961 and 1990. In a historical perspective, both sides of the Patagonian Andes between 46 and 55°S where the NPI and SPI are located, have suffered the warmest conditions since the LIA over the past 40 years, with indications that the decadal oscillations observed in the region are related to atmospheric-oceanic anomalies in the Pacific Ocean related to ENSO events. A warming trend was also observed at an altitude of approximately 1350 m based upon NCEP/NCAR 40 year reanalysis data.

Mass balance

A negative mass balance has been calculated for Glaciar Chico between 1975 and 2001, resulting in a total volume loss of -4.46 ± 1.43 km^3 of w. eq. This negative mass balance is primarily explained by an increase in ablation, especially around the ELA of the glacier, in response to the higher temperatures observed at meteorological and radiosonde stations. Accumulation has also been reduced, especially at the lower altitudes of the accumulation zone, with the area surrounding the mast installed in 1996 having suffered high inter-annual variations and a negative accumulation trend during recent years. The mass balance of the glacier is very sensitive to changes in temperature, as demonstrated by modelling scenarios of climate changes in Patagonia, which resulted in mass balance values approximately 90% more negative during the scenario of warming trends of +3°C and reduced precipitation of -30%, than have been observed.

Dynamic component

The climate changes observed at the reference stations used to calculate the mass balance model could not account for all the ice elevation changes observed on the glacier, with approximately one quarter of the ice elevation potentially related to dynamic components. Dynamic factors including the role of calving, dynamic thinning due to ice advection/higher velocities, snow/firn densification and geothermal activity generated from nearby Volcán Lautaro have been discussed. The most likely process affecting the glacier has been related to higher rates of ablation at higher than expected

altitudes, generating larger volumes of melt water which have fed internal cavities and percolated through the glacier to the subglacial topography, there lubricating the bedrock and encouraging basal sliding. Unfortunately, very limited ice velocity data are available from Glaciar Chico, therefore it has been impossible to test the hypothesis that the glacier is experiencing an acceleration in ice flow to explain the high thinning rates observed at lower altitudes of the accumulation area.

7.3 Future research directions

One of the main challenges in future research on Glaciar Chico and the SPI will be the initiation of a systematic mass balance programme. Due to the logistical constraints existing in the region, a combined method similar to the one presented here will be necessarily adopted, where remote sensing techniques are complemented by, and validated with, direct measurements. In recent years there has been a rapid advance in the glaciological knowledge and understanding of the area, however, new data from the field will be essential to accomplish the task of an improved estimation of the mass balance of the region, the sensitivity of the glaciers to climate change and their possible contribution to sea level rise. One of the priorities must be the installation of a network of AWS at different sites across the SPI, with the aim of capturing the high spatial variability demonstrated by recent research. One possibility is to adopt the approach proposed by Kaser (2002) to install AWS traverses along both sides of the SPI, and including measurements to account for the mass balance gradient, ELA and energy balance. Moreover, such data would provide valuable ground truthing for

remote sensing data that could be used to extrapolate the specific measurements to the whole icefield.

The region around Paso de Los Cuatro Glaciares, where Glaciar Chico is located, is one of the most suitable areas of the SPI to initiate such a mass balance programme. The common logistical constraints of the SPI could be easily addressed in this area, with the support of airborne operations, as has been the case during the Hielo Azul campaigns of the Chilean Air Force. A hut has recently been installed at Nunatak García (Figure 1.3), which could provide a permanent base camp from where scientists can move along the whole northern sector of the SPI using snowmobiles. From a glaciological point of view, the area is also very suitable for mass balance studies because Glaciar Chico is probably one of the few glaciers of the SPI where calving is not the main driving factor behind the glacier behaviour, as has been demonstrated in this thesis. Accordingly, a transect from Glaciar Pío XI in the west, up to the top of Cerro Mariano Moreno, and then to the east to Glaciar Chico could be representative of the range of maritime and continental environments of the SPI.

Glaciar Pío XI on the western side of the SPI was characterized as having anomalous behaviour (Section 1.2.2), however, it is the major glacier of the SPI; has one of the easiest approaches to the accumulation area through the Exmouth fjord where a day's walk separates the fjord from the high plateau of the glacier (Meseta del Comandante); has one of the highest mass turnovers of the SPI, and has the longest historical record of

frontal variations in Patagonia (Rivera and others, 2000), therefore it is worthy of inclusion in a mass balance transect.

The summit of Cordón Mariano Moreno at an altitude of approximately 3200 m (Figure 1.3) has been included in a recently approved Chilean National Science Foundation grant, as one of several sites proposed to drill shallow ice cores of ~20 m in southern Chile. This grant was complemented with a National Geographic grant, also approved in 2004, with the specific aim of drilling the ice summit of the mountain and analysis of the mass balance and glacio-chemistry characteristics of the glacier.

Future activities at Glaciar Chico will include monitoring of the mast installed in 1996, and the expansion of the stake network to other areas presently not measured. One of these areas would be the ice divide between Glaciares GAEA and Chico, where it has been proposed in this thesis that a migration of the divide could be possible. For that purpose, geodetic quality GPS receivers would be used to survey the area, and the results with previous data (SRTM and DEMs), or used to validate remotely sensed data obtained by ICESat or CryoSat.

Despite all the above techniques and proposals for direct measurements, the main approach for improving our understanding of the SPI must come from remote sensing techniques, including satellite data (passive and active sensors), as well as laser altimeters from satellites (ICESat) and aircraft. The spatially restricted measurements obtained for this thesis could be significantly improved by using these remote sensing techniques,

especially in the accumulation area of the glaciers where accessibility for field measurements is very limited.

The combination of different sources of data used here to estimate ice elevation changes and the mass balance of Glaciar Chico have proven to be useful when a detailed error assessment is carried out. This approach could be extended to other glaciers of the SPI, however the degree-day model used here must be significantly improved in order to include other parameters that affect the mass balance of the glaciers. The geodetic approach to estimating ice elevation changes must also be improved, by including remote sensing techniques and direct measurements in the accumulation areas.

Finally, the dynamic thinning affecting Patagonian glaciers must be considered as an important component of changes in the mass balance of the glaciers. In order to account for this component new and improved GPS, interferometry and other remote sensing data (for example feature tracking) will be necessary, especially with respect to measurements of ice velocities and their possible acceleration during recent and future years.

REFERENCES

Abdalati, W., Krabill W., Frederick E., Manizade S., Martin C., Sonntag J., Swift R., Thomas R., Wright W. and Yungel J. 2001. Outlet glacier and margin elevation changes: Near-coastal thinning of the Greenland ice sheet. Journal of Geophysical Research, 106(D24), 33729-33741.

Aceituno, P. 1988. On the functioning of the Southern Oscillation in the South American sector. Part I: Surface climate. Monthly Weather Review, 116, 505-524.

Agostini, A. 1945. Andes Patagónicos. Viajes de Exploración a la Cordillera Patagónica Austral. Segunda edición, Guillermo Kraft Ed., Buenos Aires, 445 p.

Alley, R., Shuman C., Meese D., Gow A., Taylor K., Cuffey K., Fitzpatrick J., Grootes P., Zielinski G., Ram M., Spinelli G. and Elder B. 1997. Visual-stratigraphic dating of the GISP2 ice core: Basic, reproducibility, and application. Journal of Geophysical Research, 102 (C12), 26367-26381.

Aniya, M. 1995. Holocene Glacial Chronology in Patagonia: Tyndall and Upsala Glaciers. Arctic, Antarctic and Alpine Research, 27(4), 311-322.

Aniya, M. 1996. Holocene variations of Ameghino glacier, southern Patagonia. The Holocene, 6, 247-252.

Aniya, M. 1999. Recent glacier variations of the Hielos Patagónicos, South America, and their contribution to sea-level change. Arctic, Antarctic and Alpine Research, 31(2), 165-173.

Aniya, M. 2001. Glacier variations of Hielo Patagónico Norte, Chilean Patagonia, since 1944/45, with special reference to variations between 1995/96 and 1999/2000. Bulletin of Glaciological Research, 18, 55-63.

Aniya, M. and Naruse R. 1999. Late-Holocene Glacial advances at Glaciar Soler, Hielo Patagonico Norte, South America. Transactions, Japanese Geomorphological Union, 20(2), 69-83.

Aniya, M., Sato H., Naruse R., Skvarca P. and Casassa G. 1996. The use of satellite and airborne imagery to inventory outlet glaciers of the Southern Patagonia Icefield, South America. Photogrammetric Engineering and Remote Sensing, 62, 1361-1369.

Aniya, M., Sato H., Naruse R., Skvarca P. and Casassa G. 1997. Recent variations in the Southern Patagonia Icefield, South America. Arctic, Antarctic and Alpine Research, 29(1), 1-12.

Aniya, M., Dhakal A., Park S. and Naruse R. 2000. Variations of Patagonian Glaciers, South America, Using RADARSAT and Landsat Images. Canadian Journal of Remote sensing, 26(6), 501-511.

Aristarain, A. and Delmas R. 1993. Firn-core study from the southern Patagonia ice cap, South America. Journal of Glaciology, 39(132), 249-254.

Baldwin, D. 2003. InSAR processing for Glaciar Chico, Southern Patagonia Icefield. Technical report, Bristol Glaciology Centre, University of Bristol, Bristol, 6 figures, 11 p.

Biondi, F., Gershunov A. and Cayan D. 2001. North Pacific Decadal Climate Variability since 1661. Journal of Climate, 14, 5-10.

Braithwaite, R. 1995. Positive degree-day factors for ablation on the Greenland ice-sheet studied by energy-balance modelling. Journal of Glaciology, 41(137), 153-160.

Buturovic, N. 2001. Meteorological summary 2000, "Jorge C. Schythe" station. Anales del Instituto de la Patagonia, Series Ciencias Naturales, 29, 173-182.

Caldenius, C. 1932. las Glaciaciones Cuaternarias en la Patagonia y Tierra del Fuego. Geografiska Annaler, 14, 1-164.

Carrasco, J., Casassa G. and Rivera A. 1998. Climatología actual del Campo de Hielo Sur y posibles cambios por el incremento del efecto invernadero. Anales Instituto de la Patagonia, Serie Ciencias Naturales, 26, 119-128.

Carrasco, J., Casassa G. and Rivera A. 2002. Meteorological and climatological aspects of the Southern Patagonia Icefield. In G. Casassa, F. Sepúlveda and R. Sinclair (Eds.) The Patagonian Icefields. A unique natural laboratory for environmental and climate change studies. Kluwer Academic/Plenum Publishers, p. 29-41.

Casassa, G., Brecher H., Rivera A. and Aniya M. 1997. A century-long record of glacier O'Higgins, Patagonia. Annals of Glaciology, 24, 106-110.

Casassa, G. and Rivera A. 1999. Topographic mass balance model for the Southern Patagonia Icefield. Abstract International Symposium on the Verification of Cryospheric models, Bringing data and modelling scientists together, 16-20 August 1999, Zürich, p. 44.

Casassa, G., Damm V., Eisenburger E., Jenett M., Cárdenas C., Acuña C., Rivera A. and Lange H. 2001. Estudios glaciológicos en Patagonia y Chile central utilizando un sistema aerotransportado de radio eco sondaje. Anales del Instituto de la Patagonia, Serie Ciencias Naturales, 29, 25-44.

Casassa, G., Rivera A., Aniya M. and Naruse R. 2002. Current knowledge of the Southern Patagonia Icefield. In G. Casassa, F. Sepúlveda and R. Sinclair (Eds.) The Patagonian Icefields. A unique natural laboratory for environmental and climate change studies. Kluwer Academic/Plenum Publishers, p. 67-83.

Clapperton, C. 1993. Quaternary geology and geomorphology of South America. Amsterdan, Elsevier.

Clapperton, C. And Sugden D. 1988. Holocene glacier fluctuations in South America and Antarctica. Quaternary Science Reviews 7, 185-198.

Church, J. and 37 others. 2001. Changes in Sea level. In J. Houlton, Y. Ding, D. Griggs, M. Noguer, P. Van der Linden, X. Dai, K. Maskell and C. Johnson (Eds.) Climate Change 2001: The Scientific Basis. Contribution of Working Group I to the Third Assessment Report of the Intergovernmental panel on Climate Change Cambridge University press, Cambridge, UK and New York, NY, USA, p. 639-693.

Cogley, J. and Adams W. 1998. Mass balance of glaciers other than ice sheets. Journal of Glaciology, 44(147), 315-325.

Conway, H., Rasmussen L. and Marshall H. 1999. Annual mass balance of Blue Glacier, USA: 1955-97. Geografiska Annaler, 81A(4), 509-520.

Delgado, S., Masiokas M., Villalba R., Trombotto D., Ripalta A., Hernández J. and Calí S. 2002. Evidencias históricas y dendrocronológicas de las variaciones climáticas en la Patagonia durante los últimos 1000 años (Patagon-1000). In D. Trombotto and R. Villalba (Eds.) IANIGLA, 30 años de investigación básica y aplicada en ciencias ambientales. Mendoza, Argentina, p. 47-51.

DGA (Dirección General de Aguas), 1987. Balance Hídrico de Chile. Ministerio de Obras Públicas, Santiago, Chile, 59 p.

Dugmore, A. and Sugden D. 1990. Do the anomalous fluctuations of Sólheimajökull reflect ice-divide migration? Boreas, 20, 105-113.

Dyurgerov, M. 2002. Glacier mass balance and regime: Data of Measurements and Analysis. In M. Meier and R. Armstrong (Eds.) Occasional paper 55, INSTAAR, Colorado, USA, 88 p.

Dyurgerov, M. and Meier M. 1997a. Mass balance of mountain and subpolar glaciers: A new global assessment for 1961-1990. Arctic Antarctic and Alpine Research, 29(4), 379-391.

Dyurgerov, M. and Meier M. 1997b. Year-to-year fluctuations of global mass balance of small glaciers and their contribution to sea level. Arctic Antarctic and Alpine Research, 29(4), 392-402.

Elsberg, D., Harrison W., Echelmeyer K. and Krimmel R. 2001. Quantifying the effects of climate and surface change on glacier mass balance. Journal of Glaciology 47(159), 649-658.

Endlicher, A. and Santana A. 1988. El Clima del sur de la Patagonia y sus aspectos ecológico. Un siglo de mediciones climatológicas en Punta Arenas. Anales del Instituto de la Patagonia, Serie Ciencias Naturales, 18, 57-86.

ERDAS, 2001. IMAGINE OrthoBASE Tour Guide. Erdas Imagine 8.5. Erdas Inc., Atlanta, Georgia, USA, 206 p.

ERSDAC, 2001. ASTER User's guide. Part I. General (Ver.3.1). Earth Remote Sensing Data Analysis Center, USA, 101 p.

Escobar, F., Vidal F. and Marín C. 1992. Water balance in the Patagonia Icefield. In R. Naruse and M. Aniya (Eds.) Glaciological Research in Patagonia, 1990. Japanese Society of Snow and Ice, p. 109-119.

Escobar, F., Casassa G. and Pozo V. 1995. Variaciones de un Glaciar de Montaña en los Andes de Chile Central en las últimas dos décadas. Bulletin de l'Institut Francais d'Études Andines, 24(3), 683-695.

Falkner, E. 1995. Aerial Mapping. Methods and Applications. CRC Press Inc, USA, 322 p.

Francou, B., Ribstein P., Sémiond H., Portocarrero C. and Rodríguez A. 1995. Balances de Glaciares y Clima en Bolivia y Perú: Impacto de los Eventos ENSO. Bulletin de l'Institut Francais d'Études Andines, 24(3), 661-670.

Fukami, H. and Naruse R. 1987. Ablation of ice and heat balance on Soler Glacier, Patagonia. Bulletin of glacier Research, 4, 37-42.

Funk, M. and Röthlisberger H. 1989. Forecasting the effects of a planned reservoir which will partially flood the tongue of Unteraargletscher in Switzerland. Annals of Glaciology, 13, 76-81.

Garreaud, R. 1995. Regional atmospheric configurations during major storms in Central Chile. Meteorológica, 19, 73-81.

Gershunov, A. and Barnett T. 1998. Interdecadal modulation of ENSO teleconnections. Bulletin of the American meteorological Society, 79, 2715-2725.

Giese, B., Urizar C. and Fuckar N. 2002. Southern Hemisphere Origins of the 1976 Climate Shift. Geophysical Research Letter, 29(2), 10.1029-2001GL013268.

Grove, J. 1988. The little ice age. Methuen, London, UK, 498 p.

Gustafsson, D., Stähli M. and Jansson P. 2001. The surface energy balance of a snow cover: comparing measurements to two different simulation models. Theoretical and Applied Climatology, 70, 81-96.

Haakensen, N. 1986. Glacier mapping to confirm results from mass-balance measurements. Annals of Glaciology, 8, 73-77.

Haeberli, W. 1995. Glacier fluctuations and climate change detection-operational elements of a worldwide monitoring strategy. World Meteorological Organization Bulletin, 44(1), 23-31.

Haeberli, W. 1998. Historical evolution and operational aspects of worldwide glacier monitoring. In   W. Haeberli, M. Hoelze and Suter (Eds.) Into the second century of World Wide glaciers Monitoring: Prospects and Strategies. World Glacier Monitoring Service. Studies and Reports in Hydrology 56, Zürich, p. 35-51.

Haeberli, W., Frauenfelder R., Hoelze M. and Maisch M. 1999. On rates and acceleration trends of global glacier mass changes. Geografiska Annaler, 81A(4), 585-591.

Harper, J. and Bradford J. 2003. Snow stratigraphy over a uniform depositional surface: spatial variability and measurement tools. Cold Regions Science and Technology, 37, 289-298.

Harrison, S. and Winchester V. 1998. Historical fluctuations of the Gualas and Reicher Glaciers, North Patagonian Icefield, Chile. The Holocene, 8(4), 481-485.

Harrison, S. and Winchester V. 2000. Nineteenh- and twentieth-century Glacier Fluctuations and Climatic Implications in the Arco and Colonia Valleys, Hielo Patagónico Norte, Chile. Arctic, Antarctic and Alpine Research, 32(1), 55-63.

Hawkins, F. 1985. Equilibrium-line altitudes and paleoenvironment in the Merchants Bay area, Baffin Island N.W.T., Canada. Journal of Glaciology 31(109), 205-213.

Hensley, S., Rosen P. and Gurrola E. 2000. Microwave Remote Sensing of the Atmosphere and Environment II. In T. Wilheit, H. Masuko and H. Wakabayashi (Eds.) Proceedings of SPIE. Volume 4152, Sendai, Japan.

Heucke, E. 1999. A light portable steam-driven ice drill suitable for drilling holes in ice and firn. Geografiska Annaler, 81A(4), 603-609.

Hirano, A., Welch R. and Lang H. 2003. Mapping from ASTER stereo image data: DEM validation and accuracy assessment. ISPRS Journal of Photogrammetry and Remote Sensing, 57, 356-370.

Hock, R. 1999. A distributed temperature-index ice- and snowmelt model including potential direct solar radiation. Journal of Glaciology, 45(149), 101-111.

Hock, R. 2003. Temperature index melt modelling in mountain areas. Journal of Hydrology, 282(1-4), 104-115.

Huybrechts, P., Letreguilly A. and Reeh N. 1991. The Greenland ice sheet and greenhouse warming. Palaeogeography, Palaeoclimatology, Palaeoecology, 89, 399-412.

IAHS/UNESCO, 2001. Glacier Mass Balance Bulletin N°6. (1998-1999). World Glacier Monitoring Service, Zürich, 93 p.

Ibarzabal y Donángelo, T., Hoffmann J. and Naruse R. 1996. Recent climate changes in southern Patagonia. Bulletin of Glacier Research, 14, 29-36.

IPCC, 2001. Climate Change 2001: The Scientific Basis. Contribution of Working Group I to the Third Assessment Report of the Intergovernmental panel on Climate Change. In J. Houlton, Y. Ding, D. Griggs, M. Noguer, P. Van der Linden, X. Dai, K. Maskell and C. Johnson (Eds.) Cambridge University press, Cambridge, UK and New York, NY, USA, 881 p.

Isaksson, E. and Melvold K. 2002. Trends and patterns in the recent accumulation and oxygen isotopes in coastal Dronning Maud Land, Antarctica: interpretations from shallow ice cores.   Annals of Glaciology, 35, 175–180.

Jóhannesson, T., Raymond C. and Waddington E. 1989. Time-scale for adjustment of glaciers to changes in mass balance. Journal of Glaciology, 35(121), 355-369.

Jóhannesson, T., Sigurdsson O., Laumann T. and Kennett M. 1995. Degree-day glacier mass-balance modelling with applications to glaciers in Iceland, Norway and Greenland. Journal of Glaciology, 41(138), 345-358.

Jones, P., Wigley T. and Brifa K. 1994. Global and hemisphere temperature anomalies-land and marine instrumental records. In T. Boden, D. Kaiser, R. Sepanski and F. Stoss (Eds). Trends '93; A Compendium of data on Global Change. ORNL/CDIAC-65, Carbon Dioxide Information Analysis Center, Oak Ridge National laboratory, Oak Ridge, Tn, USA, p. 603-608.

Kääb, A. 2002. Monitoring high-mountain terrain deformation from repeated air- and spaceborne optical data: examples using digital aerial imagery and ASTER data. ISPRS Journal of Photogrammetry & Remote Sensing, 57(1-2), 39-52.

Karoly, D. 1989. Southern-hemisphere circulation features associated with El Niño - Southern Oscillation events. Journal of Climate, 2 (11), 1239-1252.

Kaser, G. 2002. Glacier mass balance and climate in the south American Andes. An example from the tropics and a long-term and large scale concept for the Southern Patagonia icefield. In G. Casassa, F. Sepúlveda and R. Sinclair (Eds.) The Patagonian Icefields. A unique natural laboratory for environmental and climate change studies. Kluwer Academic/Plenum Publishers, p. 89-99.

Kerr, A. and Sudgen D. 1994. The sensitivity of the South Chilean Snowline to Climatic Change, 28, 255-272.

Koizumi, K. and Naruse R. 1992. Measurements of meteorological conditions and ablation at Tyndall Glacier, Southern Patagonia, in December 1990. Bulletin of Glacier Research, 10, 79-82.

Kölliker, A., Kühn F., Reichert F., Tomsen A. and Witte L. 1917. Patagonia. Resultados de las expediciones realizadas en 1910 a 1916. Sociedad Científica Alemana. Tomos I y II, Buenos Aires, Argentina.

Krimmel, R. 1999. Analysis of difference between direct and Geodetic Mass Balance Measurements at South Cascade Glacier, Washington. Geografiska Annaler, 81A(4), 653-658.

Lang, H. 1986. Forecasting meltwater runoff from snow-covered areas and from glacier basins. In D. Kraijenhoff and J. Moll (Eds.) River flow modelling and forecasting. Dordrecht, D. Reidel Publishing C., p. 99-127.

Lawford, R. 1993. Regional hydrologic response to global change in western North America. In H. Mooney, E. Fuentes and B. Kronberg (Eds.) Earth System Responses to Global Change: Contrasts between North and South America. Academic press, p. 73-99.

Laumann, T. and Reeh N. 1993. Sensitivity to climate change of the mass balance of glaciers in southern Norway. Journal of Glaciology 39(133), 656-665.

Leiva, J. and Cabrera G. 1996. Glacier Mass Balance Analysis and Reconstruction in the Cajón del Rubio, Mendoza, Argentina. Zeitschrift fur Gletscherkunde und Glazialgeologie, 32, 101-107.

Lliboutry, L. 1956. Nieves y Glaciares de Chile. Fundamentos de Glaciología. Ediciones de la Universidad de Chile, Santiago, 471 p.

Lliboutry, L. 1957. Banding and volcanic ash on Patagonian glaciers. Journal of Glaciology, 3(21), 18-25.

Lliboutry, L. 1998. Glaciers of Chile and Argentina. In R. Williams Jr. and J. Ferrigno (Eds.) Satellite Image Atlas of Glaciers of the World. U.S. Geological Survey Professional paper 1386-I, Glaciers of South America, p. I109-I206.

Luckman, B. and Villalba V. 2001. Assessing the Synchroneity of Glacier Fluctuations in the Western Cordillera of the Americas During the Last Millennium. In V. Markgraf (Ed.) Interhemispheric climate linkages. London, Academic press, p. 119-140.

Lythe, M., Vaughan D. and the BEDMAP consortium.2001. BEDMAP: A new ice thickness and subglacial topographic model of Antarctica. Journal of Geophysical Research, 106(b6), 11335-11351.

Maisch, M. 2000. The long-term signal of climate change in the Swiss Alps: Glacier retreat since the end of the Little Ice Age and future ice decay scenarios. Geografia fisica e dinamica Quaternaria, 23, 139-151.

Mantua, N., Hare S., Zhang Y., Wallace J. and Francis R. 1997. A pacific interdecadal climate oscillation with impacts on salmon production. Bulletin of the American meteorological Society 78, 1069-1079.

Marden, C. and Clapperton C. 1995. Fluctuations of the South Patagonian Ice-Field during the last glaciation and the Holocene. Journal of Quaternary Science, 10, 197-210.

Martinic, M. 1999. Cartografía Magallánica 1523-1945. Ediciones de la Universidad de Magallanes, Punta Arenas, Chile, 345 p.

Matsuoka, K. and Naruse R. 1999. Mass Balance Features Derived from a Firn Core at Hielo Patagónico Norte, South America. Arctic, Antarctic and Alpine Research, 31(4),333-340.

McConnell, J., Arthern R., Mosley-Thompson E., Davis C., Bales R., Thomas R., Burkhart J. and Kyne J. 2000. Changes in Greenland ice sheet elevation attributed primarily to snow accumulation variability. Nature, 406 (6798), 877-879.

Meier, M. 1984. Contribution of small glaciers to global sea level. Science, 226, 1418-1420.

Meier, M. 1989. Relation between water input, basal water pressure, and sliding of Columbia Glacier, Alaska. Annals of Glaciology, 12, 214.

Meier, M., Dyurgerov M. and Mccabe G. 2003. The health of glaciers: recent changes in glacier regime. Climatic Change, 59, 123–135.

Mercer, J. 1965. Glacier variations in Southern Patagonia. The Geographical Review, 55, 390-413.

Mercer, J. 1968. Variations of some Patagonian glaciers since the Late-glacial. American Journal of Science, 266, 91-109.

Mercer, J. 1970. Variations of some Patagonian glaciers since late-Glacial II. American Journal of Science, 269, 1-25.

Mercer, J. and Sutter J. 1982. Late Miocene-Earliest Pliocene glaciation in southern Argentina: Implications for global ice-sheet history. Paleogeography, Paleoclimatology, Paleoecology, 38, 185-206.

Michel, R. and Rignot E. 1999. Flow of Glaciar Moreno, Argentina, from repeat-pass Shuttle Imaging Radar Images: comparison of the phase correlation method with radar interferometry. Journal of Glaciology, 45(149), 93-100.

Montecinos, A. and Aceituno P. 2003. Seasonality of the ENSO-Related Rainfall Variability in Central Chile and Associated Circulation Anomalies. Journal of Climate, 16, 281-296.

Naruse, R. and Aniya M. 1992. Outline of Glacier Research Project in Patagonia, 1990. Bulletin of Glacier Research, 10, 31-38.

Naruse, R., Peña H., Aniya M. and Inoue J. 1987. Flow and surface structure of Tyndall glacier, Southern Patagonia Icefield. Bulletin of Glacier Research, 4, 133-140.

Naruse, R., Aniya M., Skvarca P. and Casassa G. 1995. Recent Variations of Calving Glaciers in Patagonia, South America, Revealed by Ground Surveys, Satellite-data Analyses and Numerical Experiments. Annals of Glaciology, 21, 297-303.

Naruse, R., Skvarca P. and Takeuchi Y. 1997. Thinning and Retreat of Glaciar Upsala, and an estimate of annual ablation Changes in Southern Patagonia. Annals of Glaciology, 24, 38-42.

Naruse, R. and P. Skvarca 2000. Dynamic features of thinning and retreating Glaciar Upsala, a lacustrine calving glacier in Southern Patagonia. Arctic, Antarctic and Alpine Research, 32(4), 485-491.

Nereson, N., Raymond C., Waddington E. and Jacobel R. 1998. Migration of the Siple Dome ice divide, West Antarctica. Journal of Glaciology, 148, 643–652.

Nishida, K., Satow K., Aniya M., Casassa G. and Kadota T. 1995. Thickness change and flow of Tyndall Glacier, Patagonia. Bulletin of Glacier Research, 13, 29-34.

Paul, F., Kääb A., Maisch M., Kellenberger T. and Haeberli W. 2002. The new remote sensing derived Swiss glacier inventory I: Methods. Annals of Glaciology, 34, 355-362.

Paterson, W. 1994. The Physics of Glaciers. Pergamon Press, London, 480 p.

Peña, H. and Gutiérrez R. 1992. Statistical analysis of precipitation and air temperature in the Southern Patagonia Icefield. In R. Naruse and M. Aniya (Eds.) Glaciological Researches in Patagonia, 1990, Japanese Society of Snow and Ice, p. 95-107.

Popovnin, V., Danilova T. and Petrakov D. 1999. Pioneer mass balance estimate for a Patagonian glacier: Glaciar De los Tres, Argentina, Global and Planetary Change, 22, 255-267.

Porter, S. 1975. Equilibrium-line altitudes of late Quaternary glaciers in Southern Alps, New Zealand. Quaternary Research, 5(1), 27-47.

Porter, S. 2000. Onset of Neoglaciation in the Southern Hemisphere. Journal of Quaternary Science, 15(4), 395-408.

Rasmussen, L., Conway H. and Hates O. 2000. The accumulation regime of Blue Glacier, USA, 1914-96. Journal of Glaciology, 46(153), 326-334.

Rasmussen, L., Conway H. and Raymond C. (in press). Influence of upper air conditions on the Patagonia Icefields. Global and Planetary Change.

Raymond, C., Neumann, T., Rignot, E., Echelmeyer, K., Rivera A. and Casassa G. (in press). Retreat of Tyndall Glacier, Patagonia, over the last half century. Journal of Glaciology.

Reeh, N. 1989. Parameterization of melt rate and surface temperature on the Greenland ice sheet. Polarforschung, 59(3),113-128.

Reinwarth, O. and Rentsch H. 1994. Volume and mass balance of Vernagtferner/Oetztal Alps. Zeitschrift für Gletscherkunde und Glazialgeologie, 30, 99-107.

Rignot, E., Echelmeyer K. and Krabill W. 2001. Penetration depth of interferometric synthetic-aperture radar signals in snow and ice. Geophysical Research Letters, 28 (18), 3501-3504.

Rignot, E., Rivera A. and Casassa G. 2003. Contribution of the Patagonia Icefields of South America to Global Sea Level Rise. Science, 302, 434-437.

Risopatron, L. 1905. La Cordillera de los Andes, entre las latitudes 46° i 50° S. Imprenta Cervantes, Santiago, Chile.

Rivera, A. 1992. El Glaciar Pío XI: avances y retrocesos, el impacto sobre su entorno durante el presente siglo. Revista Geográfica de Chile Terra Australis, 36, 33 - 62.

Rivera, A., Aravena J. and Casassa G. 1997a. Recent fluctuations of Glaciar Pío XI, Patagonia: discussion of a glacial surge hypothesis. Mountain Research and Development, 17(4), 309-322.

Rivera, A., Lange H., Aravena J. and Casassa G. 1997b. The 20th century advance of Glaciar Pío XI, Southern Patagonia Icefield. Annals of Glaciology, 24, 66-71.

Rivera, A. and Casassa G. 1999. Volume changes of Pío XI glacier:1975-1995. Global and Planetary Change, 22(1-4), 233-244.

Rivera, A. and Casassa G. 2000. Variaciones recientes del Glaciar Chico, Campo de Hielo Sur. Actas IX Congreso Geológico Chileno, P. Varas, 31 Julio-4 Agosto, p. 244-248.

Rivera, A., Casassa G., Acuña C. and Lange H. 2000. Variaciones recientes de glaciares en Chile. Revistas Investigaciones Geográficas, 34, 25-52.

Rivera, A., Acuña C., Casassa G. and Bown F. 2002. Use of remote sensing and field data to estimate the contribution of Chilean glaciers to the sea level rise. Annals of Glaciology, 34, 367-372.

Rivera, A. and Casassa G. 2002. Detection of Ice Thickness using radio echo sounding on the Southern Patagonia Icefield. In G. Casassa, F. Sepúlveda and R. Sinclair (Eds.) The Patagonian Icefields. A unique natural laboratory for environmental and climate change studies. Kluwer Academic/Plenum Publishers, pp. 101-115.

Rivera, A. and Casassa G. 2004. Ice elevation, areal and frontal changes of glaciers from Torres del Paine National Park, Southern Patagonia Icefield. Arctic, Antarctic and Alpine Research, 36(4), 379-389.

Rott, H., Stuefer M., Siegel A., Skvarca P. and Eckstaller A. 1998. Mass fluxes and dynamics of Moreno Glacier, Southern Patagonia Icefield. Geophysical Research Letters, 25(9), 1407-1410.

Rosenblüth, B., Casassa G. and Fuenzalida H. 1995. Recent climate changes in western Patagonia. Bulletin of Glacier Research, 13, 127-132.

Rosenblüth, B., Fuenzalida H. and Aceituno P. 1997. Recent temperature variations in southern South America. International Journal of Climatology, 17, 67-85.

Röthlisberger, F. 1987. 10,000 Jahre Gletschergeschichte der Erde. Ein Vergleich zwischen Nord- und Südhemisphäre. Alpen-Skandinavien-Himalaya-Alaska-Südamerika-Neuseeland. Aarau, 315 p.

Rutllant, J. and Fuenzalida H. 1991. Synoptic aspects of the central Chile rainfall variability associated with the Southern Oscillation. International Journal of Climatology, 11, 63-76.

Schneider, C. and Gies D. 2004. Effects of El Niño-Southern Oscillation on Southernmost South America precipitation at 53°S revealed from NCEP-NCAR Reanalyses and weather station data. International Journal of Climatology, 24, 1057-1076.

Schöner, M. 1995. Determination of changes in volume of Gasbreen using different geodetic methods. Zeitschrift für Gletscherkunde und Glazialgeologie, 31, 85-91.

Schwikowski, M., Brütsch S., Saurer M., Casassa G. and Rivera A. 2002. First shallow firn core records from Gorra Blanca, Patagonia, Annual Report 2001, Labor für Radio- und Umweltchemie, Paul Scherrer Institut, 5.

Sessions, M. 1975. The meteorological report. Unpublished report of the Joint Services expedition to Chilean Patagonia 1972-1973. Royal Geographical Society, London, 82 p.

Shipton, E. 1963. Land of Tempest: Travels in Patagonia 1958-1962. Hodder and Stoughton, London, 224 p.

Shiraiwa, T., Kohshima S., Uemura R., Yoshida N., Matoba S., Uetake J. and Godoi M. 2002. High net accumulation rates at Campo de Hielo Patagónico Sur, South America, revealed by analysis of a 45.97 m long ice core. Annals of Glaciology, 35, 84-90.

Skvarca, P. and Naruse R. 1997. Dynamic behaviour of Glaciar Perito Moreno, Southern Patagonia. Annals of Glaciology, 24, 268-271.

Skvarca, P., De Angelis H., Naruse R., Warren C. and Aniya M. 2002. Calving rates in fresh water: new data from southern Patagonia. Annals of glaciology 34, 379-384.

Skvarca, P., Raup B. and De Angelis H. 2003. recent behaviour of Glaciar Upsala, a fast-flowing calving glacier in Lago Argentino, southern Patagonia. Annals of glaciology 36, 184-188.

Strelin, J., Malagnino E., Sone T., Casassa G., Iturraspe, R., Mori J. and Torielli C. 2002. Cronología Neoglacial del extremo Sur de Sudamérica, Arco de Scotia y península Antártica. Actas del XV Congreso Geológico Argentino, 6 p.

Streten, N. and Troup A. 1973. A synoptic climatology of satellite observed cloud vortices over the Southern Hemisphere. Quarterly Journal of the Royal Meteorological Society 99(419), 56-72.

Stuefer, M. 1999. Investigations on Mass Balance and Dynamics of Moreno Glacier based on Field Measurements and Satellite Imagery. PhD dissertation, Leopold-Franzens-Universität, Innsbruck, 173 p.

Takeuchi, Y., Naruse R. and Satow K. 1995. Characteristics of heat balance and ablation on Moreno and Tyndall glaciers, Patagonia, in the summer 1993/94. Bulletin of Glacier Research, 13, 45-56.

Takeuchi, Y., Naruse R. and Skvarca P. 1996. Annual air-temperature measurement and ablation estimate at Moreno Glacier, Patagonia. Bulletin of Glacier Research, 14, 23-28.

Thomas R., Csatho B., Davis D., Kim C., Krabill W., Manizade S., McConnell J. and Sonntag J. 2001. Mass balance of higher-elevation parts of the Greenland ice sheet. Journal of Geophysical Research, 106 (D24), 33707-33716.

Thomas, R. Abdalati W., Frederick E., Krabill W., Manizade S. and Steffen K. 2003. Investigation of surface melting and dynamic thinning on Jakobshavn Isbrae, Greenland. Journal of Glaciology, 49(165), 231-239.

Toutin, T. and Cheng P. 2001. DEM generation with ASTER stereo data. Earth Observation Magazine, 10(6), 10-13.

Trenberth, K. and Shea D. 1987. On the Evolution of the Southern Oscillation. Monthly Weather Review, 115, 3078-3096.

Trenberth, K. and Hurrell J. 1994. Decadal atmosphere-ocean variations in the Pacific. Climate Dynamics, 9, 303-319.

Tucker, C., Grant D. and Dykstra J. 2004. NASA's Global Orthorectified Landsat Data. Photogrammetric Engineering and Remote Sensing, 70(3), 111-125.

UNESCO, 1998. Into the second century of worldwide glacier monitoring-prospects and strategies. In W. Haeberli, M. Hoelzle and S. Suter (Eds.) World Glacier Monitoring Service. Studies and Reports in Hydrology 56, Zürich, 227 p.

USGS, 1998. Satellite Image Atlas of Glaciers of the World: South America. In R. Williams and J. Ferrigno (Eds.) U.S. Geological Survey Professional paper 1386-I, Washington DC, USA, 1206 p.

Van der Veen, C. 1996. Tidewater calving. Journal of Glaciology, 42(141), 375-385.

Van der Veen, C. 1999. Fundamentals of Glacier Dynamics. Balkema, Rotterdam, Brookfield, Netherlands, 462 p.

Van der Veen, C. 2002. Calving glaciers. Progress in Physical geography, 26(1), 96-122.

Vaughan, D., Marshall G., Connolley W., Parkinson C., Mulvaney R., Hodgson D., King J., Pudsey C. and Turner J. 2003. Recent rapid regional climate warming on the Antarctic Peninsula. Climatic Change, 60 (3), 243-274.

Venteris, E. 1999. Rapid tidewater glacier retreat: a comparison between Columbia Glacier, Alaska and Patagonia calving glaciers. Global and Planetary Change, 22(1-4), 131-138.

Verbunt, M., Gurtz J., Jasper K., Lang H., Warmerdam P. and Zappa M. 2003. The hydrological role of snow and glaciers in alpine river basins and their distributed modelling. Journal of Hydrology, 282, 36-55.

Villalba, V., D'Arrigo R., Cook E., Wiles G. and Jacoby G. 2001. Decadal-Scale Climatic Variability along the Extratropical Western Coast of the Americas: Evidences from Tree-Ring Records. In V. Markgraf (Ed.), Inter-Hemispheric Climate Linkages, Academic Press, San Diego, California, U.S.A., p. 155–172.

Villalba, R., Lara A., Boninsegna J., Masiokas M., Delgado S., Aravena J., Roig F., Schmelter A., Wolodarsky A. and Ripalta A. 2003. Large-scale temperature changes across the southern Andes: 20th-century variations in the context of the past 400 years. Climatic Change, 59 (1-2), 177-232.

Waddington, E. and Marriott R. 1986. Ice divide migration at Blue Glacier, USA. Annals of Glaciology, 8, 175-176.

Warren, C. 1992. Iceberg calving and the glacioclimatic record. Progress in Physical geography, 16(3), 253-282.

Warren, C. and Sugden D. 1993. The Patagonian icefields: a glaciological review. Arctic, Antarctic and Alpine Research, 25(4), 316-331.

Warren, C. and Rivera A. 1994. Non linear Climatic Response of Calving Glaciers: A case study of Pío XI Glacier, Chilean Patagonia. Revista Chilena de Historia Natural, 67, 385-394.

Warren, C., Sugden D. and Clapperton C. 1995a. Asynchronous response of Patagonian glaciers to historic climate change. Quaternary of South America and Antarctic Peninsula, 9, 89-108.

Warren, C., Glasser N., Harrison S., Winchester V., Kerr A. and Rivera A. 1995b. Characteristics of tide-water calving at Glaciar San Rafael, Chile. Journal of Glaciology, 41(138), 273-289.

Warren, C., Rivera A. and Post A. 1997. Greatest Holocene advance of glaciar Pío XI, Chilean Patagonia: possible causes. Annals of Glaciology, 24, 11-15.

Warren, C. and Aniya M. 1999. The calving glaciers of South America. Global and Planetary Change, 22(1-4), 59-77.

Warren, C., Benn D., Winchester V. and Harrison S. 2001. Buoyancy-driven lacustrine calving, Glaciar Nef, Chilean Patagonia. Journal of Glaciology, 47(156), 135-146.

Wenzens, G. 1999. Fluctuations of Outlet and Valley Glaciers in the Southern Andes (Argentina) during the Past 13,000 Years. Quaternary Research, 51, 238-247.

Wenzens, G. 2002. The influence of tectonically derived relief and climate on the extent of last Glaciation east of the Patagonian ice fields (Argentina, Chile). Tectonophysics, 345, 329-344.

Winchester, V., and Harrison S. 2000. Dendrochronology and Lichenometry, an investigation into colonization, growth rates and dating on the east side of the North Patagonian Icefield, Chile. Geomorphology, 34, 181-194.

Winchester, V., Harrison S. and Warren C. 2001. Recent retreat Glaciar Nef, Chilean Patagonia, dated by Lichenometry and Dendrochronology. Arctic, Antarctic and Alpine Research, 33(3), 266-273.

Yamada, T. 1987. Glaciological Characteristics Revealed by 37.6 m deep core drilled at the Accumulation area of San Rafael Glacier, the Northern Patagonia Icefield. Bulletin of Glacier Research, 4,59-68.

Yamaguchi, S., Naruse R., Matsumoto T. and Ohno H. 2003. Multiday variations in flow velocity at Glaciar Soler, Northern Patagonia, Chile. Arctic, Antarctic and Alpine Research, 35(2), 170-174.